MODELLING THE IMPACT OF CLIMATE CHANGE ON GROUNDWATER RESOURCES: CASE STUDY OF KONYA CLOSED BASIN

by

Onur Cem Yologlu

B.Sc. in Environmental Engineering, Middle East Technical University, 2020

Submitted to the Institute of Environmental Sciences
in partial fulfillment of the requirements for the degree of
Master of Science
in
Environmental Sciences

Boğaziçi University
2023

MODELLING THE IMPACT OF CLIMATE CHANGE ON GROUNDWATER RESOURCES: CASE STUDY OF KONYA CLOSED BASIN

APPROVED BY:

Prof. Dr. Nadim K. Copty Thesis Advisor	. . . . .
Prof. Dr. Alper Elçi	. . . . .
Assist. Prof. Dr. İrem Daloğlu Çetinkaya	. . . . .

DATE OF APPROVAL: 12/09/2023

ACKNOWLEDGEMENTS

First and foremost, working under the supervision of my advisor, Prof. Dr. Nadim K. Copty, was an experience beyond words – I simply adored it. I am thankful for his guidance, patience, and support from beginning till the end of my research period. His office was always accessible, providing me the opportunity to engage in fruitful discussions with him. He was incredibly generous in sharing his knowledge whenever I need. His belief in my potential and encouragement gave me commitment to put greater effort and do my best. I consider myself lucky to work under his supervision.

I would like to extend my gratitude to the members of the examining committee, Prof. Dr. Alper Elçi and Assist. Prof. Dr. İrem Daloğlu Çetinkaya, for their significant suggestions and contributions. Additionally, I extend my sincere gratitude to Assist. Prof. Dr. İrem Daloğlu Çetinkaya for sharing knowledge and discussions. Her comments and questions have always helped to improve my understanding and encouraged me to explore new perspectives. Her consultation and contributions have significantly enhanced my work, leading to better achievements.

I would like to express my appreciation to Prof. Dr. Ali Kerem Saysel and İzel Uygur for their exceptional and indispensable contributions to this project. Their expertise and efforts have significantly enhanced the outcomes of the project. Also, I would like to thank my fellow lab mates at Environmental Systems Laboratory, Mehmet Can Tunca and Elif Bal, for sharing their valuable knowledge and having invaluable discussions.

Lastly, I would like to convey my most sincere appreciation to my beloved family members and friends for their tremendous support during my journey. Among them, I especially have to mention my mom Eylem, my father Hilmi and my brother Erencan for their endless support and encouragement. Their love and support have played a vital role in enabling me to achieve my goals, and for that, I am genuinely thankful. I would also like to express my gratitude to my friends, Utku Berkalp Ünalan and İlksen Şenocak, for inspiring brainstorming and their help throughout the years.

I would like to acknowledge InTheMED Project which has provided me a unique opportunity to work within interdisciplinary team at international scale. I am sincerely grateful to InTheMED which is supported by the PRIMA programme under grant agreement No 1923. The PRIMA programme is supported by the European Union.

ABSTRACT

MODELING THE IMPACT OF CLIMATE CHANGE ON GROUNDWATER RESOURCES: CASE STUDY OF KONYA CLOSED BASIN

The Konya Closed Basin (KCB), located in central Turkey, is one of the major agricultural regions of the country. KCB which has semi-arid climate relies heavily on groundwater for irrigation purposes. This has led to serious decrease in groundwater levels. To enhance water resources management in the basin and ensure its long-term sustainability, a groundwater flow model for the entire basin is developed. The model simulates vertical water flow in the vadose zone as well as horizontal flow in the underlying aquifer system. The model was calibrated using observed head data at 29 monitoring wells from 2000 to 2022. It is estimated that the average water table drop is 0.43 m/year over the entire domain and 0.62 m/year in the agricultural regions. The calibrated model was then used to reveal the potential impacts of climate change on groundwater resources for different water use scenarios. Seventeen regional climate models under two climate pathways (RCP 4.5 and RCP 8.5) were considered for the period of 2023-2040. Five different water management scenarios were developed based on the surveys with farmers, NGOs, and water authorities. With the business as usual scenario, the model predicts 0.28 meters per year average drop in groundwater head over entire basin between 2023 and 2040. On the other hand, through improved irrigation efficiency and reverting to traditional rainfed crops, it is shown that groundwater water drop can be reversed to net increase of 0.04 m/year for the same period allowing for more sustainable use of the groundwater resource.

ÖZET

KONYA KAPALI HAVZASI'NDA İKLİM DEĞİŞİKLİĞİNİN YERALTI SUYU KAYNAKLARINA ETKİSİNİN MODELLENMESİ

Türkiye'nin merkezinde yer alan Konya Kapalı Havzası (KKH), ülkenin en önemli tarım bölgelerinden biridir. Yarı-kurak iklime sahip havzada sulama amacıyla büyük ölçüde yeraltı suyu kullanılmaktadır. Bu durum yeraltı su seviyesinde ciddi düşüşlere yol açmıştır. Havzadaki su kaynakları yönetimini iyileştirmek ve uzun vadeli sürdürülebilirliğini sağlamak için tüm havzayı kapsayan bir yeraltı suyu akış modeli geliştirilmiştir. Geliştirilen model, vadoz bölgedeki dikey su akışının yanı sıra alttaki akifer sistemindeki yatay akışı simüle etmektedir. Model, 2000'den 2022'ye kadar ölçüm yapılan 29 yeraltı suyu izleme kuyusundan toplanan yeraltı suyu seviyelerinin kullanılmasıyla kalibre edilmiştir. Havzanın tamamında ortalama yeraltı suyu seviyesi düşüşünün 0.43 m/yıl ve bu rakamın tarım bölgelerinde 0.62 m/yıl olduğu tahmin edilmektedir. Kalibre edilen model daha sonra farklı su kullanım senaryolarının simulasyonunda ve iklim değişikliğinin havzanın yeraltı su kaynakları üzerindeki potansiyel etkilerini ortaya çıkarılmasında kullanılmıştır. 2023-2040 dönemi için sıcaklık ve yağış projeksiyonu için RCP 4.5 ve RCP 8.5 olmak üzere iki iklim yolu altındaki on yedi bölgesel iklim modeli dikkate alınmıştır. Ayrıca, çiftçiler, STK'lar ve su üstüne çalışan politika yapıcılar ile yapılan anketlere dayalı olarak beş farklı su yönetimi senaryosu geliştirilmiştir. Model, tüm koşulların aynı kalması durumunda 2023 ile 2040 yılları arasında tüm havzada yeraltı suyu seviyesinde yılda ortalama 0.28 metre düşüş olacağını öngörüyor. Öte yandan, iyileştirilmiş sulama verimliliği ve geleneksel yağmurla beslenen mahsullere geri dönülmesiyle, tüm havzadaki ortalama yeraltı suyu seviyesi aynı dönem için yılda 0,04 metre artabilir ve bu da yeraltı suyu kaynaklarının daha sürdürülebilir bir şekilde kullanılmasına olanak sağlayacağı öngörülmektedir.

TABLE OF CONTENTS

ACKNOWLEDGEMENTS iii

ABSTRACT iv

ÖZET v

TABLE OF CONTENTS vi

LIST OF FIGURES x

LIST OF TABLES xv

LIST OF SYMBOLS/ABBREVIATIONS xvi

1. INTRODUCTION 1

2. LITERATURE REVIEW 4

2.1. Problem Statement 4

2.2. Objectives 6

2.3. Literature Review 7

2.3.1. Introduction 7

2.3.2. Hydrological Studies 8

2.3.3. Studies on Climate Change 10

2.3.4. Model Selection 11

3. STUDY AREA 15

3.1. Location of Study Area 15

3.2. Topography 16

3.3. Climate 17

3.4. Land Use 24

3.5. Hydrology 25

3.6. Hydrogeology 25

3.6.1. Pumping Tests 26

3.6.2. Hydraulic Conductivity 27
3.6.3. Head Distribution 28
4. METHODOLOGY 30
4.1. Research Workflow 30
4.2. Data Preprocessing 30
4.3. Numerical Model 31
4.3.1. Software Interface Selection 31
4.3.2. Spatial Discretization 31
4.3.3. Temporal Discretization 32
4.3.4. Hydrological and Storage Parameters 33
4.3.5. Boundary Conditions 33
4.3.6. UZF1 Package 33
4.3.7. Simulation Scenarios 34
4.3.7.1. Business as Usual Scenario. 35
4.3.7.2. Corn Phased Out Scenario. 36
4.3.7.3. Increase in Irrigation Efficiency Scenario. 37
4.3.7.4. Mavi Tunnel Scenario. 37
4.3.7.5. Combining of Corn Phased Out and Increased Irrigation Efficiency Scenario. 37
4.4. Conceptual Hydrological Model 38
4.4.1. Schematization 38
4.4.2. Water Balance Zones and Components 39
4.5. Driving Forces 40
4.5.1. Precipitation 40
4.5.2. Potential Evapotranspiration (PET) 40
4.5.3. Surface Water 42

4.5.4. Groundwater Abstraction 42
4.5.4.1. Domestic water demand. 43
4.5.4.2. Agricultural water demand. 44
4.5.4.3. Groundwater extraction. 48
4.6. Spatial Interpolation 49
5. RESULTS 52
5.1. Spatial Data 52
5.1.1. Hydraulic Conductivity (K_h) 52
5.1.2. Top Elevation 52
5.2. Spatiotemporal Data 53
5.2.1. Precipitation 53
5.2.2. Groundwater Abstraction 54
5.3. Calibration Results 55
5.4. Sensitivity Analysis 60
5.5. Simulations of Scenarios 63
5.5.1. Business as Usual Scenario 63
5.5.2. Corn Phased Out Scenario 68
5.5.3. Increase in Irrigation Efficiency Scenario 71
5.5.4. Mavi Tunnel Scenario 74
5.5.5. Combination of Corn Phased Out and Efficient Irrigation Scenario 77
5.6. Evaluation of Scenarios 80
6. CONCLUSIONS 83
REFERENCES 85
APPENDIX A: PLOT OF PRECIPITATION FOR ALL STATIONS 97
APPENDIX B: FORECASTED LAND USE 106
APPENDIX C: PUMPING TEST RESULTS 125

APPENDIX D: PRECIPITATION AND TEMPERATURE UNDER REGIONAL CLIMATE MODELS FOR ALL STATIONS 130

LIST OF FIGURES

Figure 1.1. Map of Konya Closed Basin 2

Figure 2.1. Total agricultural products in Konya and Karaman 4

Figure 2.2. (a) & (b) Sinkholes in Karapınar, Konya, (c) Dead Flamingos in Tuz Lake, (d) Drought in Akşehir Lake 6

Figure 2.3. Coupled 1-D unsaturated zone flow and 3-D groundwater flow 12

Figure 3.1. Map of cities in Konya Closed Basin. 15

Figure 3.2. Elevation map of Konya Closed Basin. 16

Figure 3.3. Flow directions based on Eight Direction Pour Point Model. 17

Figure 3.4. Annual mean of monthly precipitation (mm) and reference evapotranspiration(mm) over the basin. 18

Figure 3.5. Mean aridity index over the basin. 19

Figure 3.6. Mean aridity index over the basin between 2000 and 2022. 19

Figure 3.7. Climate classification for Konya Closed Basin. 20

Figure 3.8. Location of meteorological stations. 21

Figure 3.9. Monthly cumulative precipitation for Konya Closed Basin. 21

Figure 3.10. Monthly mean temperature for Konya Closed Basin. 22

Figure 3.11. Mean projected changes for precipitation and temperature among RCMs during the period of 2023-2040 relative to 1976-2005 under pathway of RCP4.5. 23

Figure 3.12. Mean projected changes for precipitation and temperature among RCMs during the period of 2023-2040 relative to 1976-2005 under pathway of RCP8.5. 23

Figure 3.13. Land use classification in the basin. 24

Figure 3.14. Simplified groundwater flow system in the basin 26

Figure 3.15. Pumping tests from the Green Reports. 27

Figure 3.16. Initial groundwater head distribution of the basin. 28

Figure 3.17. Summary of the groundwater level recording. 29

Figure 4.1. Schematic representation of research methodology. 30

Figure 4.2. Tests for grid size in ArcGIS 32

Figure 4.3. Schematic diagram of UZF-MODFLOW model 34

Figure 4.4. Land use for main crops for business as usual scenario in Konya Basin: (a) normal plot and (b) log-log plot.....35

Figure 4.5. Schematic representation for the components of UZF-MODFLOW. 38

Figure 4.6. Discharge from Apa Dam. 42

Figure 4.7. Domestic wells in Konya province. 43

Figure 4.8. Town allocated grids over the basin. 46

Figure 4.9. Agricultural land use for Konya Closed Basin: (a) normal plot and (b) log-log plot. 47

Figure 5.1. Hydraulic conductivity for the basin. 52

Figure 5.2. Top elevation in the model 53

Figure 5.3. Precipitation distribution over the basin by applying SK. 53

Figure 5.4. Groundwater abstraction in the basin. 54

Figure 5.5. Simulation heads and observed heads of observation locations for the entire period. ...55

Figure 5.6. Observed groundwater level versus simulated groundwater level (continue). 56

Figure 5.7. Observed groundwater level versus simulated groundwater level (continued) 57

Figure 5.8. Percent discrepancy for calibrated model. 58

Figure 5.9. Simulated groundwater level across the whole KCB after calibration process for December 2022 58

Figure 5.10. Water budget for the basin from January 2000 to December 2022. 59

Figure 5.11. Impact of Brooks-Corey exponent on recharge (a) normal plot and (b) log-log plot.....60

Figure 5.12. Impact of residual water content (θ_r) on recharge (a) normal plot and (b) log-log plot.....61

Figure 5.13. Impact of saturated water content (θ_s) on recharge (a) normal plot and (b) log-log plot 62

Figure 5.14. Predicted groundwater level averaged over the entire basin for the business as usual scenario for RCP 4.5 and 8.5.....64

Figure 5.15. Net inflow graph for the business as usual scenario for the KCB based on RCP4.5 65

Figure 5.16. Net inflow graph for the business as usual scenario for the KCB based on RCP8.5 66

Figure 5.17. Spatial distribution of mean groundwater level for year 2040 based on 17 RCMs under RCP4.5 climatic pathway according to business as usual scenario. 67

Figure 5.18. Spatial distribution of mean groundwater level for year 2040 based on 17 RCMs under RCP8.5 climatic pathway according to business as usual scenario. 67

Figure 5.19. Groundwater level over entire basin for corn phased out scenario.....68

Figure 5.20. Net inflow graph for the corn phased out scenario for the KCB based on RCP4.5 69

Figure 5.21. Net inflow graph for the corn phased out scenario for the KCB based on RCP8.5 69

Figure 5.22. Spatial distribution of mean groundwater level for year 2040 based on 17 RCMs under RCP4.5 climatic pathway according to corn phased out scenario. 70

Figure 5.23. Spatial distribution of mean groundwater level for year 2040 based on 17 RCMs under RCP8.5 climatic pathway according to corn phased out scenario. 70

Figure 5.24. Groundwater level over entire basin for efficiency increase scenario. 71

Figure 5.25. Net inflow graph for the efficiency increase scenario for the KCB based on RCP4.5 72

Figure 5.26. Net inflow graph for the efficiency increase scenario for the KCB based on RCP8.5 73

Figure 5.27. Spatial distribution of mean groundwater level for year 2040 based on 17 RCMs under RCP4.5 climatic pathway according to efficiency increase scenario. 73

Figure 5.28. Spatial distribution of mean groundwater level for year 2040 based on 17 RCMs under RCP8.5 climatic pathway according to efficiency increase scenario. 74

Figure 5.29. Groundwater level over entire basin for Mavi Tunnel scenario. 74

Figure 5.30. Net inflow graph for the Mavi Tunnel scenario for the KCB based on RCP4.5 75

Figure 5.31. Net inflow graph for the Mavi Tunnel scenario for the KCB based on RCP8.5 76

Figure 5.32. Spatial distribution of mean groundwater level for year 2040 based on 17 RCMs under RCP4.5 climatic pathway according to Mavi Tunnel scenario. 76

Figure 5.33. Spatial distribution of mean groundwater level for year 2040 based on 17 RCMs under RCP4.5 climatic pathway according to Mavi Tunnel scenario. 77

Figure 5.34. Groundwater level over entire basin for the combination of corn phased out and efficient irrigation scenario. 77

Figure 5.35. Net inflow graph for the combination of corn phased out and efficient irrigation scenario for the KCB based on RCP4.5 78

Figure 5.36. Net inflow graph for the combination of corn phased out and efficient irrigation scenario for the KCB based on RCP8.5 79

Figure 5.37. Spatial distribution of mean groundwater level for year 2040 based on 17 RCMs under RCP4.5 climatic pathway according to combination of corn phased out and efficiency increase scenario. 79

Figure 5.38. Spatial distribution of mean groundwater level for year 2040 based on 17 RCMs under RCP8.5 climatic pathway according to combination of corn phased out and efficiency increase scenario. 80

LIST OF TABLES

Table 3.1. Land Area of City Overlaying the Basin and Percentage of Overlaying Area to Total City Area. 16

Table 3.2. Climatic Condition According to Aridity Index 18

Table 3.3. GCM-RCM models for the study from EURO-CORDEX. 22

Table 4.1. Summary of key input parameter 39

Table 4.2. Water resources for domestic use in Konya province 43

Table 5.1. Average drivers of water budget from January 2000 to December 2022. 59

LIST OF SYMBOLS/ABBREVIATIONS

Symbol	Explanation
hm^3	Cubic Hectometer
L	Liter
Km	Kilometer
M	Meter
Mm	Millimeter
ºC	Celsius

Abbreviation	Explanation
DEM	Digital Elevation Model
DSI	State Hydraulic Works (Devlet Su İşleri)
GCM	General Circulation Model
HGM	General Directorate of Mapping (Haritalar Genel Müdürlüğü)
GIS	Geographical Information System
KCB	Konya Closed Basin
N	Neogene
P	Paleogene
RCM	Regional Climate Model
RCP	Representative Concentration Pathway
SIM	Spatial Interpolation Methods
SK	Simple Kriging
SZB	Sakarya Zone Block
TAB	Tauride-Anatolide Block
TSMS	Turkish State Meteorological Service
UZF1	Unsaturated Zone Flow Package
WWF	World Wide Fund for Nature

1. INTRODUCTION

Historically, water from aquifers, lakes, and rivers has generally been sufficient to meet agricultural, domestic, and industrial water demand (Falkenmark & Molden, 2008). However, in recent years, water resources have been depleted dramatically in many regions of the world due to the unsustainable use of this resource especially due to excessive groundwater extraction for irrigation purposes to meet ever-increasing food demand. During the 20th century, water consumption has increased at nearly twice the population growth rate (Food and Agriculture Organization of the United Nations, 2017). Today, water resources are devoted to a diverse ever-increasing array of anthropogenic activities that cause the depletion of this vital resource and degradation of water quality and ecosystems. Therefore, water policies and interventions are needed to preserve and enhance the status of water resources. Water management is necessary to increase the efficiency of water usage, identifying the sources of the pollution, mitigating the pollution, enhancing the ecosystems, and conserving biodiversity (Gregersen et al., 2007; G. Wang et al., 2016).

Basins all over the world have been facing numerous challenges such as groundwater overdraft, steadily growing freshwater demand, and freshwater contamination. These challenges are likely to be exacerbated in many regions of the world due to climate change that are anticipated to lead to more frequent extreme weather events, fluctuations in amount and frequency of precipitation, heatwaves, droughts, and wildfires. Furthermore, environmental changes considerably impact subsurface hydrology, water quality, and interactions between surface and groundwater. Consequently, basin management studies should include a comprehensive understanding of the hydrologic cycles and interactions for sustainable governance (Jensen et al., 2007)

Basins can be categorized as open and closed (endorheic) basins. In an open basin, water flows towards an outlet such as a stream, sea, or ocean. On the other hand, in an endorheic watershed, water can only get out of the system through evapotranspiration. Endorheic watersheds cover approximately 11.4% of the total land area in the world. Closed basins are primarily located in arid and semi-arid lands (X. Li et al., 2018). Many endorheic watersheds face the threat of collapse of water systems due to drought, rapid increase in population growth, unsustainable economic development, and overuse of water resources (X. Li et al., 2018). The water capacity of an endorheic basin is highly sensitive to fluctuations in water fluxes due to global warming and human activities since there is limited precipitation and a high potential for evaporation. Combining satellite observations and hydrological model shows that the water loss of global endorheic systems was approximately 106.3 Gt.yr-1

between 2002 and 2016 (J. Wang et al., 2018).

Groundwater resources are particularly crucial for endorheic basins since the water-food-energy nexus highly depends upon groundwater. Soil moisture and deep aquifers are two essential water reserves as they support the terrestrial subsurface ecosystem and water needs of domestic use, agricultural activities, and industries. While soil moisture is valuable for vegetation and crop, deep aquifers can provide less contaminated water for anthropogenic activities, acting as a storage reservoir (Okello et al., 2020). Groundwater resources in arid and semi-arid areas are a strategic water resource for irrigation due to their relatively high reliability compared to surface waters, availability, and ease of use, contributing approximately 43% of global water usage for irrigation (L. Wang et al., 2020). Moreover, adverse impacts of climate change in many endorheic basins can disrupt the fragile water balance because climate change is expected to cause an increase in evaporation and decrease in precipitation, which generally lead to a reduction of the groundwater recharge rate and a rise in groundwater consumption.

There are 25 basins in Turkey, with a variety in size of catchment area and hydrological characteristics including precipitation, evaporation, geologyand land use. Most of the basins in Turkey are open apart from Burdur Lakes, Lake Van, Akarçay, and Konya watersheds (Topcu et al., 2019). Konya Closed Basin (KCB), located in Central Anatolia, is the biggest endorheic basin in Turkey, covering an area of 49,963 km^2 (Figure 1.1). KCB lies within administrative boundaries of Konya, Aksaray, Karaman, Niğde, Isparta, Ankara, Mersin and Antalya.

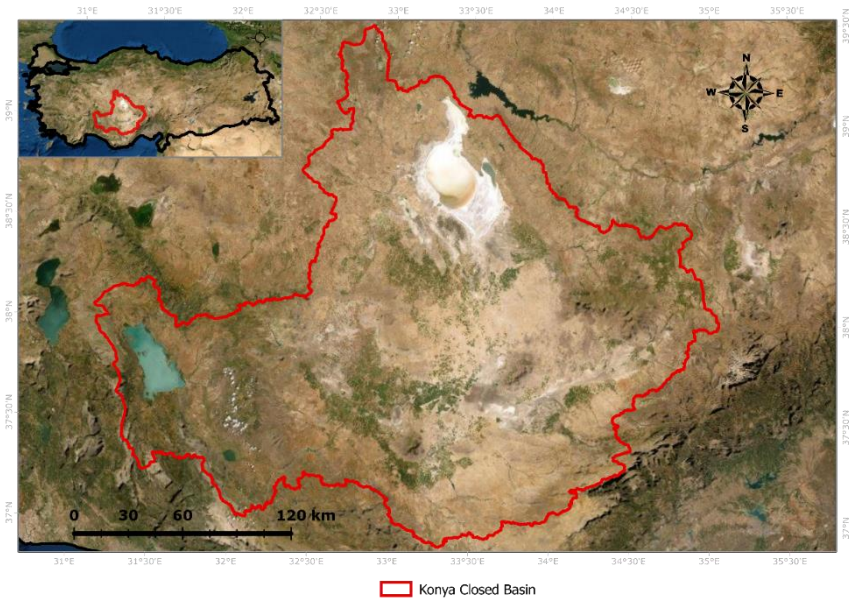

Figure 1.1. Map of Konya Closed Basin.

The Konya basin which occupies 6.4% of the country's land area, has a semi-arid climate. Agriculture is the dominant economic activity within the basin. The area of irrigated agriculture accounts for 865,059 ha, approximately 30% of the total agricultural land (WWF, 2014). Dry agriculture is applied on the rest of the agricultural land (WWF, 2014). The basin's primary water use is irrigation. Annual precipitation in the basin varies between 280 to 350 mm (FAO & GEF, 2019) but the distribution of rainfall over the basin is uneven with irregular temporal and spatial patterns. Historically, surface water resources have been inadequate for crop water requirements. Therefore, many initiatives and projects have been developed to supply the deficiency between need and demand since the 19th century (Muşmal, 2015).

Groundwater extraction in the basin began in the 1960s. At first, wells were drilled by local authorities and non-profit community associations. State Hydraulic Works (DSİ) has ultimate control over groundwater management according to Law on Ground Waters (Law No: 167) which gives permission for the exploration for and extraction of groundwater. Water extraction has increased steadily due to rise in agricultural, domestic, and industrial water demands in addition to insufficient surface water resources. As a result, the number of authorized and unregister wells have skyrocketed in the basin, especially for irrigation purposes. According to a study conducted by the 4th Regional Directorate of State Hydraulic Works in 2007, there was a total of 93,948 wells in the basin, 66,808 of them unregulated. The number of wells in the basin by the end of the 2012 was estimated as more than 100,000 wells (KOP, 2012).

Agricultural activities in the basin consume approximately 88% of water resources of the basin while 61% of irrigation water is supplied from groundwater resources (World Bank Group, 2016). The report of WWF (2014) estimates the annual available surface and groundwater as 1.93 and 2.45 billion m^3 respectively, while annual basin-wide demand is predicted as 2-2.5 and 4-4.5 billion m^3 for surface water and groundwater, respectively. The amount of annual deficiency for water is stated as 1.62-2.62 billion m^3, so water resources in the basin are consumed roughly 50% more than its safe yield according to this study. Rainfall occurs mostly in the winter and spring seasons whereas irrigation water demand is concentrated mostly in the late spring and summer months.

2. LITERATURE REVIEW

2.1. Problem Statement

There are several reasons for excessive utilization of water resources in the Konya Closed Basin. The basin has wide fertile lands which is a major source of agricultural production of the country. Revenues of total agricultural output in Konya were 30 billion Turkish Liras in 2020, ranked first in Turkey, so highlighting the basin's strategic importance for food security of the country (KTO, 2021). Thus, the primary focus of government policies has been on increasing agricultural production and food supply, rather than the protection of water and groundwater availability in the basin. This ultimately led to the persistent over-utilization of this vital resource. A recent study carried out by Yılmaz et al. (2021) examined the increase in agricultural production and a transition of crop pattern in Konya and Karaman. Figure 2.1 from this study shows the increase in irrigation demand, number of livestock and amount of agricultural product. Particularly since 2010, due in large part to high profit and financial support from the state, the agricultural sector in the basin has undergone a transition to more water intensive crops such as corn, potatoes, clover and various kinds of vegetables and fruits in addition to sugar beet farming which had a great impact for the development of the basin since mid-20th century (WWF, 2014). In addition to these reasons, the basin has started to experience negative impacts of climate change such as fluctuations in precipitation, extreme climates, and weather events, and increase in temperature. For instance, it is reported by farmers that dryland farming in the region demands more water than needed in the past due to insufficient precipitation, so irrigation requires additional water utilization and cost since groundwater is usually used to meet the deficiency.

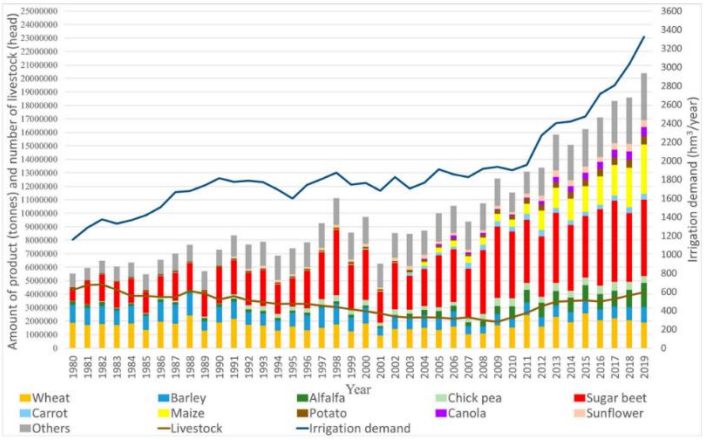

Figure 2.1. Total agricultural products in Konya and Karaman (Yılmaz et al., 2021a).

While the basin has faced several adverse impacts of climate change, these cause two major problems to the groundwater resource. First, fluctuation in precipitation may lead to less amount of aquifer recharge. Second, farmers are faced with the need to utilize more groundwater since the basin receives less precipitation along with higher evaporation and heat waves. Unauthorized wells contribute a tremendous amount of groundwater extraction. Because of the sharp increase in unauthorized wells, it has become very difficult to tackle this problem. As a result, farmers use these unauthorized wells at will, just by paying for the operational and maintenance costs. This has significantly contributed to the over and uncontrolled exploitation of the water resource in the basin. Thus, excessive utilization of groundwater in addition to less amount of percolation and recharge have led to faster groundwater depletion.

As a result of overexploitation of groundwater and the continuous drop of water levels, operational and maintenance costs have created increased economic burden on farmers since utilization of groundwater from deeper levels requires higher power, leading to higher electricity bill, new pipelines, equipment, and eventually drilling of new deeper wells. Furthermore, groundwater depletion may reduce quality of groundwater as the water table approaches the bottom of the aquifer. Saline water in particular can lead to decreased crop yields. All in all, strong understanding of groundwater budget is essential for the sustainable groundwater management in Konya. Although the regional economy relies heavily on the groundwater, there is no documented detailed modelling study to assess groundwater budget, safe amount of extraction yield and recharge as yet. Also, the impact of climate change over groundwater for such a sensitive area is another issue that must be examined.

Another major environmental problem that has risen in the area is the formation of sinkholes in the basin due to the overexploitation of the resources. Several hundred sinkholes have formed in Obruk Plateau, located in northwest of Karapınar, Konya where the soil profile is lacustrine limestone with consolidated non-karst caprocks overlying the limestones (Figure 2.2, a & b). The diameter of these sinkholes can vary between a few meters to tens of meters. Sinkholes have become like small lakes when their depth reaching to the groundwater table. Formation of sinkholes is unpredictable and instantaneous, thus posing a great risk to public safety. Climate variables and overexploitation of groundwater has increase the potential of their formation (Doğan & Yilmaz, 2011).

Excessive groundwater abstraction and climate change also cause a dramatic harm to the ecology of the basin. For example, in recent news from the basin, hundreds of flamingos died in Tuz Lake, located in the north of the basin, since streams draining to it have been depleted for irrigation purposes (Figure 2.2, c). Akşehir Lake, has dried out in 2008 where people are now capable of drive their cars

over the lake (Sener et al., 2009) (Figure 2.2, d).

Overall, it is evident that groundwater is a major component of the economical, agricultural social and environmental aspects of the basin and that excessive over-exploitation of the basin along with potential decrease in precipitation reaching the basin have become a severe and urgent threat to the sustainability of this resource. There is a need to develop novel approaches and take informed decisions involving all stake holders to sustainably utilize this resource.

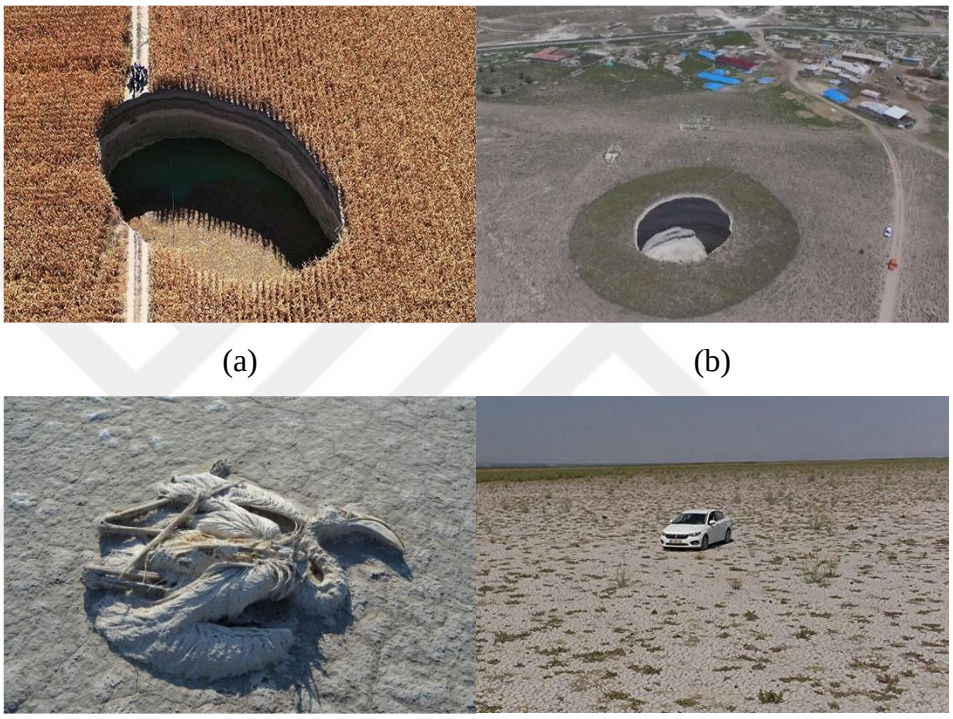

(a) (b)

(c) (d)

Figure 2.2. (a) & (b) Sinkholes in Karapınar, Konya, (c) Dead Flamingos in Tuz Lake, (d) Drought in Akşehir Lake (Diken, 2021; Sputnik, 2021a, 2021b).

2.2. Objectives

KCB which plays a strategic role for the food supply of Turkey relies heavily on groundwater resources to supply the demand for irrigation water. The number of unauthorized wells has led to tremendous increase in the amount of groundwater abstraction which poses a risk for the future of the basin, the livelihood and future security of the region and the country.

The aim of the research is to develop a numerical surface/subsurface hydrological model of the entire KCB that can estimate the net recharge to the basin, the spatial and temporal change in

groundwater levels, and the impacts of climate change on the groundwater resources. Outcomes of the study will help decision makers to develop sustainable water management of the basin and halt the drop in groundwater levels that has been observed in recent years. Outcomes will be shared with local community since there is lack of knowledge about impacts of climate change over the basin.

Specific outcomes of the study are usage of downscaled outputs of General Climate Models (GCMs) and Regional Climate Models (RGMs) for the KCB, assessment impacts of climate change on groundwater resources, and usage of calibrated vadose zone module coupled to the MODFLOW model for the simulation of climate scenario's impacts on groundwater.

2.3. Literature Review

2.3.1. Introduction

The hydrologic interaction between surface water and groundwater occurs by lateral fluxes through the unsaturated zone and vertical fluxes due to infiltration into or extrafiltration from the saturated zone. In the case of fractured rocks or karst, the interactions can also take place through flows in fractures or solution channels. The flow direction is driven by the difference in head between water resources (Sophocleous, 2002). In other words, the flow will be towards the aquifer when surface head is greater than aquifer head. When surface head is less, the flow will be from groundwater towards surface water. The flux path is dynamic which means that it can change both spatially and temporally (Brunner et al., 2004; Keery et al., 2007). While groundwater is excessively withdrawn in part of the basin, other part may rely less on groundwater abstraction. Moreover, the water demand can change due to the change in population, cropping pattern or pattern of industrial growth. In brief, the management of water resources must be carried out with an integrated approach. Estimation of groundwater recharge is critical for the management of water resources in arid and semi-arid region (Kinzelbach et al., 2002).

Groundwater models are important tools for simulating the amount of groundwater recharge and abstraction, impacts of land cover and climate change, and transport of pollution to develop sustainable watershed management. Though surface water-groundwater interaction is crucial to understanding the watershed's hydrological cycle, surface water and groundwater traditionally were considered as two separate systems. Groundwater models can be categorized as single and coupled models. The single numerical model focuses either on water flow at the surface and through the vadose zone by simplifying groundwater flow such as HYDRUS (Šimůnek et al., 2016) and SWAT

(Arnold et al., 1998) or groundwater by simplifying surface water hydrology such as MODFLOW (McDonald & Harbaugh, 1988). However, this type of model may in some instance not give accurate simulation result since the model neglects the interaction between surface water and groundwater. Hence, coupled model, which simulates surface water and groundwater flow, has emerged recently (Wang & Chen, 2021). MIKE SHE (DHI, 2023), HYDRUS-3D (Šimůnek et al., 2008), UZF1 (Unsaturated Zone Flow) Package for MODFLOW-2005 (Niswonger et al., 2006) and HYDRUS Package for MODFLOW-2000 (Twarakavi et al., 2008) are the most recent examples of surface-water and groundwater integrated models (Kampf & Burges, 2007; Twarakavi et al., 2008). MIKE SHE and HYDRUS-3D are not publicly available (Warsta et al., 2013). UZF1-MODFLOW and HYDRUS-MODFLOW are publicly available models, both of which provide the source code (Niswonger et al., 2006; Twarakavi et al., 2008). Both models simulate groundwater flow with MODFLOW which utilizes three-dimensional groundwater flow equation. Both are modular hydrological models, allowing the user to include the module necessary for the problem at hand.

2.3.2. Hydrological Studies

This section reviews some numerical modeling studies to assess the groundwater studies of the KCB. Caló et al. (2017) pointed out that unsustainable agricultural practices and non-monitored irrigation lead to groundwater depletion for the Konya basin. The authors underlined that irrigation fields had increase around 120 km^2 between 2000 and 2012 according to land use change analysis. Demir et al. (2021) found that groundwater level data shows significantly decreasing trend in the basin. From the results of the study, it can be concluded that the decline in groundwater level disturbs the balance between soil stress and water pressure. The imbalance causes deformation of soil and collapse formation in the region. Yılmaz et al. (2021) reported that significant increase in agricultural production and transition to water incentive crops in the basin led to significant groundwater abstraction to support agricultural water demand in the basin. The authors showed that change in land use and groundwater abstraction to maintain the growth in agricultural production in addition to climate change led to dramatic decrease in the surface area of lakes within the basin.

The Report of WWF (2010) focused on the groundwater budget estimation for the basin. According to the report, the amount of groundwater abstraction is greater than the percolation amount. Allowable water consumption consisting of groundwater and surface water was simulated for the year of 2009, 2015, 2030, 2050 and 2057. ECHAM5 and RegCM3 models under SRES A2 scenario were utilized for the simulation of temperature, precipitation, evaporation and runoff. The report claimed the current rate of water consumption as 4228.5 hm^3/year. However, allowable water consumptions

according to simulation results are 2575.3, 1873.6, 2134.9, 1753 and 1117.9 hm^3/year for 2009, 2015, 2030, 2050 and 2057 respectively. Thus, consumption rate is far higher than the allowable amount according to the study.

The study also includes simulation with four different scenarios: business as usual, less water intensive cropping pattern without changing irrigation techniques, transition to pressurized irrigation systems without changing cropping pattern and transition to both less water intensive cropping pattern and pressurized irrigation systems. The transition in cropping pattern and transition in irrigation technique scenarios decreased the water need by 25% respectively. The other scenario with less water intensive cropping pattern and pressurized irrigation systems decreased water need by 43%. Although the study has focused on groundwater budget in Konya, the model or methodology have not been explained clearly. According to the report, hydrological model was built by experts of Danish Hydraulic Institute. However, their work has not been described in detail.

Naing (2011) developed a MODFLOW-based regional model for the basin to estimate groundwater fluxes. It was reported however that the model failed in transient run due to the high abstraction rates in Çumra and Karapınar region. On the other hand, steady state simulation of the model shows the total recharge to groundwater, estimated as 2.2 hm^3/day. Özyurt et al. (2017) studied the impact of groundwater on land subsidence in the basin using MODFLOW-SUB Package. Surucu (2018) investigated the impact of climate change and different climate scenarios on water supply resources (Surface Water – Groundwater) for the basin based on IWFM (Integrated Water Flow Model), using the Finite Element numerical method.

A number of groundwater modelling studies were performed for various regions of Turkey. Ersoy & Gültekin (2008) developed hydrological model based on the MODFLOW-RIVER Package to assist groundwater management practices for Gümüşhacıköy Plane in the northern part of Turkey. The aim of the study of Rukundo & Doğan (2019) was to estimate the amount of recharge and help groundwater resources management. They also developed their model on mGROWA for the Ergene Basin (river catchment) in north-west part of Turkey. Tonkul et al. (2019) and Ertürk et al. (2014) developed a HYDRUS 1-D regional model for Gediz Basin and a SWAT-based regional model for Köyceğiz-Dalyan Coastal Watershed to estimate net recharge. Mansour et al. (2017) simulated sea water intrusion in a coastal aquifer of Karaburun Peninsula, located in west part of Turkey, based on SEAWAT (MODFLOW-MT3DMS) model.

A number of coupled surface subsurface models have been developed for various regions of the world. These studies are briefly reviewed below because of their relevance to the current study. Cao et al. (2016) investigated the rapid groundwater depletion in the North China Plain (NCP) by developing an integrated soil water balance (SWB) and UZF-MODFLOW coupled model between 1993 and 2008. The study showed that aquifer thickness can influence the magnitude of recharge, unsaturated storage and lag time between percolation and recharge. Thick unsaturated zone delays recharge, so unsaturated storage may increase while groundwater recharge may be reduced significantly. Nazarieh et al. (2018) developed UZF-MODFLOW coupled model for simulating vadose and saturated zones for Neishaboor Plain in Iran between 2000 and 2012. The calibrated model was utilized to assess deep percolation through the vadose zone and estimate its impact on recharge dynamics. According to study, vadose zone has a significant impact on recharge dynamics.

Another study carried out by Lekula & Lubczynski (2019) developed a UZF-MODFLOW coupled regional model that uses various remote sensing data to estimate water balance dynamics for evaluating groundwater resources in Central Kalahari Basin, South Africa. According to the study, rainfall and subsurface evapotranspiration are driving forces for water flux in semi-arid aquifer system. Also, the groundwater only can be considered as a sustainable resource during wet years in semi-arid aquifer systems. The study also reported that Remote Sensing data can provide data with better spatial and temporal resolution for integrated hydrological models. Mali et al. (2021) estimated the amount of recharge based on coupled HYDRUS 1-D and MODFLOW regional model for the unconfined aquifers in the Eastern Indo-Gangetic Plains of India. The aim of study was to investigate the impact of cropping pattern on groundwater level. The study also showed that groundwater levels will decline if the excessive use of groundwater due to irrigation is not compensated. The authors underlined that increasing demand to produce more food for growing population should be planned on a balanced approach.

2.3.3. Studies on Climate Change

Assessment of impacts of climate change and anthropogenic activities on groundwater is crucial since these factors may alter the amount of evaporation and soil moisture content, the frequency of precipitation and surface runoff, and groundwater abstraction. Numerical modelling tools have been used for the simulation of complex environmental systems for many decades (Kumar, 2016). For the estimation of the effects of climate change in the KCB, numerical models will be useful in the study.

Global Circulation Models (GCMs) simulate current global climate and future climate projections. However, GCMs are not suitable to use directly in many hydrological models since the resolution varies between 70 to 250 km which is much coarser than the resolution of typical hydrological models (Iles et al., 2020; IPCC, 2008). Moreover, these results must be corrected for bias using local data. Therefore, downscaling with Regional Climate Models (RGMs) have been developed to get finer resolutions that overcomes disproportion of the grid scale. For example, Bozkurt et al. (2011) evaluated three GCMs, ECHAM5, CCSM3 and HadCM3, using RegCM3 as regional climate model to downscale winter and summer climate data for the East Mediterranean and Black Sea region. It was reported that ECHAM5 and HADCM3 performed well for prediction of temperature and precipitation in summer whereas simulation result of CCSM3 gave dryer and warmer condition than observed conditions.

RCP scenarios described in the Fifth Assessment Report (AR5) of the Intergovernmental Panel on Climate Change (IPCC) published in 2014. RCP scenarios includes four pathway: RCP2.6 (strict mitigation scenario), RCP4.5 & RCP6 (intermediate scenarios) and RCP8.5 (high GHG emission scenario) (IPCC, 2014). In this study, RCP 4.5 and RCP 8.5 scenarios are selected since many parts of the earth have already experienced over 1.5 ^{o}C warming increase in at least one season (M. R. Allen et al., 2022). After calibrating the KCB model with historical data between 2000 and 2022, the model will be extended between 2023-2040 to assess the future groundwater level until the end of the century.

2.3.4. Model Selection

In this study two codes will be considered for simulating the water budget for the basin: Hydrus package coupled to the MODFLOW and UZF1 module coupled to MODFLOW. The HYDRUS Package for MODFLOW is mainly composed of two sub-models: HYDRUS and MODFLOW-2000 that interact with each other in time and space (Hyeyoung et al., 2007; Twarakavi et al., 2008). The HYDRUS sub-model is based on the HYDRUS-1D software which simulates one-dimensional water flows in vadose zone by utilizing Richards' equation for the unsaturated zone flow (J. Šimůnek, M. Šejna, H. Saito, M. Sakai, 2008). On the other hand, MODFLOW is a three-dimensional modular finite-difference hydrologic model and considered as an international standard for simulating groundwater flow. HYDRUS-MODFLOW does not provide any graphical user interface (GUI). Therefore, the modeler needs to prepare inputs externally using different programs or programming languages. However, input files should be prepared according to required format.

UZF1 (Unsaturated Zone Flow) Package is another model developed by the USGS that simulates water flow through the vadose zone. UZF1 couples with the saturated flow model, MODFLOW. Unlike HYDRUS Package for MODFLOW, UZF1 package simulates flow in vadose zone based on the kinematic wave equation, a simplified version of Richards' equation (Niswonger et al., 2006; Twarakavi et al., 2008). Hydraulic properties, climatic conditions and depth to the groundwater table are important for the application of the kinematic wave equation. Also, kinematic wave equation limits the model application since unsaturated zone is assumed as homogenous (Hou et al., 2020; Twarakavi et al., 2008). Similar to the HYDRUS Package, groundwater flow is simulated by MODFLOW. UZF1 package can simulate surface runoff, evapotranspiration, infiltration, vadose flow and groundwater flow as depicted in Figure 2.3 (Niswonger et al., 2006).

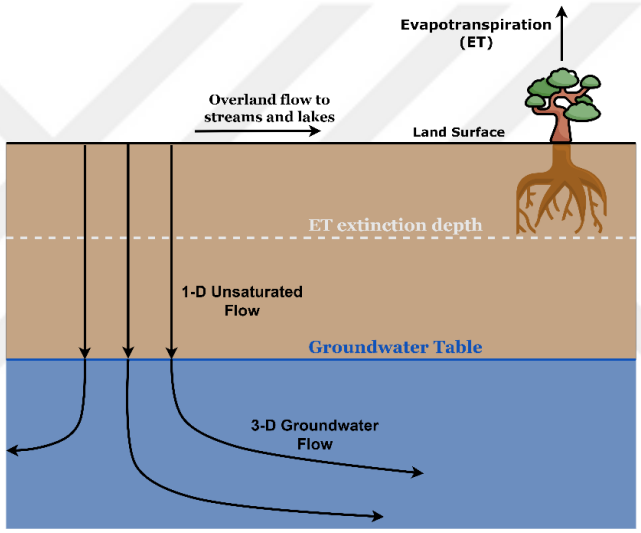

Figure 2.3. Coupled 1-D unsaturated zone flow and 3-D groundwater flow (modified from Niswonger et al., 2006).

Although HYDRUS-MODFLOW was suggested for the larger spatial domains thanks to its less computational demands, the program does not simulate properly especially for the initial time steps according to couple of trial run for the case (Twarakavi et al., 2008). Therefore, UZF1 package coupled to MODFLOW is chosen for the groundwater simulation.

UZF1 package assumes that water movement occurs only in the vertical direction and solves the vertical flow using kinematic waves approximation. The approximation is the simplification of Richards' equation, which is as follows (Niswonger et al., 2006):

$$\frac{\partial \boldsymbol{\theta}}{\partial \boldsymbol{t}} = \frac{\partial \boldsymbol{q}}{\partial \boldsymbol{z}} - \boldsymbol{i} = \frac{\partial}{\partial \boldsymbol{z}}\left[\boldsymbol{D}(\boldsymbol{\theta})\frac{\partial \boldsymbol{\theta}}{\partial \boldsymbol{z}} - \boldsymbol{K}(\boldsymbol{\theta})\right] - \boldsymbol{i} \quad (2.1)$$

where:

θ the volumetric water content (dimensionless),

q the water flux ($L^3T^{-1}L^{-2}$),

t time (T),

z the vertical coordinate (L),

i the ET rate per unit depth ($LT^{-1}L^{-1}$)

D(θ) the hydraulic diffusivity (LT^{-1}),

K(θ) the unsaturated hydraulic conductivity (LT^{-1}).

Equation 2.1 is simplified by removing the diffusive term when assuming that vertical flow is driven only by gravity force. Vertical flux with the assumption of ignoring diffusive term yields the following equation:

$$\mathbf{q} = -\boldsymbol{K}(\boldsymbol{\theta}) \quad (2.2)$$

The flux is negative since the flow is downward in Equation 2.2. Substitution of assumed flux equation in Equation 2.1 shows that the flow is downward in the vertical direction yielding the following equation:

$$\frac{\partial \boldsymbol{\theta}}{\partial \boldsymbol{t}} + \frac{\partial \boldsymbol{K}(\boldsymbol{\theta})}{\partial \boldsymbol{z}} + \boldsymbol{i} = \mathbf{0} \quad (2.3)$$

The Brooks-Corey unsaturated hydraulic conductivity model is used to evaluate rate of change of unsaturated hydraulic conductivity as a function of water content with respect to volumetric water content ($\partial K(\theta)/\partial\theta$). Equation 2.4 shows the mathematical formulation of the Brooks-Corey model.

For the evaluation of the rate of change of unsaturated hydraulic conductivity as a function of water content with respect to volumetric water content ($\partial K(\theta)/\partial\theta$), Brooks-Corey model for unsaturated hydraulic conductivity can be employed. The mathematical representation of the Brooks-Corey model is illustrated by Equation 2.4.

$$\boldsymbol{K(\theta) = K_s \left[\frac{\theta - \theta_r}{\theta_s - \theta_r}\right]^{\varepsilon}} \quad (2.4)$$

where:

K_s the saturated hydraulic conductivity,

θ_r the residual water content,

θ_s the saturated water content,

ε the Brooks-Corey exponent.

MODFLOW uses three-dimensional incompressible groundwater flow through porous earth material for simulation. Equation 2.5 describes the mathematical formulation of three-dimensional groundwater flow process. It can be simulated under steady or transient flow in any condition of aquifer systems such as unconfined, confined or combination of them.

$$\boldsymbol{\frac{\partial}{\partial x}\left(K_{xx}\frac{\partial h}{\partial x}\right) + \frac{\partial}{\partial y}\left(K_{yy}\frac{\partial h}{\partial y}\right) + \frac{\partial}{\partial z}\left(K_{zz}\frac{\partial h}{\partial z}\right) + W = S_s\frac{\partial h}{\partial t}} \quad (2.5)$$

where:

K_{xx}, K_{yy} *and* K_{zz} hydraulic conductivities along x, y and z coordinate axis (LT^{-1}),

h the potentiometric head (L),

t time (T),

W a volumetric flux per unit volume (T^{-1}),

S_s the is the specific storage of the porous material (L^{-1}).

3. STUDY AREA

3.1. Location of Study Area

There are 25 basins in Turkey, with a variety in size of catchment area and hydrological characteristics such as precipitation, evaporation, and land use. Most of the basins in Turkey are open apart from Burdur Lakes, Lake Van, Akarçay, and Konya watersheds (Topcu et al., 2019). Konya Closed Basin (KCB), located in Central Anatolia, is the biggest endorheic basin and fourth largest basin in Turkey. The basin covers 49,963 km^2, which is geographically located between 31^o 7’ 29.01’’ E - 35^o 3’ 28.94’’ E and 36^o 53’ 45.17’’ N - 39^o 29’ 10.33’’ N. The total land area of Turkey is 780,350 km^2, so the basin comprises 6.4% of the total land.

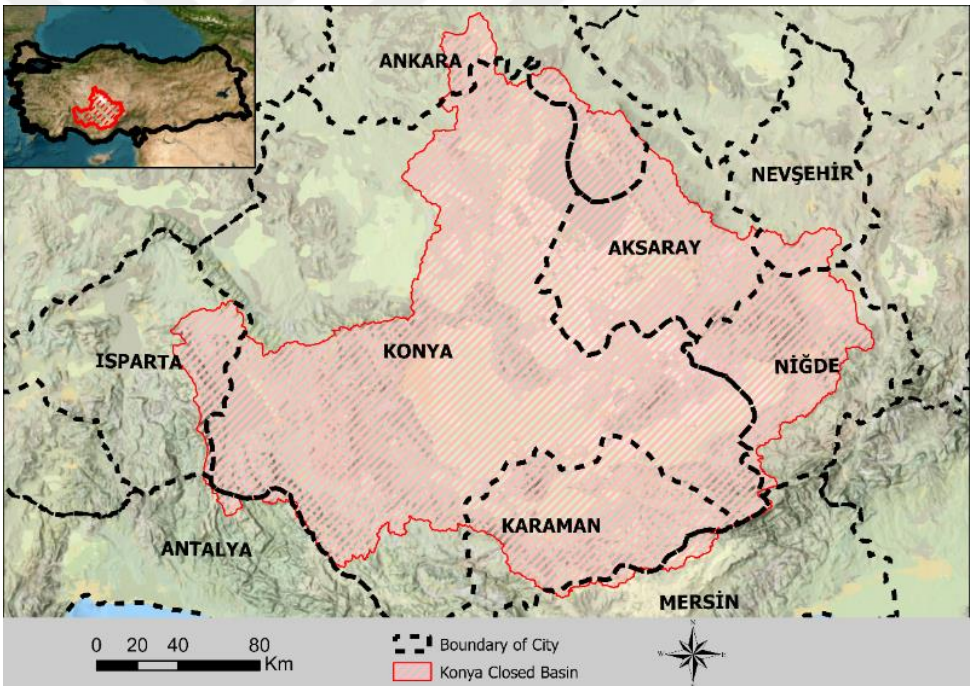

Figure 3.1. Map of cities in Konya Closed Basin.

Figure 3.1 shows the map of cities in the basin. The basin lies in administrative boundaries of Konya, Aksaray, Karaman, Niğde, Ankara, Isparta, Nevşehir, Mersin and Antalya. Table 3.1 indicates the land area of each city falling within the basin and the percentage of overlaying area to total city area. The data in indicates that Konya province occupies the largest land area in the basin, comprising more than half of the entire basin area.

Table 3.1. Land Area of City Overlaying the Basin and Percentage of Overlaying Area to Total City Area.

City	Overlaying Area (Km^2)	Percentage (%)
Konya	28453.5	69.8
Aksaray	6348.3	82.9
Karaman	5799.2	66.9
Niğde	4481.7	62.0
Ankara	2282.3	8.9
Isparta	1334.8	14.9
Nevşehir	657.0	12.0
Mersin	406.3	2.5
Antalya	200.1	1.0

3.2. Topography

Digital Elevation Model (DEM) with 100-meter resolution in DTED1 format is acquired form General Directorate of Mapping (HGM). Figure 3.2 shows the elevation in the basin which varies from 900 meters near Lake Tuz to 3400 meters.

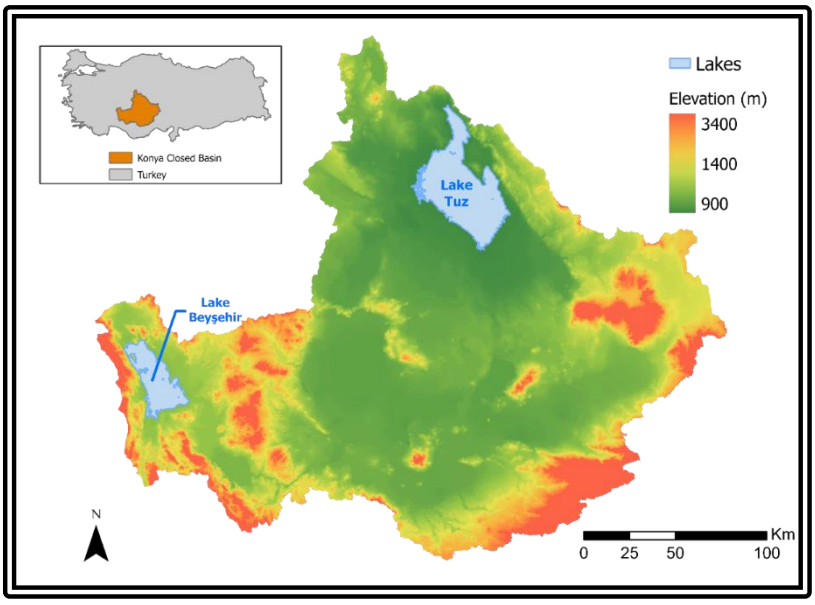

Figure 3.2. Elevation map of Konya Closed Basin.

The highest elevation ranges are located in the southern part of the basin where Toros mountains located. The lowest elevation is in the northern part of the region, around Lake Tuz. The central part of the region is flat, with a general surface slope towards Lake Tuz. Figure 3.3 shows the surface

slope direction that is created by using eight directions pour point model for 10 km by 10 km resolution with DEM data.

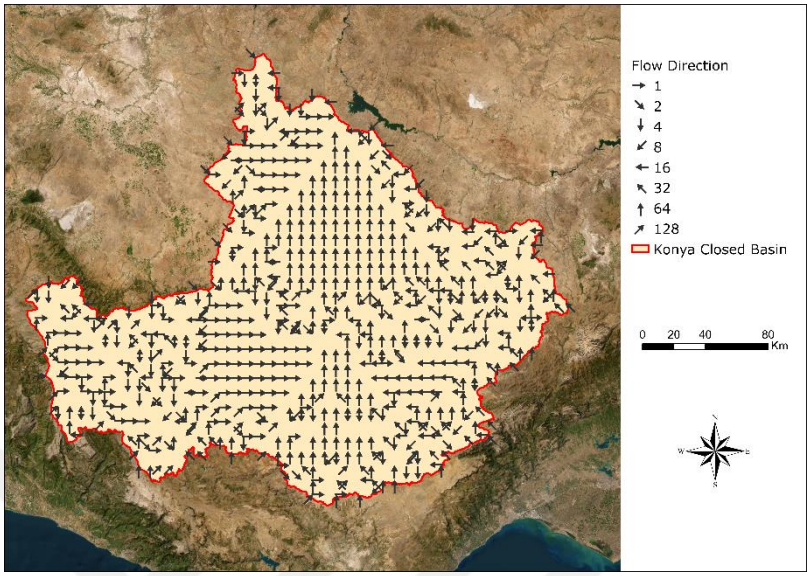

Figure 3.3. Flow directions based on Eight Direction Pour Point Model.

3.3. Climate

Understanding the state of climatic conditions within basin can provide valuable information about availability and distribution of water resources. The aridity index (AI) is one of the most relevant indicators which provides measures of the aridity or humidity of a particular region. It is the ratio of precipitation (P) to reference evapotranspiration (ET_0) (Middleton & Thomas, 1992; Spinoni et al., 2015; Zomer et al., 2022). Aridity index is unitless. Equation 3.1 shows the calculation of aridity index. Table 3.2 shows the classification of the climate classes according to the aridity index.

$$\boldsymbol{AI = \frac{P}{ET_0}} \tag{3.1}$$

AI aridity index,

P mean annual precipitation (mm),

ET_0 mean annual reference evapotranspiration (mm).

Table 3.2. Climatic Condition According to Aridity Index (Middleton & Thomas, 1992).

Aridity Index Value	Climate Class
<0.03	Hyper Arid
0.03–0.2	Arid
0.2–0.5	Semi-Arid
0.5–0.65	Dry sub-humid
>0.65	Humid

In Google Earth Engine (GEE), Aridity Index (AI) is calculated using mean annual precipitation (P) and mean annual reference evapotranspiration (ET0). These values were obtained from TerraClimate monthly climatic dataset available on GEE for the period between 2000 and 2022 (Abatzoglou et al., 2018). Figure 3.4 shows annual mean of monthly precipitation and reference evapotranspiration over the basin. Figure 3.5 shows the calculated spatially mean aridity index over the basin. According to graph, the basin has semi-arid characteristic mostly. For the period between 2009 and 2012, the basin showed dry sub-humid characteristics.

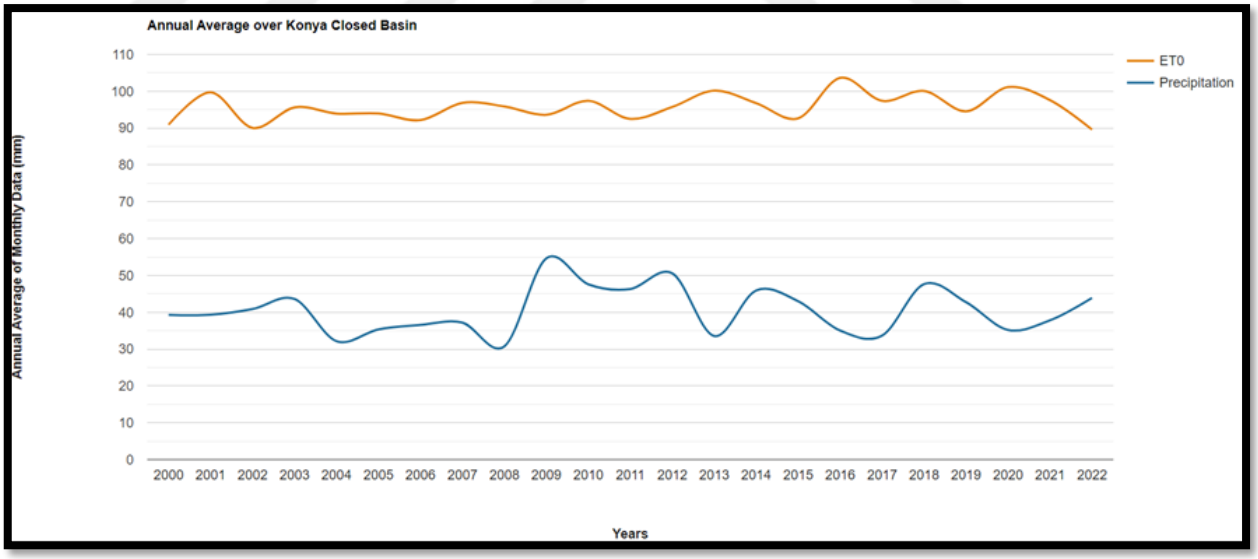

Figure 3.4. Annual mean of monthly precipitation (mm) and reference evapotranspiration (mm) over the basin.

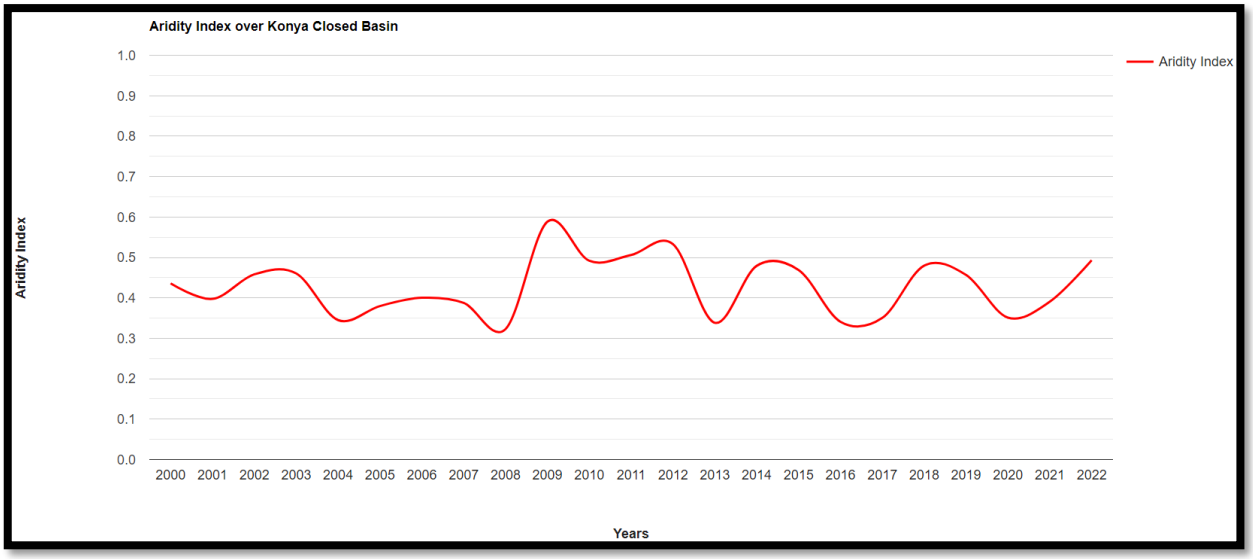

Figure 3.5. Mean aridity index over the basin.

Aridity index for the basin indicates the basin is in water-limited environments. In these environments, the water is limited due to the fact that annual precipitation is generally lower than the annual potential evapotranspiration. This leads to a ratio of P (annual precipitation) to Ep (annual potential evapotranspiration) ranging from approximately 0.03 to 0.75, indicating a significant deficit in water availability. Furthermore, the extreme temporal variability in precipitation patterns often results in prolonged periods with minimal to no rainfall, exacerbating the water limitations in these regions (Newman et al., 2006).

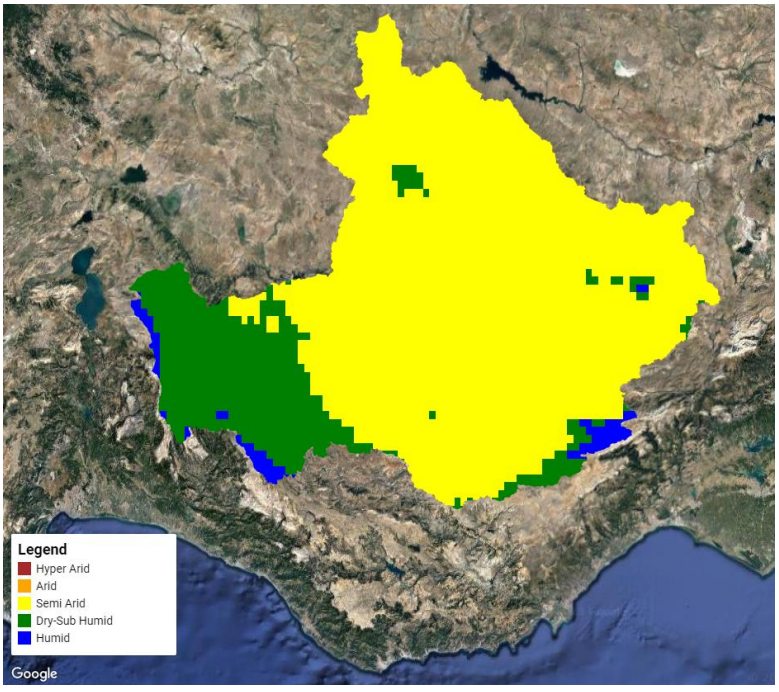

Figure 3.6. Mean aridity index over the basin between 2000 and 2022.

The spatial distribution of aridity index is also important to identify aridity of a particular region. Figure 3.6 shows the temporal mean of aridity map between 2000 and 2022 over the basin. Konya Closed Basin has dry-sub humid climate in southwestern part (Beyşehir-Kaşaklı Subbasin) and semi-arid climate on the rest of the basin. As mentioned earlier, southern edges of the basin where Toros mountains are located, shows humid characteristics due to high altitude. Figure 3.7 shows the percentage for each climatic category over the basin for the same period.

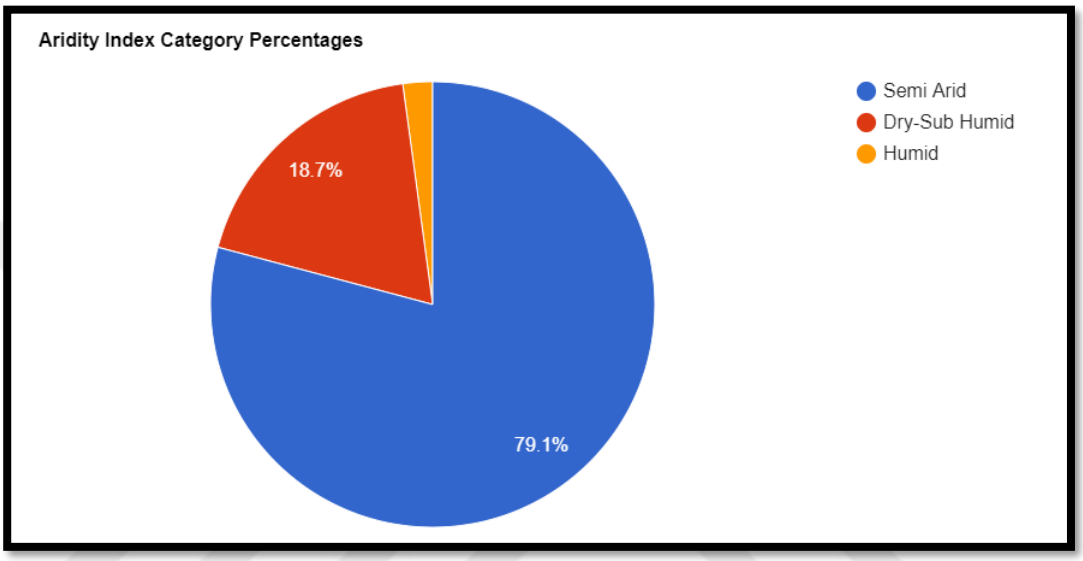

Figure 3.7. Climate classification for Konya Closed Basin.

As noted above, the aridity index for the basin indicates that it predominantly falls within the semi-arid region, signifying a water limited environment. This implies that the basin experiences little precipitation and is characterized by a potential scarcity of water resources. The aridity index performs as important indicator for evaluating the overall water availability, potential water management challenges and water use allocation in the region. Developing better understanding of the basin's water limitation is crucial for implementing sustainable water management strategies and mitigation of water scarcity in the area.

Following the climatic investigation utilizing publicly available databases, meteorological data was requested from Turkish State Meteorological Service (TSMS) to enhance the accuracy of analysis. TSMS provided daily mean temperature and daily accumulated precipitation data for a total of eighteen meteorological stations located within or adjacent to the basin. The geographical distribution of these stations is depicted in Figure 3.8, showing their locations within and outside the basin boundary. Notably, ten of these stations are situated inside the basin boundary while the remaining stations are in various areas surrounding the basin.

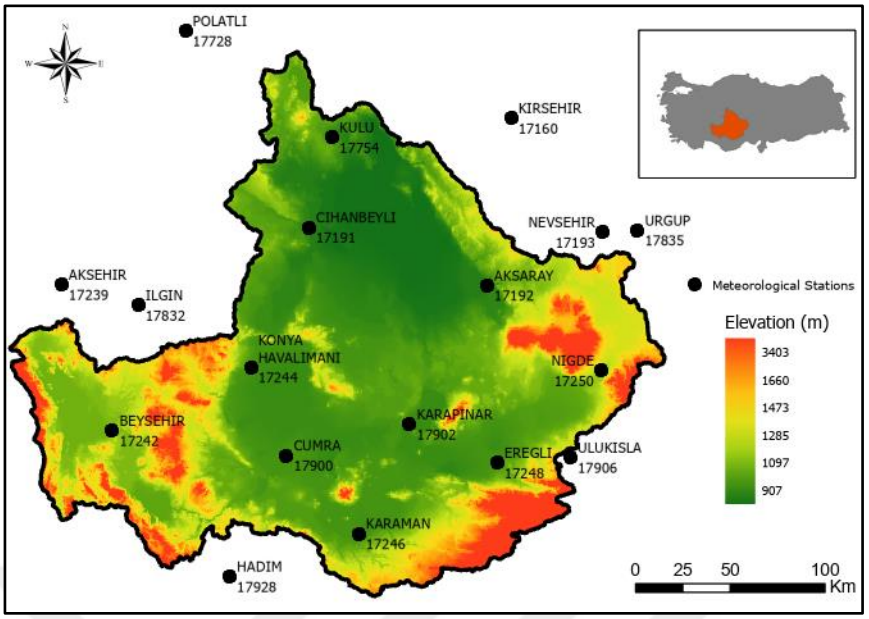

Figure 3.8. Location of meteorological stations.

The annual cumulative precipitation in the basin is calculated as 343.23 mm for the period between 1980 and 2020 by using Simple Kriging methodology. Figure 3.9 displays the monthly cumulative mean precipitation over the period between 1980 and 2020 in the basin. The analysis reveals that the highest levels of precipitation occur from October to May. On the other hand, there is no or limited precipitation during summer. Moreover, the annual mean temperature during the 1980-2020 period was recorded as 11.38 Celsius. Figure 3.10 shows the mean temperature for each month between 1980 and 2020.

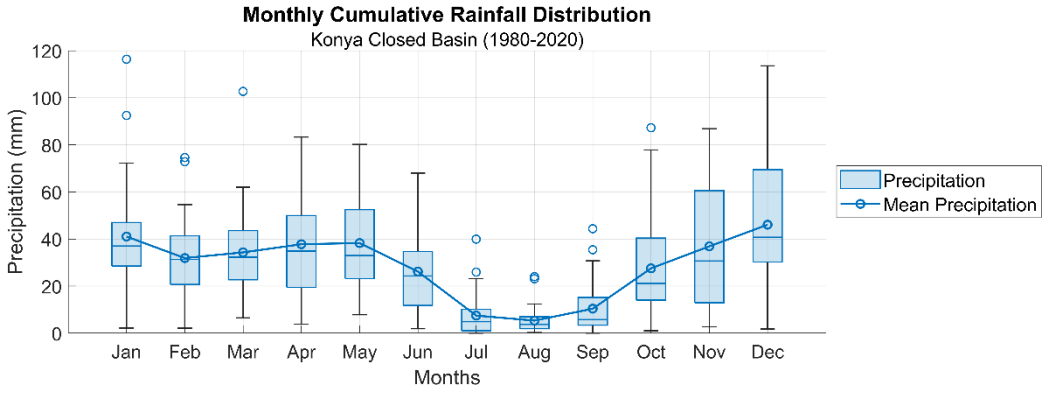

Figure 3.9. Monthly cumulative precipitation for Konya Closed Basin.

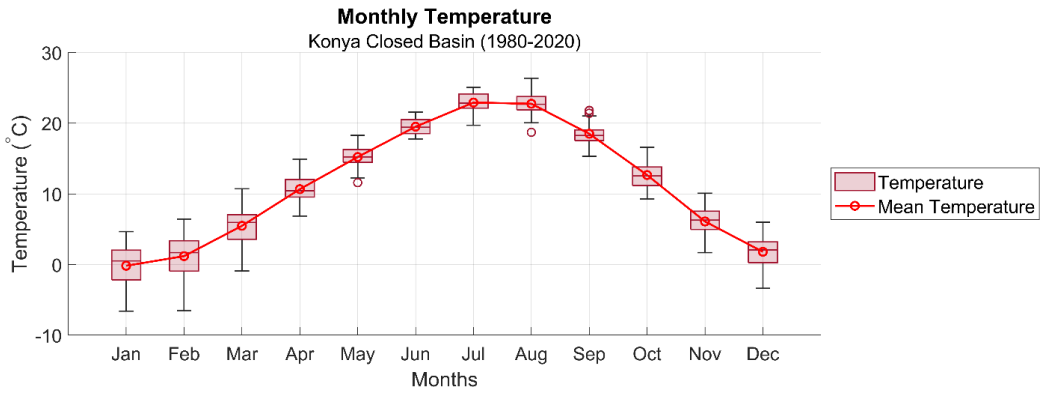

Figure 3.10. Monthly mean temperature for Konya Closed Basin.

Future climate data is one of the input data for the projection of groundwater levels, is provided by University of Parma as part of the InTheMED project (https://inthemedprima.com/), supported by the PRIMA program. Todaro et al. (2022) has analyzed 17 GCM-RCM climate projections under two representative pathways (RCP4.5 and RCP8.5) for the basin, based on the data from EURO-CORDEX database. They utilized temperature and precipitation data on a daily scale. Grid based model results are downscaled to meteorological stations in the Konya basin by using inverse squared distance method with closest nine grid points. Then, bias correction is applied for the period between 1976 and 2005 (control period) by using distribution transfer method. Table 3.3 shows the name of the global climate models considered in paper.

Table 3.3. GCM-RCM models for the study from EURO-CORDEX.

	GCM		**RCM**	
	Institute	**Model**	**Institute**	**Model**
1	CNRM-	CNRM- CM5	CLMcom	CCLM4-8-17
2	CNRM-	CNRM- CM5	SMHI	RCA4
3	MOHC	HadGEM2-ES	DMI	HIRHAM5
4	NCC	NorESM1-M	DMI	HIRHAM5
5	ICHEC	EC-EARTH	KNMI	RACMO22E
6	ICHEC	EC-EARTH	SMHI	RCA4
7	ICHEC	EC-EARTH	CLMcom	CCLM4-8-17
8	ICHEC	EC-EARTH	DMI	HIRHAM5
9	IPSL	IPSL-CM5A-	IPSL	WRF381P
10	IPSL	IPSL-CM5A-	SMHI	RCA4
11	IPSL	IPSL-CM5A-	IPSL-INERIS	WRF331F
12	CNRM-	CNRM- CM5	KNMI	RACMO22E
13	MOHC	HadGEM2-ES	CLMcom	CCLM4-8-17
14	MOHC	HadGEM2-ES	KNMI	RACMO22E
15	MOHC	HadGEM2-ES	SMHI	RCA4
16	MPI-M	MPI-ESM-LR	CLMcom	CCLM4-8-17
17	MPI-M	MPI-ESM-LR	SMHI	RCA4

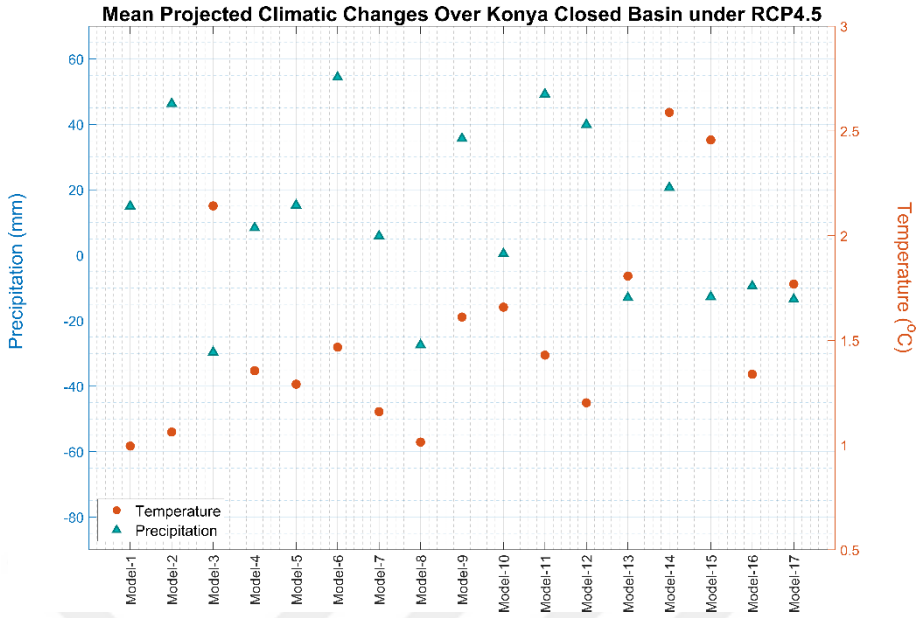

Figure 3.11. Mean projected changes for precipitation and temperature among RCMs during the period of 2023-2040 relative to 1976-2005 under pathway of RCP4.5.

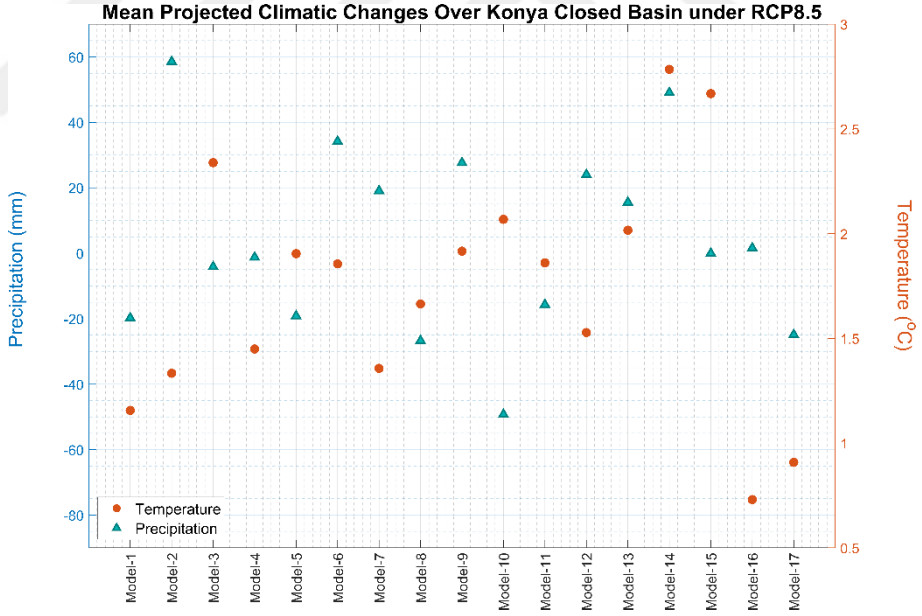

Figure 3.12. Mean projected changes for precipitation and temperature among RCMs during the period of 2023-2040 relative to 1976-2005 under pathway of RCP8.5.

Although these climate models are projected until the end of the century, the data between 2023 and 2040 only were used in groundwater flow model developed as part of this thesis. Figure 3.11 and Figure 3.12 shows the annual mean temperature difference and annual cumulative precipitation difference between 2023 and 2040 with respect to the level in reference period of 1976 and 2005 for

both climatic pathways. According to the RCP4.5 climatic pathway, the annual mean temperature deviation between the years 2023 and 2040, relative to the reference period of 1976-2005, is calculated to be 1.55 Celsius. Additionally, the annual cumulative precipitation increase during the same period is projected to be 10.91 mm. Similarly, under the RCP8.5 climatic pathway, the annual mean temperature deviation between 2023 and 2040, relative to the reference period of 1976-2005, is expected to be 1.74 Celsius. Furthermore, the annual cumulative precipitation increase during this timeframe is projected to be 4.05 mm.

3.4. Land Use

Land use in the basin shows a diverse range of anthropogenic activities. Agriculture plays a significant role in the region, with high cultivation of cereals, corn, and sugar beet. The fertile soils support a thriving agricultural sector. Livestock farming with sheep, cattle, and poultry is another significant land use component, contributing to the region's economy. Apart from agriculture, the basin is characterized by industrial zones and urban areas, reflecting the growth and development of commercial and residential sectors. The land use dynamics in the Konya Closed Basin highlights the complex socio-economic and ecological aspects of the region. Figure 3.13 presents the land use classification of the Konya Closed Basin based on the Corine database for the years 2000, 2006, 2012, and 2018.

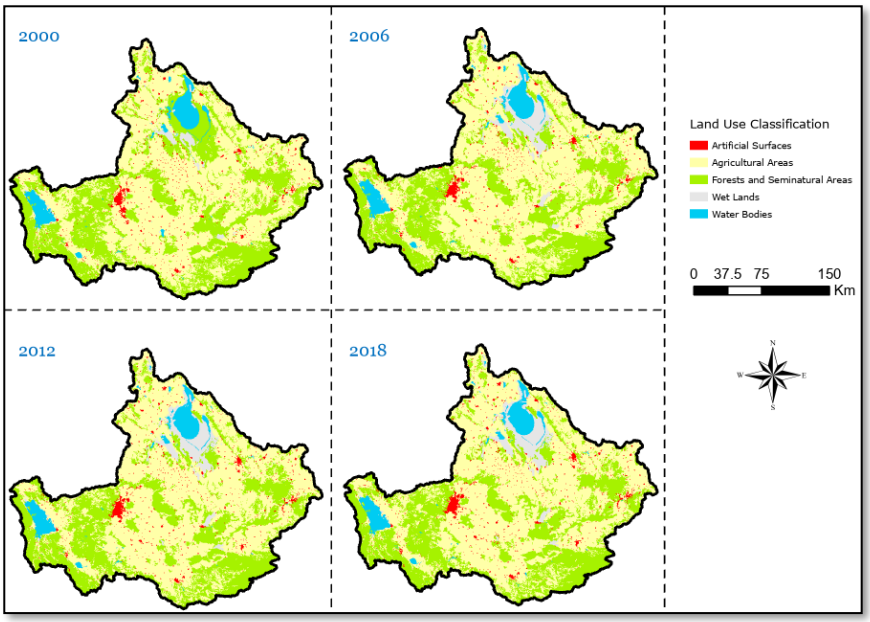

Figure 3.13. Land use classification in the basin.

3.5. Hydrology

The basin experiences seasonal variations in precipitation, with a limited precipitation during summer months. The semi-arid climate and low levels of precipitation make the basin a water-limited environment, causing challenges for water availability. The basin is home to two significant lakes: Lake Tuz and Lake Beyşehir. Figure 3.2 shows their location inside the basin. Lake Tuz is the second largest lake in Turkey and one of the largest hypersaline lakes in the world (Aydoğdu et al., 2014). Lake Tuz encompasses an expansive area of 1725.9 km^2 according to SRTM Water Body Data. Lake Beyşehir is the largest freshwater lake in Turkey, situated in western part of the basin. The lake has served as upstream storage in the basin, supplying the irrigation and domestic water demand for the basin (Bucak et al., 2018; Croitoru et al., 2016; Yılmaz et al., 2021b). The lake has a surface area of 641.5 km^2 according to SRTM Water Body Data. The water from Lake Beyşehir follows a hydrological pathway, starting with the Çarşamba stream, which carries the water to the Suğla Reservoir. From there, the water continues to center of the basin and eventually the Lake Salt (Bucak et al., 2018). The hydrological system of the Konya Closed Basin does not have a dominant stream.

The aquifer system underlying the basin is the primary water storage and transmission system. The groundwater is more reliable than surface water for the basin since the basin is a water-limited environment with high evaporation potential. Groundwater plays a vital role for meeting the water demand in the basin. However, unsustainable use of groundwater has led to decrease in groundwater levels. As mentioned earlier, transition of crop pattern to more water demanding crops in summer such as maize is one of the reasons for the decline. Due to the deficiency between the water demand and supply, number of the authorized and unregister wells have increased dramatically. Land subsidence caused by the declining groundwater levels is one of the main drivers for the formation of sinkholes (Özyurt et al., 2017).

3.6. Hydrogeology

The simplified hydrogeological cross-section of the basin, shown in Figure 3.14, includes Tauride-Anatolide Block (TAB), Sakarya Zone Block (SZB), Neogene(N) and Paleogene(P). The basin mainly comprises two aquifer systems: productive freshwater aquifers at the top (Neogene) and poor deep aquifers (TAB) with saline water. Surface water and groundwater flowing from the Taurus Mountains through Palezoic-Mesozoic karstic carbonates of TAB lithospheric plate feed mainly both aquifer systems. The general groundwater flow in the region is from Taurus Mountains at south towards to Lake Tuz in the north (Bayari, Ozyurt, et al., 2009; Bayari, Pekkan, et al., 2009; Ozyurt &

Bayari, 2018).

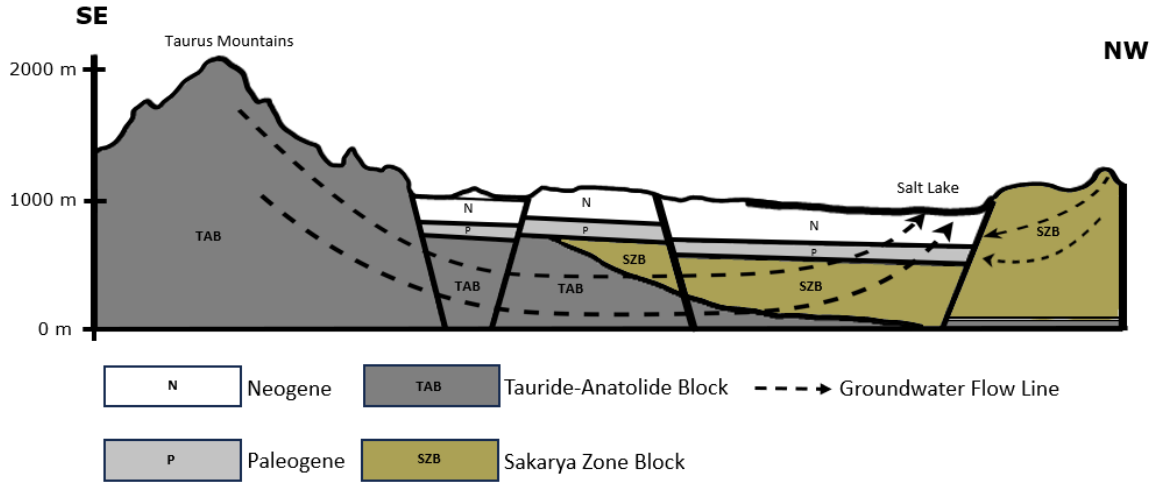

Figure 3.14. Simplified groundwater flow system in the basin, modified from Bayari et al. (2009).

3.6.1. Pumping Tests

Pumping tests are an essential component of hydrogeological surveys to estimate hydrological parameters such as storage coefficient, transmissivity, and hydraulic conductivity. In a pumping test, the drawdown is measured over time while water is extracted at a controlled rate. However, it is both time-consuming and not easy to conduct (dashti et al., 2023).

Hydrogeological studies have been conducted for plains in Konya Closed Basin by State Hydraulic Works (DSİ). These hydrogeological studies were carried out between 1970 and 1975, and as a result, reports (green reports) were published for 6 subplains within the basin. In these reports, annual safe reserves, and water balance for each subbasin were calculated. These reports also included the pumping tests for multiple locations in the each plain. These reports reported flow rate (lt/sec), drawdown (m), specific capacity (lt/sec/m), depth to the top (m), aquifer thickness(m) and estimated transmissivity coefficient (m^3/day/m) and specific storage for each test. Furthermore, chemical analysis was conducted with collected groundwater samples to evaluate the water quality in each subplain. The Green reports published by DSI and used in this study are:

- Hydrogeological Investigation Report of Konya-Çumra-Karapınar Plain (1975),
- Hydrogeological Investigation Report of Karaman-Ayrancı-Akçaşehir Plain (1975),
- Hydrogeological Investigation Report of Altınekin Plain (1973),

- Hydrogeological Investigation Report of Cihanbeyli-Yeniceoba-Kulu Plains (No Date),
- Hydrogeological Investigation Report of Ereğli-Bor Plain (1972),
- Hydrogeological Investigation Report of Misli Plain (1970).

3.6.2. Hydraulic Conductivity

The reports included a total of 77 pumping tests spread throughout the basin; however, the data was not in digital format and not with spatial coordinates. Consequently, the digitalization of the data was conducted by relying on the maps included within the reports. Georeferencing tool is utilized to locate these maps according to the locations name available in old maps. Figure 3.15 shows the location of pumping tests around the basin.

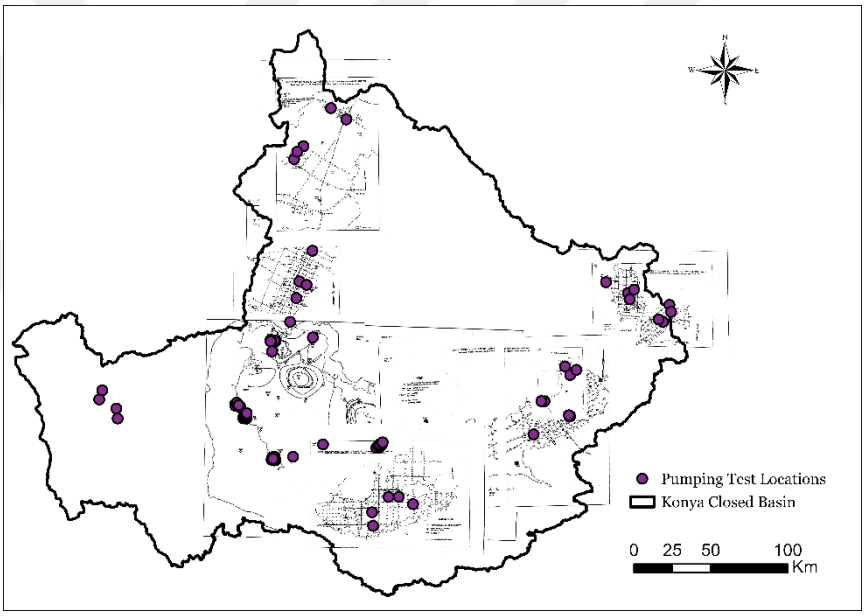

Figure 3.15. Pumping tests from the Green Reports. (DSI, n.d., 1970, 1972, 1973, 1975b, 1975a; SUİŞ-PROJE, n.d.)

As can be observed from the Figure 3.15, Beyşehir subbasin has not been studied in the Green reports. However, Beyşehir subbasin is important for the basin. SUİŞ-PROJE (n.d.) have studied for the hydrogeological report of the basin. In the report, there is hydrogeological investigation of the Beyşehir subbasin including four pumping test results. Therefore, the values obtained from these four locations for Beyşehir subbasin in the report were used.

Green reports provided transmissivity and thickness, so hydraulic conductivity is calculated by dividing the transmissivity by thickness. As a result, there are 81 pumping test locations over the basin. Hydraulic conductivity in the basin varies between 0.43 and 592.59 m/day according to these

test results.

3.6.3. Head Distribution

Another input data needed by the model is the initial distribution of groundwater levels. Figure 3.16 shows the initial groundwater head for January 2000. The data from 29 monitoring wells were interpolated by utilizing Simple Kriging (SK). Groundwater head in north-eastern region of the basin is highest relative to the rest of the basin. Relatively, the ground elevation is high in that particular region. Southeast of the basin around the Beyşehir Lake has high piezometric records as well. This region receives also more precipitation than the rest of the basin. The lowest heads in the basin are located around Lake Tuz.

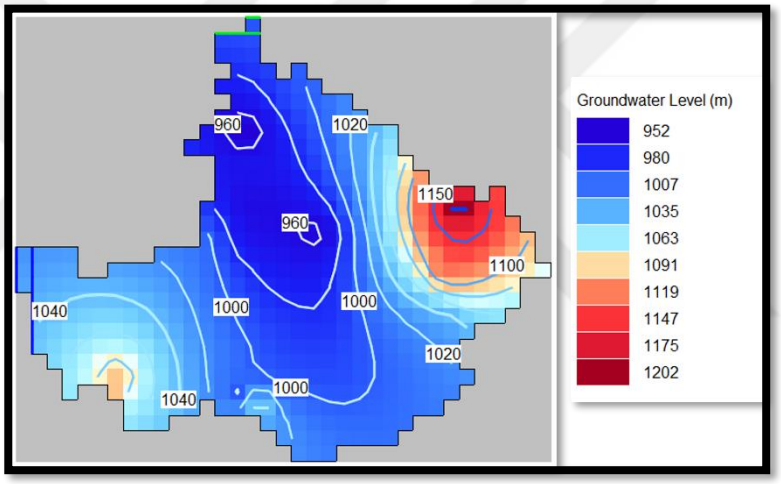

Figure 3.16. Initial groundwater head distribution of the basin.

State Hydraulic Works (DSI) has monitored the groundwater level in the basin since 1967. In our model, the initial condition corresponds to January of 2000. However, it is essential to note that at the beginning of the model, the heads of only 29 were available from State Hydraulic Works (DSI). After 2010, there is significant increase in groundwater monitoring wells. There are total of 99 monitoring wells since 2015. Monitoring of the groundwater head in the basin was carried out manually between 1967 and 2019. Following this period, automatic high resolution monitoring wells were installed. These sensors provide high resolution data at the time intervals ranging from 3-12 minutes. As of today, all of the wells are monitored automatically. Figure 3.17 shows the summary of the groundwater level recording by State Hydraulic Works (DSI) during the interested period.

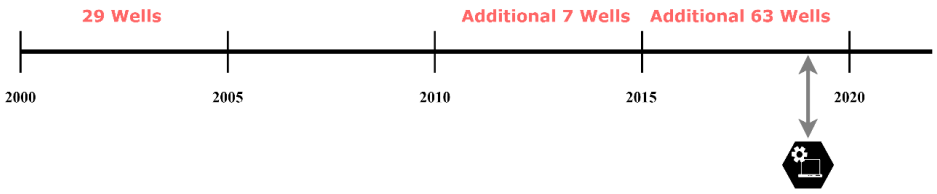

Figure 3.17. Summary of the groundwater level recording.

4. METHODOLOGY

4.1. Research Workflow

Figure 4.1 presents the schematic representation of the workflow involved in the development of the groundwater model for the entire KCB. Orange colour represents processing while blue colour represents data and results. Each of the major steps is described in the following sections.

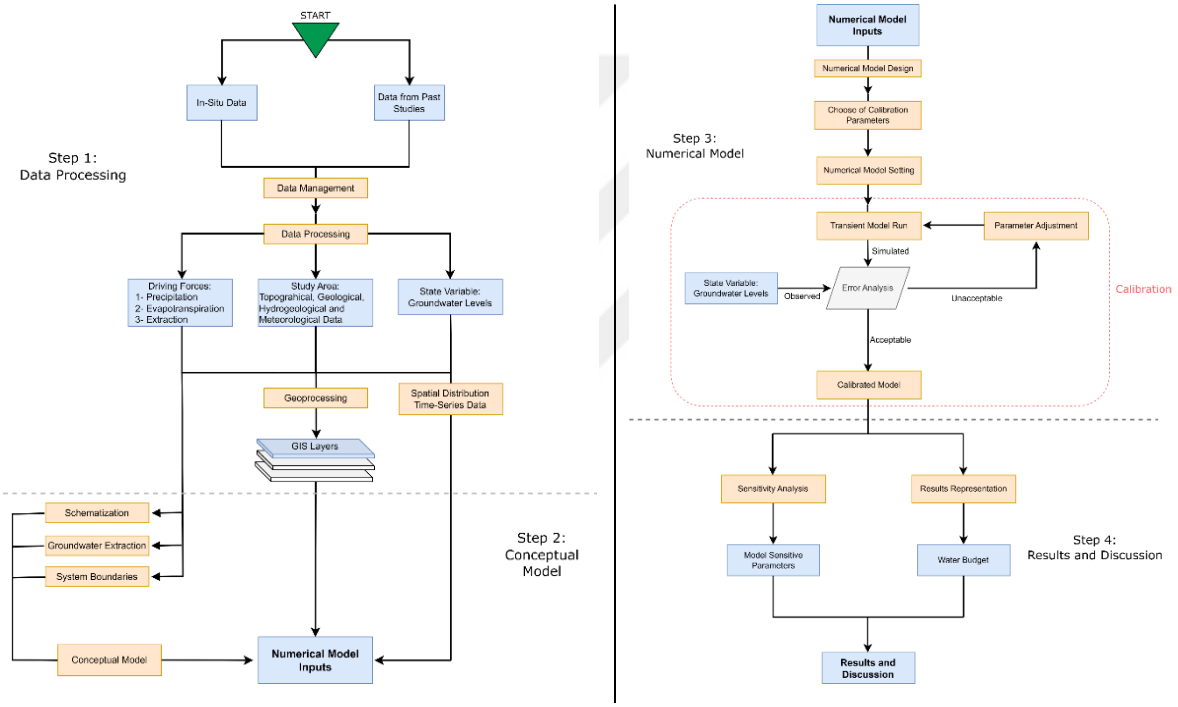

Figure 4.1. Schematic representation of research methodology.

4.2. Data Preprocessing

The input datasets needed for the modeling were gathered from various sources, such as previous studies and in-situ measurements in different formats. Consequently, data preprocessing was necessary to arrange the data required by MODFLOW, convert it to appropriate structure and store it in the appropriate format required by MODFLOW. Programming and geoprocessing are the most effective tools for handling these works. Geographical Information System (GIS) is helpful while managing different types of geospatial data. The use of it is quite common for handling and processing

spatial data in hydrologic science (Vieux, 2001). On the other hand, programming is useful for data visualization and spatial processing of multiple time-series datasets. Groundwater flow models calculate the dependent variable, hydraulic heads, as a function of location and time given a series of input variables such as precipitation, groundwater extraction which dependent on crop type and crop water demand, and aquifer parameters such as transmissivity and storage coefficient. Generally, dependent variables are measured to define the state of the system such as hydraulic heads, pressure and concentration. Independent variables can change spatially and temporally such as land use type, population size and the type of top soils. Parameters include hydrologic parameters, such as recharge, injection and pumping rates, and material property such as hydraulic conductivity and storativity (Anderson et al., 2015; Konikow, 2008; Nourbakhsh & Yousefi, 2017).

4.3. Numerical Model

4.3.1. Software Interface Selection

USGS developed two graphical user interface (GUI) -ModelMuse and FloPy- to help in the preparation of MODFLOW input data and for the visualization of results. In this study, ModelMuse was utilized to generate the fundamental files for simulation such as Name File, Basic Package, Discretization File, Layer Package File, Preconditioned Conjugate-Gradient Package and Output Control File. However, Well File and UZF1 File which vary on a monthly basis are not easy to define for such a complex system. The calculations are needed to estimate the amount of abstraction for Well File which depend on other parameters such as the precipitation, the cultivated fraction of each grid point and the type of crop. Therefore, a code was written to prepare these files in the format needed by MODFLOW. The code was written using the MATLAB tool.

4.3.2. Spatial Discretization

MODFLOW is grid based numerical model (Harbaugh, 2005). It requires that the study area be divided into structured rectangular grids. The area of KCB is quite large, so different grid sizes were initially considered. ArcGIS environment was used to select the grid size for the hydrological model using the Create Fishnet under Data Management toolbox in ArcGIS Pro. Few tests were carried out for gridding the area and gathering the data (Figure 4.2 a, b, c & d). There are 12,920 active cells for the grid size of 4 km^2 (2x2km), 5,843 active cells for 9 km^2 (3x3 km) and 508 active cells for 100 km^2 (10x10 km) respectively. Finer grids allow for the more accurate simulation of the heads.

However, given the size of the domain and the length of the simulations (monthly stress periods extending over a period of 40 years), the finer grids would require prohibitively long time. Moreover, the preparation and control of the input files becomes more complex as the resolution increases. Therefore, inputs for the model are prepared according to grid size of 10x10 km. Grid cells located more than half outside the domain boundary were defined as non-active cells.

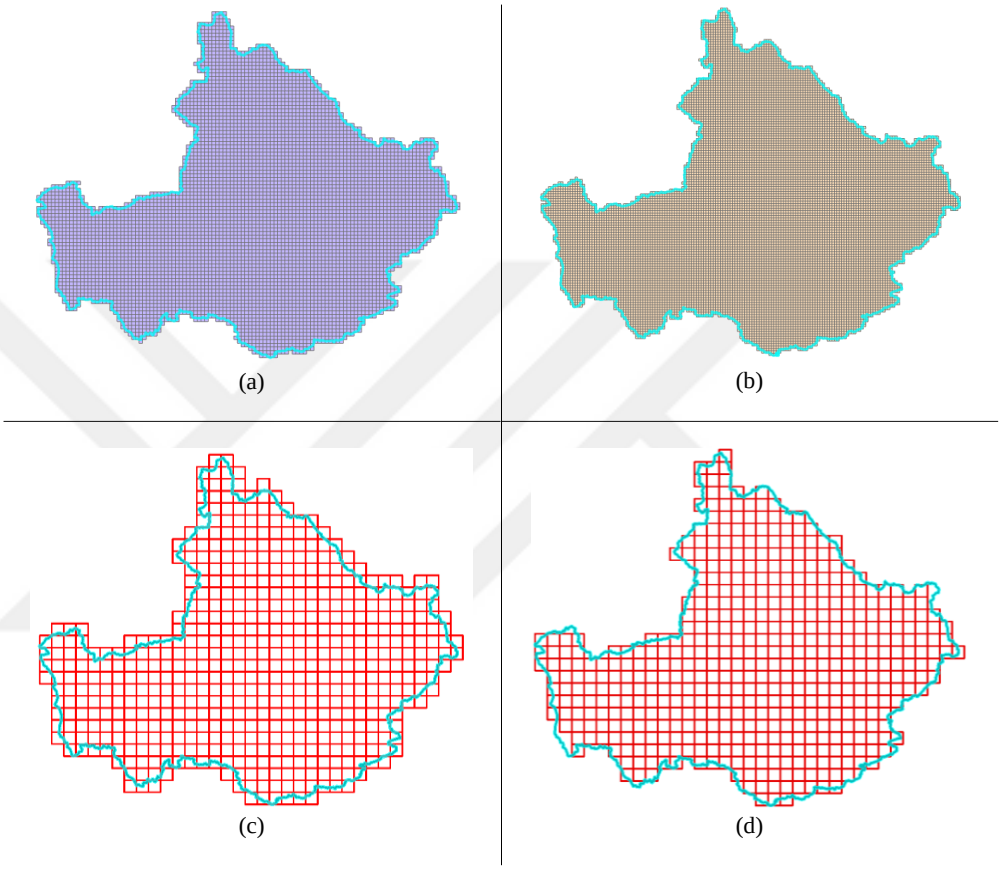

Figure 4.2. Tests for grid size in ArcGIS: (a) 3x3 km, (b) 2x2 km, (c) 10x10 km and (d) modified 10x10km.

Vertically, the model is represented in term of a single unconfirmed layer that describes the total horizontal flow in the aquifer system. The model calculates the transmissivity of this layer as the product of the variable thickness of the aquifer multiplied by the hydraulic conductivity.

4.3.3. Temporal Discretization

To model the water levels over the entire basin, the transient simulation option was used. The model duration was 23 years, divided into 276 stress periods. The duration of each stress period was set at one month due to variability of the precipitation, water extraction and irrigation data. The

computational time step was defined as 1 day. Preliminary tests indicated that the numerical solution is stable for a time step of 1 day and that the numerical error is negligible.

4.3.4. Hydrological and Storage Parameters

The hydrological parameters play a key role in governing both unsaturated and saturated flow dynamics. The two main input hydrologic parameters are the hydraulic conductivity and specific storage. These parameters control the downward rate of flow in the unsaturated zone and the horizontal flow through the aquifer system. The saturated hydraulic are defined in the Layer Package File. Hydraulic conductivity in horizontal direction (K_h) is obtained from the pumping tests described in Yeşil Reports interpolated over the entire domain using kriging, as mentioned earlier. Anisotropy (K_h/K_v) is assumed to be 10 which is consistent with various references (Tanachaichoksirikun et al., 2020). The aquifer system was defined as a single layer with variable thickness and hydraulic conductivity.

The Layer Package File also requires the specific storage (S_s) and specific yield (S_y) are defined. Specific storage was assumed as 10^{-5} m^{-1} whereas specific yield was assumed as 0.05. Later, both specific storage and specific yield were adjusted during calibration.

4.3.5. Boundary Conditions

To solve the governing flow equation (Equation 2.5) boundary conditions must be defined along all boundaries of the basin. since the basin is stated as endorheic, the outer boundary conditions were assumed as no flow boundary conditions. The bottom of the aquifer was also assumed to be a no flow boundary. The water application on the surface was assumed to be equal to the monthly precipitation rates plus irrigation that depends on the type of crop and its water requirements as described in the following section.

4.3.6. UZF1 Package

In the study, UZF1 Package (Niswonger et al., 2006) is selected for simulating flows in the unsaturated zone. Figure 4.3 illustrates the interaction between UZF1 Package and MODFLOW model. The figure also summarizes the data need of each component. UZF1 Package requires infiltration rate (FINF) and potential evapotranspiration rate (PET) applied on the surface. Infiltration rate can be defined as the volume of water that infiltrates the soil per surface area per time. UZF1

package firstly removes evapotranspiration rates by removing the water from the root zone located at the top of the unsaturated zone. If the soil moisture above the extinction depth is adequate, the total potential evapotranspiration is removed from the soil. If the soil moisture above the extinction depth is inadequate, the actual evapotranspiration which is calculated by UZF1 would be less than the potential evapotranspiration rate. Evapotranspiration can occur from the water table if it falls above the extinction depth (not the case in the Konya basin).

For the research, infiltration rate is assumed to be sum of the precipitation and irrigation per unit grid area as depicted in Figure 4.3.

$$q_{in} = P + I \tag{4.1}$$

where:

q_{in} the infiltration rate (length per time),

P precipitation (length per time),

I irrigation (length per time).

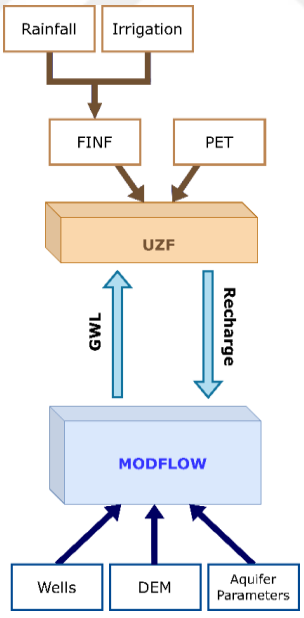

Figure 4.3. Schematic diagram of UZF-MODFLOW model

4.3.7. Simulation Scenarios

The calibrated model was used to test different future water use scenarios. A total of 5 different water management scenarios were developed based on the input from farmers, NGOs, and water

authorities for simulations. Each of water management scenarios is simulated 34 times since there are 34 precipitation predictions from 17 RCMs under two climatic pathways. Hence, the calibrating model was simulated a total of 170 simulations.

4.3.7.1. *Business as Usual Scenario.* The business as usual scenario, which assumes no significant changes in policy or behavior, accounts for the effects of climate change with the trend of cropping pattern continuing into the coming years. Crop pattern for the future is estimated by using linear regression model. In other words, the primary assumption for the scenario was that the existing trend of crop pattern change is likely to persist. The assumed cropping trends for various crops are shown in Figure 4.4.

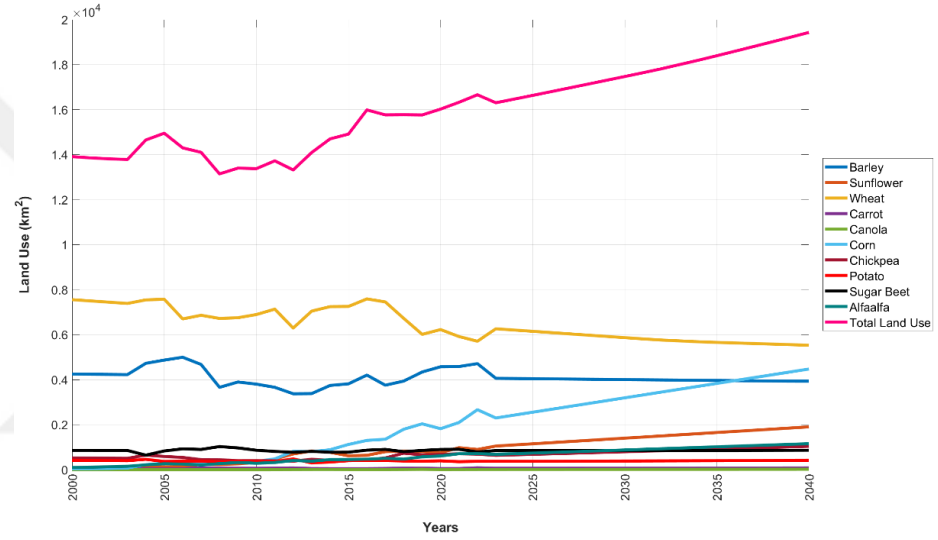

(a)

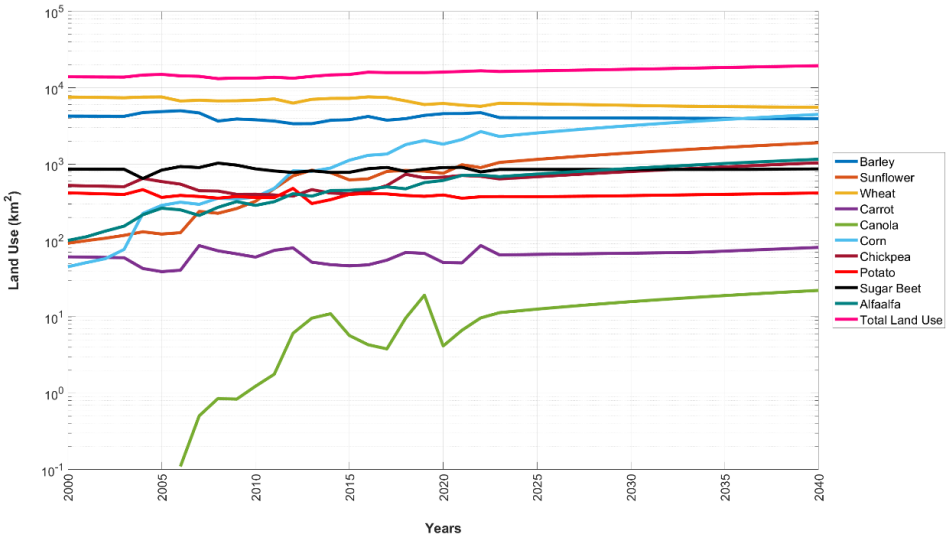

(b)

Figure 4.4. Land use for main crops for business as usual scenario in Konya Basin: (a) normal plot and (b) log-log plot

The irrigation efficiency that appears in equation 4.11 covers the potential losses during both conveyance and irrigation application. It is defined as the multiplication of conveyance efficiency and field application efficiency (Brouwer et al., 1989). Typical values are 0.2-0.3 for low efficiency conditions to about 0.6 for high efficiency irrigation systems (Rai et al., 2017). The calibration parameter for the years 2000-2022 was used as the primary calibration parameter. As will be discussed in Section 4.5.4.3, the following values were used in the model calibration:

- e=0.3 for years 2000-2004
- e=0.4 for years 2005-2009
- e=0.5 for years 2010-2014
- e=0.65 for years 2015-2022

The higher irrigation efficiency of recent years reflects farmers' switch to more efficient irrigation systems. For the business as usual scenario, the irrigation efficiency is assumed to remain 0.65 in the coming years until the end of the simulation (years 2023-2040).

Also, water discharge and storage at Apa Dam is assumed to be used to offset some of irrigation demand in Çumra province. The details of discharge amount and forecasting is explained in Chapter 4.5.3. All of the future scenarios were based on this assumption.

First order linear regression was applied from 2000 to 2003 and from 2023 to 2040. Average coefficient of determination (R2) for all towns and all crops for first order linear regression is 0.36. Between 2000 and 2022, observed precipitation data were used for the climate data. From 2023 to 2040, climate model precipitation predictions are interpolated onto the entire basin and used for simulating water heads.

4.3.7.2. *Corn Phased Out Scenario.* For this scenario, observed precipitation and crop areas (from TURKSTAT) were used for the historical period between 2000 and 2022. Following this, a transition period from 2023 to 2028 was assumed, during which corn cultivation will be partially phased out, with the goal of reducing its cultivation levels to that of the year 2005. Phased out corn cultivated lands were assumed to switch to wheat cultivation, with relatively much lower irrigation demand than corn. This phased approach was intended to gradually return over a 5-year period to historical levels of corn cultivation thereby reversing the recent increase in corn production observed in the last 2 decades. Similar to the previous scenario, future climate projections are used for the estimation of precipitation.

4.3.7.3. *Increase in Irrigation Efficiency Scenario.* A set of simulations were developed to explore the potential impacts of increasing irrigation efficiency. Other things being identical to the business as usual scenario, efficiency was assumed to increase linearly between 2023 and 2028 from 0.65 to 0.8 and remain constant at 0.8 thereafter. Higher efficiency corresponds to pressurized drip systems with minimal distribution losses and farmers following irrigation guidelines without over-irrigation of crops.

4.3.7.4. *Mavi Tunnel Scenario.* The Mavi Tunnel project will transfer water from the Göksu River in the Eastern Mediterranean Basin to the southern portions of Konya Closed Basin. The project, which was just completed, has a capacity of 400 hm^3/year, of which 100 hm^3/year will be allocated for drinking water. Since the 400 hm^3/year is the project's capacity and in reality may not be for all years particularly for dry years, it was assumed that Mavi Tunnel will transfer 200 hm^3/year water for irrigation purposes to Çumra region in the southern part of KCB after 2023. The scenario is developed based on business as usual scenario but with the addition of Mavi Tunnel water transfers. Apa Dam had been already included in scenario, so the water transfer with Mavi Tunnel is the only addition in the scenario. Mavi Tunnel Scenario can be potentially combined with other scenarios.

4.3.7.5. *Combining of Corn Phased Out and Increased Irrigation Efficiency Scenario.* A set of model simulations were developed to explore the potential impacts of increasing irrigation efficiency simultaneously with the phasing out of corn cultivation back to 2005 levels. Efficiency was assumed to increase linearly between 2023 and 2028 from 0.65 to 0.80 and remain constant thereafter. For corn cultivation, a transition period from 2023 to 2028 was assumed, during which corn cultivation will be partially phased out, with the goal of reducing its cultivation levels to that of the year 2005. Phased out corn cultivation lands were replaced with wheat cultivation.

4.4. Conceptual Hydrological Model

4.4.1. Schematization

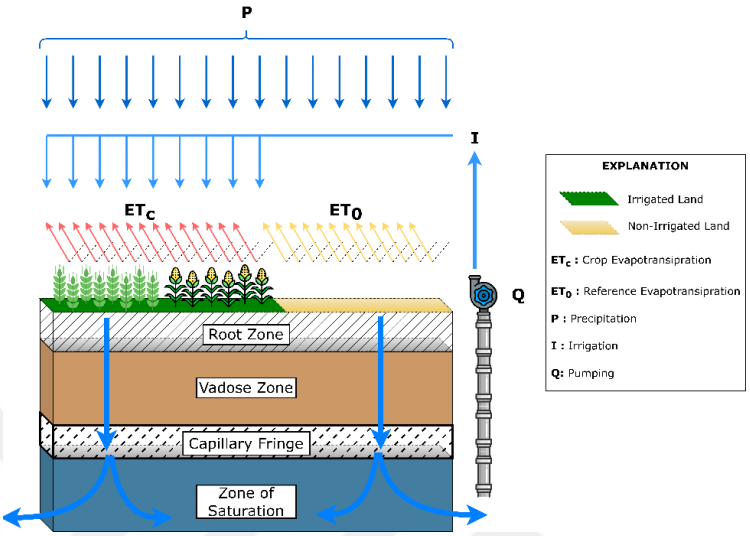

Figure 4.5. Schematic representation for the components of UZF-MODFLOW.

A schematic of the UZF-MODFLOW groundwater flow is shown in Figure 4.5. The sketch depicts a single cell. The land use of this area consists of agricultural and non-agricultural lands, the former defined by TURKSTAT. If the precipitation is not enough, agricultural irrigation (i.e. groundwater abstraction) is accounted as surface water application along with precipitation. Water infiltrates through the vadose zone. This is simulated by the UZF1 program. ET occurs from moisture above the extinction depth. water passing the extinction infiltrates downwards and eventually feeds the aquifer. The groundwater extraction combines domestic use and irrigation when the precipitation is not sufficient for the cultivated crops. MODFLOW calculates the water level at each cell on a daily basis. Based on water level differences and the aquifer transmissivity, water can flow between adjacent cells. Table 4.1 is a summary of the essential input parameters, providing a comprehensive overview of the key factors that shape the model's dynamics.

Table 4.1. Summary of key input parameter

Parameter	Data Availability	Data	Frequency	Unit
Ground Elevation	Available	DEM (Digital Elevation Model) by General Directorate of Mapping (HGM)	x	m
Precipitation	Available	Turkish State Meteorological Service (TSMS).	Daily	mm/day
Groundwater Level	Available	Records of State Hydraulic Works (DSI)	Monthly	m
Hydraulic Conductivity	Available	Yeşil Reports prepared by DSI (n.d., 1970, 1972, 1973, 1975a, 1975b)	x	m/day
Groundwater Abstraction	Unavailable	It has not been recorded. Therefore, it was estimated.	x	m^3/day
Potential Crop Evapotranspiration	Available	TAGEM & DSİ (2017)	10 Days	mm/day
Dam Discharge	Available	Discharge of Apa Dam, recorded by State Hydraulic Works (DSI)	Annual(partial), Monthly(partial)	m^3/day
Evaporation	Available	Average monthly evaporation by TAGEM & DSİ (2017)	Monthly	mm/day

4.4.2. Water Balance Zones and Components

Groundwater levels indicate that aquifer system of the Konya basin is deep, so the interaction between surface water bodies (lakes) and groundwater is assumed to be particularly limited. The interested hydrological system subdivided into two components: unsaturated zone and groundwater zone. Equation 4.2 illustrates the total water balance for the basin. Total catchment storage consists

of unsaturated zone storage and groundwater zone storage.

$$\boldsymbol{P = ET \pm \Delta S} \tag{4.2}$$

where:

P	precipitation,
ET	total evapotranspiration,
ΔS	total catchment storage.

4.5. Driving Forces

The groundwater model requires the definition of the meteorological and hydrogeological data on a monthly basis over the entire simulation duration and the entire basis. Each of these datasets, including their source, is described below.

4.5.1. Precipitation

In Turkey, precipitation is historically monitored manually on daily basis by Turkish State Meteorological Service (TSMS). As mentioned earlier, eighteen meteorological observations stations are located in or adjacent KCB, covering the period of the model between years of 2000 and 2022. The location of these stations is shown in Figure 3.8. Climate projections were obtained from the EURO-CORDEX project which is the European division of the international CORDEX initiative (Jacob et al., 2014). Precipitation predictions incorporated in the groundwater model were generated by RCM (regional climate models) aligned with the Fifth Assessment Report (AR5) of IPCC. Precipitation data based on historical, and projections only provides data for specific locations. These data were then interpolated of the entire KCB using the geostatistical tool kriging.

4.5.2. Potential Evapotranspiration (PET)

The evapotranspiration (ET) isone of the key components of the water balance in the unsaturated zone. The soil moisture content, the recharge into the aquifer, and the estimated amount of water lost from the system are determined using the ET rate calculated by the UZF1 program. The calculation is performed on a 10 km by 10 km grid and monthly basis.

$$ET_{total} = \frac{ET_{c,agri}\ x\ A_{agri} + ET_0\ x\ A_{non-agri}}{A_{agri} + A_{non-agri}} \quad (4.3)$$

where:

ET_{total} cumulative evapotranspiration potential,

$ET_{c,agri}$ evapotranspiration potential from agricultural lands, depends on crop type,

ET_0 evaporation potential from non-agricultural lands,

A_{agri} area of agricultural lands,

$A_{non-agri}$ area of non-agricultural lands.

TURKSTAT only provides agricultural lands per each crop on town basis. In the calculation, it is assumed that town area is only consist of agricultural land and non-agricultural land. Thus, the formulation to calculate total evapotranspiration is altered as in the following formulas:

$$A_{town} = A_{agri} + A_{non-agri} \quad (4.4)$$

where:

A_{town} area of a town,

A_{agri} area of agricultural lands,

$A_{non-agri}$ area of non-agricultural lands.

Substituting Equation (4.3) in Equation (4.4) and rearranging terms yields:

$$ET_{total} = \frac{ET_{c,agri}\ x\ A_{agri}}{A_{town}} + \frac{ET_0\ x\ A_{non-agri}}{A_{town}} \quad (4.5)$$

$$ET_{total} = \frac{ET_{c,agri}\ x\ A_{agri}}{A_{town}} + \frac{ET_0\ x\ (A_{town} - A_{agri})}{A_{town}} \quad (4.6)$$

$$ET_{total} = ET_{c,agri} * \frac{A_{agri}}{A_{town}} + ET_0\ * (1 - \frac{A_{agri}}{A_{town}}) \quad (4.7)$$

4.5.3. Surface Water

As mentioned earlier, there are two important lakes in the basin. Lake Tuz has hypersaline characteristics, so it does not provide water for irrigation. On the other hand, Lake Beyşehir is freshwater. It provides water for irrigation through Apa Dam to Çumra town. Figure 4.6 shows annual discharge data from Apa Dam. The annual discharge rate from Apa Dam was available on report of (SUİŞ-Proje, n.d.-a) between 1968 and 2012. Therefore, the data has been asked from State Hydraulic Works (DSI). DSI shared monthly discharge rate between 2012 and 2022 (shown in orange in Figure 4.6). Ratio of monthly discharge rate is calculated based on data of DSI which is applied for the temporal distribution of discharge rate. For forecasting the discharge rate, linear regression model was applied between 2023 and 2040 (shown in red on Figure 4.6).

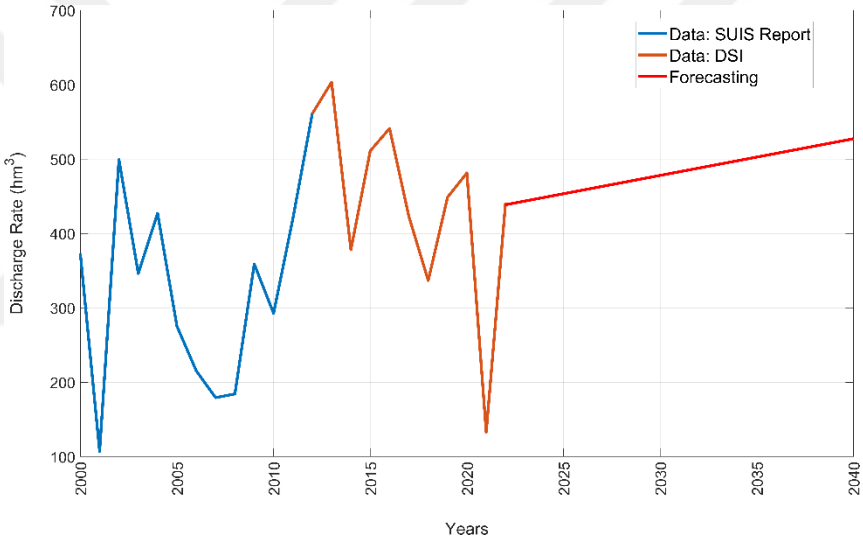

Figure 4.6. Discharge from Apa Dam. (SUİŞ-Proje, n.d.-a)

4.5.4. Groundwater Abstraction

Measurement or estimation of the water needs is crucial for sustainable management of water resources. Since the use of groundwater is not being measured or recorded for the basin, the water needs of the basin have been estimated based on two categories: agricultural water demand and non-agricultural water demand (domestic use). Estimation of water supplied from the groundwater is one of the main tasks that was performed prior to the simulation for the preparation of the WEL input file of MODFLOW.

4.5.4.1. *Domestic water demand.* Since the highest spatial resolution available on TURKSTAT is on town basis, grids of hydrological model have been allocated to towns. However, the domestic, recreational, and industrial water use supplied by municipalities, in other words water demand data in town basis, are not provided on TURKSTAT. Also, the amount of water abstracted from groundwater to supply these demands is not available on town basis.

As State Hydraulic Works is the responsible authority for the groundwater use, groundwater abstraction data for domestic and industrial use were requested from 4th Regional Directorate of State Hydraulic Works. State Hydraulic Works has shared the location of domestic wells for Konya province (Figure 4.7). Table 4.2 represents the comprehensive overview of water resources allocated for domestic use within Konya province (*TURKSTAT Database -Biruni*, n.d.).

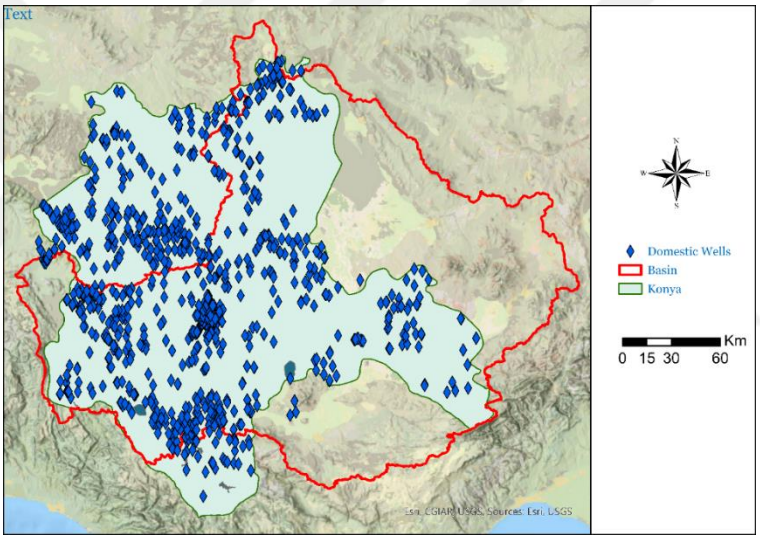

Figure 4.7. Domestic wells in Konya province.

Table 4.2. Water resources for domestic use in Konya province(*TURKSTAT Database -Biruni*, n.d.).

	Rivers	Dams	Lakes	Ponds	Spring Water	Wells	Sum	Population
	(hm^3/year)							Capita
2001	0.16	25.48	2.90	4.31	33.81	98.70	165.35	-
2002	0.33	26.00	3.09	0.21	41.28	101.09	172.00	-
2003	-	32.72	9.65	-	41.85	89.33	173.55	-
2004	-	29.50	2.36	-	38.59	102.67	173.12	-
2006	0.21	10.20	2.80	0.22	42.87	110.98	167.27	-
2008	0.22	17.00	1.73	-	38.33	84.50	141.77	1969868
2010	0.20	21.11	2.55	-	27.63	71.62	123.10	2013845
2012	0.20	26.25	2.45	-	24.38	81.54	134.81	2052281
2014	0.79	7.12	2.86	-	3.17	107.13	121.07	2108808
2016	-	16.43	2.74	-	3.13	134.94	157.23	2161303
2018	-	37.44	2.00	-	2.43	126.31	168.17	2205609
2020	-	115.61	2.69	-	-	63.89	182.19	2250020

As can be seen from Figure 4.7, the location of domestic wells is spatially distributed across the Konya province. However, there is lack of information regarding the abstraction rates from each of these wells, provided by State Hydraulic Works. TURKSTAT shares the amount of water resources used for drinking water in Konya province (Table 4.2). According to the table, supply of potable water relies heavily on both dams and wells. Average amount of drinking water per capita is calculated as 190.27 L/day/capita which is slightly less than Turkish average of 224 L/day/capita (Belediye Su İstatistikleri, 2018). For the simulations, it was assumed that domestic water need is supplied from groundwater. Domestic water demand is calculated based on Equation 4.8.

$$\boldsymbol{Q_{domestic} = P * Cons_{avg} * \frac{1}{1000}} \quad (4.8)$$

where:

$Q_{domestic}$ domestic water needs(m^3/day),

P population (capita),

$Cons_{avg}$ 190.27 (L/day/capita),

The constant appearing in the equation is for unit conversion from liter to m^3 (1 m^3 = 1000 L).

4.5.4.2. *Agricultural water demand.* Calculation of groundwater withdrawals is one of the main challenges and sources of uncertainty when building up hydrological model, particularly for large areas and if the pumping wells are not metered. Implementation of measurement device and storage of the data are highly costly for the areas with large number of extraction wells. Also, measurement does require manpower for maintenance (Meza-Gastelum et al., 2022). Although direct measurement methods are recommended for the estimation of groundwater withdrawals, these were not available options for KCB basin due to its size and large number of extraction wells. Therefore, indirect estimation of groundwater withdrawals based on crop water demands is applied.

Evapotranspiration is the combination of evaporation from a surface (soil, vegetation surface, pavement, and water bodies) and transpiration (water movement from soil into atmosphere as water vapor through vegetation) (R. G. Allen et al., 1998; U.S. Geological Survey, 2018). Estimation of potential crop evapotranspiration (ETC) under standard conditions requires potential evapotranspiration (ETP) or reference evapotranspiration (ET0). Potential evapotranspiration (ETP) was first introduced as “the amount of water transpired in a given time by a short green crop, completely shading the ground, of uniform height and with adequate water status in the soil profile” (Penman, 1948). The main problem about this method is the confusion about the short green crop

since it is not clearly defined (Xiang et al., 2020).

Later, reference evapotranspiration (ET0) was defined as rate of evapotranspiration from a hypothetical crop with specific characteristics. Reference evapotranspiration is based only on climatic conditions, also referred as evaporation power of the atmosphere. Potential crop evapotranspiration is estimated by multiplying crop coefficient and reference evapotranspiration. Equation 4.9 shows the calculation of potential crop evapotranspiration.

$$\boldsymbol{ET_C = k_c \, x \, ET_0} \tag{4.9}$$

where:

ET_c potential crop evapotranspiration,

k_c crop coefficients,

ET_0 reference evapotranspiration.

The report of TAGEM & DSİ (2017) shows the estimated of potential crop evapotranspiration (ET_C) for many towns and cities in Turkey and many but not all crops. The report estimates ET_C for 10 days intervals. Since the model requires monthly data, it is summed monthly. Furthermore, monthly average potential crop evapotranspiration ($ET_{C,agri}$) for each town is calculated as follows:

$$\boldsymbol{ET_{C,agri} = \frac{\sum_{i=1}^{n} ET_{c,i} \, x \, A_i}{\sum_{i=1}^{n} A_i}} \tag{4.10}$$

where:

$ET_{c,agri}$ average crop evapotranspiration for town (mm/month),

$ET_{c,i}$ specific crop evapotranspiration for town (mm/month),

A_i land occupied by the specific crop (m^2),

i specific crop type,

n total number of crops grown in a town.

The calculation in Equation 4.10 is to estimate water demand for a hypothetical crop for the entire town since the available data on TURKSTAT only provide land occupied by the specific crop for each town without spatial distribution (*TURKSTAT Database -Biruni*, n.d.). General Directorate of Mapping (HGM) (n.d.) provides the political map of Turkey to public freely which includes boundaries of towns. Polylines showing the boundaries are merged to create polygon by using Feature to Polygon tool in ArcGIS software. Towns located in the basin were assigned to grids of the model by utilizing the tools under selection pane in ArcGIS.

Figure 4.8 shows the town allocated grids over the entire basin. There are total of 38 towns assigned to grids in the basin. Konya province has 21 towns located in the basin. Eight towns out of 21 towns have specific crop evapotranspiration value. Therefore, to fasten up the calculation specific crop evapotranspiration for Konya values are aggregated by averaging them. These 8 towns are: Beyşehir, Seydişehir, Cihanbeyli, Çumra, Ereğli, Karapınar, Konya, Kulu. For the rest of the towns, specific crop evapotranspiration is assumed to be equal of ET_c of connected city.

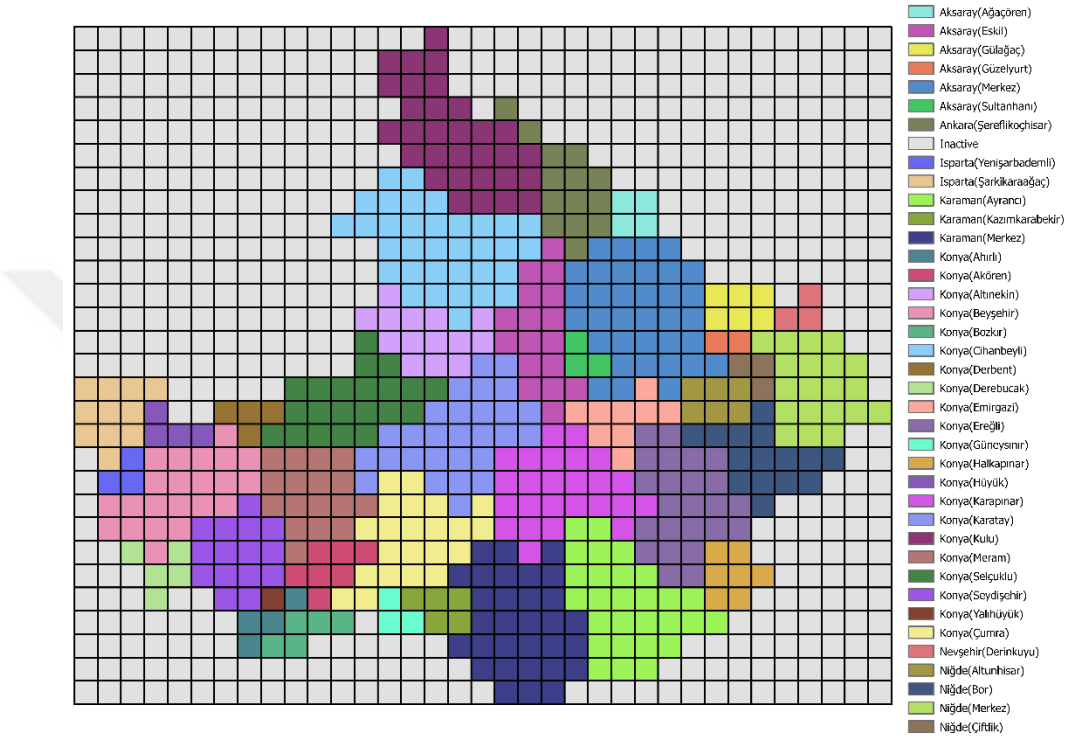

Figure 4.8. Town allocated grids over the basin.

For the calculation of hypothetical average crop evapotranspiration for town, it is not possible to account for all species cultivated in the town. Therefore, most cultivated ten crops were selected. These are alfalfa, barley, canola, carrot, chickpeas, corn, potatoes, sugar beet, sunflower and wheat (R.T. Ministry of Industry and Technology General Directorate of Development Agencies, 2021).

Land use data for various crop on TURKSTAT Database -Biruni (n.d.) are publicly available for town scale, covering the period between 2004 and 2022. The total land use for the main crops covering the entire basin is plotted in Figure 4.9. It is important to point out that the graph is plotted log-scale. The data highlighted the transition on crop pattern.

Between 2004 and 2022, the land used for corn cultivation over the entire basin was increased by 1080%. This dramatic expansion of land use is followed by an increase of 593% with sunflower cultivation. Furthermore, land occupied by alfalfa expanded 230% during the same period. Land used

for canola production increased by 871% between 2006 and 2022.

On the other hand, the dramatic land use drop for wheat cultivation is obvious from the graph. The wheat cultivation in terms of land use decreased 24% between 2004 and 2022. Also, land used for potato cultivation dropped 19% during the same period. Overall, the total land used for the main crops is expanded 14.8 % over the entire basin. Agricultural land use was forecasted by utilizing first order linear regression model between 2023 and 2040.

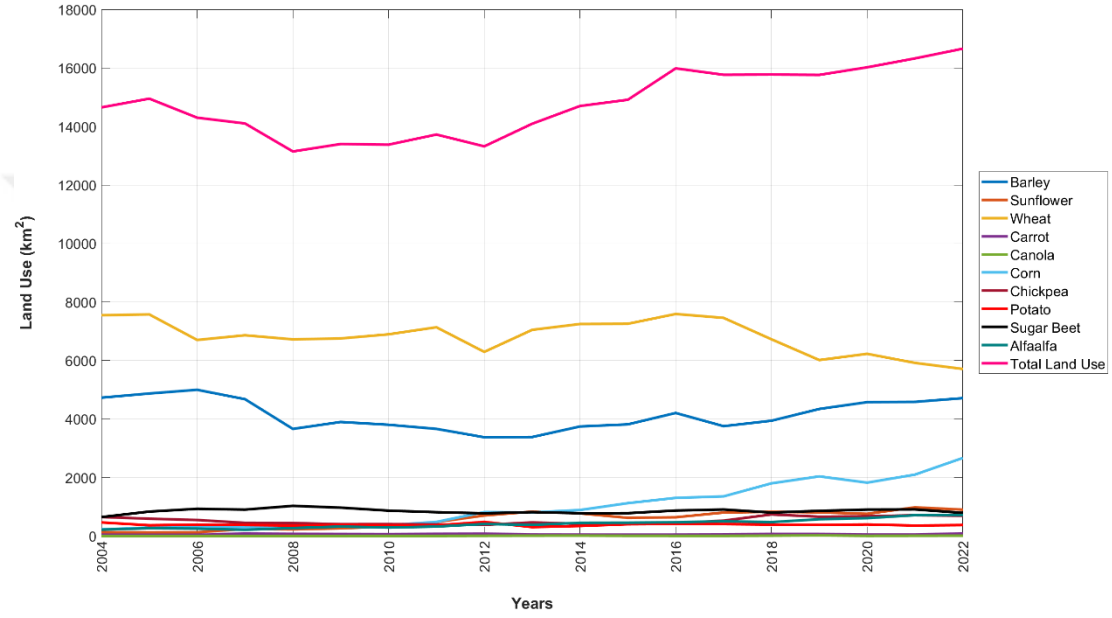

(a)

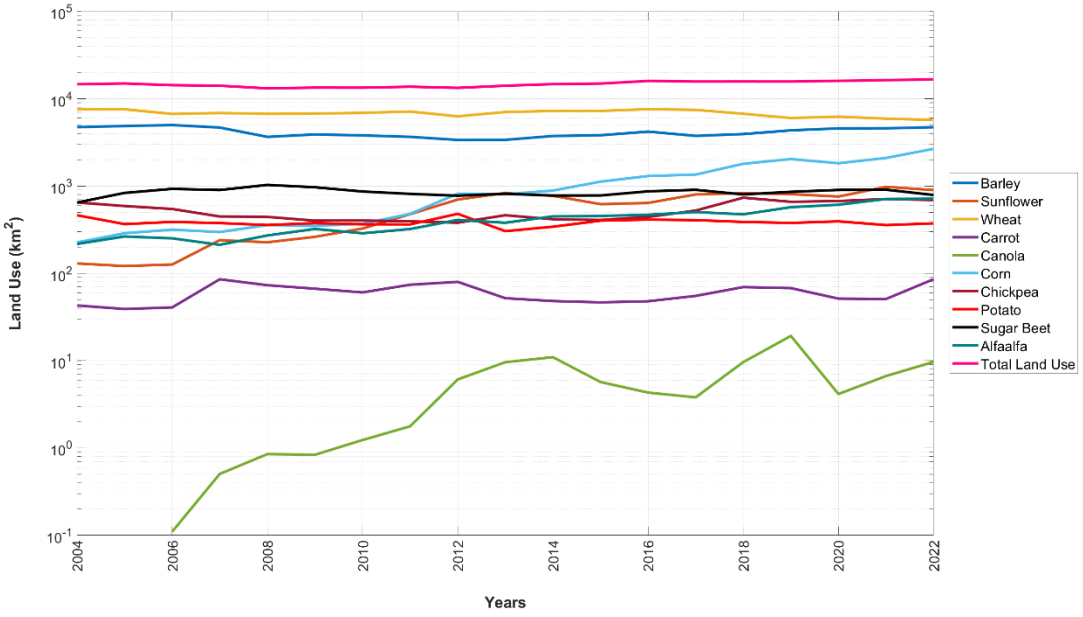

(b)

Figure 4.9. Agricultural land use for Konya Closed Basin: (a) normal plot and (b) log-log plot.

4.5.4.3. *Groundwater extraction.* Groundwater is extracted for a variety of reasons such as supplying irrigation, industrial and municipal water demand. Groundwater may be the only reliable source of water since surface water could be scarce or unreliable for some regions. One of the main reasons for groundwater extraction in agricultural regions such as KCB is to supply precipitation deficit in areas where there is rainfall is insufficient to meet the water demands of crops.

. Well Package covers the groundwater extraction for MODFLOW model. The package requires the monthly amount of abstraction rate (L^3/T) for each grid. The amount of abstraction for irrigation purposes depends also on irrigation efficiency. Groundwater abstraction is estimated formulas follows:

$$\boldsymbol{Q_{irrigation}(x,t) = \frac{\left(i_{town}(x,t) - ET_{C,agri}(x,t)\right)}{e} * A_{grid} * \frac{A_{agri}(x,t)}{A_{town}(x)} * \frac{1}{1000} * \frac{1}{30}} \quad (4.11)$$

where:

$Q_{irrigation}$	groundwater abstraction for irrigation(m^3/day),
i	precipitation (mm/month),
ET_C	agricultural water need (mm/month),
e	irrigation efficiency (unitless),
A_{grid}	area of a grid (10^8 m^2),
$\frac{A_{agri}}{A_{town}}$	ratio of agricultural areas to town area,

The constant in Equation (4.11) is for unit conversion from meter to mm and month to days (1 m = 1000 mm, 1 month = 30 days).

To quantify the proportion of irrigation water utilized effectively in comparison to the portion lost, irrigation efficiency term is used (Brouwer, C., K. Prins, Heibloem, 1989). The scheme irrigation efficiency can be divided into two components: conveyance efficiency and field application efficiency. Conveyance efficiency characterizes the effectiveness of water conveyance through canals which predominantly hinges on factors such as canal length, the type of soil and permeability alongside the characteristics of canal embankments, and the overall canal condition. Field application efficiency characterizes the effectiveness of water distribution within the cultivation area (Brouwer, C., K. Prins, Heibloem, 1989).

$$e = \frac{e_c * e_a}{100} \quad (4.12)$$

where:

e scheme irrigation efficiency (%),

e_c conveyance efficiency (%),

e_a field application efficiency (%).

An optimal scheme irrigation efficiency typically falls within the range of 50% to 60%, indicating good irrigation performance. A value of around 40% is regarded as acceptable, while a lower range of 20% to 30% indicates a poor scheme irrigation efficiency (Rai et al., 2017). However, one of the biggest uncertainties in the calculation is the irrigation efficiency since there is lack of knowledge about the irrigation technology, conveyance distance and materials of conveyance channels.

Finally, the pumping rate of a grid is thence calculated by summation of domestic and irrigation water need. Equation 4.13 shows the calculation of pumping rate.

$$Q_{pump}(x,t) = Q_{irrigation}(x,t) + Q_{domestic}(x,t) \quad (4.13)$$

where:

Q_{pump} groundwater abstraction (m^3/day),

$Q_{irrigation}$ groundwater abstraction for irrigation(m^3/day),

$Q_{domestic}$ groundwater abstraction for domestic use(m^3/day).

4.6. Spatial Interpolation

Meteorological data such as precipitation are measured at discrete locations. However, the model requires such data to be defined over the entire flow domain. Similarly, the hydraulic conductivity determined from pumping tests should be interpolated over the entire domain. In environmental science, spatial interpolation methods (SIM) are commonly used to spatially interpolate the point data. Since the study area covers vast land with limited amount of meteorological observation stations, spatial interpolation was applied to estimate unknown values at all unsampled locations within the flow domain (J. Li & Heap, 2014).

For the interpolation of precipitation data, simple kriging (SK) with known mean was used. SK

is based on the fundamental assumption that data are correlated in space and that the correlation is function of distance. Simple kriging expresses the value of an unknown function as a linear function of data at nearby locations (Wackernagel, 1995). Equation 4.14 represents the formulation of simple kriging with known mean.

$$\boldsymbol{Z^{*}_{SKM}(x_0)} = \mu + \sum_{\boldsymbol{i=1}}^{\boldsymbol{n}} \boldsymbol{\omega_i(Z(x_i)} - \mu) \tag{4.14}$$

where:

$Z_{SKM}(x_0)$ simple kriging estimate at unsampled location x_0,

μ mean,

ω_i weight of sampling point,

$Z(x_i)$ measurement at the sampling point,

n total number of sampling points.

The weights are calculated from the relative distances between the unsampled location x_0 and the locations of the available data. Simple kriging predictions require the knowledge of the mean of measured data, μ, and the covariance function as a function of separation distance, C(h) (Lichtenstern, 2013; Wackernagel, 1995) where *h* is the separation distance. The covariance function which is a measure of similarilty in the data with distance is directly related to the semi-variogram function which is a measure of the variability in the data with separation distance. The raw semi-variogram (or covariance) function is estimated directly from the available data and then fitted to some function such as the exponential or spherical model. In this study the raw semi-variogram was fitted by an exponential function which is widely used in geostatistical applications (Pardo-Iguzquiza & Chica-Olmo, 2008; Biswas & Cheng, 2013). Equation 4.15 and Equation 4.16 shows semi-variogram function and exponential covariance function respectively (Wackernagel, 1995).

$$\boldsymbol{\gamma^{exp}_{a,b}(h) = b\left(1 - exp\left(-\frac{|h|}{a}\right)\right) for\ |h| \geq 0} \tag{4.15}$$

where:

$\gamma_{a,b}$ variogram function,

b sill value,

a range parameter,

h separation distance.

$$C_{a,b}^{exp}(h) = b\left(exp\left(-\frac{|h|}{a}\right)\right) for\ |h| \geq 0 \tag{4.16}$$

where:

$C_{a,b}$ covariance function,

b sill value,

a range parameter,

h separation distance.

As can be seen from the above to equations, the sum of the semi-variogram and covariance functions is the sill which is often taken equal to the variance of the available data.

In this study, the raw and covariance and semi-variogram functions were calculated using GSLIB software. GSLIB is a suite of different geostatistical tools written in FORTRAN (Deutsch & Journel, 1998; Goovaerts, 1997).

Once the raw and covariance functions are calculated and fitted to an exponential function, they are utilized to estimate the simple kriging weights. Equation 4.17 shows the derivation of the weights for Simple Kriging. N system of linear equations must be solved for number of neighbors (n) (Wackernagel, 1995).

$$\boldsymbol{A\,w} = \mathbf{b} \tag{4.17}$$

where:

A covariance between any pairs of points,

w weight factor,

b covariance between each observation and prediction points.

Equation 4.17 can be rewritten as in Equation 4.18.

$$\underbrace{\begin{pmatrix} \mathbf{c}(\mathbf{x_1} - \mathbf{x_1}) & \cdots & \mathbf{c}(\mathbf{x_1} - \mathbf{x_n}) \\ \vdots & \ddots & \vdots \\ \mathbf{c}(\mathbf{x_n} - \mathbf{x_1}) & \ldots & \mathbf{c}(\mathbf{x_n} - \mathbf{x_n}) \end{pmatrix}}_{A} \underbrace{\begin{pmatrix} \omega_1^{SK} \\ \vdots \\ \omega_n^{SK} \end{pmatrix}}_{w} = \underbrace{\begin{pmatrix} \mathbf{c}(\mathbf{x_1} - \mathbf{x_0}) \\ \vdots \\ \mathbf{c}(\mathbf{x_n} - \mathbf{x_0}) \end{pmatrix}}_{b} \tag{4.18}$$

Since the precipitation data are defined on monthly basis in the groundwater model, a MATLAB code was written to repeat the calculations for all months (up to 480 months including future simulations.

5. RESULTS

5.1. Spatial Data

This section describes the input spatially distributed data that are required by the hydrogeologic model. The data were interpolated using simple kriging. The equations are given in Section 4.6.

5.1.1. Hydraulic Conductivity (K_h)

Hydraulic conductivity (K_h) is interpolated over the basin by utilizing Simple Kriging (The application of methodology was explained detailly in Chapter 4.6). Figure 5.1 shows the interpolated hydraulic conductivity over Konya Closed Basin. Hydraulic conductivity is used in Layer Package File. As mentioned earlier, it is assumed that 1:10 ratio of vertical hydraulic conductivity to horizontal hydraulic conductivity.

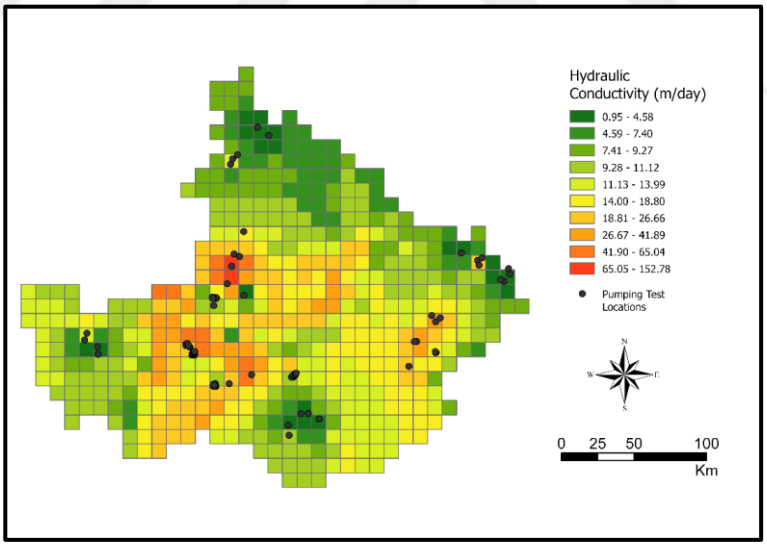

Figure 5.1. Hydraulic conductivity for the basin.

5.1.2. Top Elevation

Digital Elevation Model (DEM) was spatially continuous data, so spatial interpolation was not necessary. Zonal Statistic Tool in ArcGIS is utilized. Mean elevation is calculated by using Zonal Statistic Tool for each grid. Figure 5.2 shows the top elevation values used for Discretization File in the model.

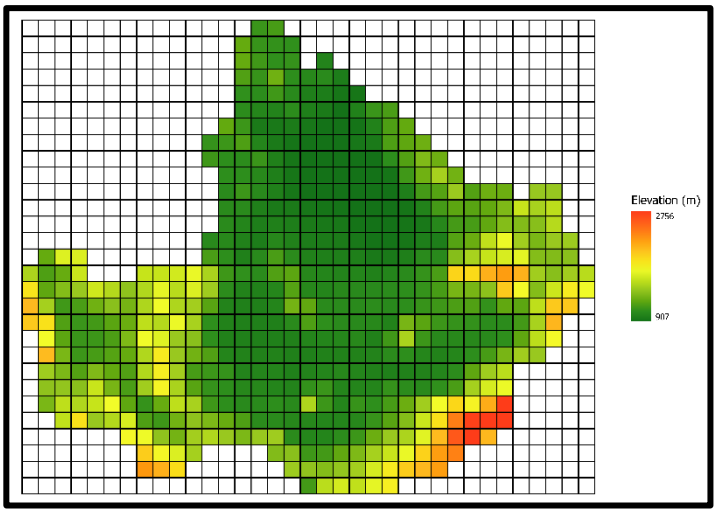

Figure 5.2. Top elevation in the model

5.2. Spatiotemporal Data

This section describes the input spatially and temporally distributed data that are required by the hydrogeologic model. Interpolation method was simple kriging which is detailly explained in Section 4.6.

5.2.1. Precipitation

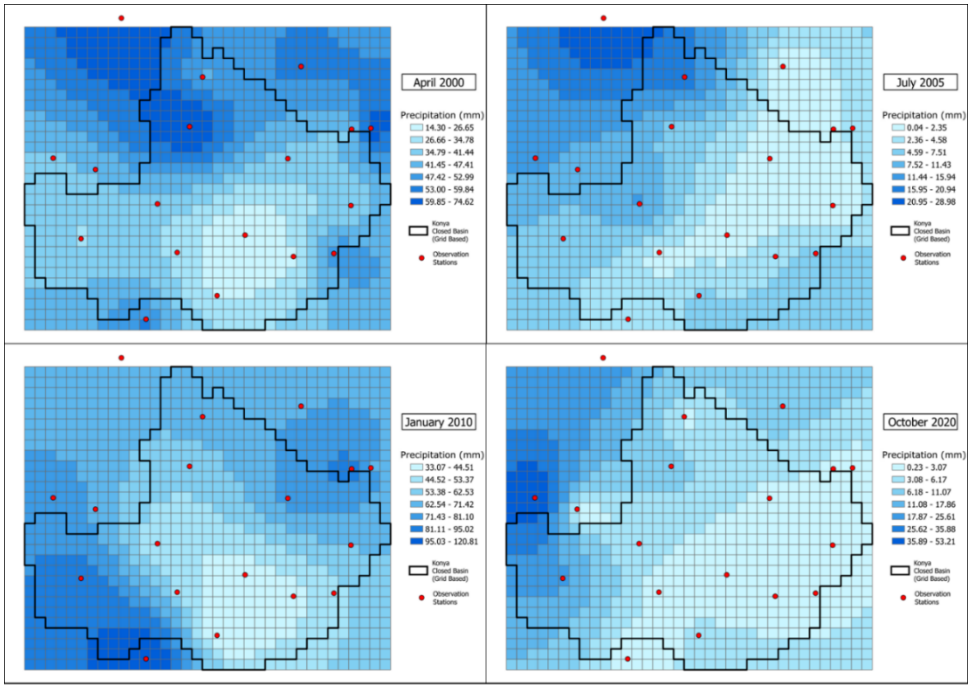

Figure 5.3. Precipitation distribution over the basin by applying SK.

Figure 5.3 shows randomly selected precipitation maps interpolated using simple kriging from the precipitation data measured at the meteorological stations. The maps shown in this figure are for 4 months randomly selected. Similar maps were generated for 23*12=276 months covering the period from January 2000 to December 2022. The central part of the basin is receiving less precipitation as can be seen in the figure. Spatially distributed precipitation data is used for both the surface water application (FINF parameters of UZF1 Package) and estimation of groundwater abstraction.

5.2.2. Groundwater Abstraction

Section 4.5.4 presents the calculation of groundwater abstraction in the basin. The Well Package requires the specification of the abstraction in each grid for each stress period. As noted earlier (Equations 4.11), agricultural groundwater extraction depends on the type of crop, the precipitation and irrigation efficiency. Farmers rely on groundwater resources for irrigation mostly in the spring months for summer crops. Examples of groundwater abstraction are shown in Figure 5.4 for the months of June of 2000, June of 2005, June of 2010, June of 2015 and June of 2020.

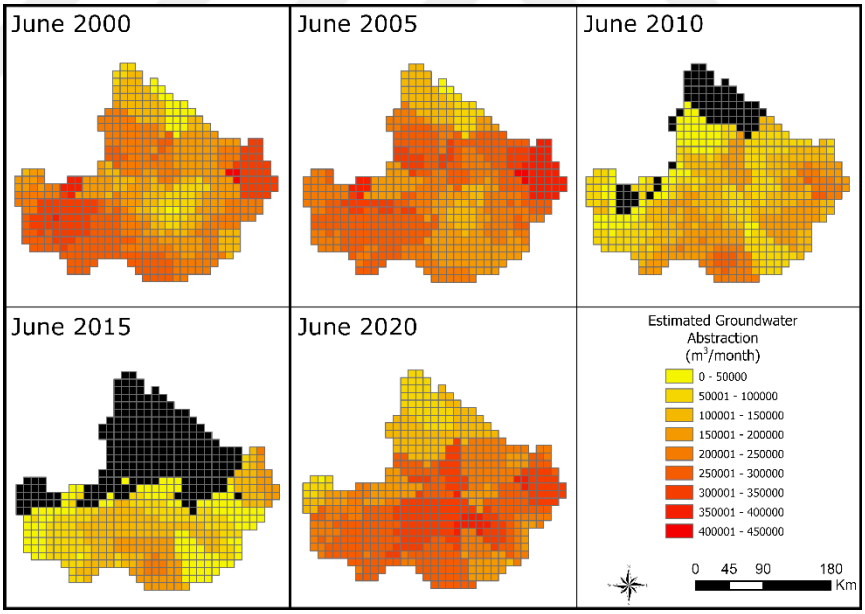

Figure 5.4. Groundwater abstraction in the basin.

As can be seen in this figure, the central part of the basin is highly reliant on groundwater resources this is attributed to the low precipitation and high aridity index of the basin (Figure 3.5). The areas shaded in black in the Figure 5.4 indicate that precipitation exceeds the water demand and therefore there is no need for groundwater abstraction. In June 2015, precipitation was quite high in the northern portions of the basin (Monthly cumulative precipitation was 130 mm at Kulu, 153.7 mm

at Cihanbeyli, and 119 mm at Aksaray) resulting in less abstraction requirement for irrigation purposes.

5.3. Calibration Results

As mentioned earlier, the primary output from the model is the groundwater level which was selected to be the calibration target. Specifically, the model was calibrated by matching the monthly measured groundwater heads at the 29 monitoring wells to the simulated heads for the period between 1st January 2000 and 31st December 2022. Since the highest uncertainty is in the irrigation efficiency, it was selected to be the main calibration parameter.

Figure 5.5 – Figure 5.7 compares the observed groundwater levels and simulated groundwater levels for 29 wells. Figure 5.5 illustrates the comparison for the entire transient period each line (shown in different color) with each dataset showing the change in water level over the period between years 2000 and 2022. Figure 5.6 and Figure 5.7 show the variation in observed and simulated heads as a function of time for each of the 29 wells. Since observed groundwater levels are confidential, the plots do not show the actual location of the groundwater monitoring wells or its name.

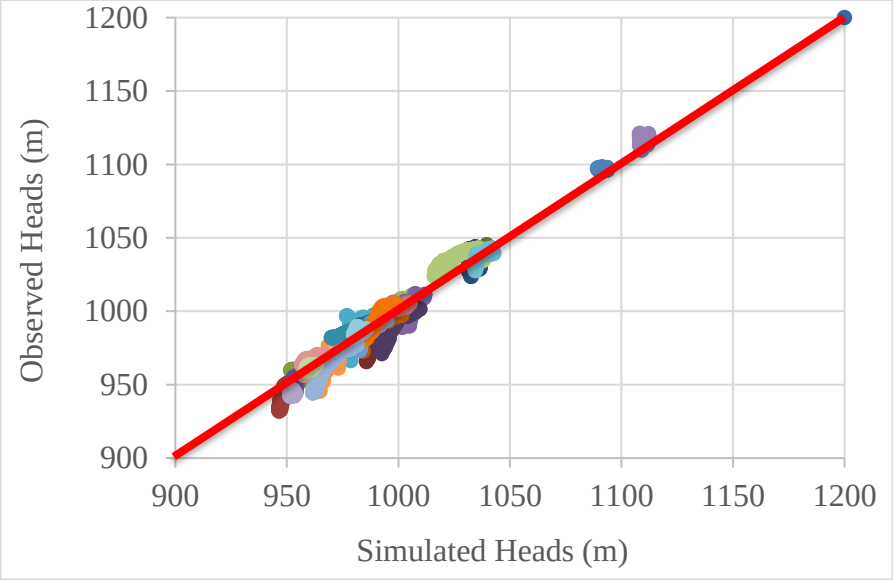

Figure 5.5. Simulation heads and observed heads of observation locations for the entire period.

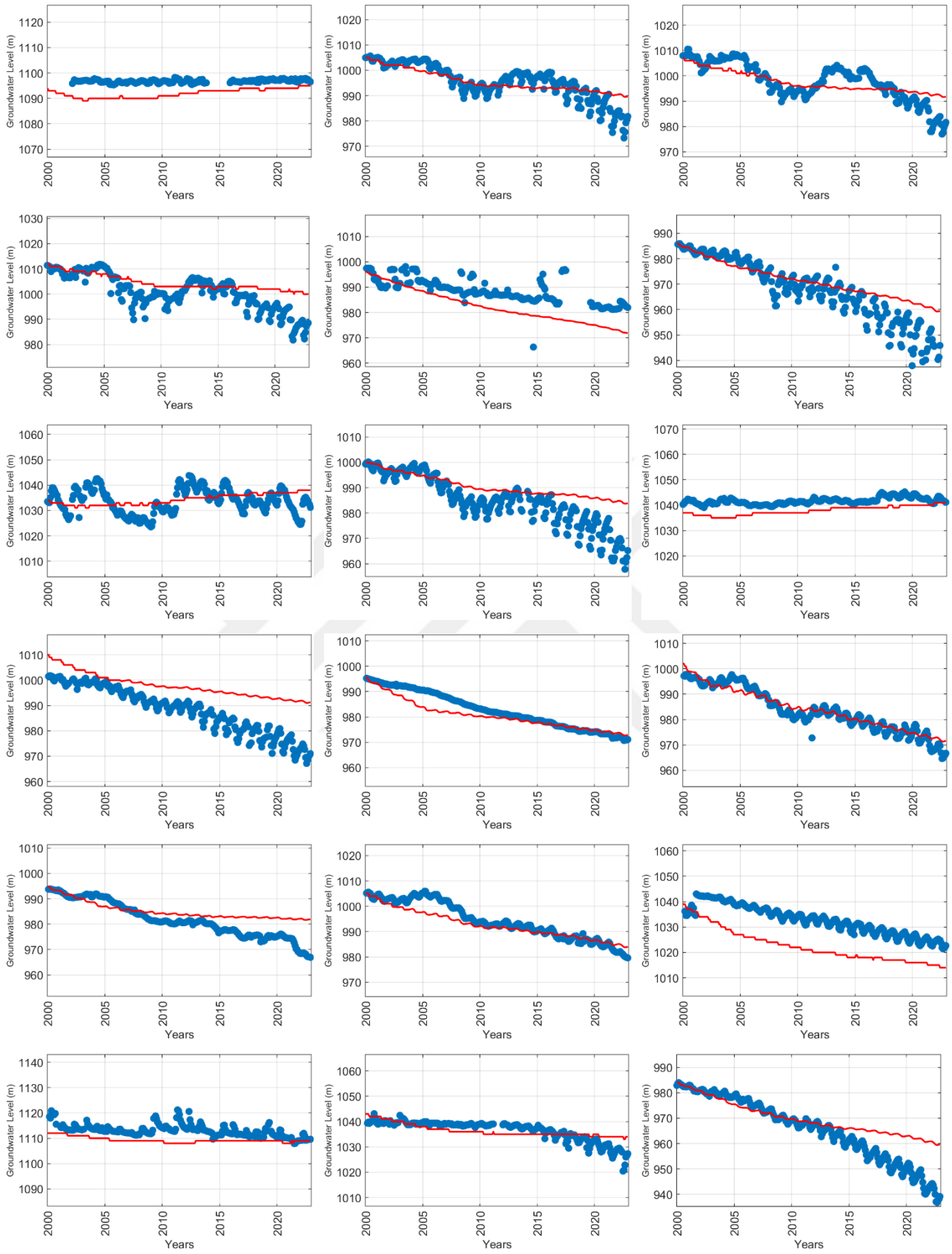

Figure 5.6. Observed groundwater level versus simulated groundwater level (continue).

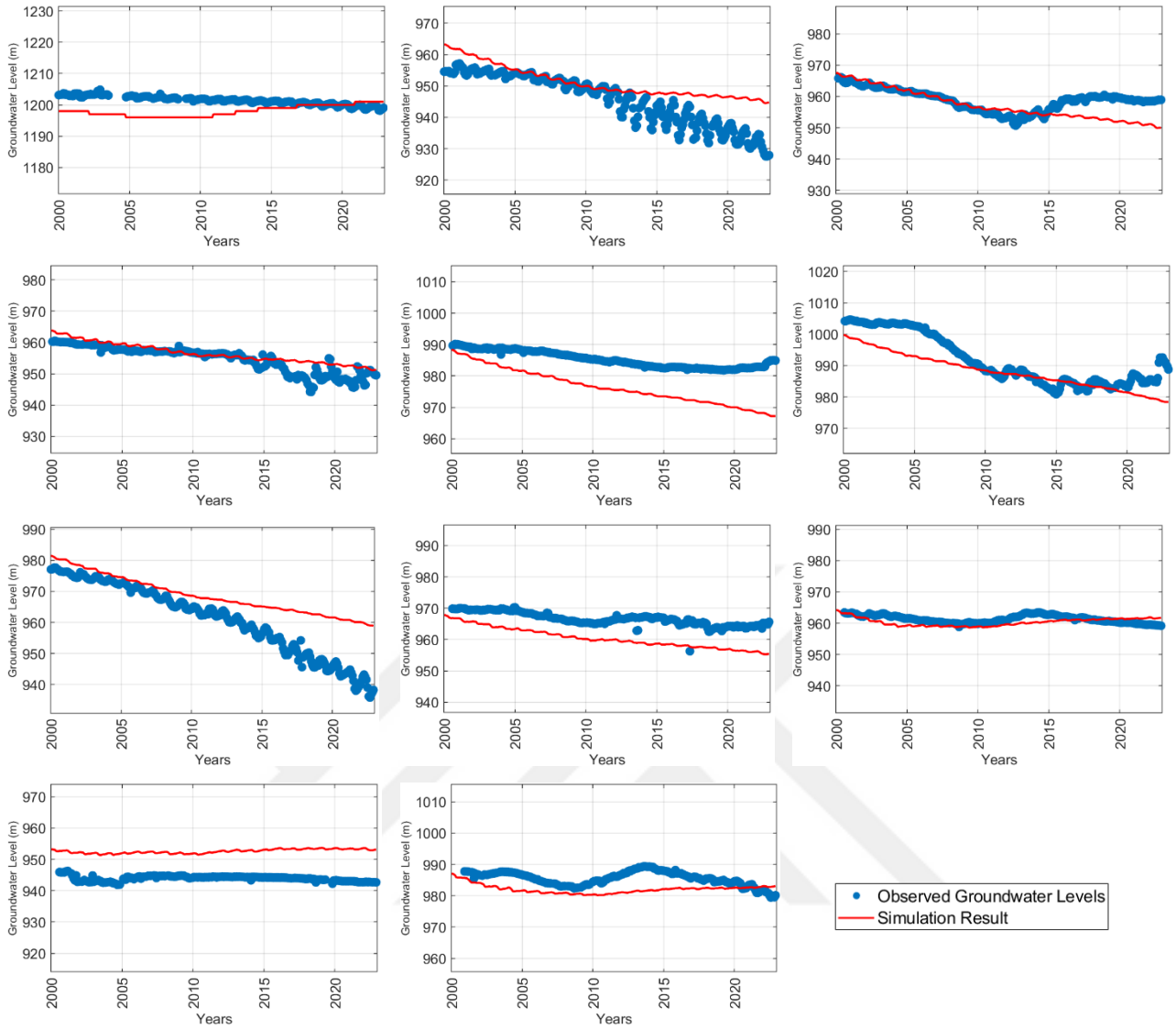

Figure 5.7. Observed groundwater level versus simulated groundwater level (continued) .

As mentioned earlier, the model computes the water level at the center of each grid point. In order to compare the simulated and observed heads, simulated groundwater levels were interpolated onto the observation well location by applying inverse distance weight method using the four closest grid centers.

In general, good match between simulated groundwater level and observed groundwater level is evident. In Figure 5.5, it is observed that the heads fall close to the 45-degree line indicating that the computed heads at individual wells are mostly consistent with the observed water levels. Variations occur in certain years due to local hydrogeologic conditions or irrigation practices not incorporated by the model. Overall, the correlation coefficient, R^2, for all control wells is 0.58 m, ranging between 0.0015 m to 0.91 m. MAE for the overall model is 4.90 m, ranging between 1.59 m and 10.39 m. Also, Nash–Sutcliffe efficiency- calculated as one minus the ratio of variance of the simulated heads to the variance of the observed heads- for the entire domain is 0.22. All these statistics suggest that

the model is capable of reproducing the main variations in water levels.

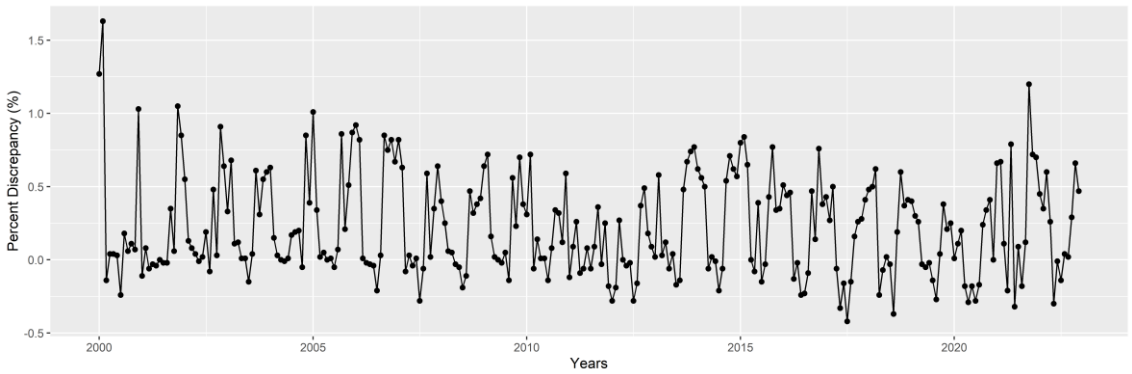

Figure 5.8. Percent discrepancy for calibrated model.

Figure 5.8 shows the percent discrepancy in the water budget for the calibrated model. Mean discrepancy value between inflow and outflow over all stress periods is 0.22%. The mean discrepancy value is within acceptable thresholds (less than or equal to 1%). The irrigation efficiency is assumed as 0.3 between 2000 and 2004, 0.4 between 2005 and 2009, 0.5 between 2010 and 2014 and finally 0.65 between 2015 and 2022.

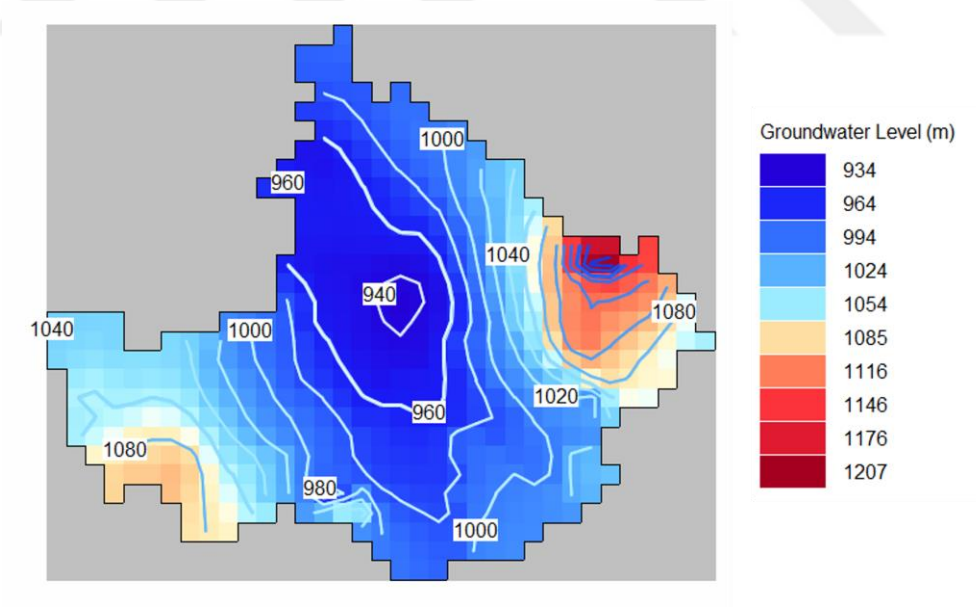

Figure 5.9. Simulated groundwater level across the whole KCB after calibration process for December 2022

Figure 5.9 illustrates the groundwater level distribution after the calibration process. When the groundwater level change is compared to the initial groundwater level in Figure 3.16, it becomes evident that the groundwater level in the central area of the basin decreased dramatically. It is

estimated that the average water table drop is 0.43 m/year over the entire domain and 0.62 m/year in the agricultural regions.

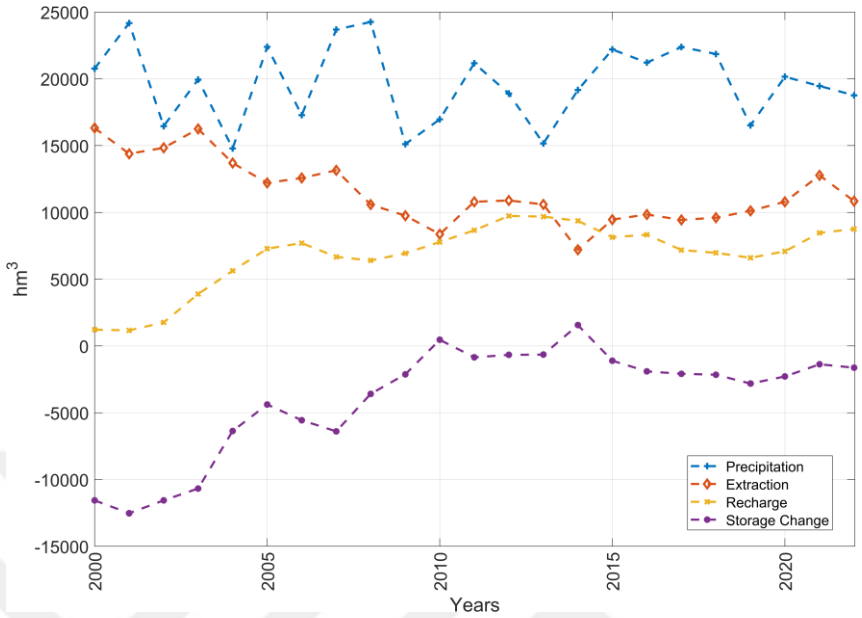

Figure 5.10. Annual water budget for the basin from January 2000 to December 2022.

Using the calibrated model, it is possible to estimate the annual budget for the entire KCB. Figure 5.10 shows the annual water budget for the period between 2000 and 2022. All quantities depicted in this figure are expressed as annual volumes in units of hm^3. For example, the precipitation volume is calculated as the precipitation rate multiplied by the basin area. It is observed that in the initial few years, the extraction was high due to low irrigation efficiency. It is estimated that the groundwater extraction in these years was about 3 times more than the total precipitation the basin received. As a result, the storage decreased dramatically. In the later years, the decrease in storage change slowed down due to enhanced irrigation efficiency, despite that irrigated lands expanded and gradual switch to more water demanding crops occurred. Table 5.1 shows the average water budget for the 23 year period between 2000 and 2022 expressed in units of hm^3 and mm. It is observed that the extraction exceeds the recharge resulting in a negative change in storage.

Table 5.1. Annual water budget from the 2000 to 2022.

Unit	**Precipitation**	**Extraction**	**Recharge**	**Storage Change**
hm^3	19685	11010	6757	-4269
mm	387	217	133	-84

5.4. Sensitivity Analysis

Unsaturated zone flow is important for groundwater modelling for several reasons. Firstly, the inclusion of unsaturated zone flow enables a more realistic representation of the complex processes occurring within the unsaturated zone, which is located above the water table and contains both air and water. Understanding saturated flow dynamics sheds light on the soil moisture distribution which plays an important role in quantifying the water that percolates through the unsaturated zone, recharging the underlying aquifer system. This information is essential for sustainable groundwater management, particularly regions highly relying on groundwater use such as the KCB. Sensitivity analysis evaluates how variations in key model input parameters impact the output of the model.

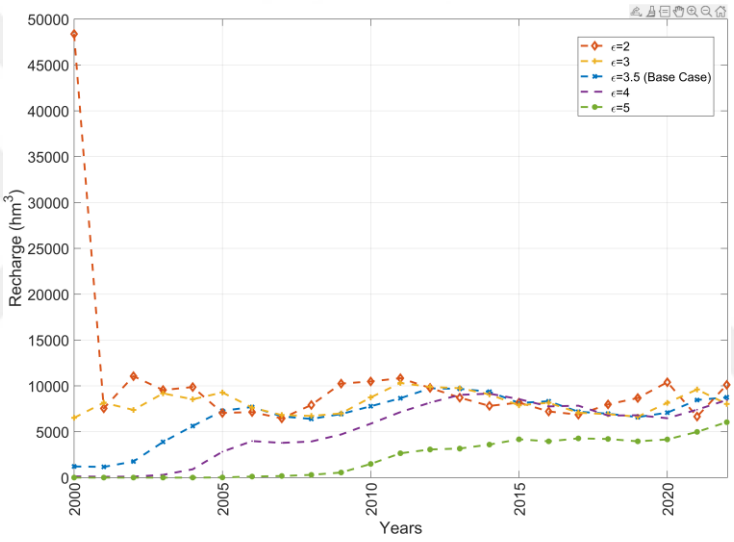

(a)

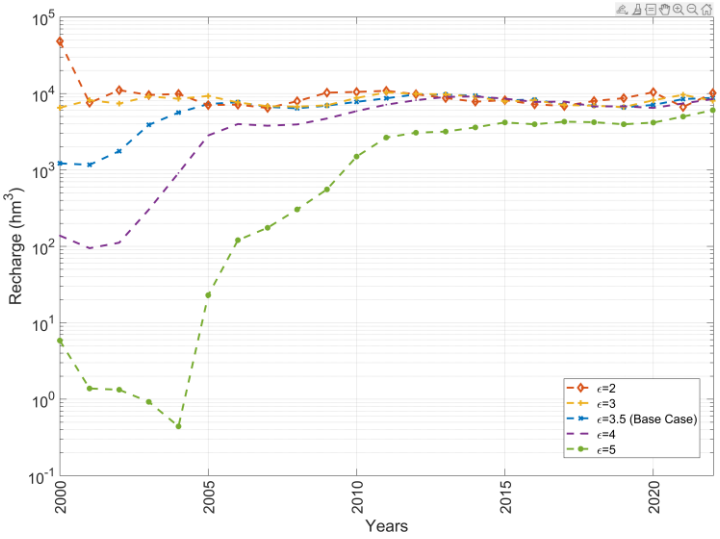

(b)

Figure 5.11. Impact of Brooks-Corey exponent on recharge (a) normal plot and (b) log-log plot.

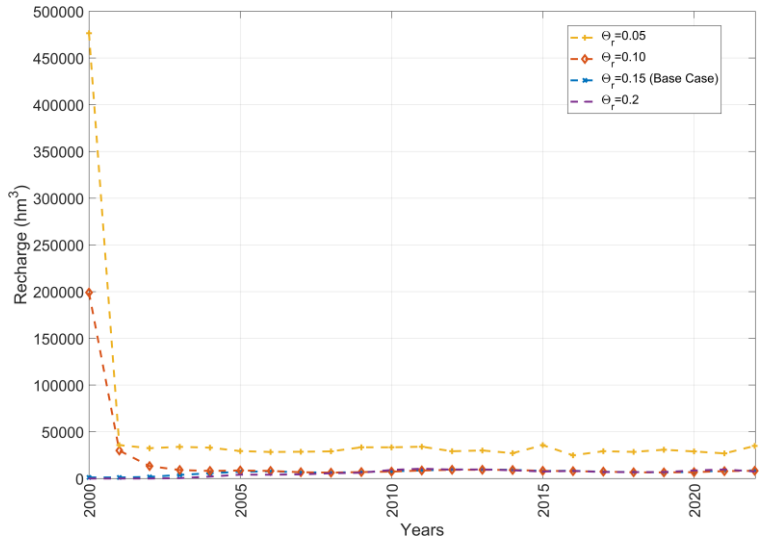

(a)

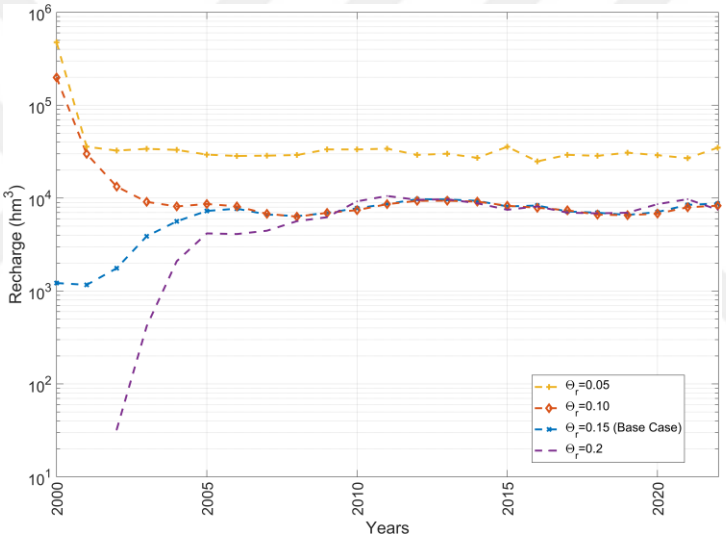

(b)

Figure 5.12. Impact of residual water content (θ_r) on recharge (a) normal plot and (b) log-log plot.

This section focuses on the sensitivity of the vadose zone parameters on the aquifer recharge rate because of the significance of the unsaturated zone processes. The parameters that are investigated as the Brooks-Corey parameters described in Equation 2.4 (Section 2.3.4). Specifically, we examine the impact of Brooks-Corey exponent and the residual and saturated moisture contents on the unsaturated hydraulic conductivity and subsequently the recharge. Figure 5.11 shows the impact of Brooks-Corey exponent on recharge expressed in units of hm^3. Higher Brooks-Corey exponent (ε) yield lower hydraulic conductivity which cause lower recharge, especially during the initial time step.

Figure 5.12 shows the impact of residual water content on recharge. During these simulation, initial water content is assumed as constant equal to 0.16. When the residual water content is high,

there is less mobile water content, resulting in less recharge. In the figure, residual content of 0.2 is greater than initial water content, so there is no recharge during the initial time steps. On the other hand, the excess moisture drains more in the first couple of years while the residual water content is low.

Figure 5.13 represents the impact of saturated water content on recharge. As saturated water content increases, the recharge decreases due to lower unsaturated hydraulic conductivity.

Overall, this analysis demonstrates the importance of accurately defining the vadose zone soil parameters. In this study, average values dependent on soil type were utilizing.

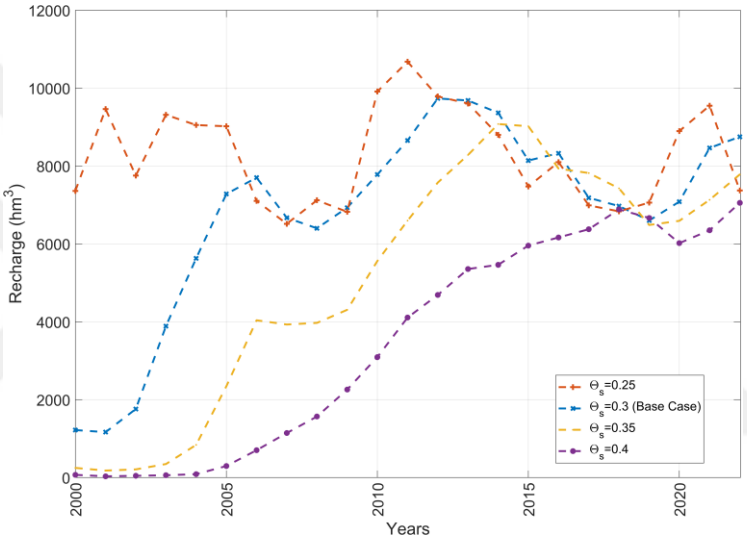

(a)

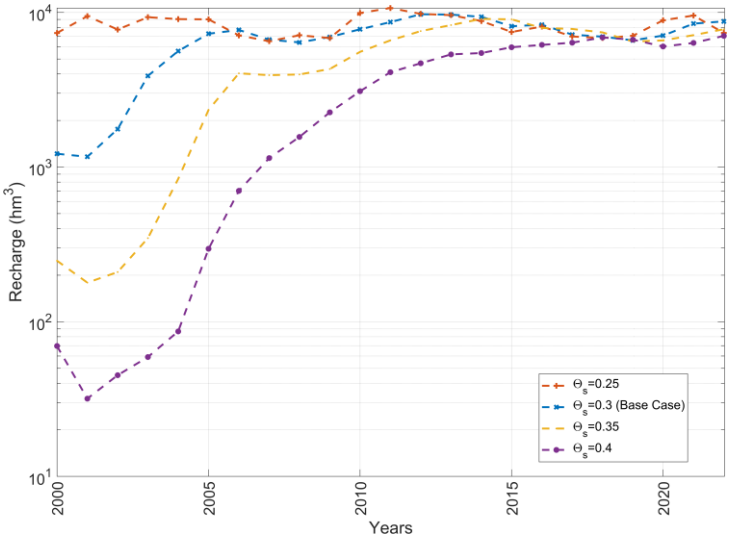

(b)

Figure 5.13. Impact of saturated water content (θ_s) on recharge (a) normal plot and (b) log-log plot.

5.5. Simulations of Scenarios

The calibrated model was then used to evaluate five different future scenarios taking into account climate projections and changes in irrigation practices. The scenarios are described in Section 4.3.7. For each scenario, 34 simulations were performed each corresponding to one of the 17 available RCMs under two climatic pathways, RCP 4.5 and 8.5. The future scenarios were simulated until the end of year 2040.

5.5.1. Business as Usual Scenario

The business as usual scenario is characterized by the absence of substantial alterations in policy or behavioral pattern. It assumed that the trend in cropping that occurred in the years 2000-2022 continues into the future (Figure 4.9). The simulations were performed with monthly stress periods with groundwater extraction calculated to cover domestic water needs and irrigation deficits.

The monthly head calculated by spatially averaging over the entire domain and for the 17 simulations (corresponding to the 17 RCMs) is plotted Figure 5.14. The blue dotted line on the figure shows the calibrated model result between 2000 and 2022. Fan plot is used to depict the uncertainty of the simulation of the various RCMs under different climatic pathways. The black line shows the median head for climatic pathways of RCP 4.5 and RCP 8.5. The shaded blue region in the plot shows the interval between first quartile (25^{th} Percentile) and third quartile (75^{th} Percentile) of groundwater level derived from simulations corresponding to the 17 RCMs for the RCP 4.5 climatic pathway. The gray filled range indicates the interval between minimum and maximum groundwater head based on the same simulations. The shaded red area indicates the interval between the first quartile (25th percentile) and the third quartile (75th percentile) of groundwater level values, corresponding to the 17 RCMs under RCP 8.5 scenario. Likewise, a light pink filled area displayed on the graph, shows the range between the minimum and maximum groundwater levels.

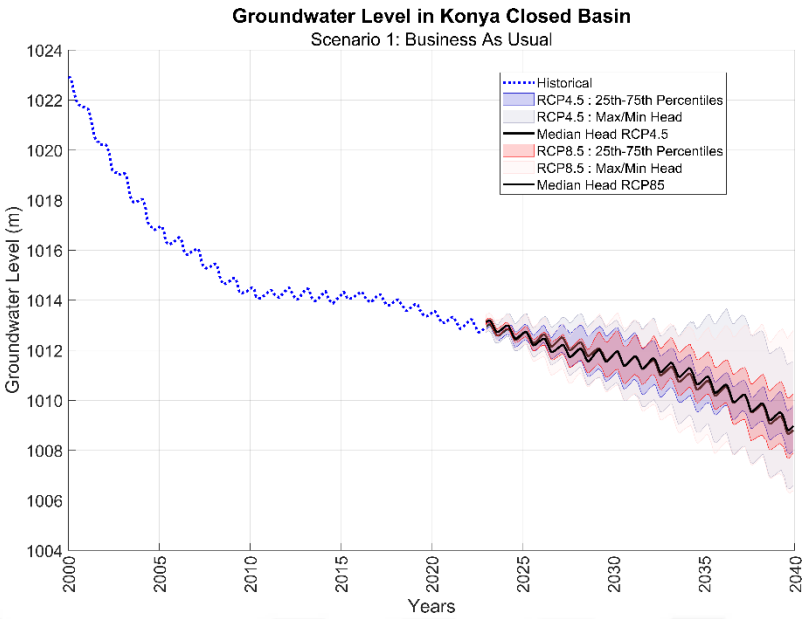

Figure 5.14. Predicted groundwater level averaged over the entire basin for the business as usual scenario for RCP 4.5 and 8.5.

Figure 5.14 shows that there is a dramatic drop in the average groundwater level, approximately 0.9 meters per year, between 2000 and 2010. Between the years 2010 and 2015 and as a result of incentives, many farmers switched to more efficient irrigation technologies (higher irrigation efficiency). This led to a temporary stabilization of the water levels. However, the switch to more demanding crops and expansion of irrigation lands again led to a drop in groundwater levels starting from 2016, albeit at a lower rate than the rate that occurred in the years between 2000 and 2010. The average drop in groundwater level between 2015 and 2022 was 0.14 meter per year.

For the business as usual scenario, it is observed that the rate of groundwater drop will continue to gradually increase in the coming years. The average annual drop in groundwater level between the years 2023 and 2040 ranged between 0.02 and 0.39 per year for individual climate projections, with an average of 0.28 meter per year.

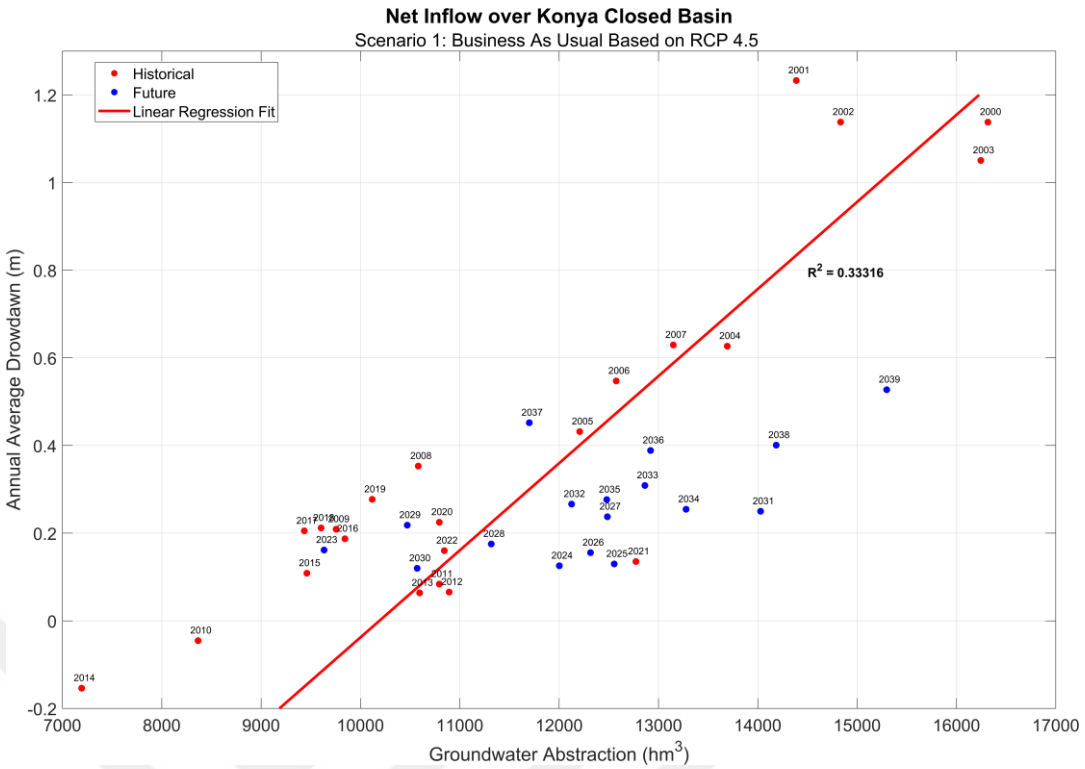

Figure 5.15. Net inflow graph for the business as usual scenario for the KCB based on RCP4.5.

The future predictions can also be evaluated using the concept of net inflow (Butler et al., 2023). The concept of inflows shows the relation between annual abstraction and annual drop in groundwater levels in heads. It considers the change in water levels due to all inflows and all outflows (lateral, precipitation, irrigation, extraction, evapotranspiration, etc.) into an aquifer system plotted against the anthropogenic groundwater extraction. For sustainable use of the available groundwater resources, it is desirable that the long-term average drawdown remains near zero. This means that the groundwater reserve is used in a sustainable way whereby small annual drawdown in dry years are balanced out by excess water in wet years.

Figure 5.15 and Figure 5.16 show the annual average groundwater level drop versus groundwater abstraction based on climatic pathways RCP 4.5 and RCP 8.5, respectively. Historical results are shown in blue whereas forecasted results are in red. The red lines in the graphs represent the linear regression fit to all points which show an average relation between groundwater abstraction and annual average drawdown. It is observed that historical years fall in 3 general clusters: relatively high annual drawdowns in the years 2000-2010 followed by near zero drawdown for the years 2010-2016 and followed by gradually increasing annual drawdown in the years 2016 to the present. Future years show a continued annual drawdown indicating that the system is far from sustainable and that the benefits from the switch to more efficient irrigation systems is gradually eroding.

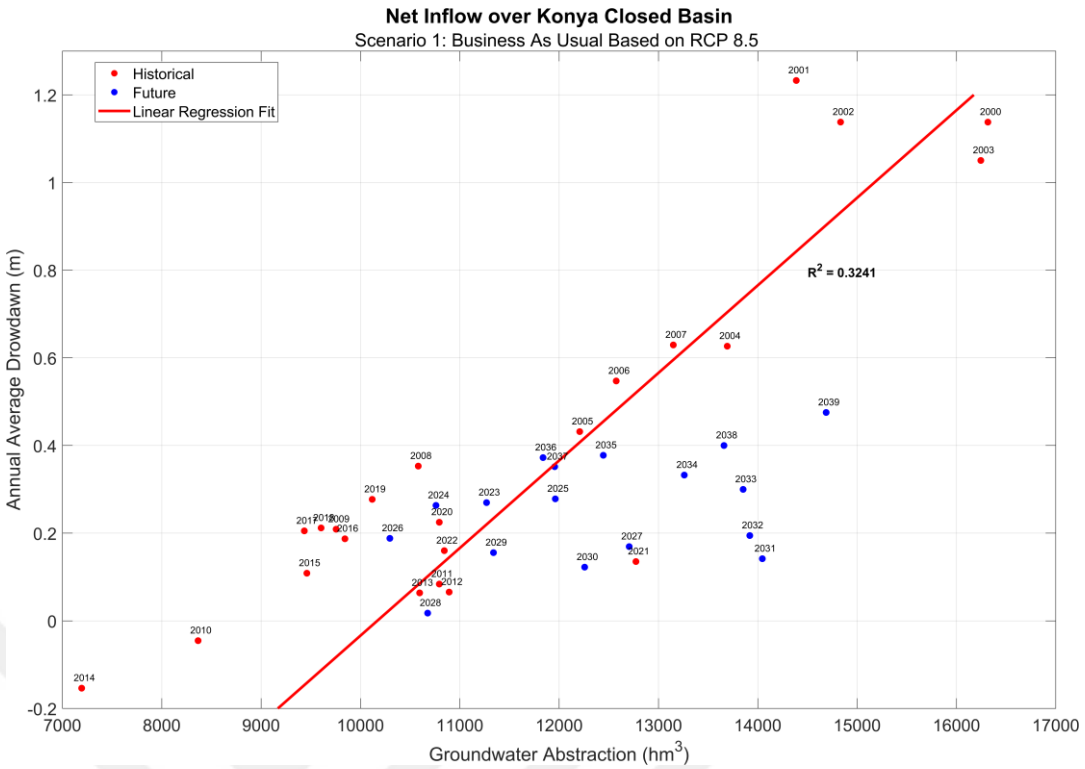

Figure 5.16. Net inflow graph for the business as usual scenario for the KCB based on RCP8.5.

Although the figures presented above give a general idea about water use over the entire basin, they do not provide any spatial information regarding the distribution of groundwater level in the study area. The spatial variation of groundwater level is particularly useful for effective water resource management and decision-making at the local scale. They provide a visual representation of the spatial distribution of groundwater levels across the study area. Spatial information is essential since it enables to identify spatial patterns and trends in groundwater level. It allows to locate areas of high or low groundwater availability and identify potential areas of concern. Figure 5.17 and Figure 5.18 provide a visual representation of the spatial distribution of groundwater levels across the study area.

It is important to note that these graphs show the mean groundwater level data derived from 17 Regional Climate Models (RCMs) under each climatic pathway. While they provide valuable spatial insights, it's crucial to emphasize their temporal limitation.

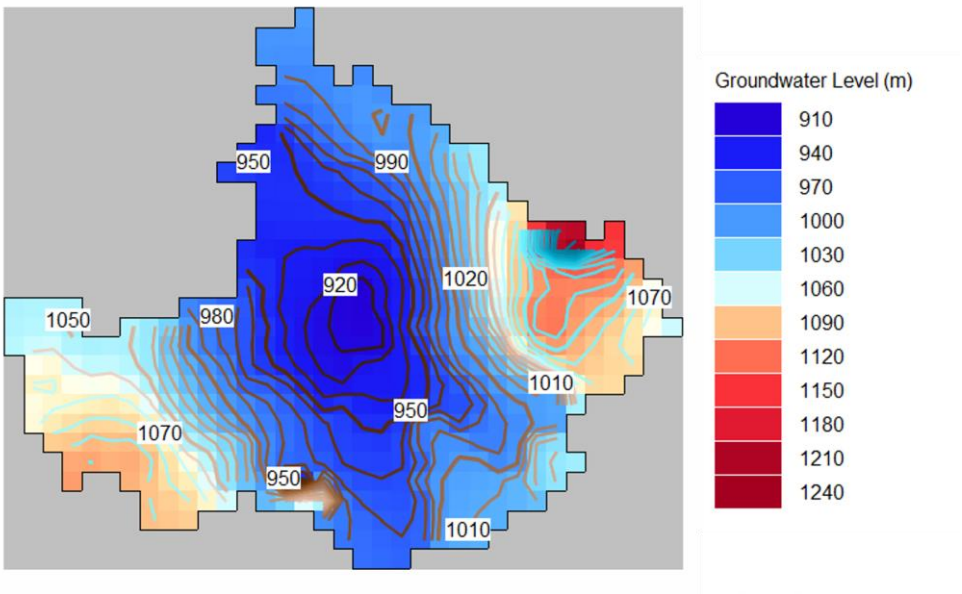

Figure 5.17. Spatial distribution of mean groundwater level for year 2040 based on 17 RCMs under RCP4.5 climatic pathway according to business as usual scenario.

When the groundwater level is compared to the groundwater level distribution at the end of historical period in Figure 5.9, the decline in groundwater levels persists under business as usual scenario particularly in the central regions of the model. It is also important to point out that the groundwater level drop continues in southern parts of the basin as well where several towns such as Çumra and Karapınar with substantial agricultural production will experience significant impacts.

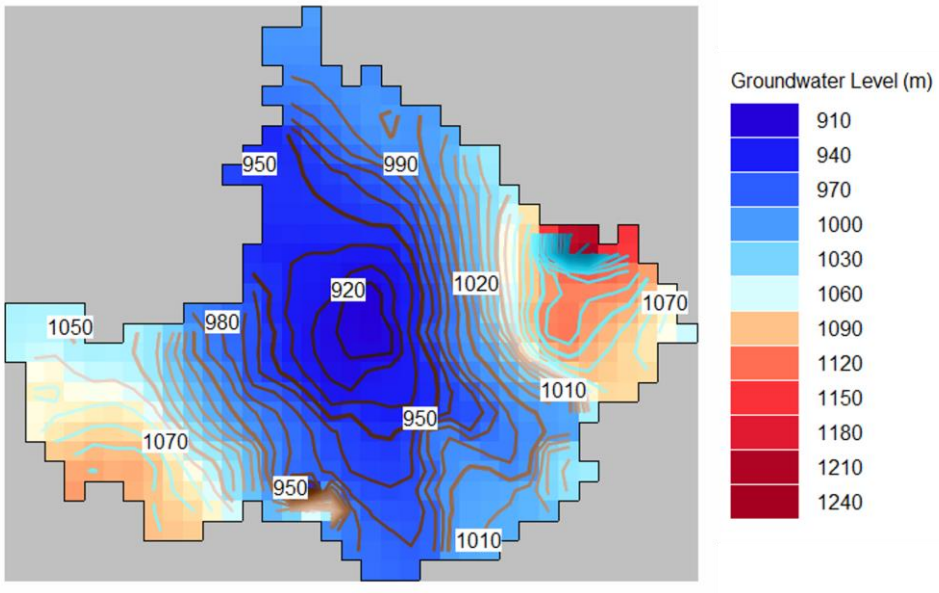

Figure 5.18. Spatial distribution of mean groundwater level for year 2040 based on 17 RCMs under RCP8.5 climatic pathway according to business as usual scenario.

5.5.2. Corn Phased Out Scenario

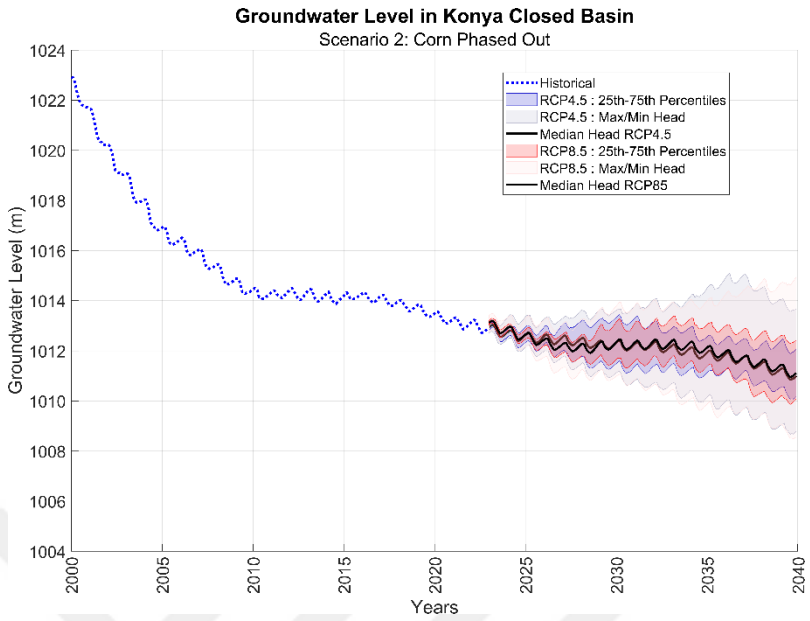

Figure 5.19. Groundwater level over entire basin for corn phased out scenario.

For the corn phased out scenario, corn cultivation is assumed to be phased out gradually between the years 2023-2028 with the goal of rolling back cultivation of corn to 2005 levels. The phased-out corn is replaced with wheat cultivation, the historical crop of the KCB. All other input data are the same as the business as usual scenario.

Figure 5.19 shows the average groundwater level for the entire Konya Closed Basin for corn phased out scenario. The historical curve is that obtained from the calibrated model as shown also for the business as usual scenario (Figure 5.14). The model predicts for this scenario the average annual drop in groundwater level between 2023-2040 ranges between 0.09 meter per year increase and 0.31 meter per year with an average of 0.11 meter per year. The groundwater drop is predicted to be about 40% of that predicted for the business as usual scenario.

Figure 5.20 and Figure 5.21 show the annual average drawdown in groundwater level versus groundwater abstraction for corn phased out scenario, based on climatic pathways of RCP 4.5 and RCP 8.5 respectively. Blue points show the historical result while red points show the forecasted results. The red line featured in both figures denote linear regression fit applied to all data points. Future years are seen closer to the zero, however annual drops remain consistently positive.

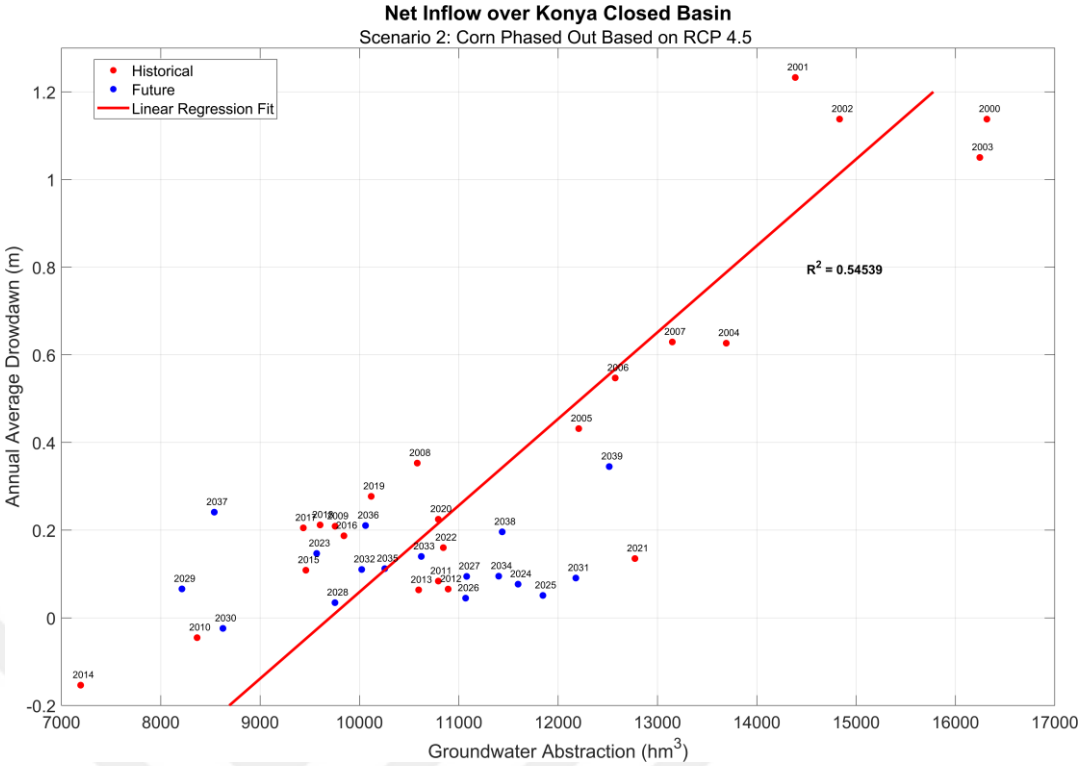

Figure 5.20. Net inflow graph for the corn phased out scenario for the KCB based on RCP4.5.

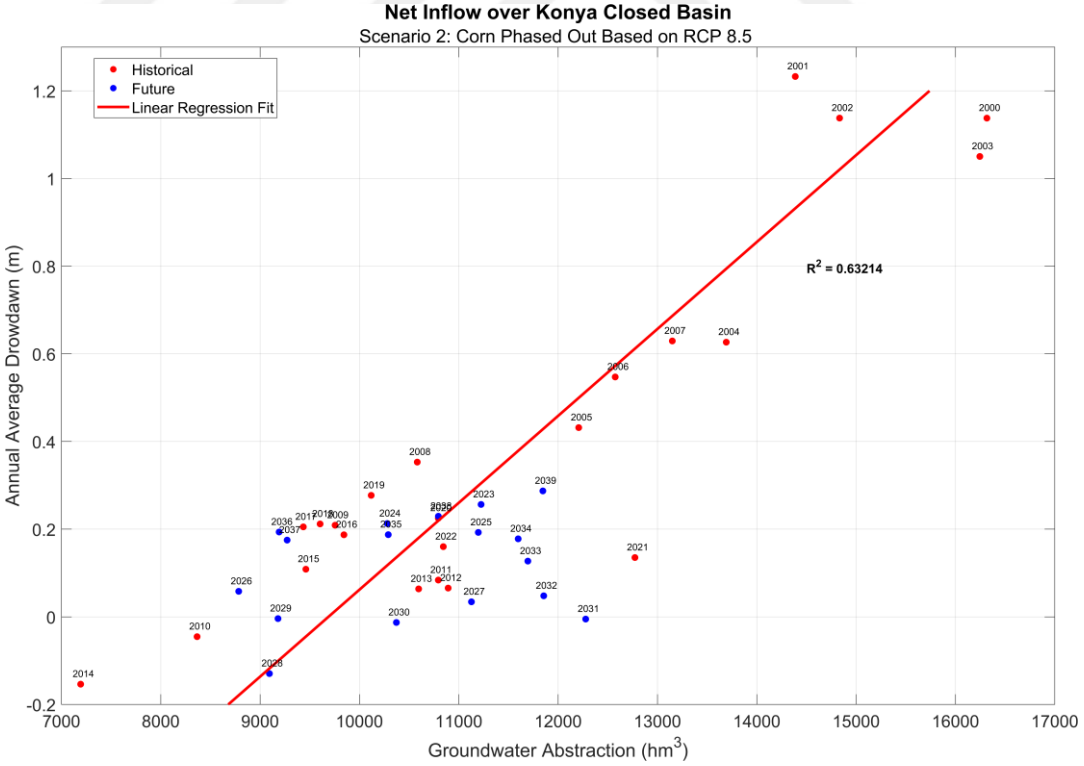

Figure 5.21. Net inflow graph for the corn phased out scenario for the KCB based on RCP8.5.

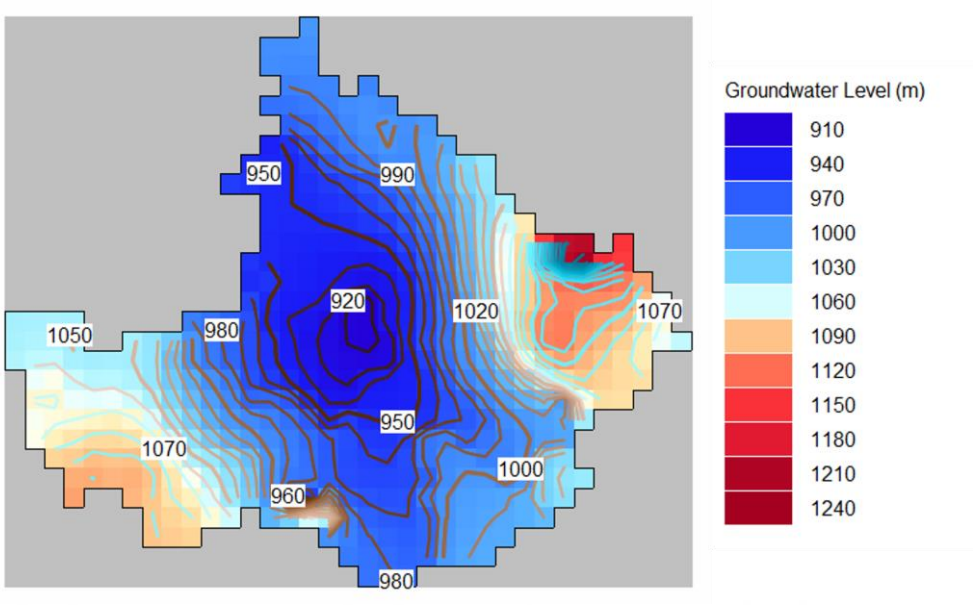

Figure 5.22. Spatial distribution of mean groundwater level for year 2040 based on 17 RCMs under RCP4.5 climatic pathway according to corn phased out scenario.

Figure 5.22 and Figure 5.23 shows the spatial distribution of groundwater level for RCP 4.5 and RCP 8.5 climatic pathway, respectively. Relative to business as usual scenario (Figure 5.17 and Figure 5.18), the corn phased out scenario show some slow down in groundwater level decline. However, heads are consistently lower than those for 2022 (Figure 5.9).

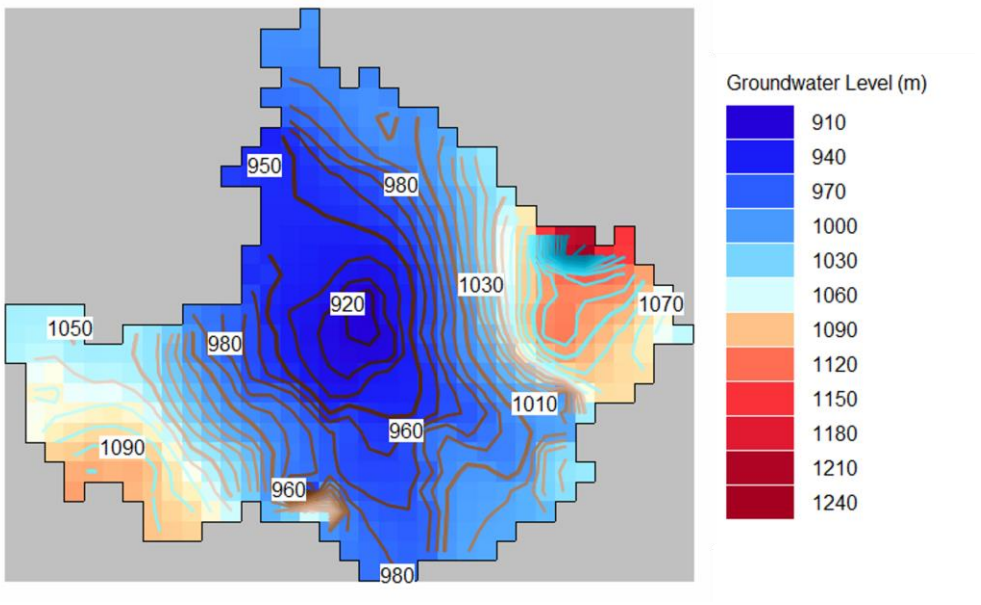

Figure 5.23. Spatial distribution of mean groundwater level for year 2040 based on 17 RCMs under RCP8.5 climatic pathway according to corn phased out scenario.

5.5.3. Increase in Irrigation Efficiency Scenario

Retaining all the other factors and components of model same, a progressive increase in irrigation efficiency scheme was assumed in this scenario. The irrigation efficiency was increased gradually to 80% between 2023 and 2028. After 2028, irrigation efficiency remains constant. All other input parameters are similar to those of the business as usual scenario. This is an ambitious scenario requiring farmers to switch to pressurized closed irrigation systems and avoiding excessive irrigation beyond that recommended for the cultivated crops.

The mean groundwater level for the entire KCB is plotted for this scenario in Figure 5.24. Between 2023 and 2040, the average annual drop in groundwater level ranges between 0.15 meter per year increase and 0.19 meter per year decrease with an average of 0.06 m/year. Although this scenario predicts close to zero average drawdown, it is observed that the drawdown is increasing in the later years 2035-2040. This suggests that the benefits of switching to more efficient irrigation by itself will keeping current cropping trends as they would be short lived.

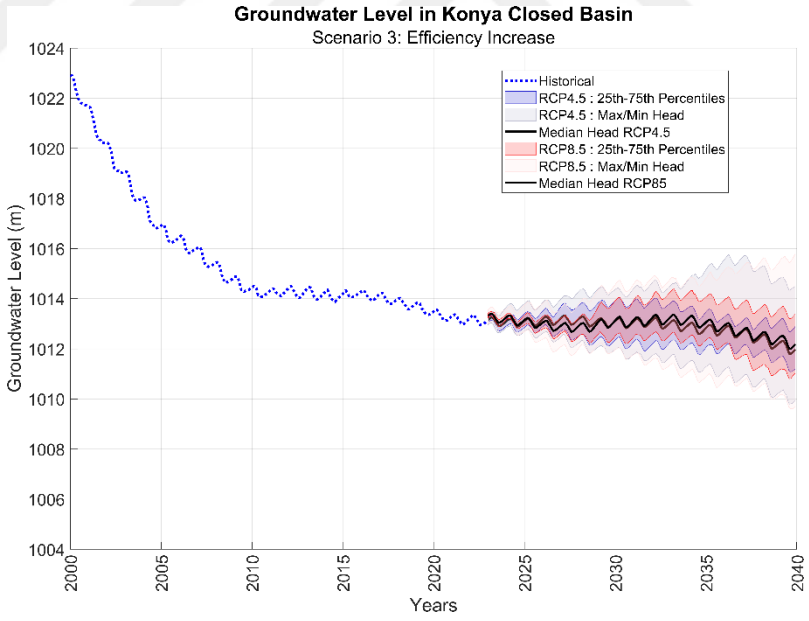

Figure 5.24. Groundwater level over entire basin for efficiency increase scenario.

Figure 5.25 and Figure 5.26 illustrate the annual mean drawdown in groundwater level versus groundwater abstraction for RCP 4.5 and RCP8.5 climatic pathway respectively based on the irrigation efficiency increase scenario. The historical outcomes are plotted with blue data points, whereas the projected outcomes are indicated by red data points. In both figures, the red line

represents fitted linear regression model. According to forecasted result, the annual average drop over the entire basin is closer to sustainable levels but that some drawdown is still predicted with this scenario.

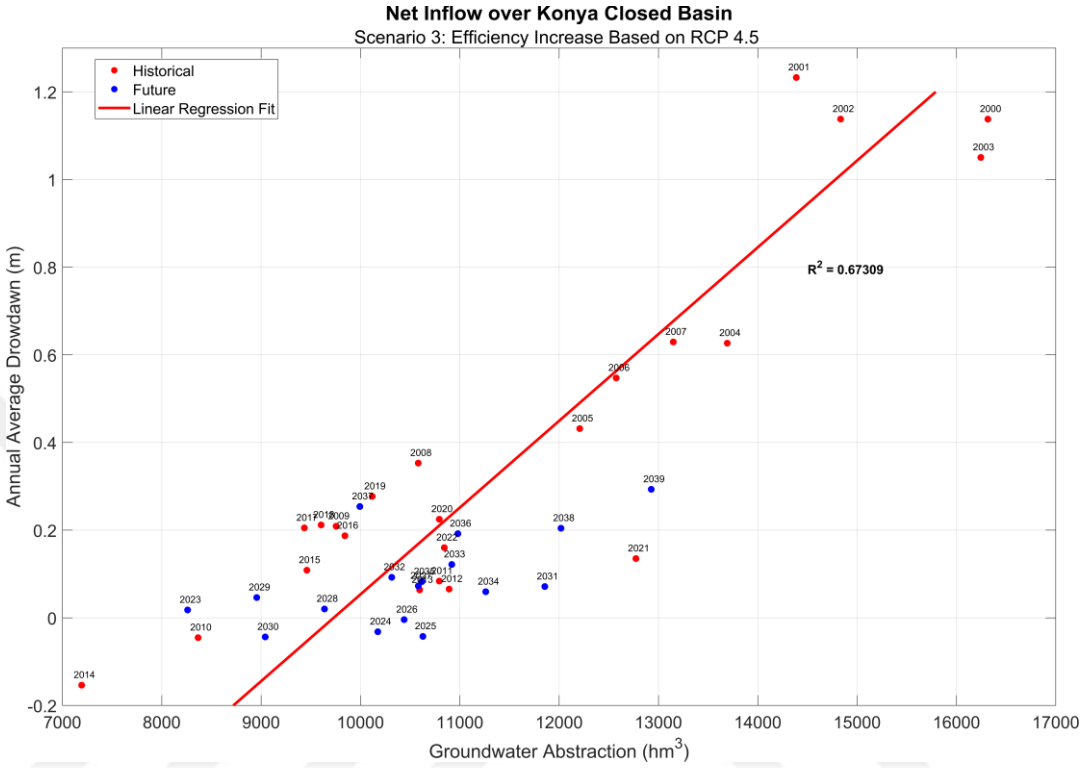

Figure 5.25. Net inflow graph for the efficiency increase scenario for the KCB based on RCP4.5.

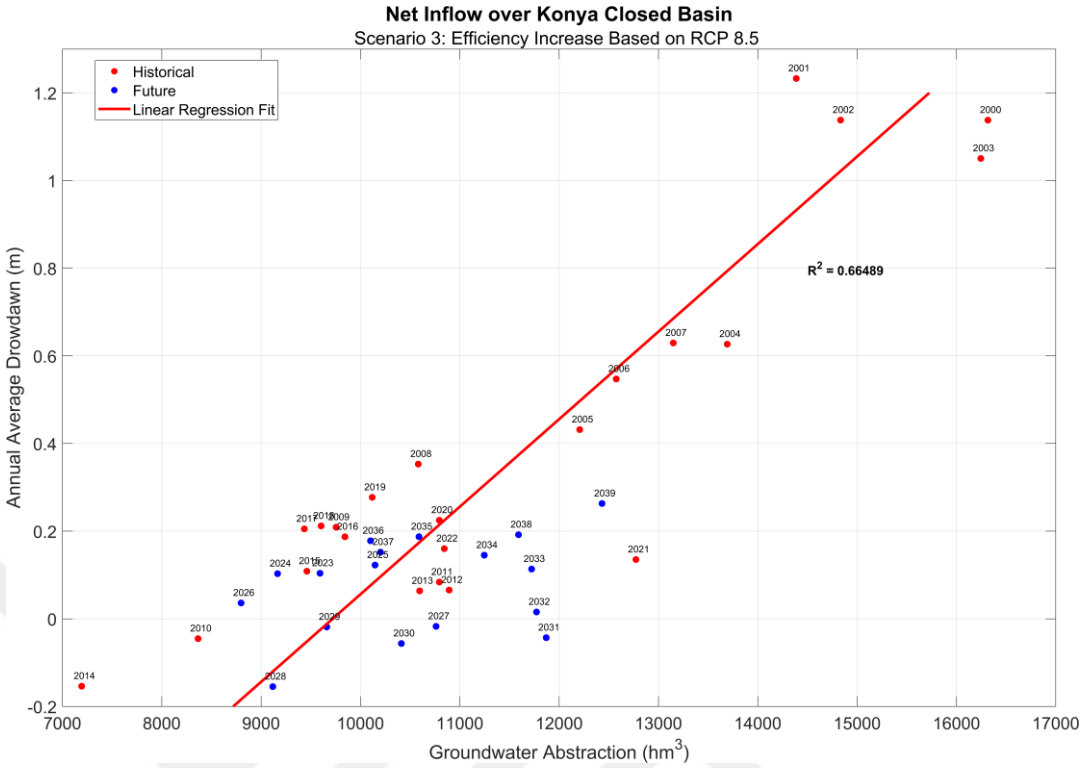

Figure 5.26. Net inflow graph for the efficiency increase scenario for the KCB based on RCP8.5.

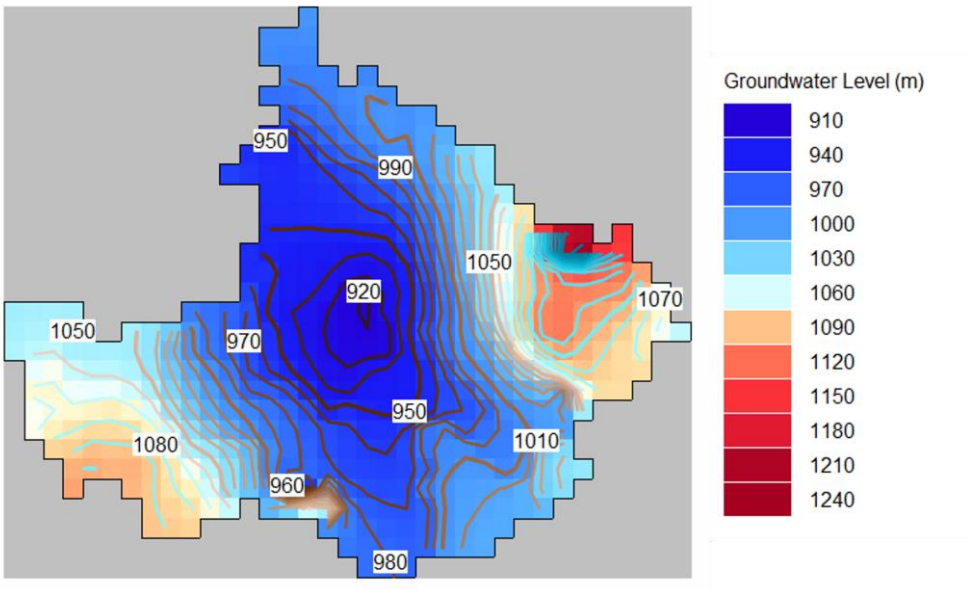

Figure 5.27. Spatial distribution of mean groundwater level for year 2040 based on 17 RCMs under RCP4.5 climatic pathway according to efficiency increase scenario.

Figure 5.27 and Figure 5.28 provides the spatial distribution of the groundwater level distribution

within the basin. Groundwater level at center of the basin shows a significant difference with respect to business as usual scenario (Figure 5.17 and Figure 5.18). Also, the drop of groundwater level in the southern region of the basin is much smaller than business as usual scenario. Efficiency increase scenario shows more significant slowdown in the groundwater level drop than corn phased out scenario. This contrast is also visually evident when examining the groundwater distribution maps.

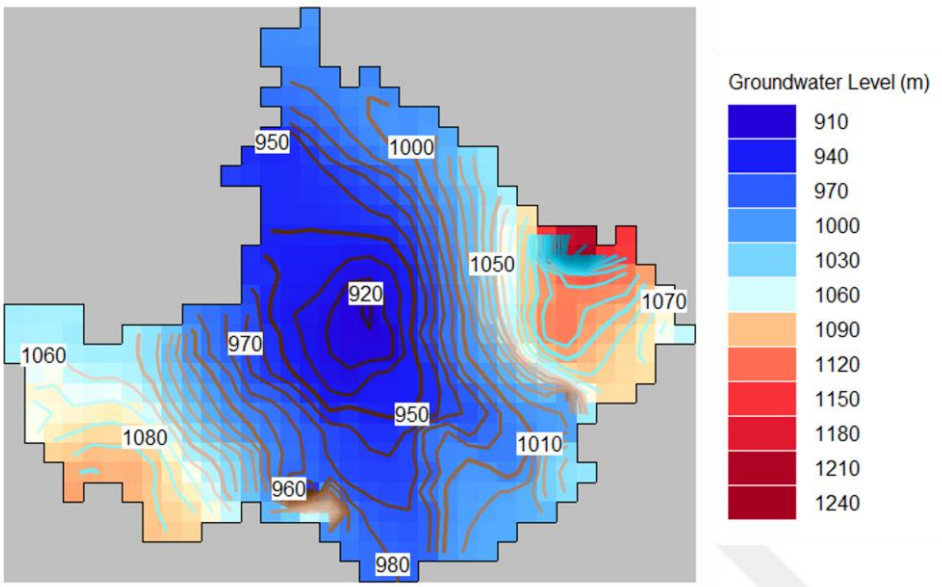

Figure 5.28. Spatial distribution of mean groundwater level for year 2040 based on 17 RCMs under RCP8.5 climatic pathway according to efficiency increase scenario.

5.5.4. Mavi Tunnel Scenario

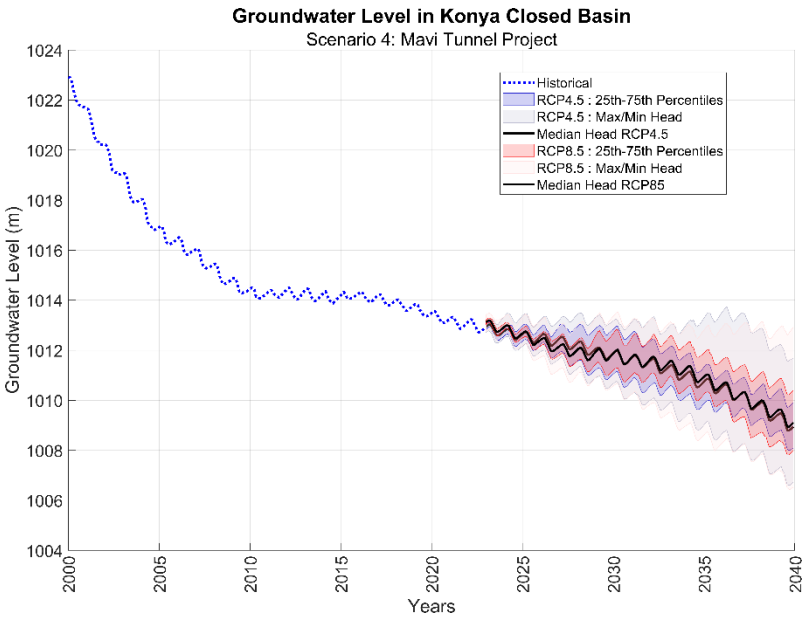

Figure 5.29. Groundwater level over entire basin for Mavi Tunnel scenario.

This scenario is similar to the business as usual scenario with additional water transfers via the Mavi Tunnel which is about to be completed. As described earlier, the Mavi Tunnel is an inter-basin water transfer project intended to bring up water from the Eastern Mediterranean Basin to the southern portions of KCB. It is assumed in this scenario that Mavi Tunnel will enable to transfer 200 hm^3 of water annually, starting the year of 2023.

The mean groundwater head over the entire basin is plotted for Mavi Tunnel scenario in Figure 5.29. The average annual groundwater level decreases 0.21 meter per year between 2023 and 2040, within the range of 0.003 meter increase per year and 0.35 meter decrease per year. The shape of the figure is similar to that of the business as usual scenario whereby the rate of drawdown will continue to accelerate with continued switch to more water-demanding crops.

Figure 5.30 and Figure 5.31 illustrate the annual mean drawdown in groundwater level versus groundwater abstraction for RCP 4.5 and RCP 8.5 respectively, corresponding to the Mavi Tunnel scenario. It is observed that the Mavi Tunnel project will have a local impact to the southern regions of KCB. However, its impact on the overall groundwater head or consumption would not be significant given that the water transfers would be a small percent of the water use within the basin.

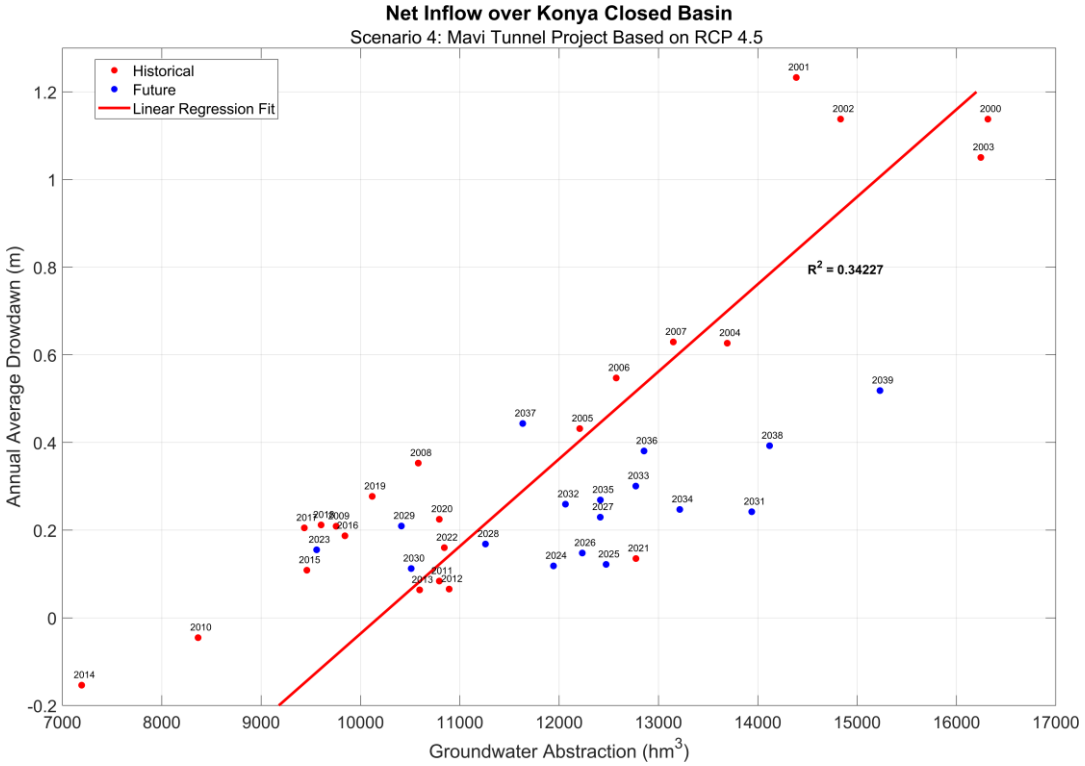

Figure 5.30. Net inflow graph for the Mavi Tunnel scenario for the KCB based on RCP4.5.

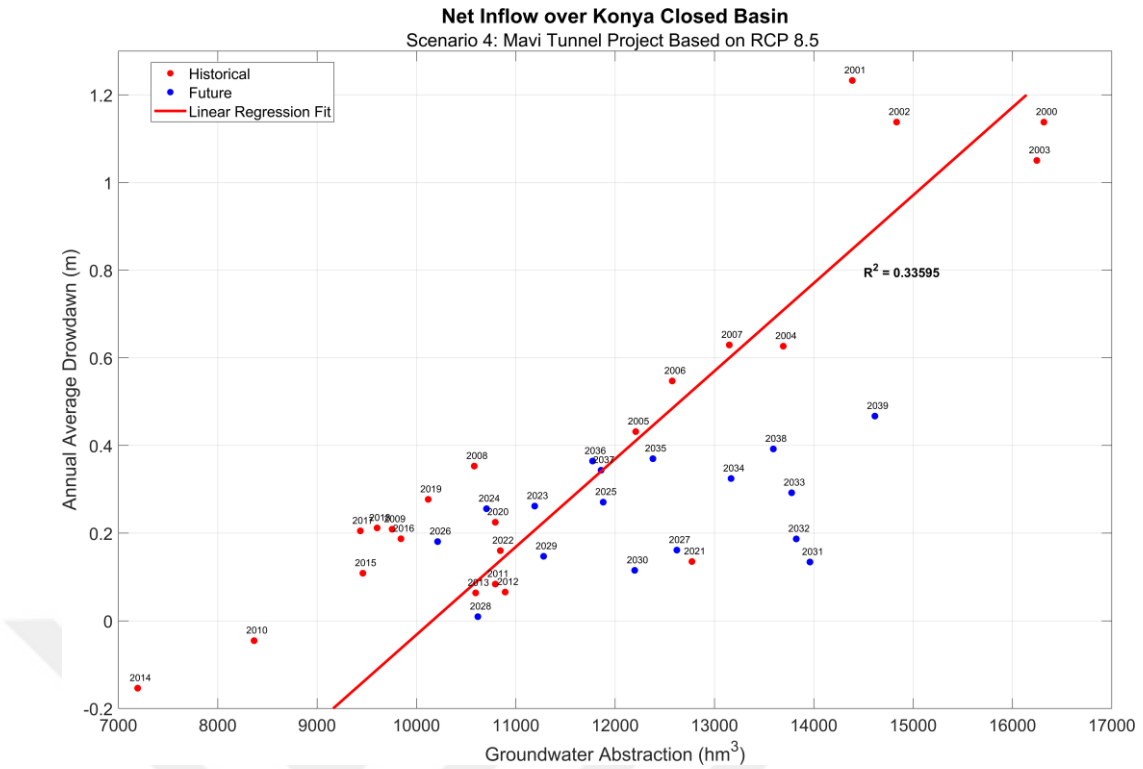

Figure 5.31. Net inflow graph for the Mavi Tunnel scenario for the KCB based on RCP8.5.

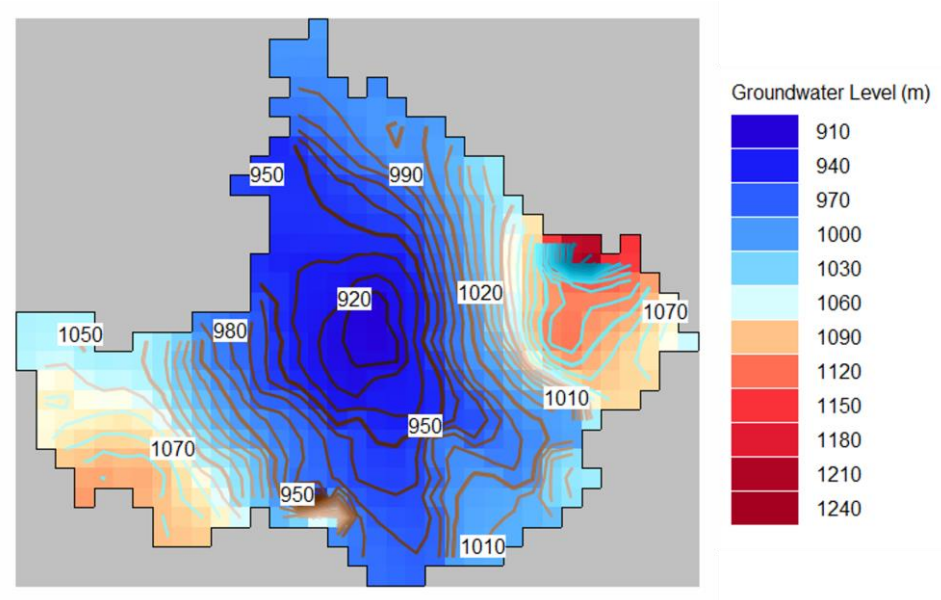

Figure 5.32. Spatial distribution of mean groundwater level for year 2040 based on 17 RCMs under RCP4.5 climatic pathway according to Mavi Tunnel scenario.

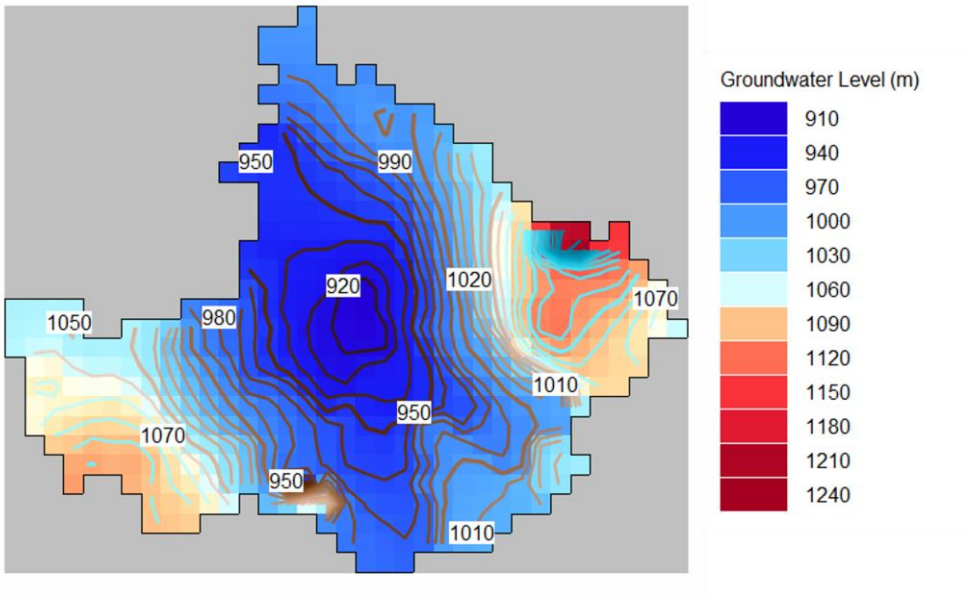

Figure 5.33. Spatial distribution of mean groundwater level for year 2040 based on 17 RCMs under RCP4.5 climatic pathway according to Mavi Tunnel scenario.

Figure 5.32 and Figure 5.33 shows the spatial distribution of the of the groundwater level throughout the basin. Since the water transfer is distributed around Çumra town for irrigation purposes, the impact of this scenario is limited to the areas around the towns of Çumra and Konya, located in the southern part of the basin.

5.5.5. Combination of Corn Phased Out and Efficient Irrigation Scenario

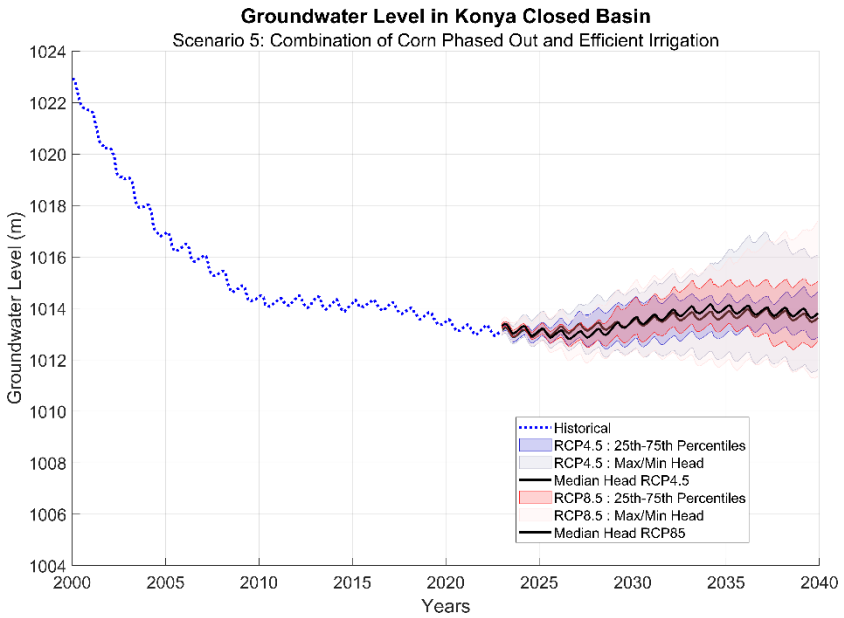

Figure 5.34. Groundwater level over entire basin for the combination of corn phased out and efficient irrigation scenario.

The last scenario considered in this study combines two previous scenarios, namely: the replacing of corn with wheat production and increasing irrigation efficiency. Figure 5.34 shows the mean groundwater head over the entire basin for this scenario. the average annual groundwater level is predicted to increase at a rate of 0.04 meter per year between 2023 and 2040, with the drop ranging between 0.22 meter increase per year and 0.10 meter decrease per year.

The annual groundwater drawdown versus annual groundwater abstraction is plotted in Figure 5.35 and Figure 5.36 for RCP 4.5 and RCP 8.5 respectively. This scenario shows that by combining advanced irrigation technology with change in cropping towards cultivating more traditional crops would lead to sustainable use of the groundwater resources in KCB.

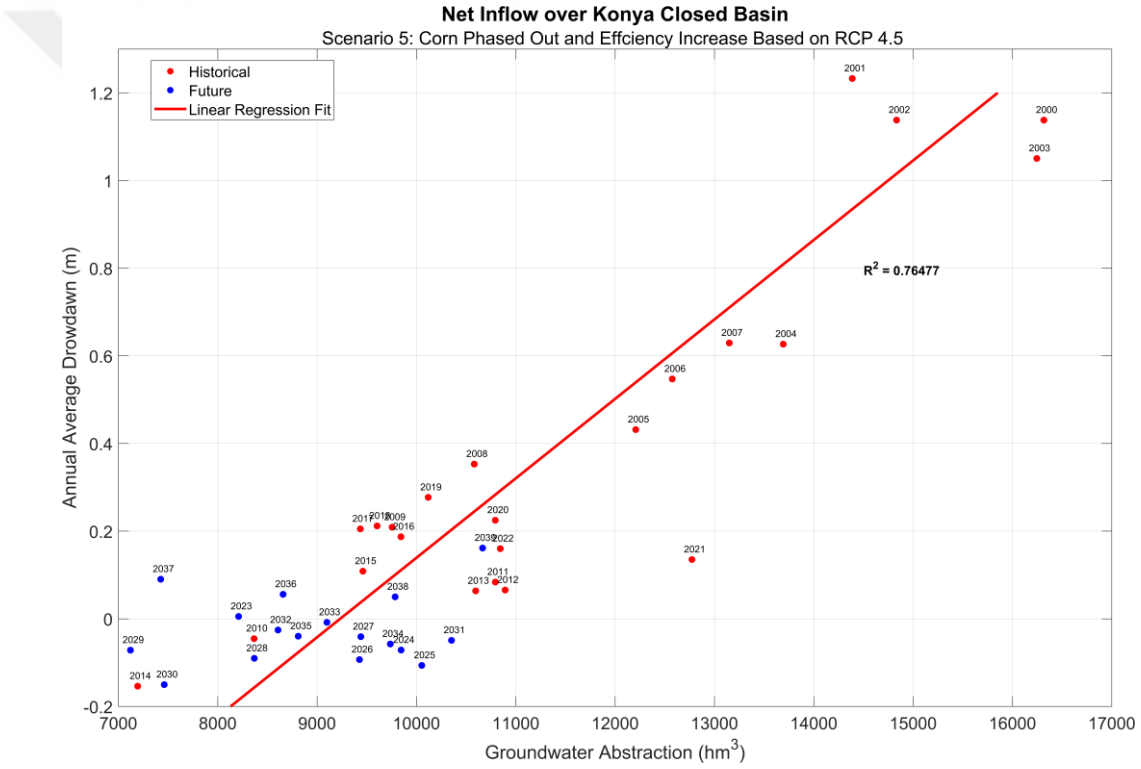

Figure 5.35. Net inflow graph for the combination of corn phased out and efficient irrigation scenario for the KCB based on RCP4.5.

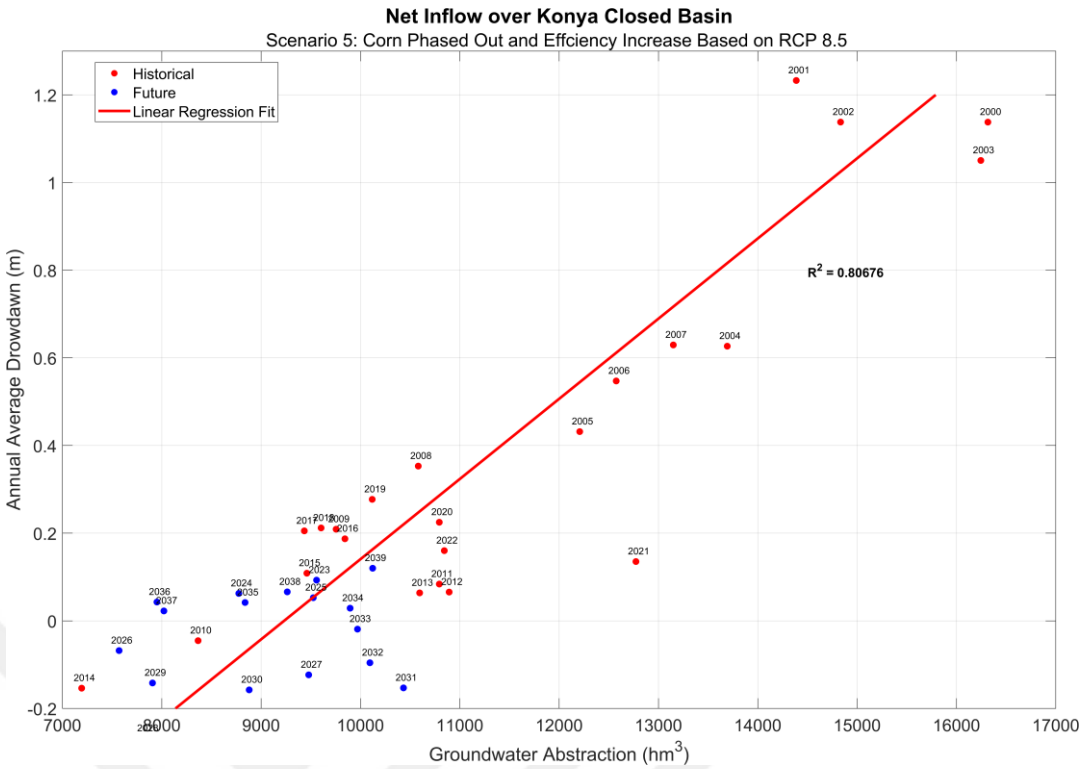

Figure 5.36. Net inflow graph for the combination of corn phased out and efficient irrigation scenario for the KCB based on RCP8.5.

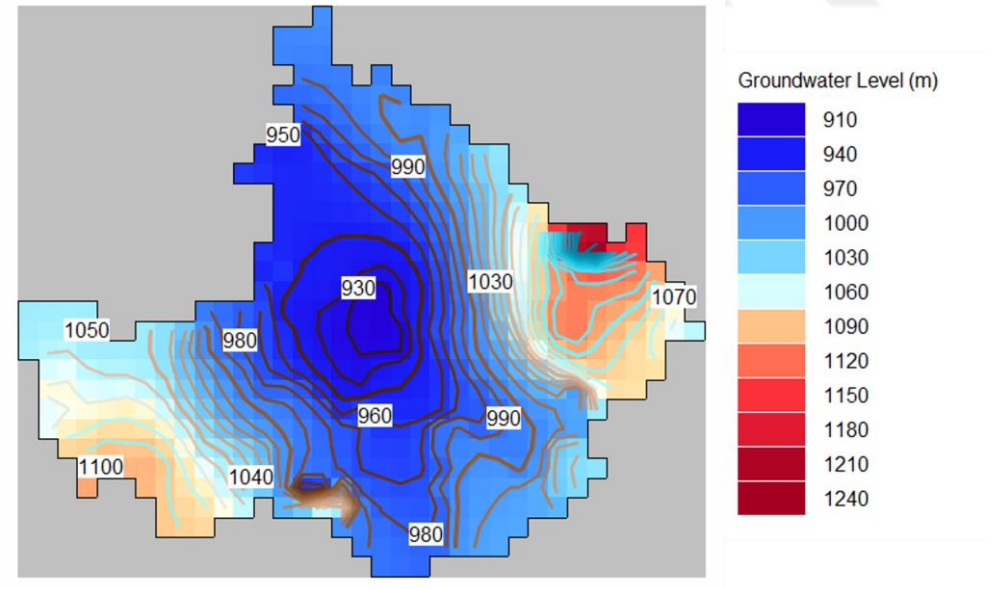

Figure 5.37. Spatial distribution of mean groundwater level for year 2040 based on 17 RCMs under RCP4.5 climatic pathway according to combination of corn phased out and efficiency increase scenario.

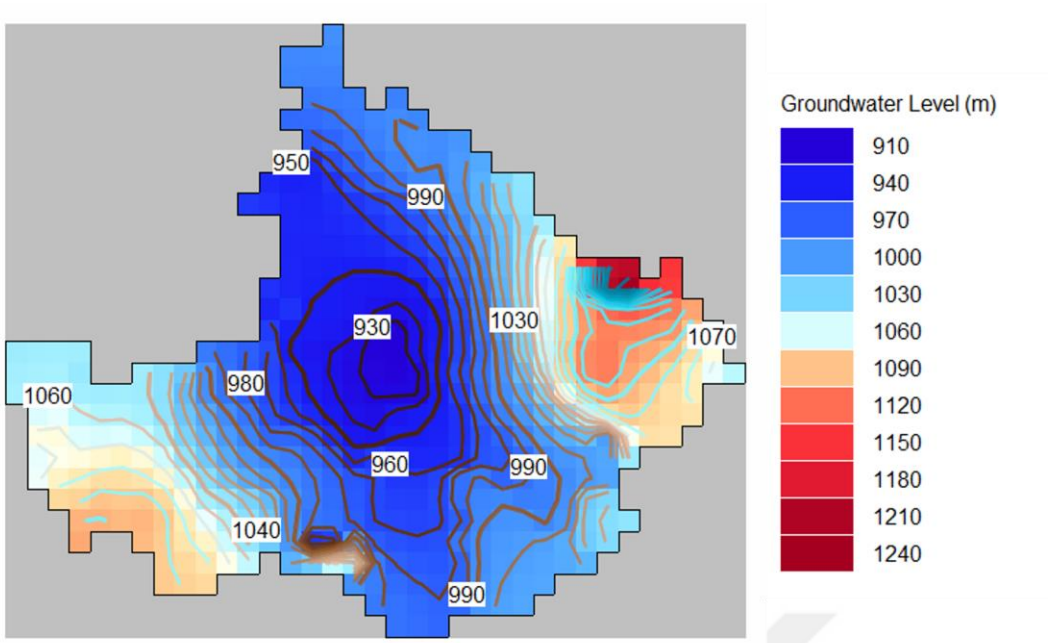

Figure 5.38. Spatial distribution of mean groundwater level for year 2040 based on 17 RCMs under RCP8.5 climatic pathway according to combination of corn phased out and efficiency increase scenario.

Figure 5.37 and Figure 5.38 depict the spatial distribution of groundwater levels across the entire basin. Notably, the concurrent application of the corn phase-out and efficiency increase scenarios shows the most effective water management strategies in terms of promoting sustainable water utilization. When compared to end of calibration period (Figure 5.9), the scenario has a positive impact on the western part of the basin.

5.6. Evaluation of Scenarios

Konya Closed Basin is a water limited environment with a semiarid climate that necessitates efficient use of its limited water resources. With agriculture being the basin's primary activity, groundwater resources become a vital resource that can buffer water demand. It can be used to provide the difference between precipitation and agricultural water demand in the summer months. However, the longevity of this resource requires that it not be used more than it is naturally replenished in the wet months. Modeling tools can be used for the management of this vital resource that is essential for food security and economic sustainability of the region.

In this study a coupled unsaturated zone and groundwater zone model was developed to provide

a tool for the detailed and reliable calculation of the basin's water balance. Water flow processes in the vadose zone have large impacts on recharge to groundwater zone. The transient calibration of the model revealed a good fit between simulated groundwater heads and observed groundwater heads. The underlying factors contributing to the disparities between simulated heads and observed heads include: uncertainty in the development of the conceptual model and the definition of the aquifer properties, errors in the manually collected observed head, errors in the interpolation of simulated head, uncertainty in defining the irrigation efficiency which, in turn, depends on a multitude of factors such as the water irrigation and distribution systems and farmer behavior, and assumption of linear increase in land use and linear increase in discharge rate from Apa Dam.

As previously noted, various studies have been carried out for Konya Closed Basin. The report of WWF(2010) highlighted that the total water consumption of the basin was 3286.1 hm^3 in 2009. Similarly, Hydrogeological Report of Konya Closed Basin (SUİŞ-Proje, n.d.-b) indicated the total water consumption rate as 3587.3 hm^3. Both reports did not provide the estimation or calculation method for the total water consumption. In this study, total water demand was estimated between 7193.9 hm^3 and 16316.3 hm^3 for historical simulation. Irrigation demand is the major driver in water demand. As explained earlier, the agricultural water demand was estimated based on potential crop evapotranspiration under optimum soil-water and agronomic conditions. However, the magnitude of difference between estimated and reported total water demand is high. The fact that the WWF analyses apply for year 2009 may partially explain the discrepancy.

The calibrated model was then used to assess a number of scenarios. These scenarios consider future climate change as predicted by various climate models and for different cropping and irrigation scenarios. The analysis of the business as usual scenario clearly shows that the alarming trend of declining groundwater heads will continue to increase in the coming years. This scenario illustrates that in the absence of any policy changes or initiatives aimed to improve irrigation technologies, drop in groundwater levels will likely accelerate with potentially drastic impacts on irrigation and agricultural production of the basin. The underlying reason for this drop in groundwater levels is expansion of agricultural land use and increase in corn cultivation. This intensification of agricultural activities, with a focus on corn, is significantly contributing to the unsustainable depletion of groundwater resources. The findings underscore the critical importance of adopting measures that address both agricultural policies and irrigation practices, as these factors are pivotal in influencing the future trajectory of groundwater levels.

The drop in groundwater level may cause an irreversible harmful impact on socio-economical

dynamics. Deeper water table means that farmers will need more electricity to pump water from deeper levels while the use of more electricity create a burden on farmers financially. In particular, small-scale farmers may allocate a larger portion of their income to energy-related expenses in future, rendering them particularly susceptible to the repercussions of policy-induced energy price hikes. This situation can influence various farmers differently. When energy prices surge, the most vulnerable groups can experience an amplified financial burden, exacerbating their existing challenges.

Examination of the other scenarios shows that inter-basin water transfer will alleviate the water deficits somewhat in the southern parts of the basin but that overall this option would be costly and have limited benefit because the volume of water transferred is only a small fraction, estimated to be about 2-4 % of the KCB water demand. Rolling back corn cultivation to its historical levels (2005 levels) or adopting higher efficiency in irrigation on their own may not be adequate for sustainable use of the groundwater resource. However, combining these two scenarios shows that the drop in groundwater level can be halted and possibly reversed in some regions of the basin. This scenario would require commitment of farmers to reduce corn cultivation in the basin, adopt high efficiency irrigation technology and avoid excessive irrigation beyond that recommended for the cultivated crops.

6. CONCLUSIONS

The primary objective of this study is to develop a coupled unsaturated/saturated-groundwater model for the Konya Closed Basin, one of the main agricultural regions of Turkey. The model serves as a tool to assess variation in groundwater levels for various cropping and irrigation patterns and due to climate change as predicted by various Regional Climate Model (RCMs) for two climatic pathways of RCP4.5 and RCP8.5. The transient model was developed and calibrated for the period between January 2000 and December 2022. The model was calibrated against 29 long term groundwater monitoring wells.

The calibrated model was then used to simulate groundwater levels until year 2040. The examination of the groundwater dynamics within the basin reveals that the groundwater levels in the past 2 decades have dropped significantly and that this rate of drop will continue into the future if drastic changes in cropping and cultivation are not adopted. The dramatic decline in groundwater levels underlain the unsustainable use of available water resources with potentially serious impacts on food production and livelihood of the inhabitants of the region. Results from simulations revealed that cultivation of corn, a key crop in the agricultural production of the region that has drastically increased in recent years, has emerged as a predominant contributor to the drop in groundwater levels. This emphasizes the significance of effective strategies to manage water usage in order to mitigate the adverse impacts of increased corn cultivation. Model simulations also show that the scenario of inter-basin water transfer which is favored by many farmers would not drastically reverse the drawdown trends observed in the past 2 decades.

Among these different scenarios considered in this study, one of the scenarios underscores a promising solution. The assessment of historical crop patterns, particularly the winter wheat cultivation, coupled with the incorporation of enhanced irrigation efficiency, showed a potential to approach sustainable utilization of groundwater resources. This strategic combination not only aligns with sustainable water management principles but also provides a practical pathway to reverse the escalating trend of declining groundwater levels.

It is evident from our findings that the challenge of the drop in groundwater levels can be effectively addressed through a serious and concerted efforts. By promoting the historical dominance of winter wheat cultivation while simultaneously increasing irrigation efficiency, a harmonious equilibrium can be achieved between agricultural productivity and the preservation of limited water

reserves. This approach demonstrates the effectiveness of sensible agricultural and water management practices in guiding the basin towards a future with more sustainable and resilient water resources.

In considering the possible avenues for future research based on the conclusions of current study, there are several remarkable directions that have potential for contributing to our understanding of water use in the Konya basin. These suggestions include:

- Development of a more comprehensive surface-subsurface water flow model: This could involve the integration of detailed geology of the region to create a more detailed representation of water movement within the aquifer system.
- Incorporation of high-resolution data: The capabilities and accuracy of the model could be improved by utilizing finer-scale data. This approach could provide more detailed picture of aquifer system's behavior. Also, it may allow for better alignment between simulation results and observations.
- Improvement of characterization of aquifer geology: Conducting additional pumping tests to define the geology of the aquifer in detailly could contribute to the accuracy of the study.
- Enhanced spatial resolution: A finer grid for the model could give more detailed insights in groundwater flow, recharge, and discharge. This higher spatial resolution could shed light on interactions that may not be noticeable at a coarser scale.
- Exploration of alternative scenarios: Expanding the scope of the study to evaluate alternative scenarios can enrich its implications.
- Model generalization: The potential to develop similar models for other regions within Turkey holds promise for extending the findings to a broader context.

REFERENCES

Abatzoglou, J. T., Dobrowski, S. Z., Parks, S. A., & Hegewisch, K. C. (2018). TerraClimate, a high-resolution global dataset of monthly climate and climatic water balance from 1958-2015. *Scientific Data*, *5*, 1–12. https://doi.org/10.1038/sdata.2017.191

Allen, M. R., Dube, O. P., Solecki, W., Aragón-Durand, F., Cramer, W., Humphreys, S., Kainuma, M., Kala, J., Mahowald, N., Mulugetta, Y., Perez, R., Wairiu, M., & Zickfeld, K. (2022). Global Warming of 1.5°C. An IPCC Special Report on the impacts of global warming of 1.5°C above pre-industrial levels and related global greenhouse gas emission pathways, in the context of strengthening the global response to the threat of climate change,. In *Global Warming of 1.5°C*. Cambridge University Press. https://doi.org/10.1017/9781009157940.003

Allen, R. G., Pereira, L. S., Raes, D., & Smith, M. (1998). *FAO Irrigation and Drainage Paper 56: Crop evapotranspiration - Guidelines for computing crop water requirements*.

Anderson, M. P., Woessner, W. W., & Hunt, R. J. (2015). *Applied Groundwater Modeling: Simulation of Flow and Advective Transport*. Elsevier Inc.

Arnold, J. G., Srinivasan, R., Muttiah, R. S., & Williams, J. R. (1998). Large area hydrologic modeling and assessment part I: Model development. *Journal of the American Water Resources Association*, *34*(1). https://doi.org/10.1111/j.1752-1688.1998.tb05961.x

Aydoğdu, A., Erk'akan, F., Keskin, N., Innal, D., & Aslan, I. (2014). Helminth communities of the Turkish endemic fish, Pseudophoxinus crassus (Ladiges, 1960): Four helminth parasites for a new host record. *Journal of Applied Ichthyology*, *30*(5), 937–940. https://doi.org/10.1111/jai.12442

Bayari, C. S., Pekkan, E., & Ozyurt, N. N. (2009). Obruks, as giant collapse dolines caused by hypogenic karstification in central Anatolia, Turkey: Analysis of likely formation processes. *Hydrogeology Journal*, *17*(2), 327–345. https://doi.org/10.1007/s10040-008-0351-9

Biswas, A., & Cheng, B. (2013). Model Averaging for Semivariogram Model Parameters. In *Advances in Agrophysical Research*. https://doi.org/10.5772/52339

Bozkurt, D., Turuncoglu, U., Sen, O. L., Onol, B., & Dalfes, H. N. (2011). Downscaled simulations of the ECHAM5, CCSM3 and HadCM3 global models for the eastern Mediterranean–Black Sea region: evaluation of the reference period. *Climate Dynamics 2011 39:1*, *39*(1), 207–225. https://doi.org/10.1007/S00382-011-1187-X

Brouwer, C., K. Prins, Heibloem, M. (1989). Irrigation Water Management: Irrigation Scheduling. In *Training manual* (Issue 4).

Brouwer, C., Prins, K., & Heibloem, M. (1989). Irrigation Water Management: Irrigation Scheduling. In *Training manual* (Issue 4).

Brunner, P., Bauer, P., Eugster, M., & Kinzelbach, W. (2004). Using remote sensing to regionalize local precipitation recharge rates obtained from the Chloride Method. *Journal of Hydrology*, *294*(4), 241–250. https://doi.org/10.1016/J.JHYDROL.2004.02.023

Bucak, T., Trolle, D., Tavşanoğlu, N., Çakıroğlu, A. İ., Özen, A., Jeppesen, E., & Beklioğlu, M. (2018). Modeling the effects of climatic and land use changes on phytoplankton and water quality of the largest Turkish freshwater lake: Lake Beyşehir. *Science of the Total Environment*, *621*, 802–816. https://doi.org/10.1016/j.scitotenv.2017.11.258

Butler, J. J., Bohling, G. C., Perkins, S. P., Whittemore, D. O., Liu, G., & Wilson, B. B. (2023). Net Inflow: An Important Target on the Path to Aquifer Sustainability. *Groundwater*, *61*(1). https://doi.org/10.1111/gwat.13233

Caló, F., Notti, D., Galve, J. P., Abdikan, S., Görüm, T., Pepe, A., & Şanli, F. B. (2017). DInSAR-Based Detection of Land Subsidence and Correlation with Groundwater Depletion in Konya Plain, Turkey. *Remote Sensing 2017, Vol. 9, Page 83*, *9*(1), 83. https://doi.org/10.3390/RS9010083

Cao, G., Scanlon, B. R., Han, D., & Zheng, C. (2016). Impacts of thickening unsaturated zone on groundwater recharge in the North China Plain. *Journal of Hydrology*, *537*, 260–270. https://doi.org/10.1016/J.JHYDROL.2016.03.049

Croitoru, L., Divrak, B. B., & Xie, J. (2016). Valuing Water Resources in Turkey: A Case Study of Beyşehir Lake. *Journal of Environmental Protection*, *07*(12), 1904–1922. https://doi.org/10.4236/jep.2016.712150

dashti, Z., Nakhaei, M., Vadiati, M., Karami, G. H., & Kisi, O. (2023). A literature review on pumping test analysis (2000–2022). *Environmental Science and Pollution Research*, *30*(4), 9184–9206. https://doi.org/10.1007/s11356-022-24440-4

Demir, V., Uray, E., Orhan, O., Yavariabdi, A., & Kuseogullari, H. (2021). Trend Analysis of Ground-Water Levels and The Effect of Effective Soil Stress Change: The Case Study of Konya Closed Basin. *European Journal of Science and Technology*, *24*, 515–522. https://doi.org/10.31590/ejosat.916026

Deutsch, C. V., & Journel, A. G. (1998). GSLIB: geostatistical software library and user's guide. Second edition. In *GSLIB: geostatistical software library and user's guide. Second edition*.

DHI. (2023). *MIKE SHE: User Guide and Reference Manual*.

Diken. (2021, July 16). *51 STK'dan ortak açıklama: Flamingo ölümlerinin nedeni yanlış tarım politikaları*. https://www.diken.com.tr/51-stkdan-ortak-aciklama-flamingo-olumlerinin-nedeni-yanlis-tarim-politikalari/

Doğan, U., & Yilmaz, M. (2011). Natural and induced sinkholes of the Obruk Plateau and Karapınar-Hotamış Plain, Turkey. *Journal of Asian Earth Sciences*, *40*(2), 496–508. https://doi.org/10.1016/J.JSEAES.2010.09.014

DSI. (n.d.). *Hydrogeological Investigation Report of Cihanbeyli-Yeniceoba-Kulu Plains*.

DSI. (1970). *Hydrogeological Investigation Report of Misli Plain*.

DSI. (1972). *Hydrogeological Investigation Report of Ereğli-Bor Plain*.

DSI. (1973). *Hydrogeological Investigation Report of Altınekin Plain*.

DSI. (1975a). *Hydrogeological Investigation Report of Karaman-Ayrancı-Akçaşehir Plain*.

DSI. (1975b). *Hydrogeological Investigation Report of Konya-Çumra-Karapınar Plain*.

Ersoy, A. F., & Gültekin, F. (2008). Modeling groundwater flow in the agricultural area of Gümüşhaciköy (Amasya, Turkey). *Bulletin of Engineering Geology and the Environment*, *67*(4), 529–535. https://doi.org/10.1007/s10064-008-0164-z

Ertürk, A., Ekdal, A., Gürel, M., Karakaya, N., Guzel, C., & Gönenç, E. (2014). Evaluating the impact of climate change on groundwater resources in a small Mediterranean watershed. *Science of the Total Environment*, *499*, 437–447. https://doi.org/10.1016/j.scitotenv.2014.07.001

Falkenmark, M., & Molden, D. (2008). Wake Up to Realities of River Basin Closure. *International Journal of Water Resources Development*, *24*(2), 201–215. https://doi.org/10.1080/07900620701723570

FAO, & GEF. (2019). *SUSTAINABLE LAND MANAGEMENT AND CLIMATE-FRIENDLY AGRICULTURE: GCP /TUR/055/GFF*. https://www.tarimorman.gov.tr/CEM/Belgeler/Havza Uluslararası Projeler/Sürdürülebilir Arazi Yönetimi ve İklim Dostu Tarım Projesi/Project Text (ENG).pdf

Food and Agriculture Organization of the United Nations. (2017). *Water for Sustainable Food and Agriculture: A report produced for the G20 Presidency of Germany*.

FOOD SECTOR ANALYSIS REPORT AND GUIDE: TR52 Region (Konya, Karaman). (2021). https://www.undp.org/sites/g/files/zskgke326/files/migration/tr/gida-tr52.pdf

General Directorate of Mapping (HGM). (n.d.). *Political Map Of Türkiye*.

Goovaerts, P. (1997). Geostatistics for natural reources evaluation. In *Geostatistics for natural resources evaluation*. https://doi.org/10.2307/1270969

Gregersen, H. M., Ffolliott, P. F., & Brooks, K. N. (2007). Integrated watershed management: Connecting people to their land and water. In *Integrated Watershed Management: Connecting People to Their Land and Water*. https://doi.org/10.1659/mrd.mm042

Harbaugh, A. W. (2005). The U.S. Geological Survey Modular Ground-Water Model — the Ground-Water Flow Process. In *U.S. Geological Survey Techniques and Methods 6-A16*. https://doi.org/10.3133/tm6A16

Hou, X., Wang, S., Jin, X., Li, M., Lv, M., & Feng, W. (2020). Using an etwatch (Rs)-uzf-modflow coupled model to optimize joint use of transferred water and local water sources in a saline water area of the north china plain. *Water*, *12*(12). https://doi.org/10.3390/w12123361

Hyeyoung, B., Seo, S., Šim, J., & Poeter, E. P. (2007). *Documentation of the Hydrus Package for Modflow-2000 , the U . S . Geological Survey Modular Ground-Water Model*.

IPCC. (2014). *Climate Change 2014: Synthesis Report*. https://www.ipcc.ch/report/ar5/syr/

J. Šimůnek, M. Šejna, H. Saito, M. Sakai, and M. T. van G. (2008). *The HYDRUS-1D Software Package for Simulating the One-Dimensional Movement of Water, Heat, and Multiple Solutes in Variably-Saturated Media* (Issue April).

Jacob, D., Petersen, J., Eggert, B., Alias, A., Christensen, O. B., Bouwer, L. M., Braun, A., Colette, A., Déqué, M., Georgievski, G., Georgopoulou, E., Gobiet, A., Menut, L., Nikulin, G., Haensler, A., Hempelmann, N., Jones, C., Keuler, K., Kovats, S., … Yiou, P. (2014). EURO-CORDEX: New high-resolution climate change projections for European impact research. *Regional Environmental Change*, *14*(2). https://doi.org/10.1007/s10113-013-0499-2

Jensen, J. R., Murray-Rust, H., Paranjpye, V., Pollard, S., & Van Der Zaag, P. (2007). River basin development and management. In D. Molden (Ed.), *Water for food, water for life* (pp. 585–624). International Water Management Institute(IWMI) - Earthscan.

Kampf, S. K., & Burges, S. J. (2007). A framework for classifying and comparing distributed hillslope and catchment hydrologic models. *Water Resources Research*, *43*(5). https://doi.org/10.1029/2006WR005370

Keery, J., Binley, A., Crook, N., & Smith, J. W. N. (2007). Temporal and spatial variability of groundwater-surface water fluxes: Development and application of an analytical method using temperature time series. *Journal of Hydrology*, *336*(1–2), 1–16. https://doi.org/10.1016/j.jhydrol.2006.12.003

Kinzelbach, W., Aeschbach, W., Alberich, C., Goni, I., Beyerle, U., Brunner, P., Chiang, W., Rueedi, J., & Zoellmann, K. (2002). *A survey of methods for groundwater recharge in arid and semi-arid regions early warning and assessment report series*.

Konikow, L. F. (2008). Use of numerical models to simulate groundwater flow and transport. In *Environmental Isotopes in the Hydrological Cycle: Principles and Applications* (Issue 2008, pp. 541–564). International Atomic Energy Agency (IAEA).

KOP. (2012). *KOP BÖLGESİ'NDE DSİ YERALTISUYU (YAS) EYLEM PLANI VE KUYULARA SU TAHSİSİ UYGULAMASI 'GENEL DEĞERLENDİRME VE ÖNERİLER' RAPORU*.

KTO. (2021). *KONYA EKONOMİ RAPORU 2020*. http://www.konyadayatirim.gov.tr/images/dosya/Konya Ekonomi Raporu-KTO.pdf

Kumar, C. P. (2016). Impact of Climate Change on Groundwater Resources. In *Handbook of Research on Climate Change Impact on Health and Environmental Sustainability* (pp. 196–221). https://doi.org/10.4018/978-1-4666-8814-8.ch010

Lekula, M., & Lubczynski, M. W. (2019). Use of remote sensing and long-term in-situ time-series data in an integrated hydrological model of the Central Kalahari Basin, Southern Africa. *Hydrogeology Journal*, *27*(5), 1541–1562. https://doi.org/10.1007/s10040-019-01954-9

Li, J., & Heap, A. D. (2014). Spatial interpolation methods applied in the environmental sciences: A review. *Environmental Modelling and Software*, *53*, 173–189. https://doi.org/10.1016/j.envsoft.2013.12.008

Li, X., Cheng, G., Ge, Y., Li, H., Han, F., Hu, X., Tian, W., Tian, Y., Pan, X., Nian, Y., Zhang, Y., Ran, Y., Zheng, Y., Gao, B., Yang, D., Zheng, C., Wang, X., Liu, S., & Cai, X. (2018). Hydrological Cycle in the Heihe River Basin and Its Implication for Water Resource Management in Endorheic Basins. *Journal of Geophysical Research: Atmospheres*, *123*(2), 890–914. https://doi.org/10.1002/2017JD027889

Lichtenstern, A. (2013). Kriging methods in spatial statistics. In *Technische Universitat München*. http://mediatum.ub.tum.de/doc/1173364/file.pdf

Mali, S. S., Scobie, M., Schmidt, E., Okwany, R. O., Kumar, A., Islam, A., & Bhatt, B. P. (2021). Modelling vadose zone flows and groundwater dynamics of alluvial aquifers in Eastern Gangetic Plains of India: evaluating the effects of agricultural intensification. *Environmental Earth Sciences*, *80*(18), 1–19. https://doi.org/10.1007/s12665-021-09915-w

Mansour, A. Y. S., Baba, A., Gunduz, O., Şimşek, C., Elçi, A., Murathan, A., & Sözbilir, H. (2017). Modeling of seawater intrusion in a coastal aquifer of Karaburun Peninsula, western Turkey. *Environmental Earth Sciences*, *76*(22). https://doi.org/10.1007/s12665-017-7124-5

McDonald, M. G., & Harbaugh, A. W. (1988). *A modular three-dimensional finite-difference ground-water flow model: US Geological Survey Techniques of Water-Resources Investigations*.

Meza-Gastelum, M. A., Campos-Gaytán, J. R., Ramírez-Hernández, J., Herrera-Oliva, C. S., Villegas-León, J. J., & Figueroa-Núñez, A. (2022). Review of Groundwater Withdrawal Estimation Methods. *Water 2022, Vol. 14, Page 2762*, *14*(17), 2762. https://doi.org/10.3390/W14172762

Middleton, N., & Thomas, D. S. G. (1992). World atlas of desertification. In *UNEP*. https://doi.org/10.2307/3060449

Muşmal, H. (2015, April 1). *THE EMERGENCE OF KONYA PLAIN IRRIGATION PROJECT IDEA AND THE FIRST STUDIES RELATED TO THE PROJECT*. The Journal of Academic Social Science Studies. https://jasstudies.com/?mod=makale_ing_ozet&makale_id=27336

Naing, Z. W. (2011). *Groundwater Fluxes in Konya Closed Basin , Turkey Groundwater Fluxes in Konya Closed Basin*. University of Twente.

Nazarieh, F., Ansari, H., Ziaei, A. N., Izady, A., Davari, K., & Brunner, P. (2018). Spatial and temporal dynamics of deep percolation, lag time and recharge in an irrigated semi-arid region. *Hydrogeology Journal*, *26*(7), 2507–2520. https://doi.org/10.1007/s10040-018-1789-z

Newman, B. D., Wilcox, B. P., Archer, S. R., Breshears, D. D., Dahm, C. N., Duffy, C. J., McDowell, N. G., Phillips, F. M., Scanlon, B. R., & Vivoni, E. R. (2006). Ecohydrology of water-limited environments: A scientific vision. *Water Resources Research*, *42*(6), 1–15. https://doi.org/10.1029/2005WR004141

Niswonger, R. G., Prudic, D. E., & Regan, R. S. (2006). *Documentation of the Unsaturated-Zone Flow (UZF1) Package for Modeling Unsaturated Flow Between the Land Surface and the Water Table with MODFLOW-2005: U.S. Geological Survey Techniques and Methods 6-A19*. U.S. Department of the Interior, U.S. Geological Survey.

Nourbakhsh, Z., & Yousefi, H. (2017). Presenting a conceptual model of data collection to manage the groundwater quality. *Journal of Water and Land Development*, *35*(1). https://doi.org/10.1515/jwld-2017-0079

Okello, C., Greggio, N., Giambastiani, B. M. S., Wambiji, N., Nzeve, J., & Antonellini, M. (2020). Modelling Projected Changes in Soil Water Budget in Coastal Kenya under Different Long-Term Climate Change Scenarios. *Water*, *12*(9), 2455. https://doi.org/10.3390/w12092455

Özyurt, N. N., Avci, P., & Bayari, C. S. (2017). Using groundwater flow modelling for investigation of land subsidence in the konya closed basin (Turkey). In *Handbook of Research on Trends and Digital Advances in Engineering Geology* (p. 569). https://doi.org/10.4018/978-1-5225-2709-1.ch016

Pardo-Iguzquiza, E., & Chica-Olmo, M. (2008). Geostatistics with the Matern semivariogram model: A library of computer programs for inference, kriging and simulation. *Computers and Geosciences*, *34*(9). https://doi.org/10.1016/j.cageo.2007.09.020

Penman, H. L. (1948). Natural evaporation from open water, bare soil and grass. *Proceedings of the Royal Society of London. Series A. Mathematical and Physical Sciences*, *193*(1032), 120–145. https://doi.org/10.1098/RSPA.1948.0037

Rai, R. K., Singh, V. P., & Upadhyay, A. (2017). Scheme Irrigation Efficiency. In *Planning and Evaluation of Irrigation Projects*. https://doi.org/10.1016/b978-0-12-811748-4.00018-2

Rukundo, E., & Doğan, A. (2019). Dominant influencing factors of groundwater recharge spatial patterns in Ergene river catchment, Turkey. *Water (Switzerland)*, *11*(4). https://doi.org/10.3390/w11040653

Sener, E., Davraz, A., & Sener, S. (2009). Investigation of Aksehir and Eber Lakes (SW Turkey) Coastline Change with Multitemporal Satellite Images. *Water Resources Management 2009 24:4*, *24*(4), 727–745. https://doi.org/10.1007/S11269-009-9467-5

Šimůnek, J., Genuchten, M. T., & Šejna, M. (2008). Development and Applications of the HYDRUS and STANMOD Software Packages and Related Codes. *Vadose Zone Journal*, *7*(2). https://doi.org/10.2136/vzj2007.0077

Šimůnek, J., van Genuchten, M. T., & Šejna, M. (2016). Recent Developments and Applications of the HYDRUS Computer Software Packages. *Vadose Zone Journal*, *15*(7), vzj2016.04.0033. https://doi.org/10.2136/vzj2016.04.0033

Sophocleous, M. (2002). Interactions between groundwater and surface water: The state of the science. *Hydrogeology Journal*, *10*(1), 52–67. https://doi.org/10.1007/s10040-001-0170-8

Spinoni, J., Vogt, J., Naumann, G., Carrao, H., & Barbosa, P. (2015). Towards identifying areas at climatological risk of desertification using the Köppen-Geiger classification and FAO aridity index. *International Journal of Climatology*, *35*(9), 2210–2222. https://doi.org/10.1002/joc.4124

Sputnik. (2021a, February 11). *Konya'da obruk tehlikesi: Sayıları 600'e ulaştı*. https://tr.sputniknews.com/20210211/konyada-obruk-tehlikesi-sayilari-600e-ulasti-1043785574.html

Sputnik. (2021b, September 5). *Kuruyan Akşehir Gölü'nün ortasında araçla gezilebiliyor*. https://tr.sputniknews.com/20210905/kuruyan-aksehir-golunun-ortasinda-aracla-gezilebiliyor-1048624633.html

SUİŞ-Proje. (n.d.-a). *16-2 Konya-Çumra-Karapınar Subbasin Hydrological Report*.

SUİŞ-Proje. (n.d.-b). *KONYA KAPALI HAVZASI YERALTISUYU VE HİDROJEOLOJİ RAPORU*.

SUİŞ-PROJE. (n.d.). *KONYA KAPALI HAVZASI MASTER PLANI HAZIRLANMASI İŞİ: HİDROJEOLOJİ ETÜT RAPORU*.

Surucu, E. (2018). *Integrated Basin Flow Modeling: A Case Study for Konya Closed Basin in Turkey*. University of California, Davis.

TAGEM, & DSİ (Eds.). (2017). *TÜRKİYE'DE SULANAN BİTKİLERİN BİTKİ SU TÜKETİMLERİ*.

Tanachaichoksirikun, P., Seeboonruang, U., & Fogg, G. E. (2020). Improving Groundwater Model in Regional Sedimentary Basin Using Hydraulic Gradients. *KSCE Journal of Civil Engineering*, *24*(5). https://doi.org/10.1007/s12205-020-1781-8

Todaro, V., D'Oria, M., Secci, D., Zanini, A., & Tanda, M. G. (2022). Climate Change over the Mediterranean Region: Local Temperature and Precipitation Variations at Five Pilot Sites. *Water (Switzerland)*, *14*(16). https://doi.org/10.3390/w14162499

Tonkul, S., Baba, A., Şimşek, C., Durukan, S., Demirkesen, A. C., & Tayfur, G. (2019). Groundwater recharge estimation using HYDRUS 1D model in Alaşehir sub-basin of Gediz Basin in Turkey. *Environmental Monitoring and Assessment*, *191*(10), 1–19. https://doi.org/10.1007/s10661-019-7792-6

Topcu, S., Kibaroglu, A., & Kadirbeyoglu, Z. (2019). Turkey. In *Global Issues in Water Policy* (Vol. 22, pp. 185–212). Springer. https://doi.org/10.1007/978-3-030-03698-0_7

TURKSTAT Database -Biruni. (n.d.).

Twarakavi, N. K. C., Šimůnek, J., & Seo, S. (2008). Evaluating Interactions between Groundwater and Vadose Zone Using the HYDRUS-Based Flow Package for MODFLOW. *Vadose Zone Journal*, *7*(2), 757–768. https://doi.org/10.2136/vzj2007.0082

U.S. Geological Survey. (2018, June 12). *Evapotranspiration and the Water Cycle* . https://www.usgs.gov/special-topics/water-science-school/science/evapotranspiration-and-water-cycle#overview

Vieux, B. E. (2001). *Distributed Hydrologic Modeling Using GIS*. 1–17. https://doi.org/10.1007/978-94-015-9710-4_1

Wackernagel, H. (1995). Multivariate geostatistics: an introduction with applications. *Multivariate Geostatistics: An Introduction with Applications*. https://doi.org/10.2307/2291758

Wang, G., Mang, S., Cai, H., Liu, S., Zhang, Z., Wang, L., & Innes, J. L. (2016). Integrated watershed management: evolution, development and emerging trends. *Journal of Forestry Research*, *27*(5), 967–994. https://doi.org/10.1007/s11676-016-0293-3

Wang, J., Song, C., Reager, J. T., Yao, F., Famiglietti, J. S., Sheng, Y., MacDonald, G. M., Brun, F., Schmied, H. M., Marston, R. A., & Wada, Y. (2018). Recent global decline in endorheic basin water storages. *Nature Geoscience*, *11*(12), 926–932. https://doi.org/10.1038/s41561-018-0265-7

Wang, L., Kinzelbach, W., Yao, H., Steiner, J., & Wang, H. (2020). How to Meter Agricultural Pumping at Numerous Small-Scale Wells?—An Indirect Monitoring Method Using Electric Energy as Proxy. *Water*, *12*(9), 2477. https://doi.org/10.3390/w12092477

Wang, Y., & Chen, N. (2021). Recent progress in coupled surface–ground water models and their potential in watershed hydro-biogeochemical studies: A review. *Watershed Ecology and the Environment*, *3*, 17–29. https://doi.org/10.1016/J.WSEE.2021.04.001

Warsta, L., Karvonen, T., Koivusalo, H., Paasonen-Kivekäs, M., & Taskinen, A. (2013). Simulation of water balance in a clayey, subsurface drained agricultural field with three-dimensional FLUSH model. *Journal of Hydrology, 476*. https://doi.org/10.1016/j.jhydrol.2012.10.053

World Bank Group. (2016). *Valuing Water Resources in Turkey: A Methodological Overview and Case Study*. World Bank, Washington, DC. https://openknowledge.worldbank.org/handle/10986/25291

WWF. (2010). *Türkiye'nin Yarınları Projesi Sonuç Raporu*.

WWF. (2014). *KONYA'DA SUYUN BUGÜNÜ RAPORU*. https://wwftr.awsassets.panda.org/downloads/konya_da_suyun_bugnu_raporu.pdf?4660/konyadasuyunbugunu

Xiang, K., Li, Y., Horton, R., & Feng, H. (2020). Similarity and difference of potential evapotranspiration and reference crop evapotranspiration – a review. In *Agricultural Water Management* (Vol. 232). https://doi.org/10.1016/j.agwat.2020.106043

Yılmaz, G., Çolak, M. A., Özgencil, İ. K., Metin, M., Korkmaz, M., Ertuğrul, S., Soyluer, M., Bucak, T., Tavşanoğlu, Ü. N., Özkan, K., Akyürek, Z., Beklioğlu, M., & Jeppesen, E. (2021a). Decadal changes in size, salinity, waterbirds, and fish in lakes of the Konya Closed Basin, Turkey, associated with climate change and increasing water abstraction for agriculture. *Inland Waters*, *11*(4), 538–555. https://doi.org/10.1080/20442041.2021.1924034/SUPPL_FILE/TINW_A_1924034_SM7120.DOCX

Yılmaz, G., Çolak, M. A., Özgencil, İ. K., Metin, M., Korkmaz, M., Ertuğrul, S., Soyluer, M., Bucak, T., Tavşanoğlu, Ü. N., Özkan, K., Akyürek, Z., Beklioğlu, M., & Jeppesen, E. (2021b). Decadal changes in size, salinity, waterbirds, and fish in lakes of the Konya Closed Basin, Turkey, associated with climate change and increasing water abstraction for agriculture. *Inland Waters*, *11*(4), 538–555. https://doi.org/10.1080/20442041.2021.1924034

Zomer, R. J., Xu, J., & Trabucco, A. (2022). Version 3 of the Global Aridity Index and Potential Evapotranspiration Database. *Scientific Data*, *9*(1), 1–15. https://doi.org/10.1038/s41597-022-01493-1

APPENDIX A: PLOT OF PRECIPITATION FOR ALL STATIONS

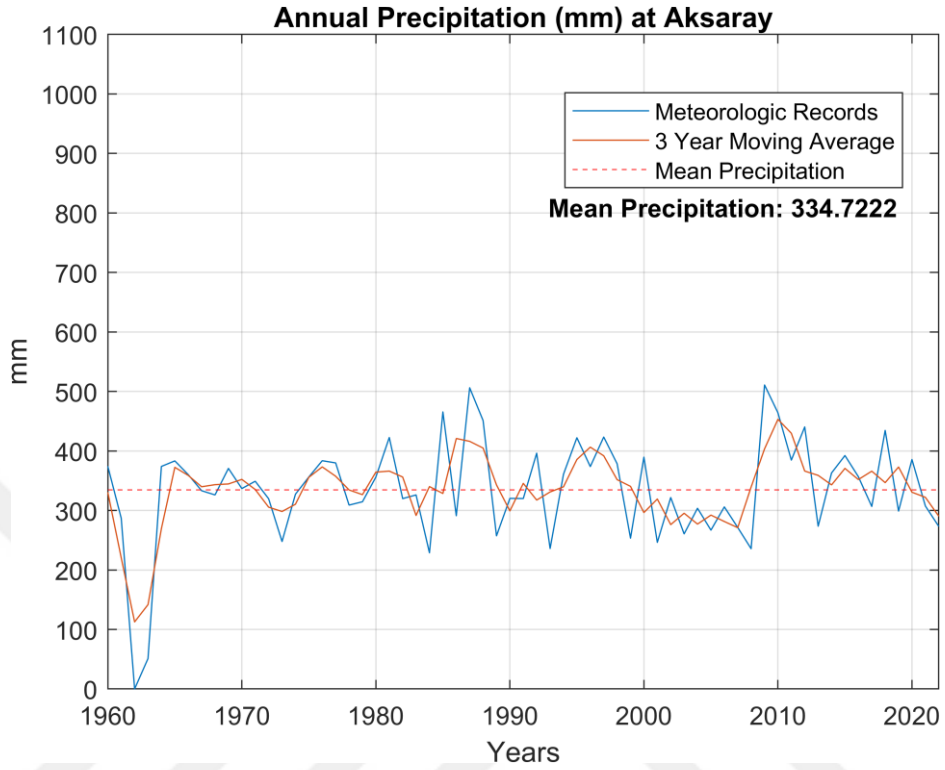

Figure A.1. Annual precipitation at Aksaray station.

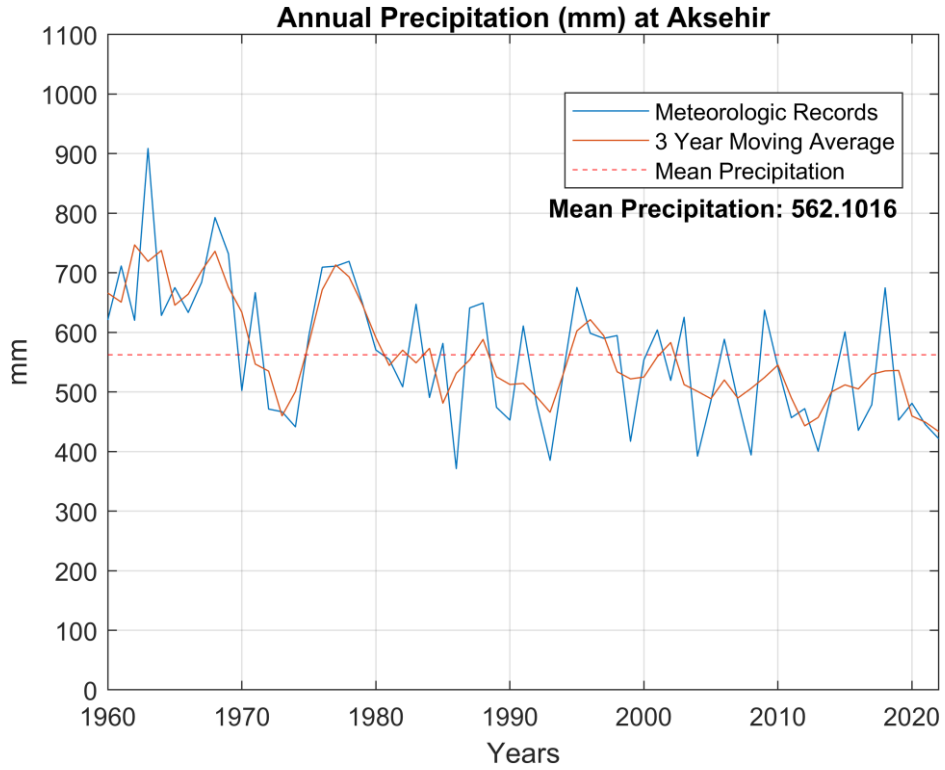

Figure A.2. Annual precipitation at Akşehir station.

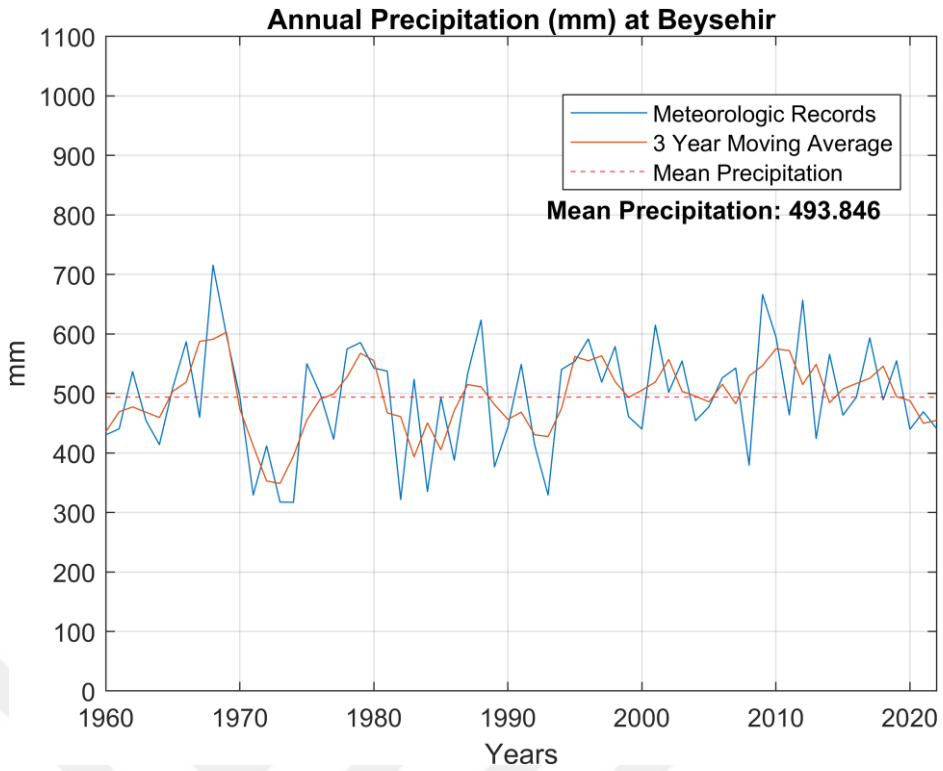

Figure A.3. Annual precipitation at Beyşehir station.

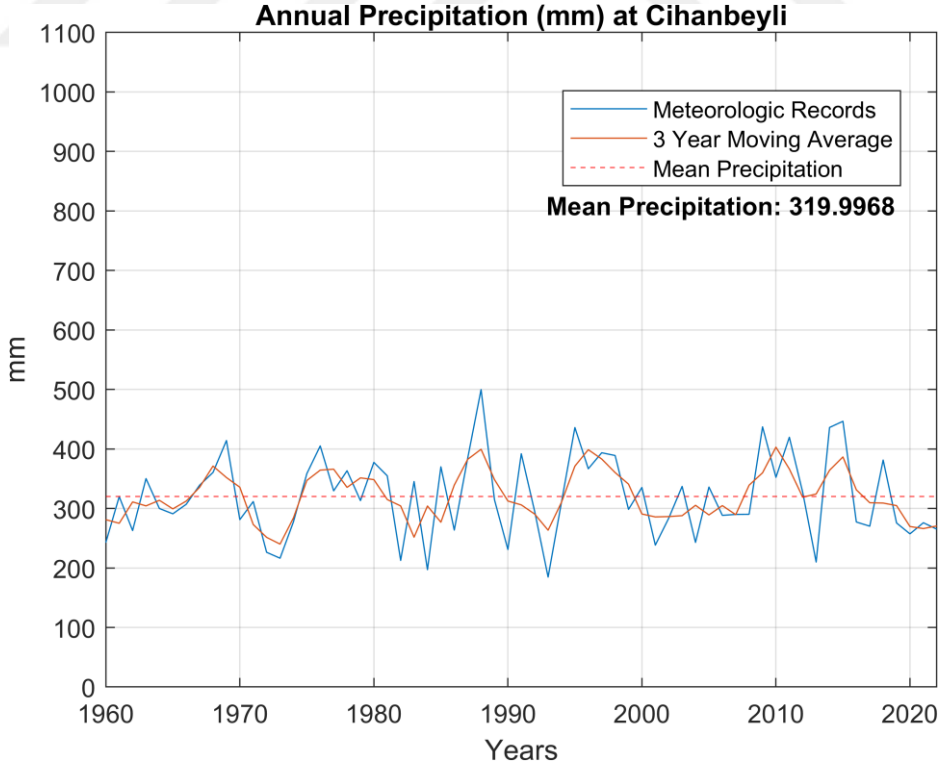

Figure A.4. Annual precipitation at Cihanbeyli station.

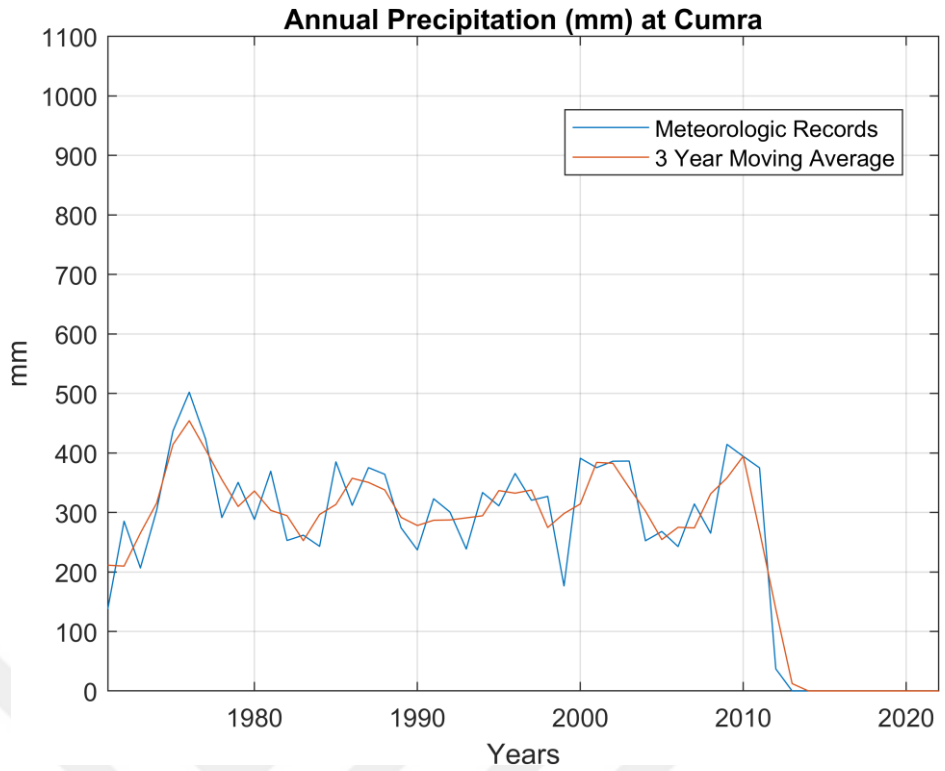

Figure A.5. Annual precipitation at Çumra station.

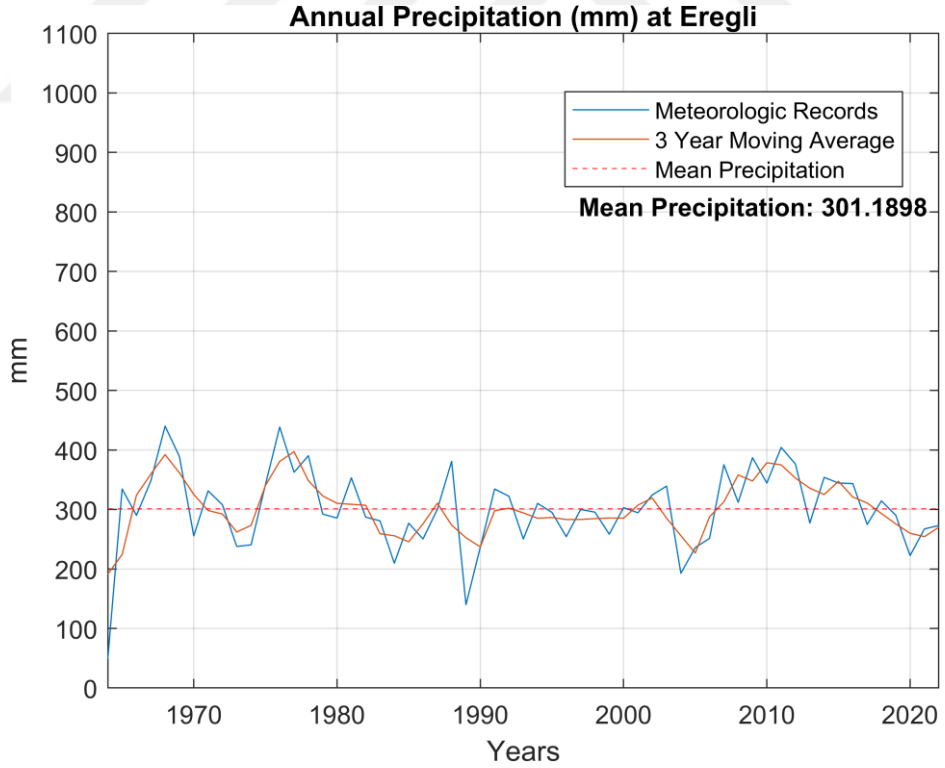

Figure A.6. Annual precipitation at Ereğli station.

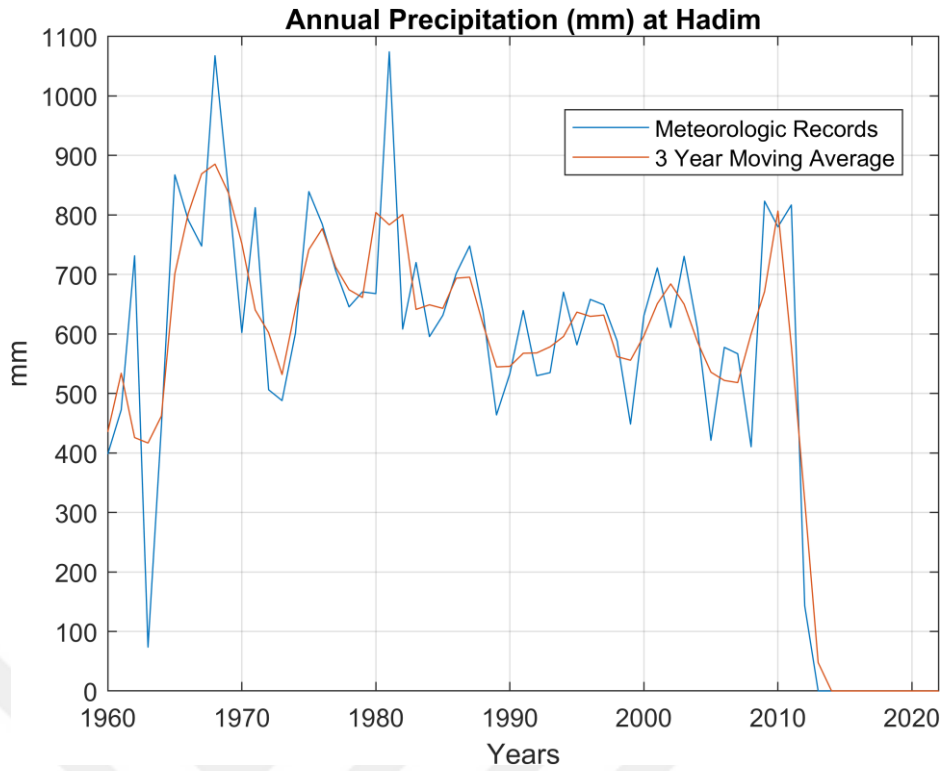

Figure A.7. Annual precipitation at Hadim station.

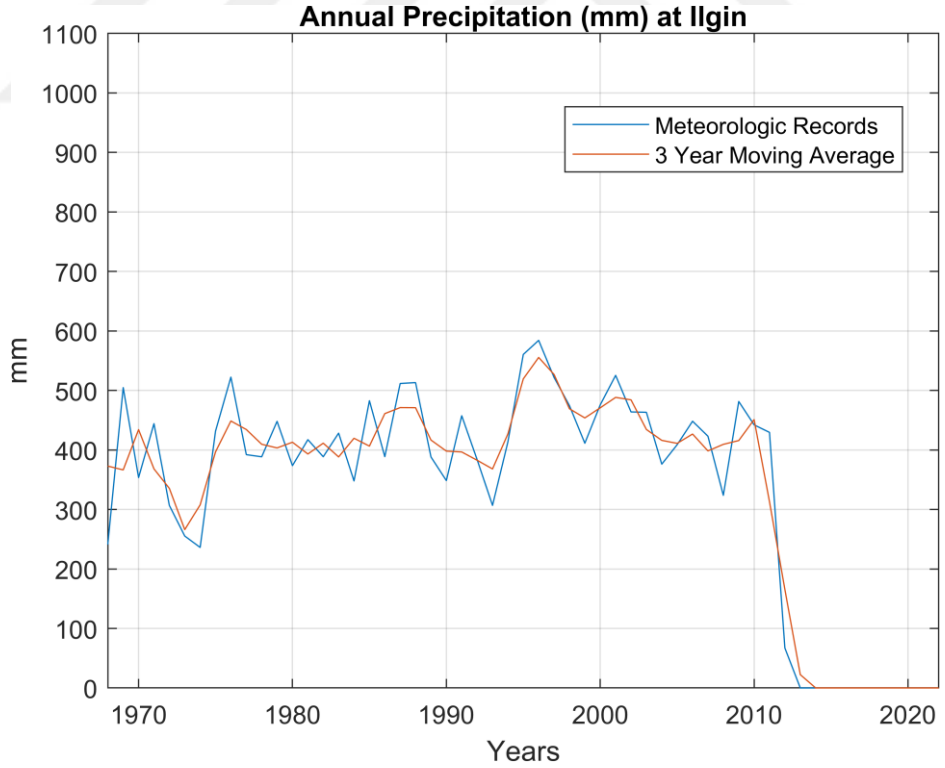

Figure A.8. Annual precipitation at Ilgın station.

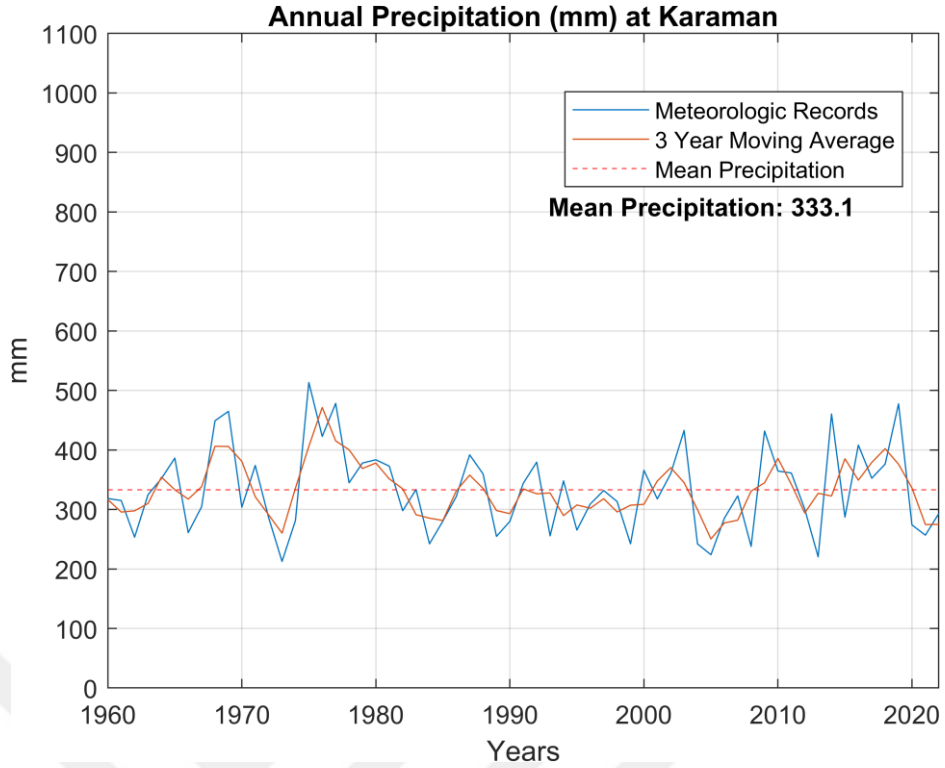

Figure A.9. Annual precipitation at Karaman station.

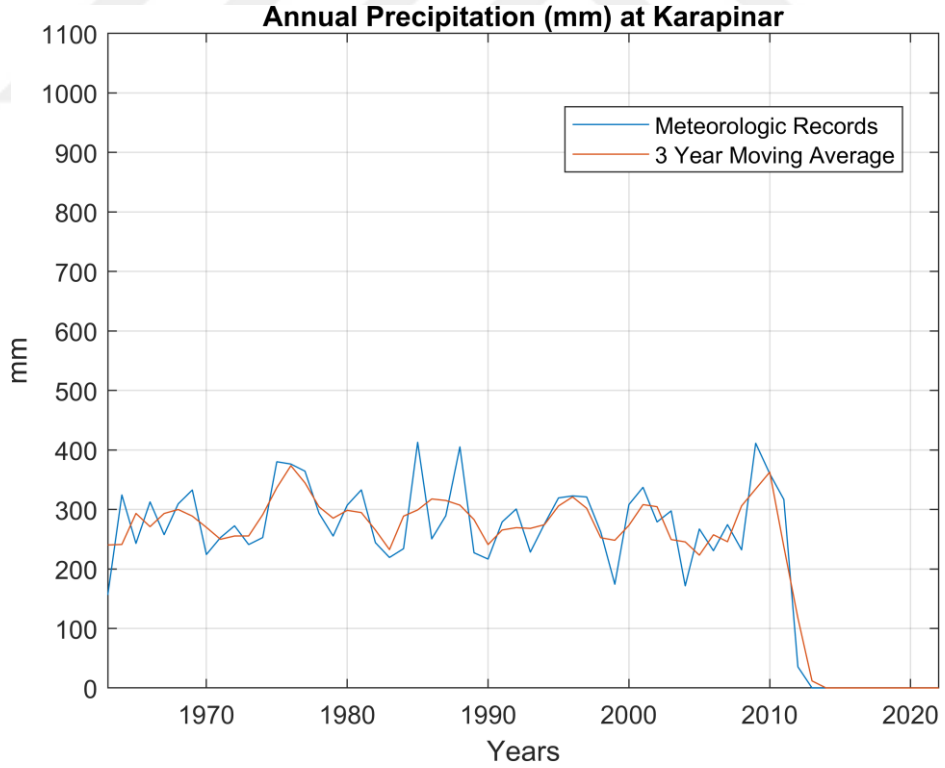

Figure A.10. Annual precipitation at Karapınar station.

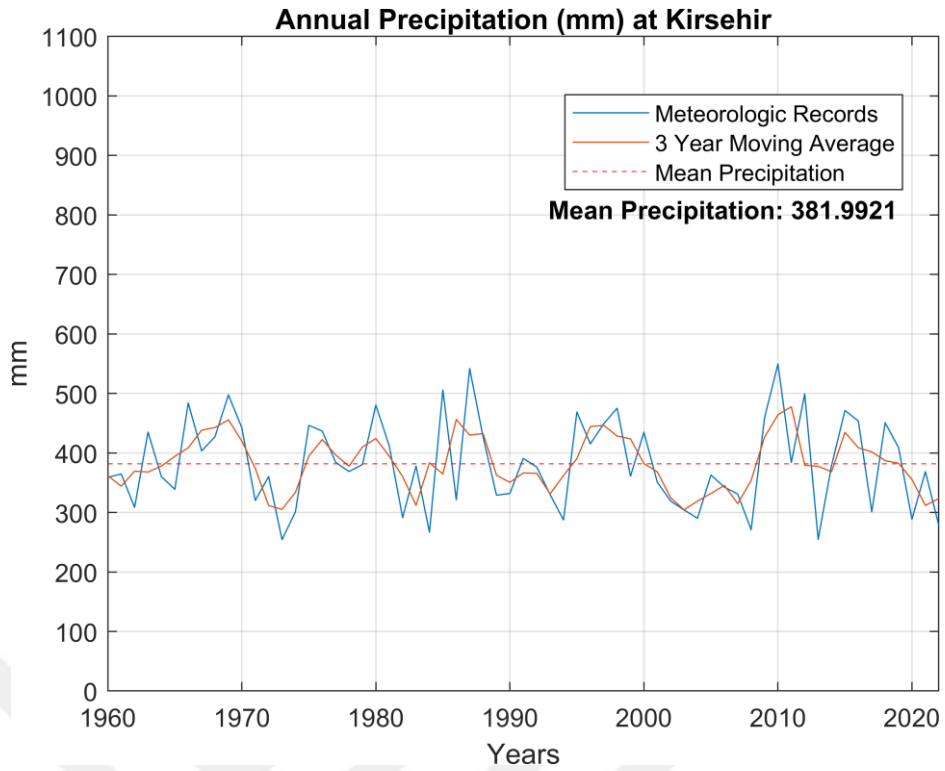

Figure A.11. Annual precipitation at Kırşehir station.

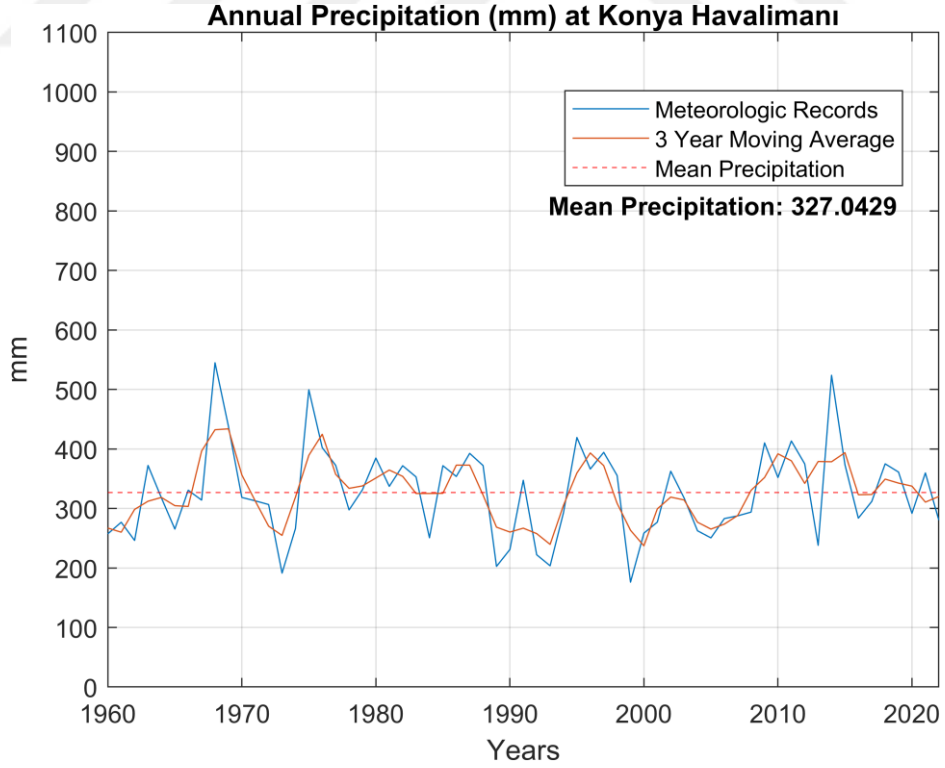

Figure A.12. Annual precipitation at Konya Airport station.

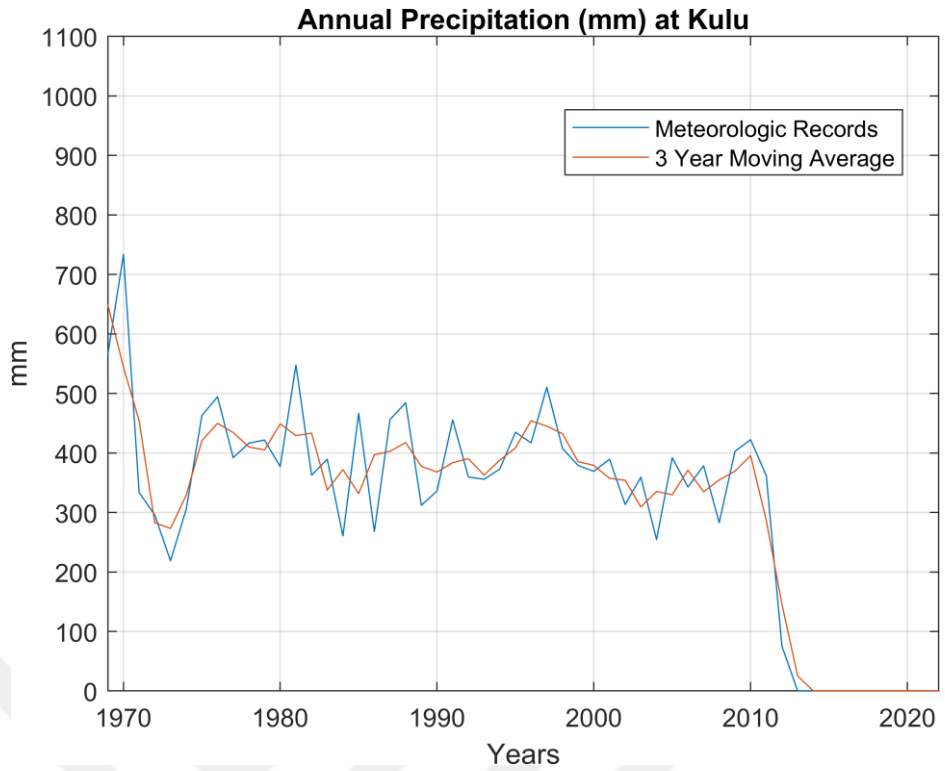

Figure A.13. Annual precipitation at Kulu station.

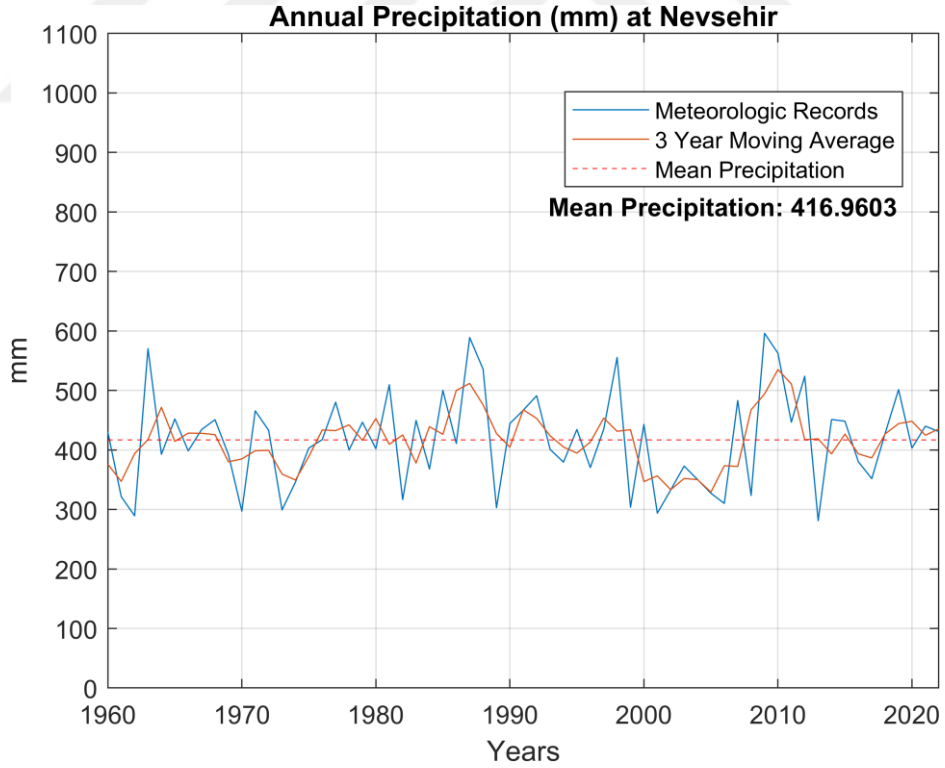

Figure A.14. Annual precipitation at Nevşehir station.

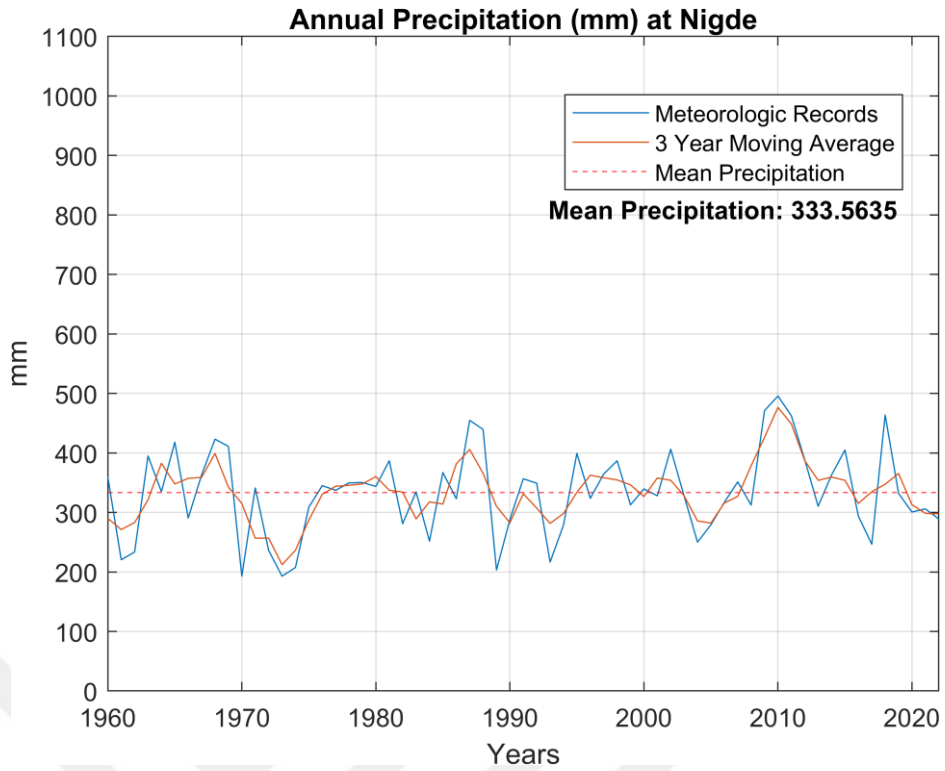

Figure A.15. Annual precipitation at Niğde station.

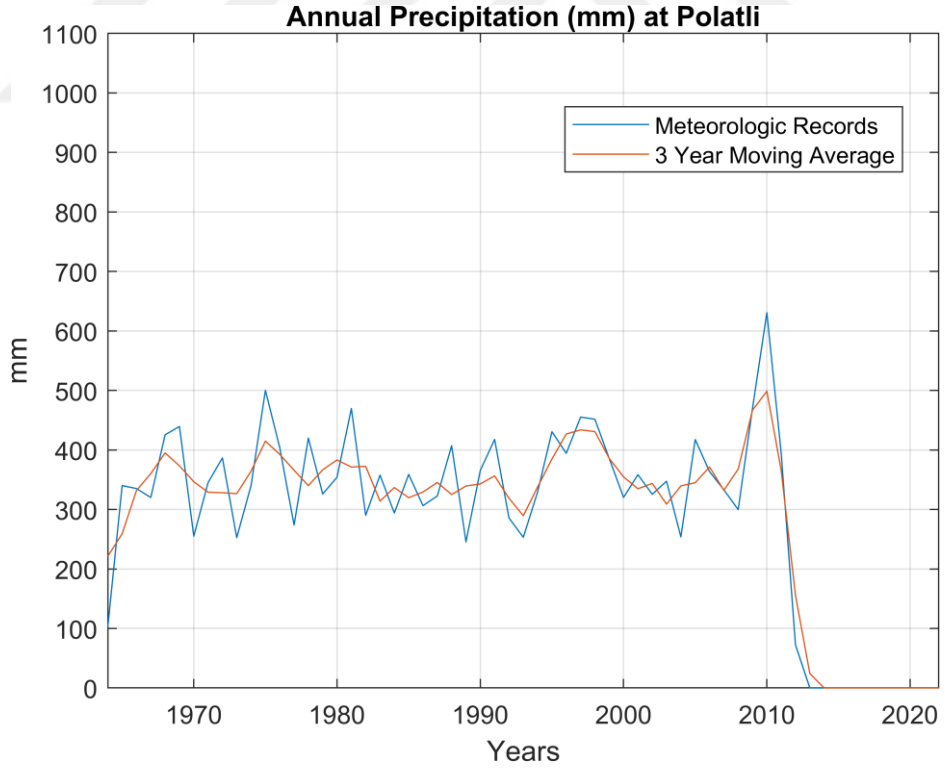

Figure A.16. Annual precipitation at Polatlı station.

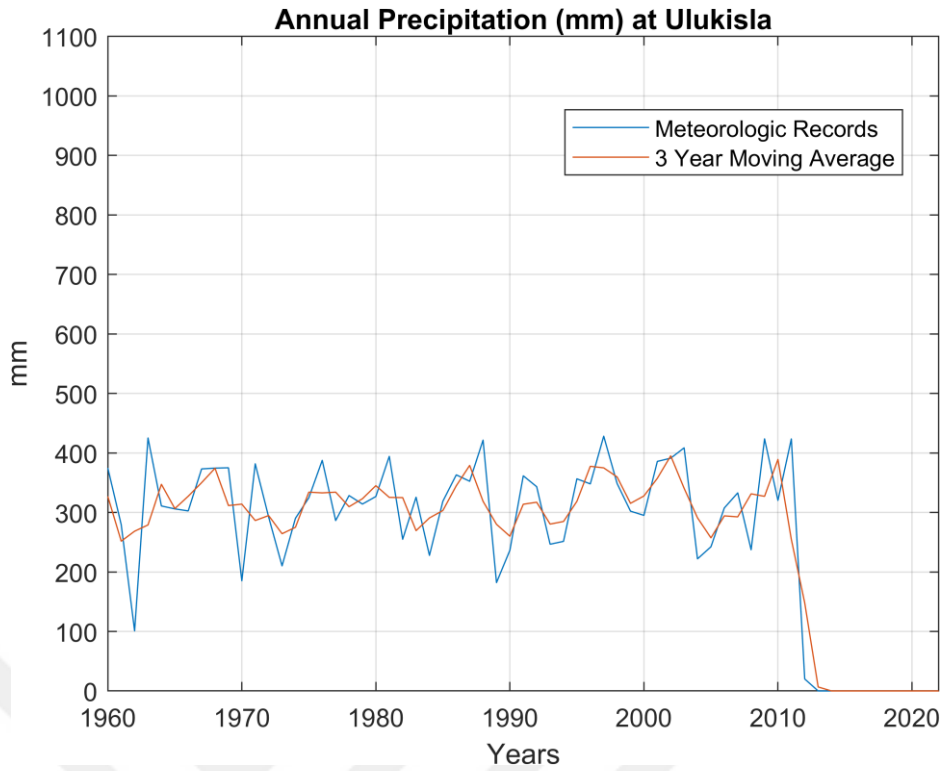

Figure A.17. Annual precipitation at Ulukışla station.

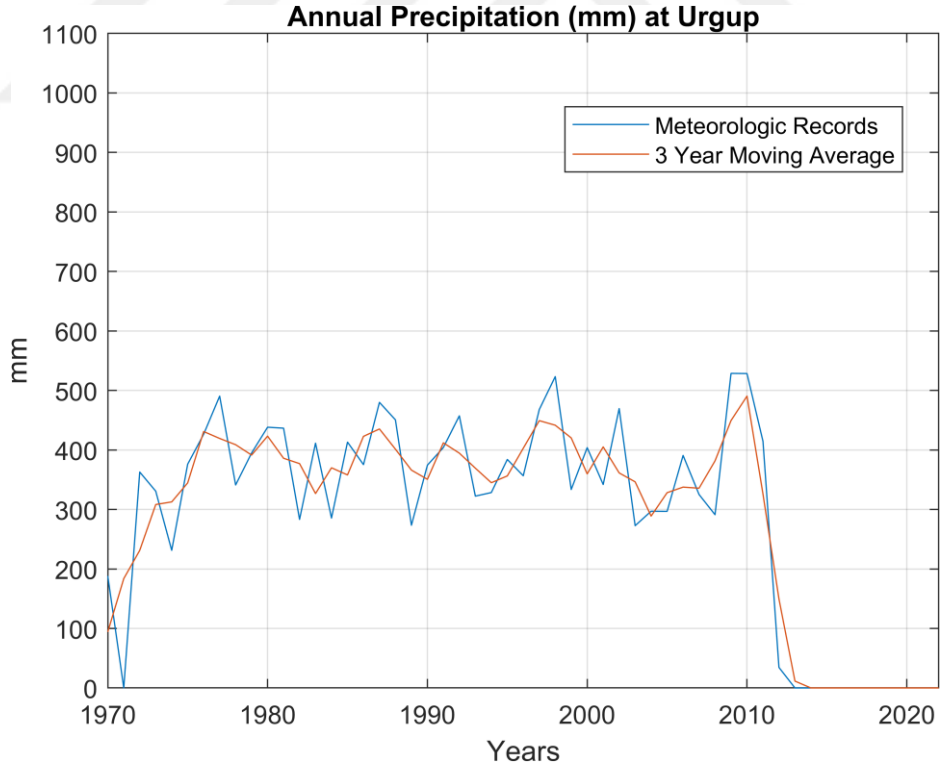

Figure A.18. Annual precipitation at Ürgüp station.

APPENDIX B: FORECASTED LAND USE

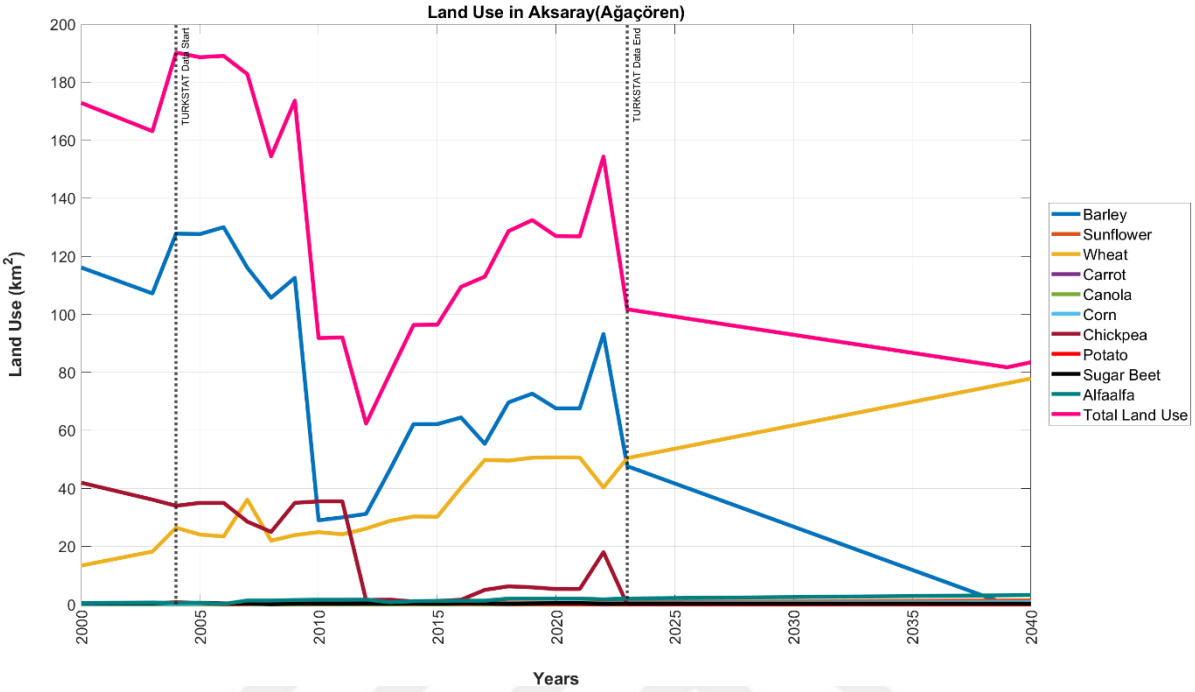

Figure B.1. Forecasted land use for the town of Ağaçören, Aksaray.

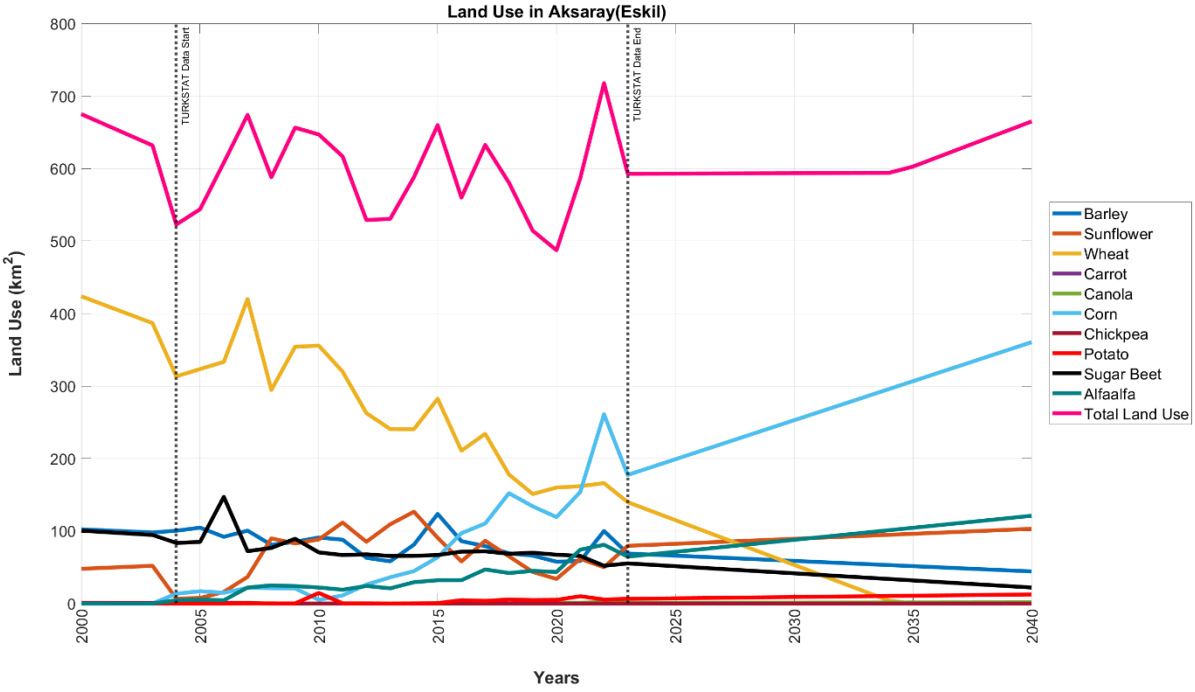

Figure B.2. Forecasted land use for the town of Eskil, Aksaray.

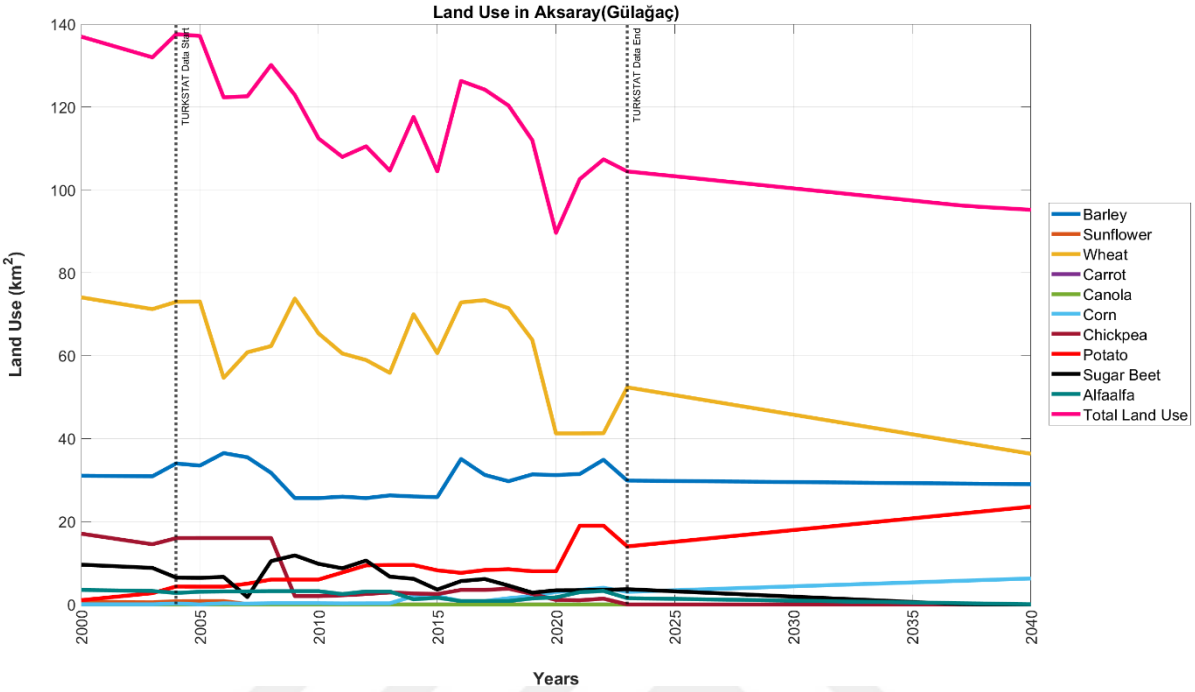

Figure B.3. Forecasted land use for the town of Gülağaç, Aksaray.

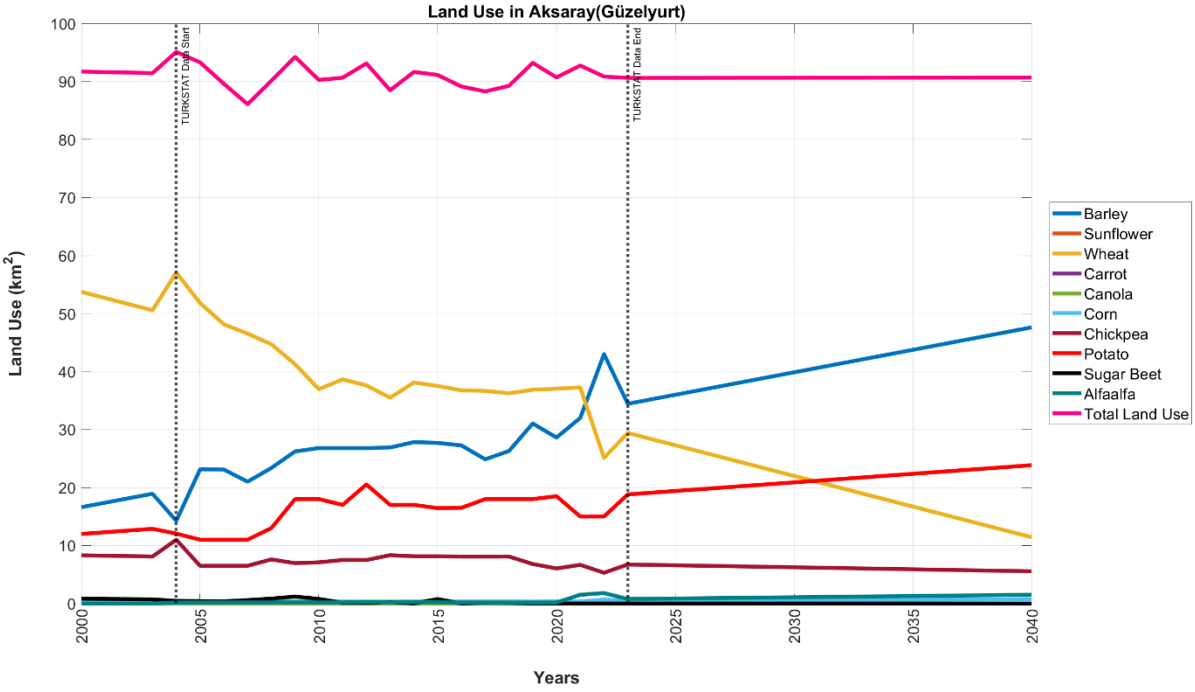

Figure B.4. Forecasted land use for the town of Güzelyurt, Aksaray.

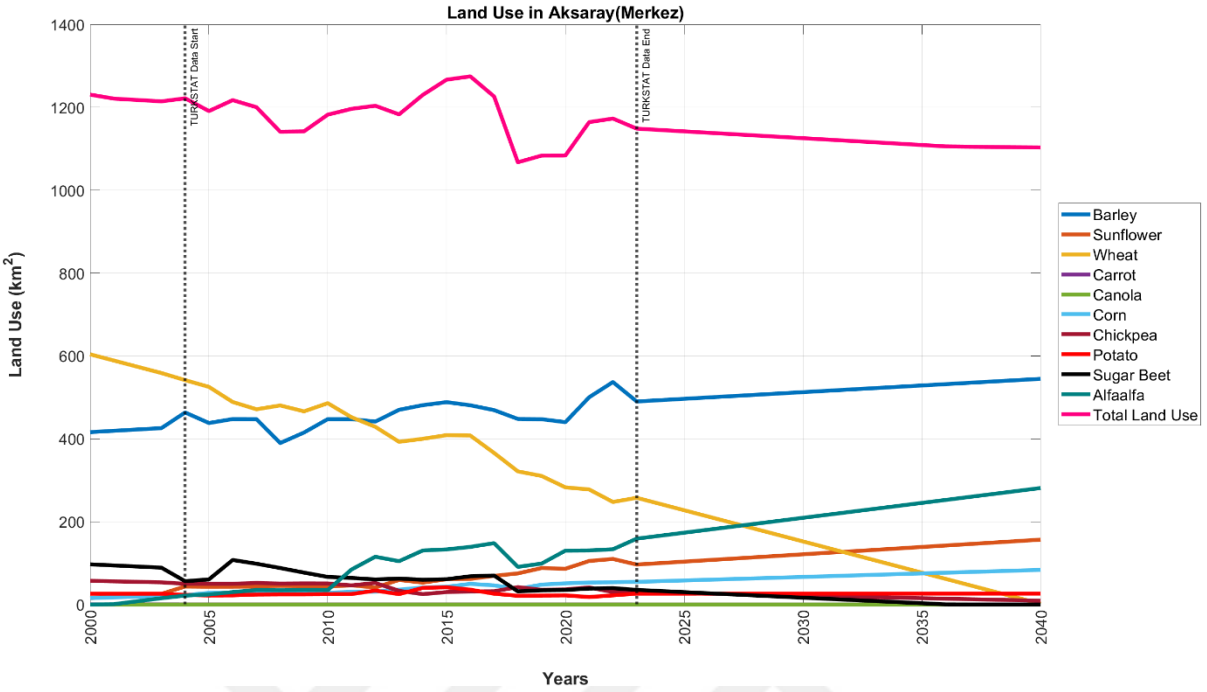

Figure B.5. Forecasted land use for the central area of province, Aksaray.

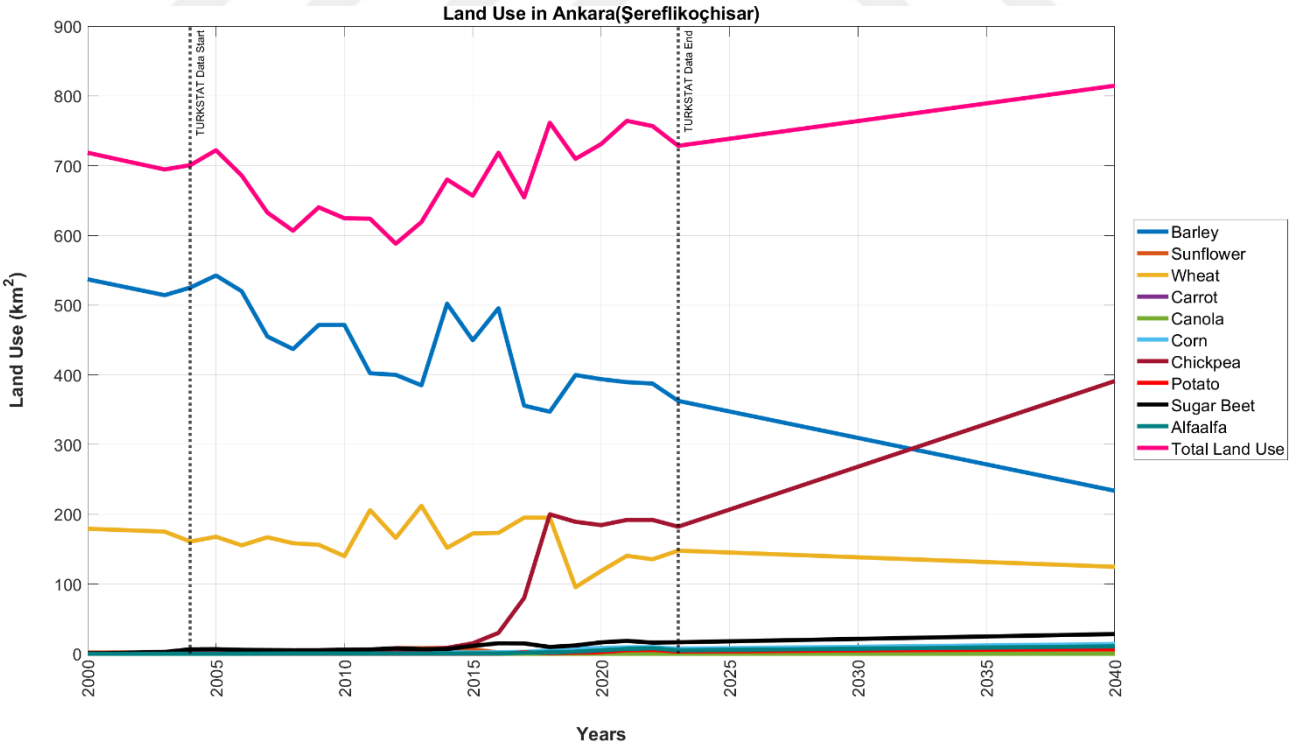

Figure B.6. Forecasted land use for the town of Şereflikoçhisar, Ankara.

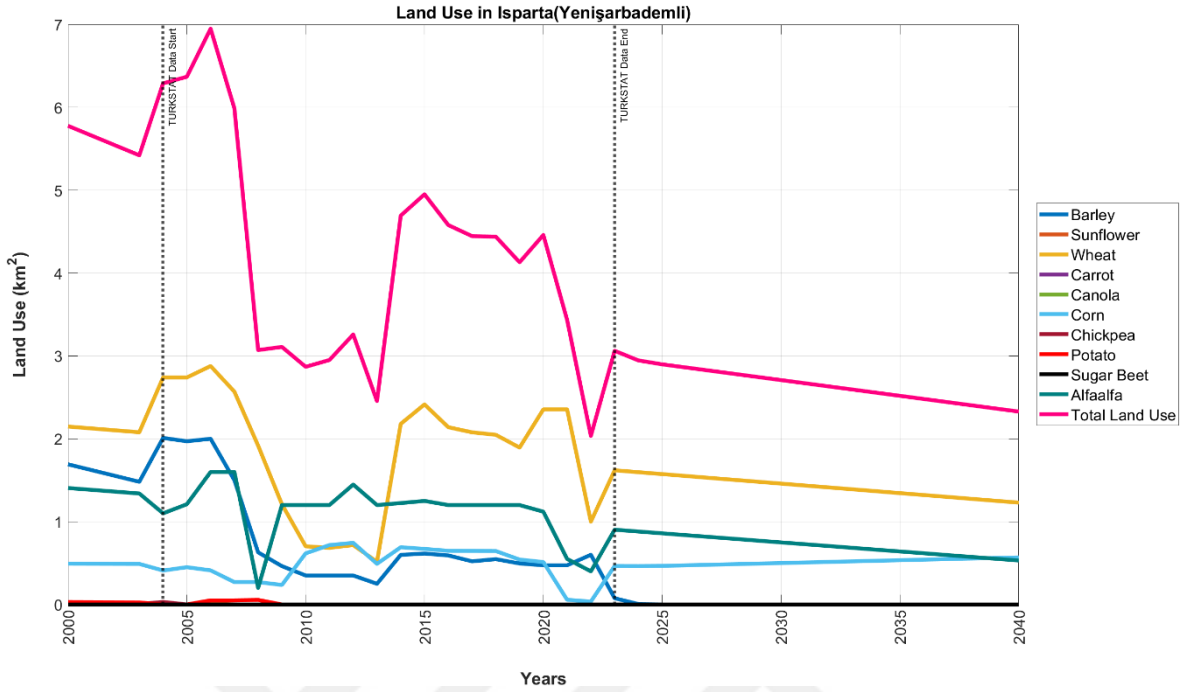

Figure B.7. Forecasted land use for the town of Yenişarbademli, Isparta.

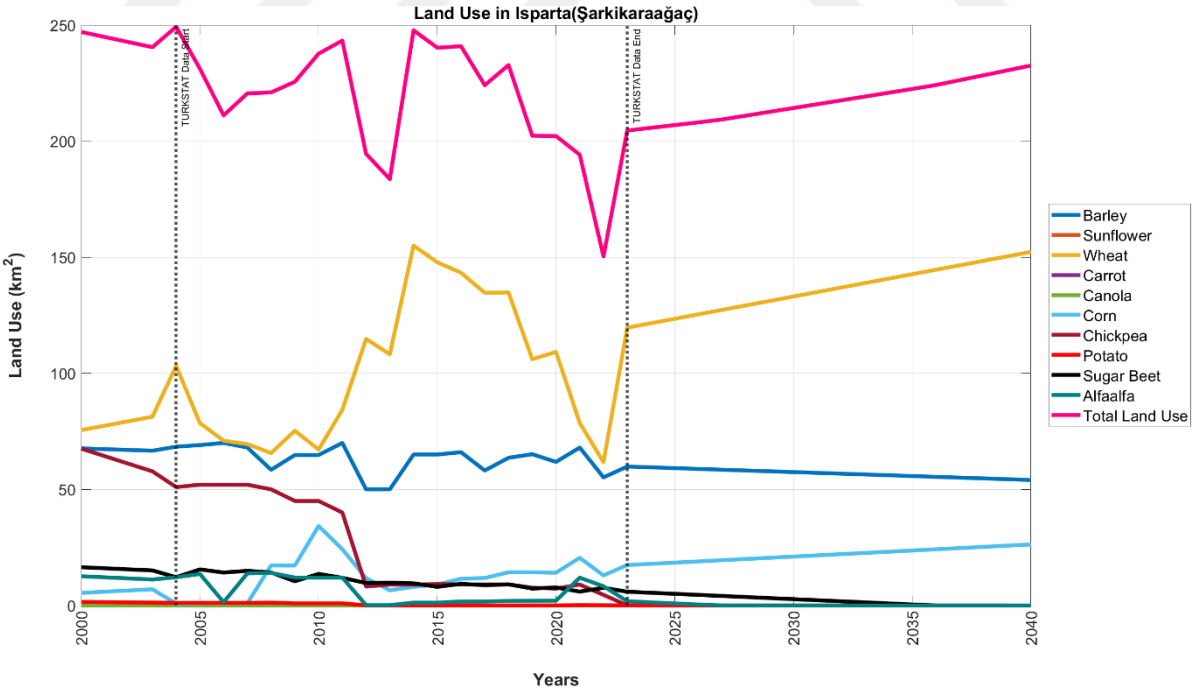

Figure B.8. Forecasted land use for the town of Şarkikaraağaç, Isparta.

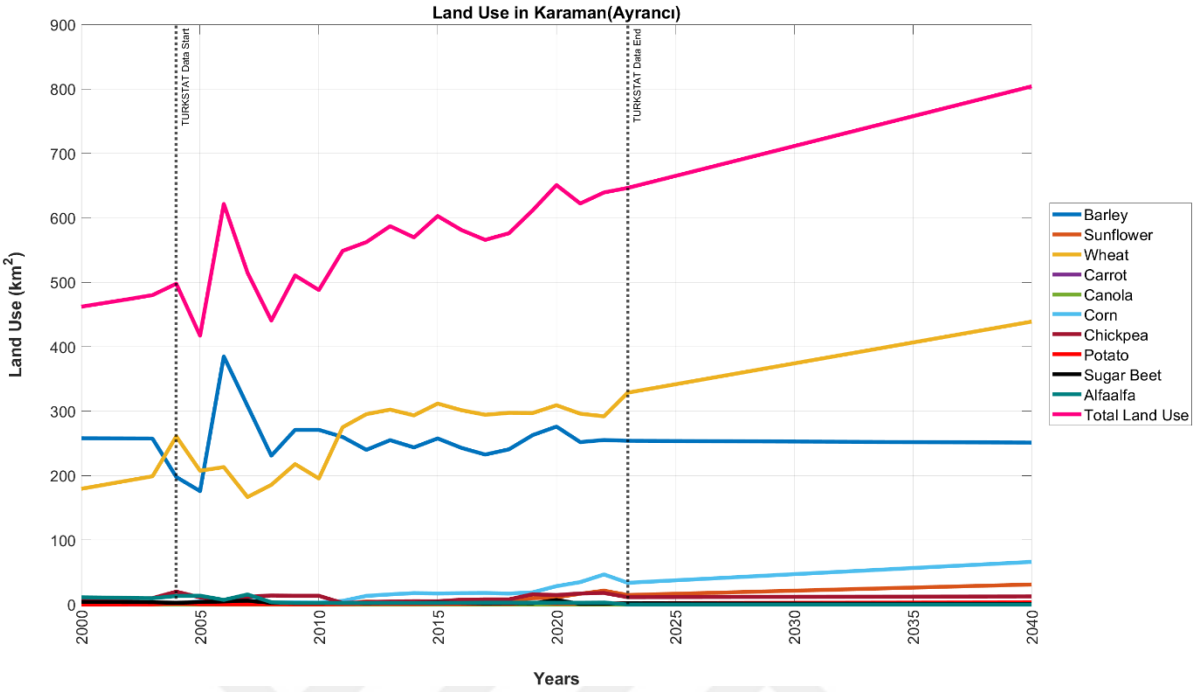

Figure B.9. Forecasted land use for the town of Ayrancı, Karaman.

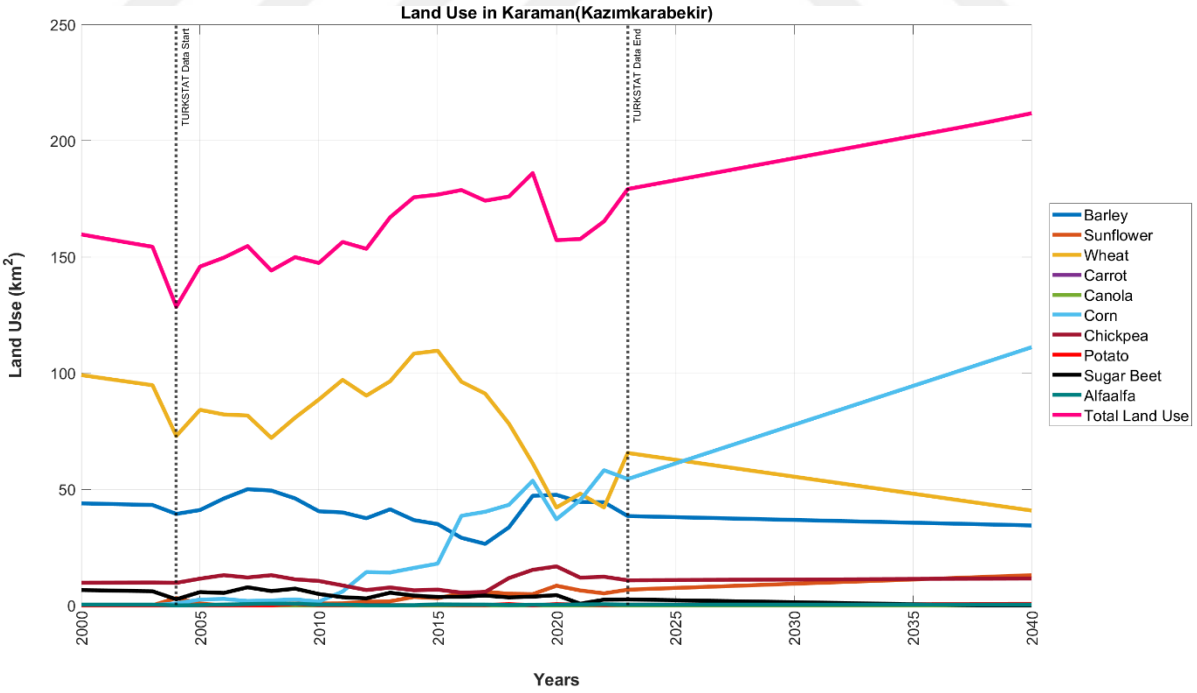

Figure B.10. Forecasted land use for the town of Kazımkarabekir, Karaman.

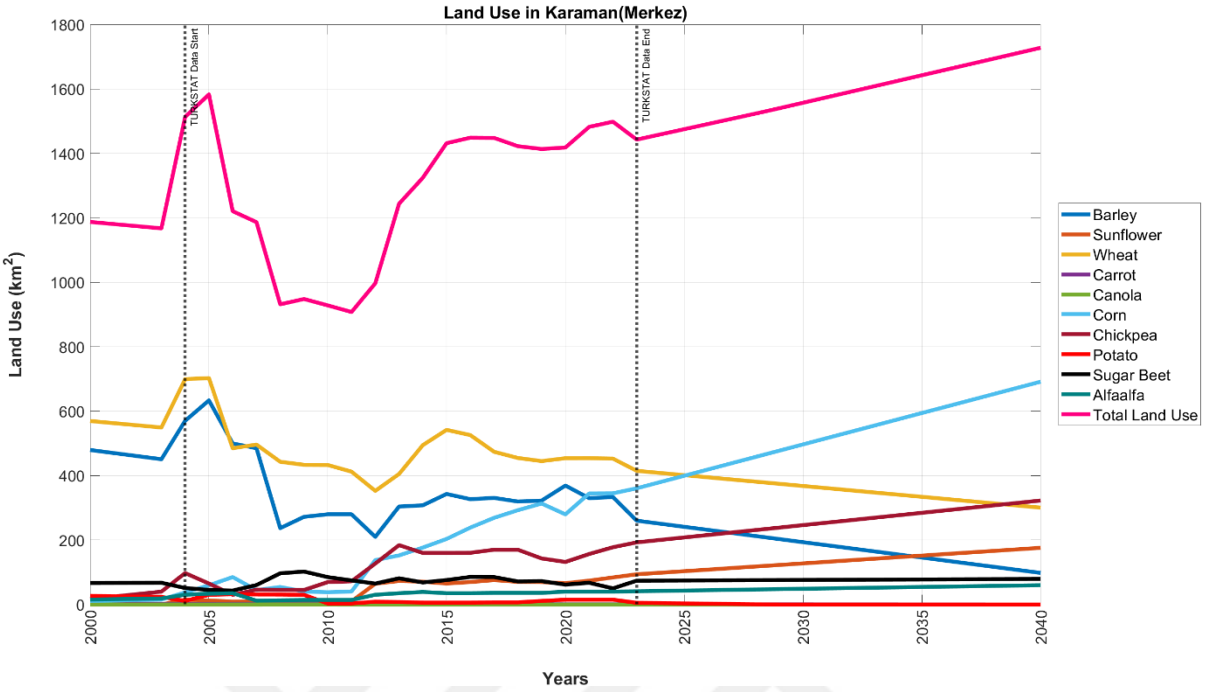

Figure B.11. Forecasted land use for the central area of province, Karaman.

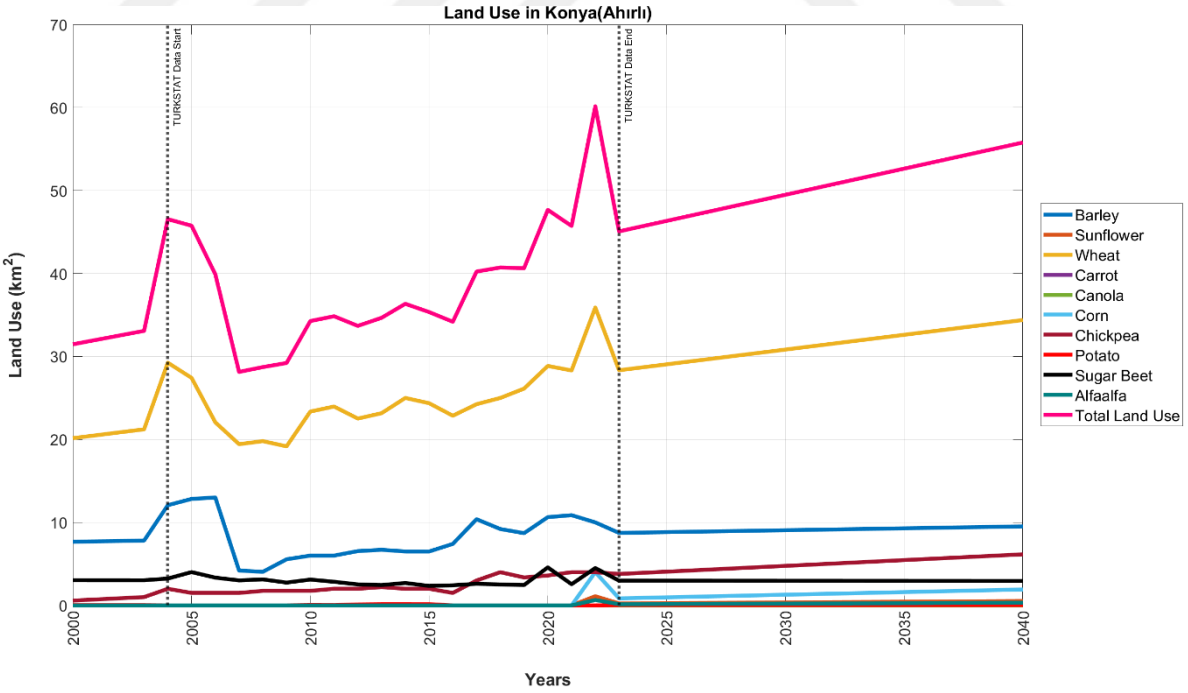

Figure B.12. Forecasted land use for the town of Ahırlı, Konya.

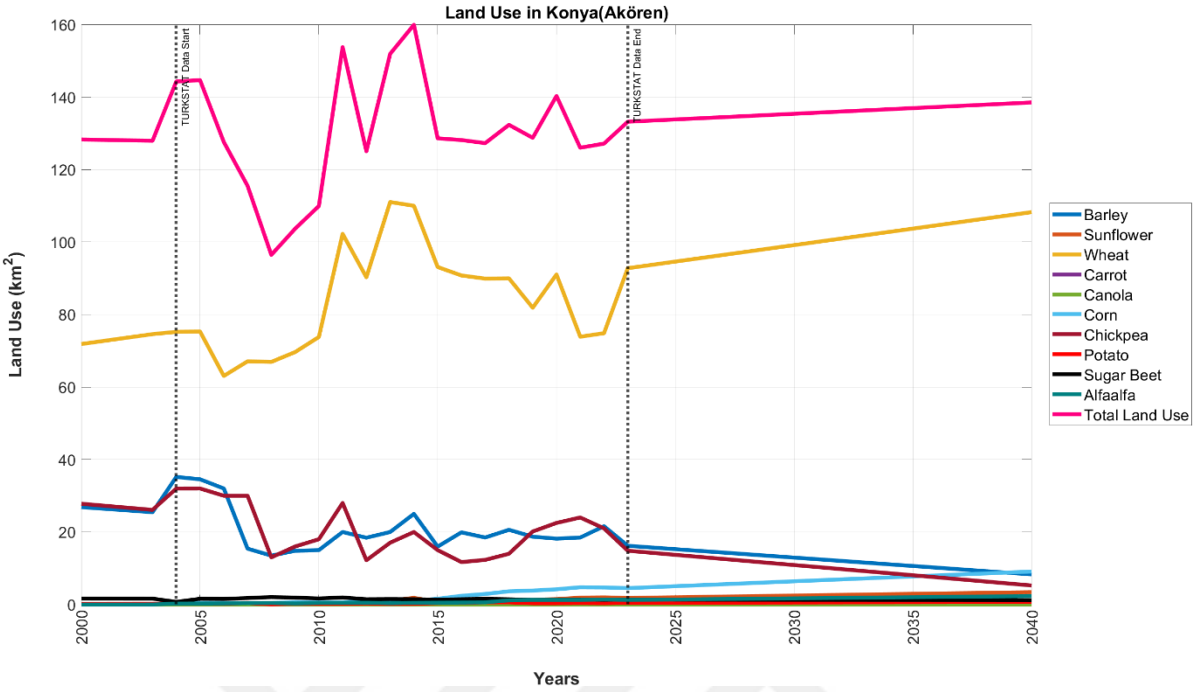

Figure B.13. Forecasted land use for the town of Akören, Konya.

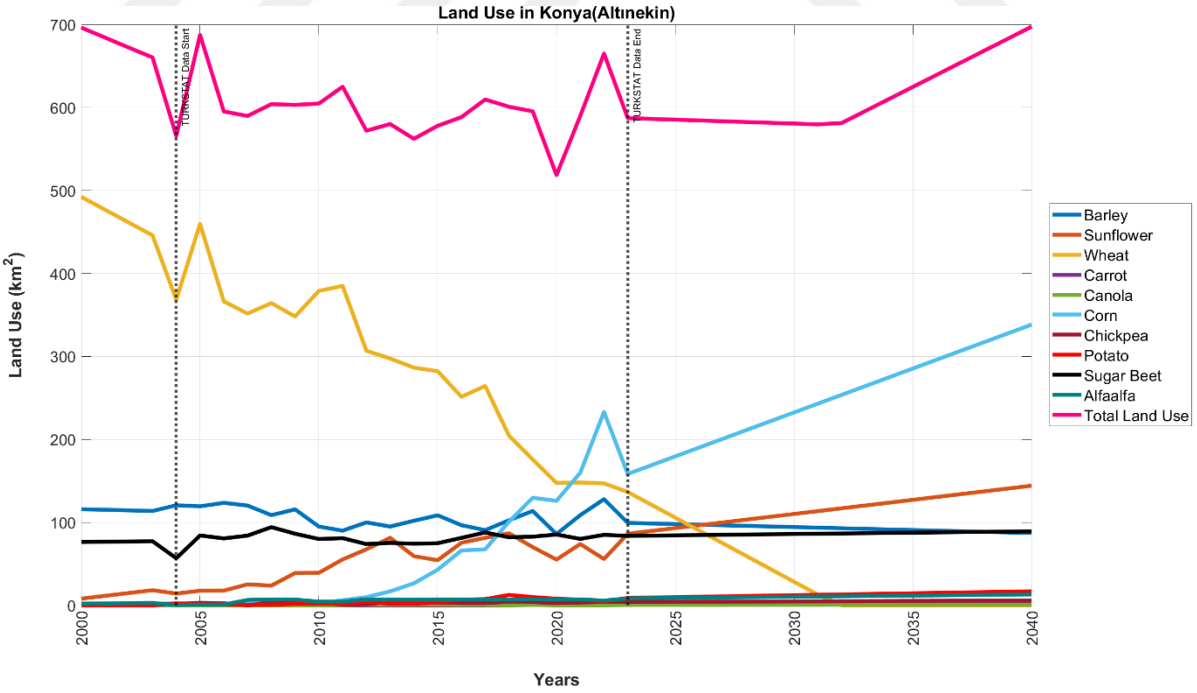

Figure B.14. Forecasted land use for the town of Altınekin, Konya.

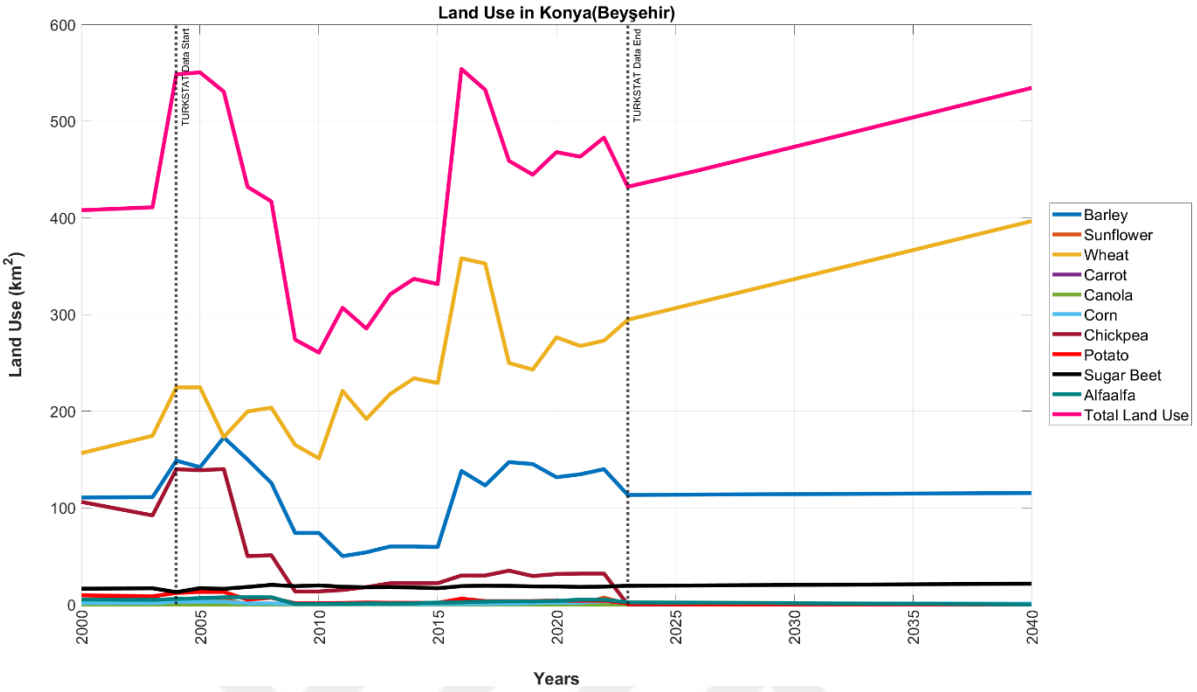

Figure B.15. Forecasted land use for the town of Beyşehir, Konya.

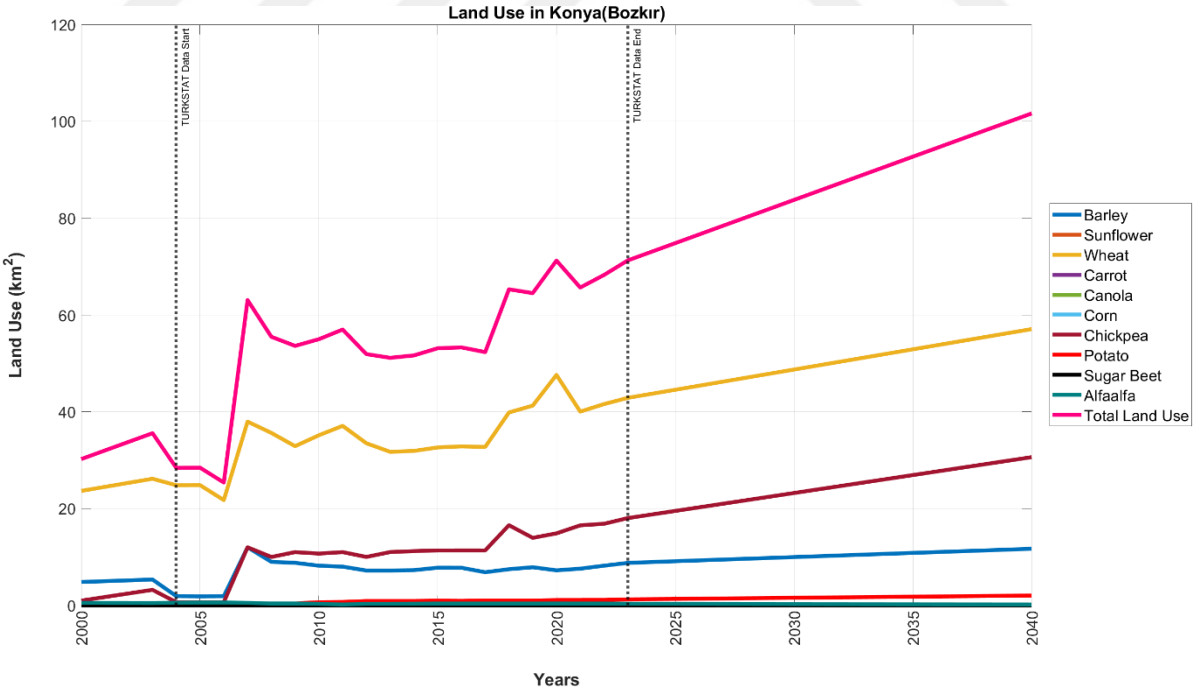

Figure B.16. Forecasted land use for the town of Bozkır, Konya.

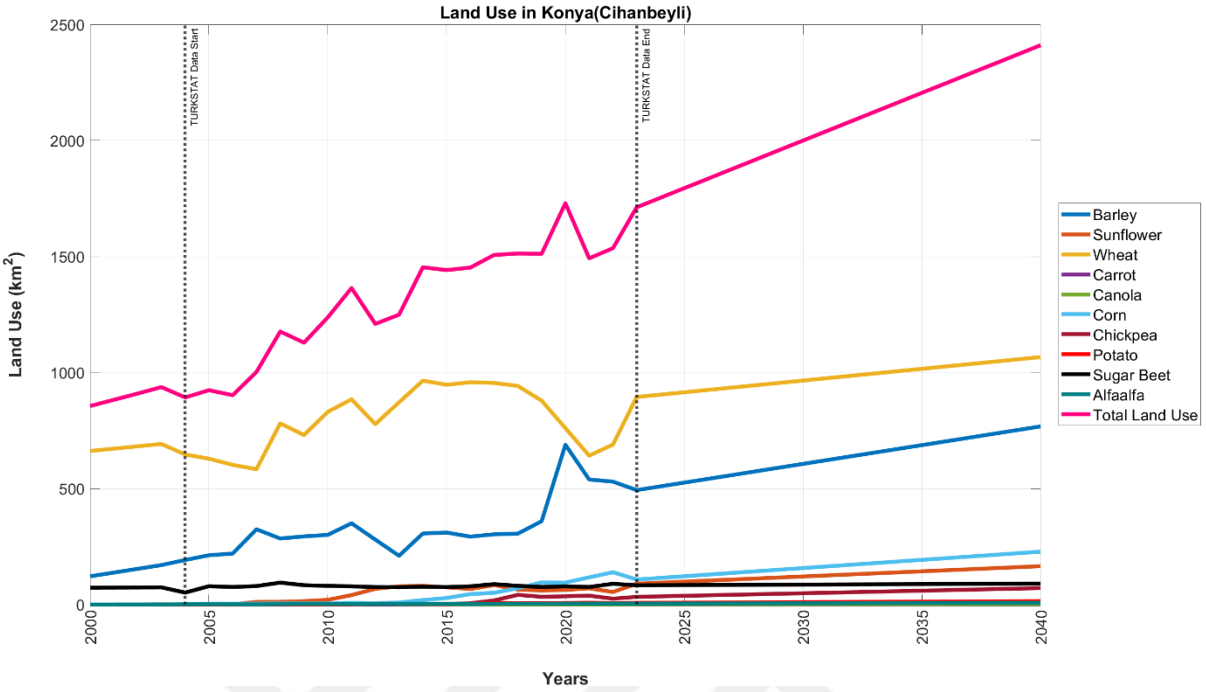

Figure B.17. Forecasted land use for the town of Cihanbeyli, Konya.

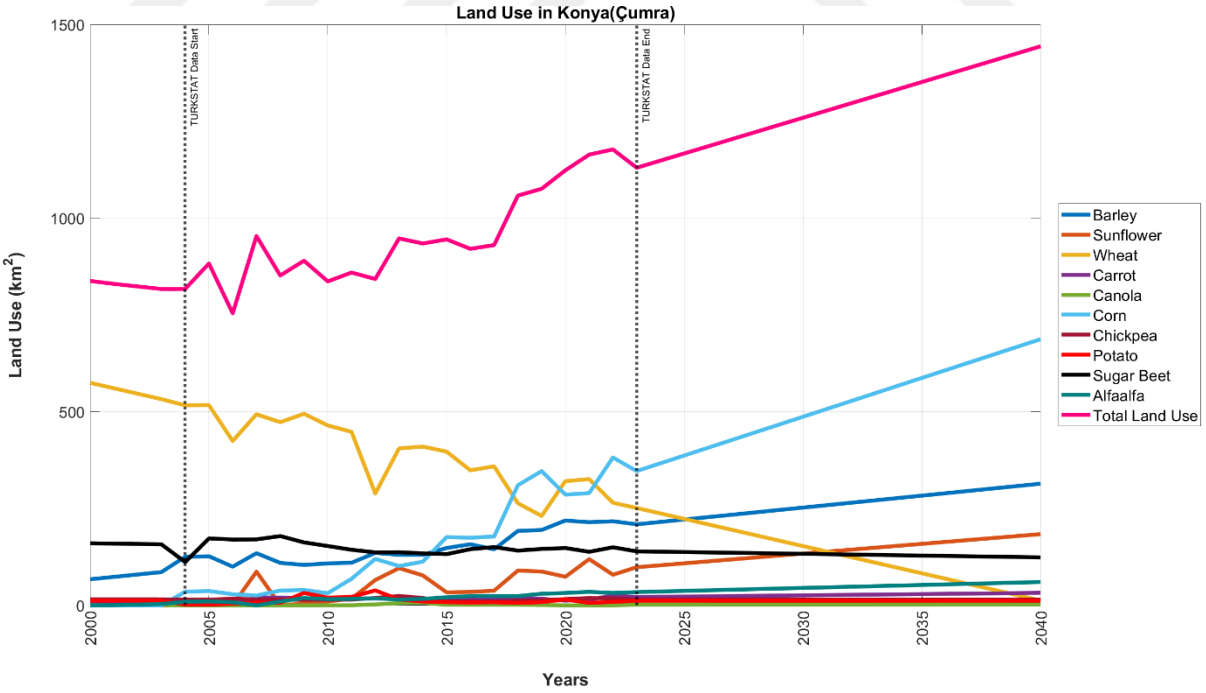

Figure B.18. Forecasted land use for the town of Çumra, Konya.

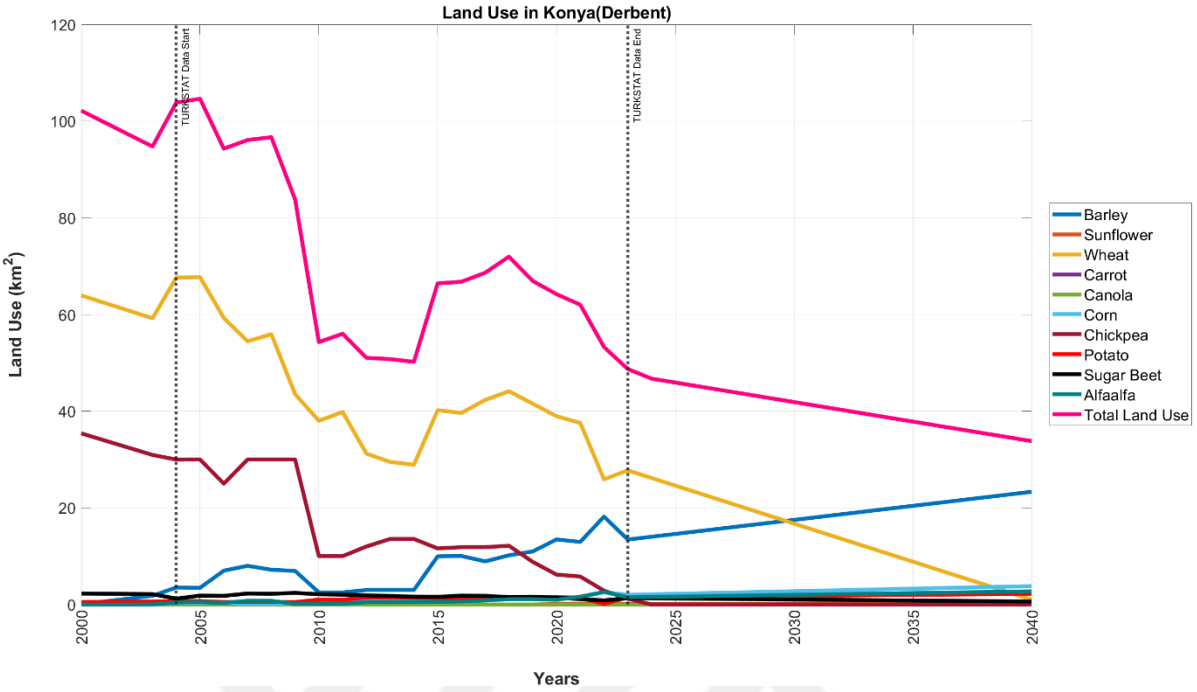

Figure B.19. Forecasted land use for the town of Derbent, Konya.

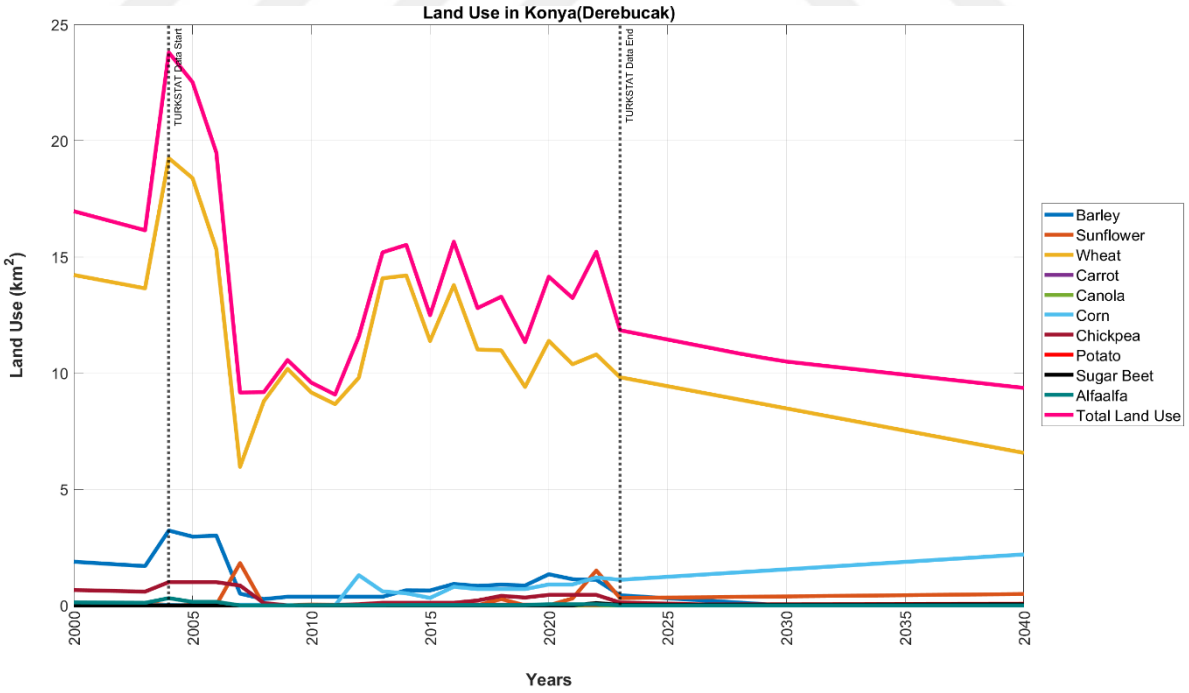

Figure B.20. Forecasted land use for the town of Derebucak, Konya.

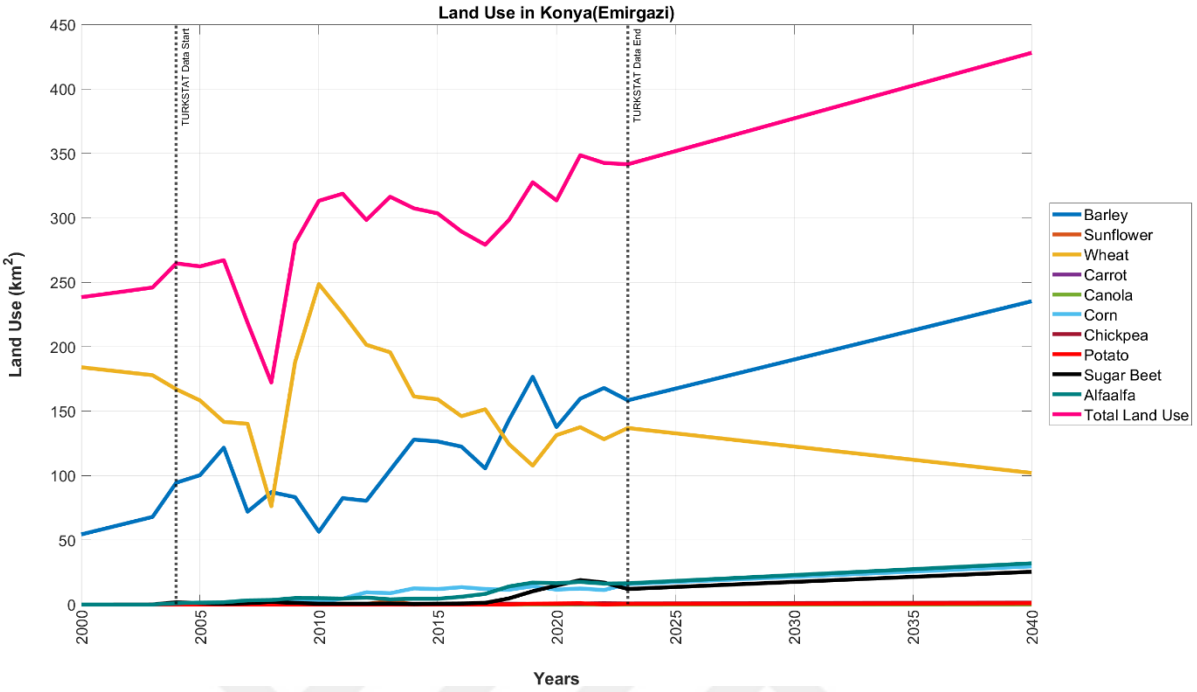

Figure B.21. Forecasted land use for the town of Emirgazi, Konya.

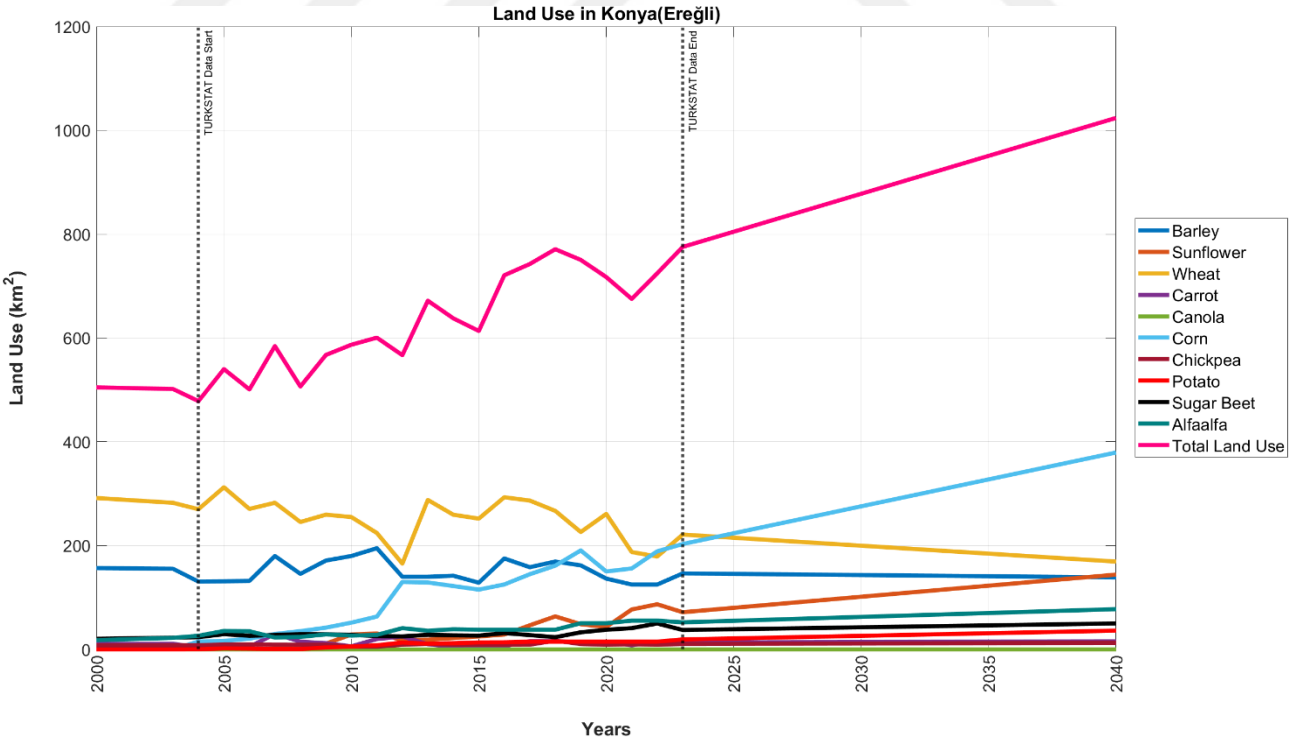

Figure B.22. Forecasted land use for the town of Ereğli, Konya.

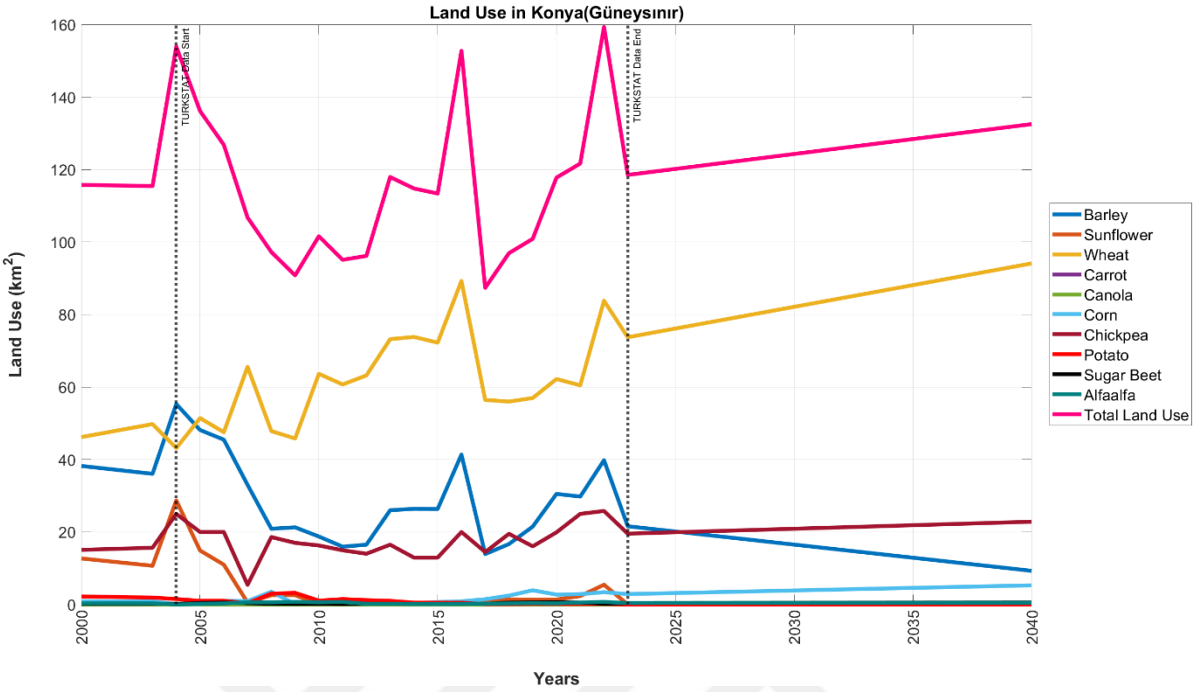

Figure B.23. Forecasted land use for the town of Güneysınır, Konya.

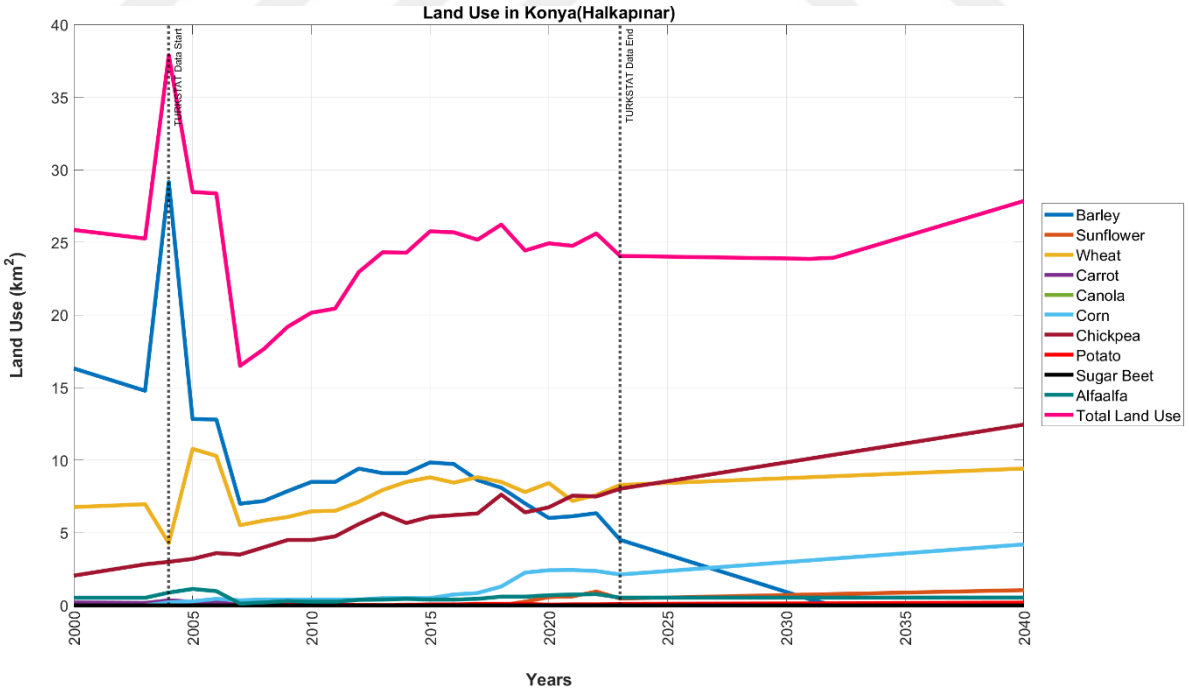

Figure B.24. Forecasted land use for the town of Halkapınar, Konya.

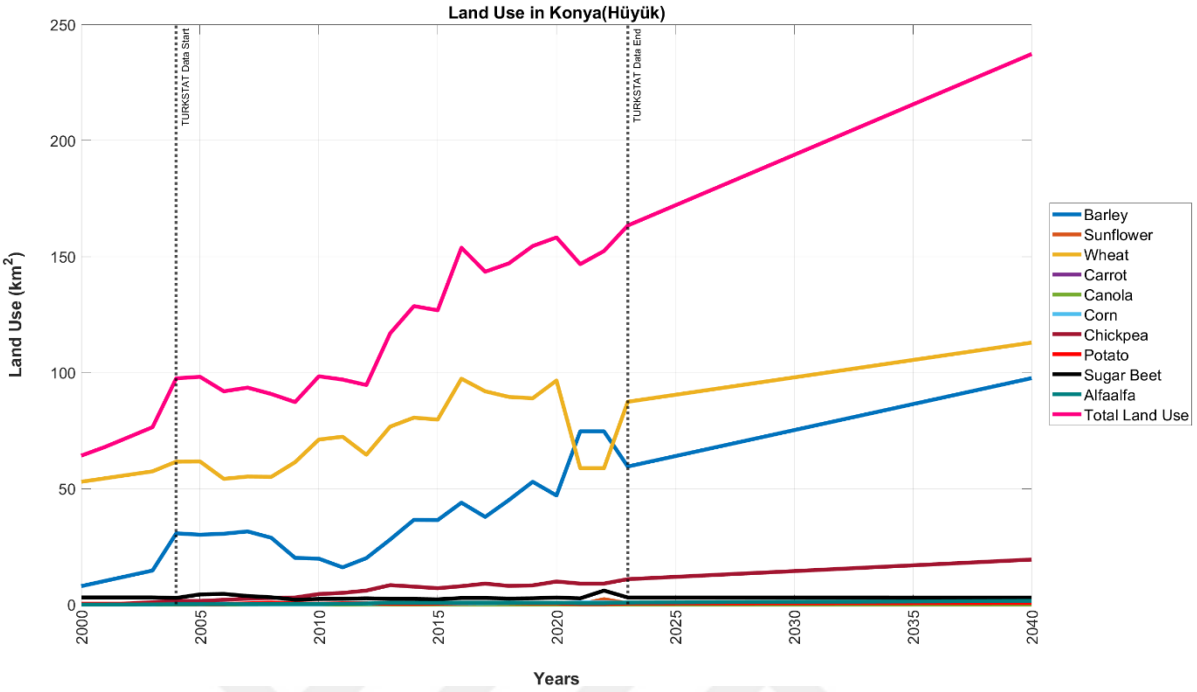

Figure B.25. Forecasted land use for the town of Hüyük, Konya.

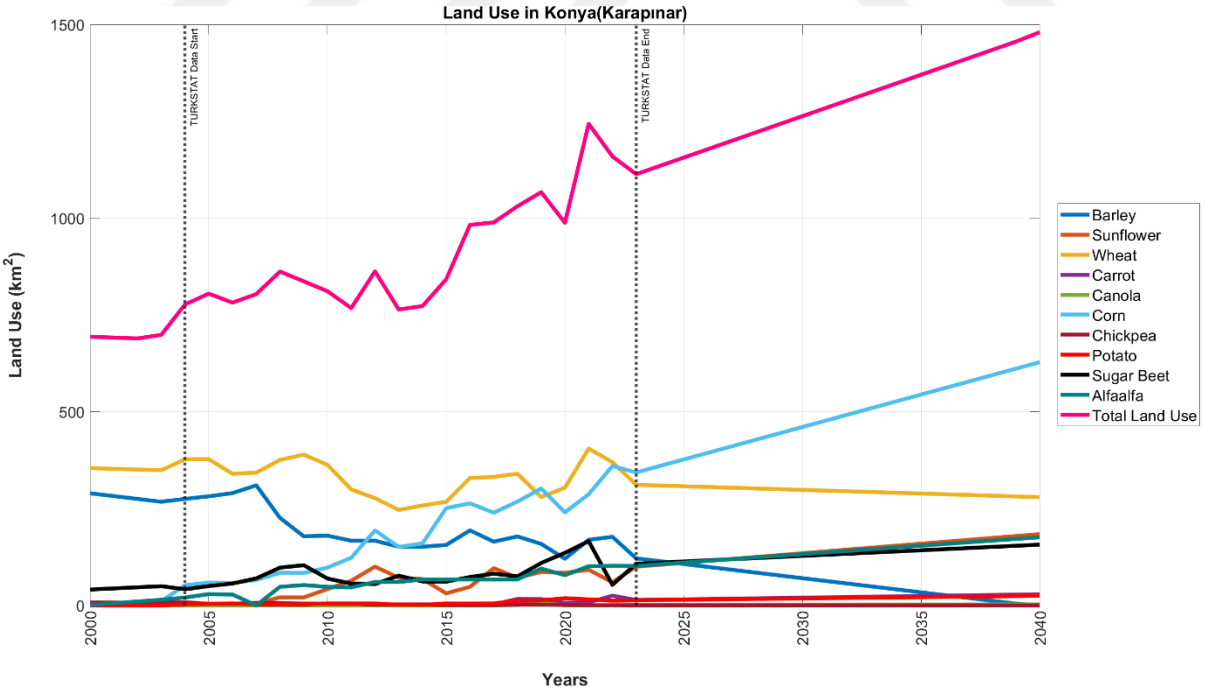

Figure B.26. Forecasted land use for the town of Karapınar, Konya.

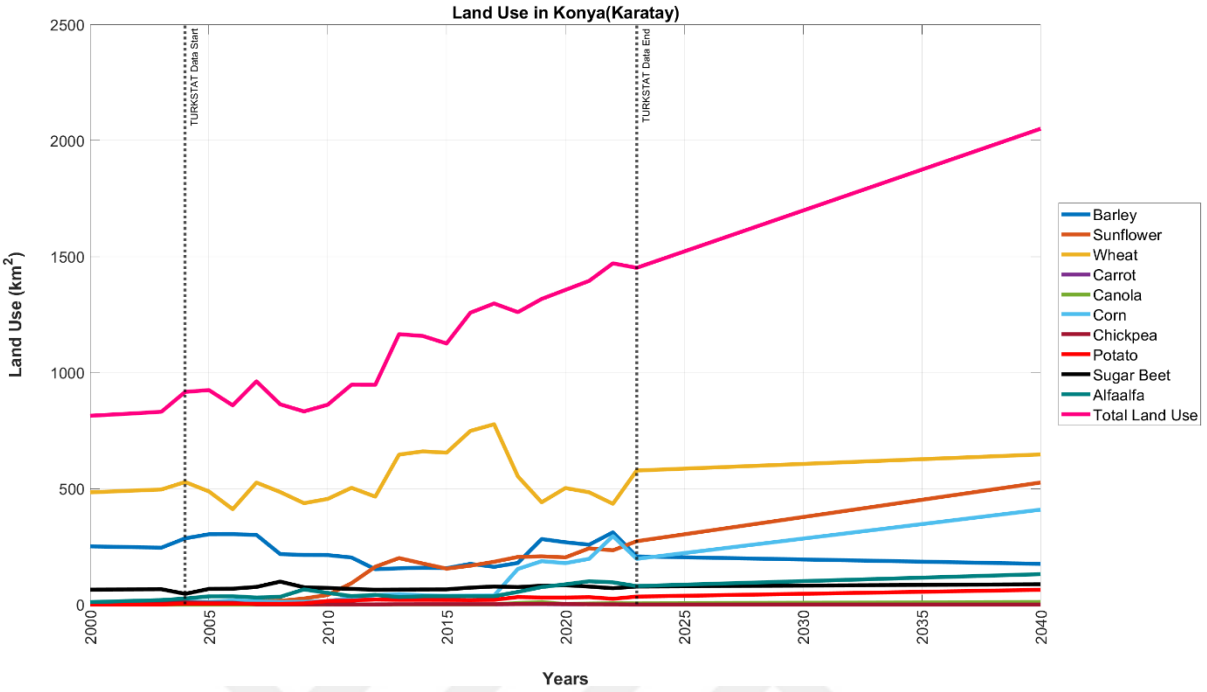

Figure B.27. Forecasted land use for the town of Karatay, Konya.

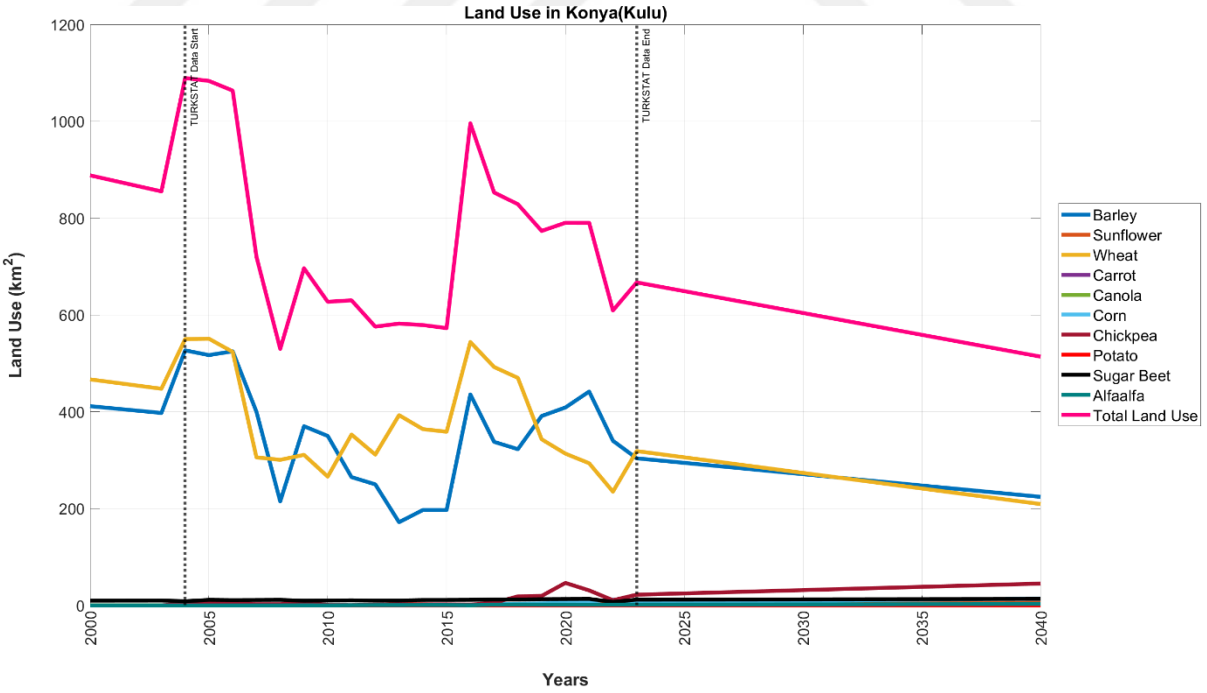

Figure B.28. Forecasted land use for the town of Kulu, Konya.

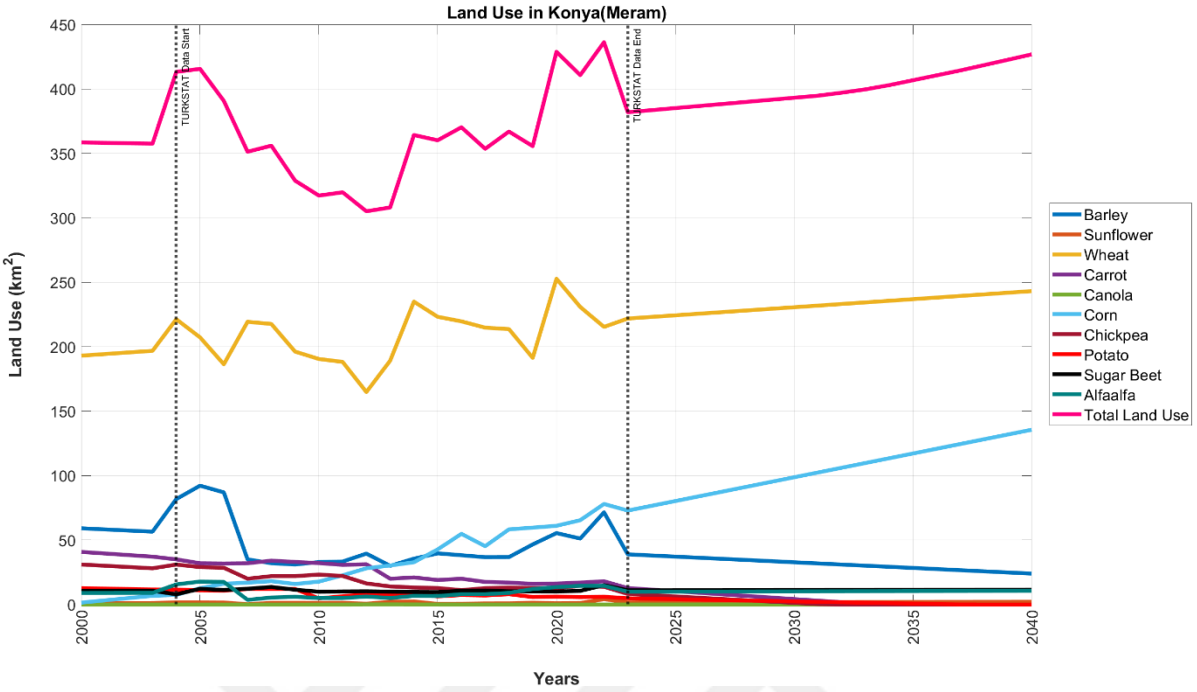

Figure B.29. Forecasted land use for the town of Meram, Konya.

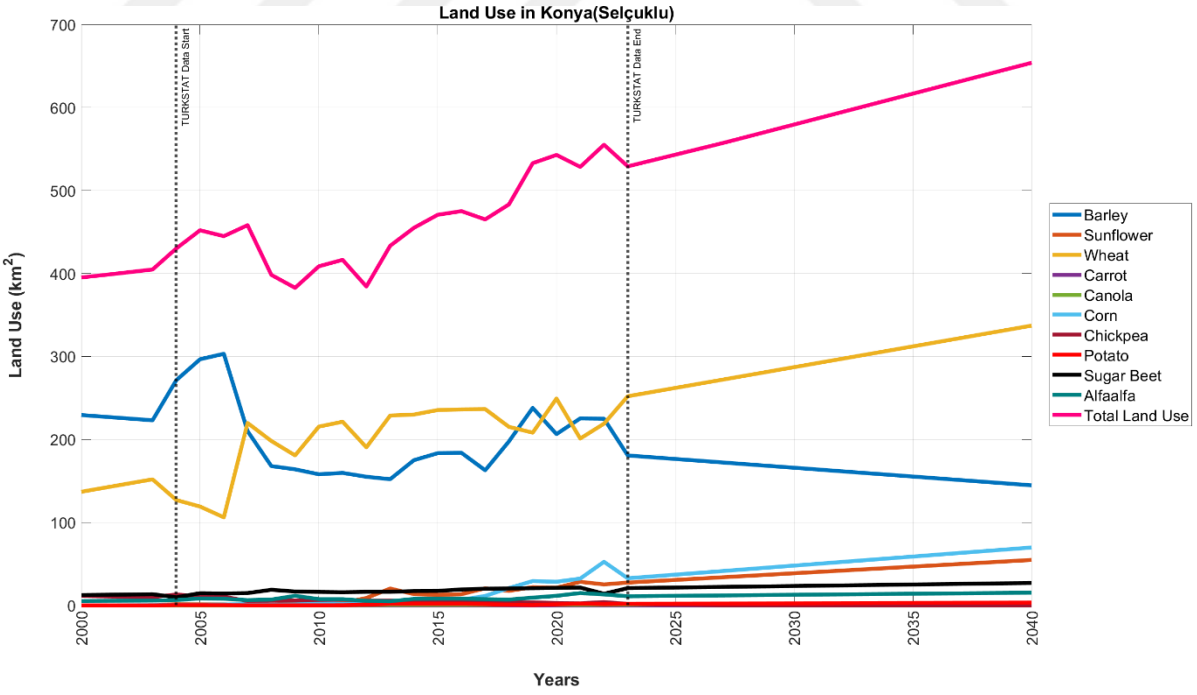

Figure B.30. Forecasted land use for the town of Selçuklu, Konya.

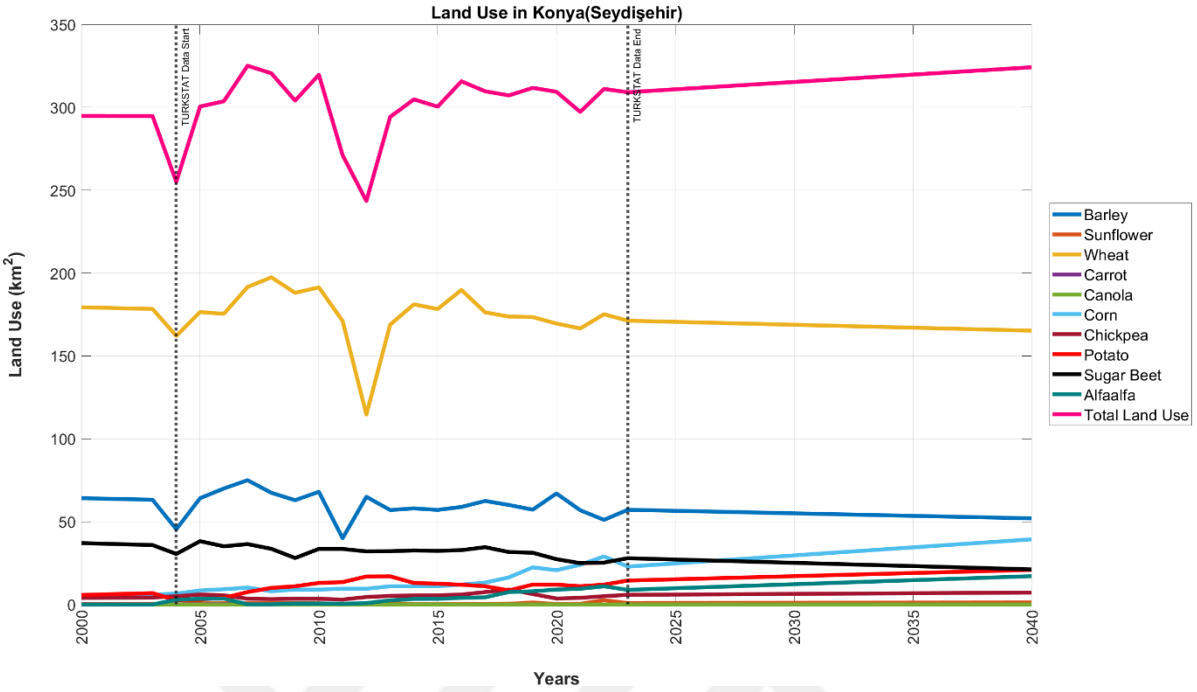

Figure B.31. Forecasted land use for the town of Seydişehir, Konya.

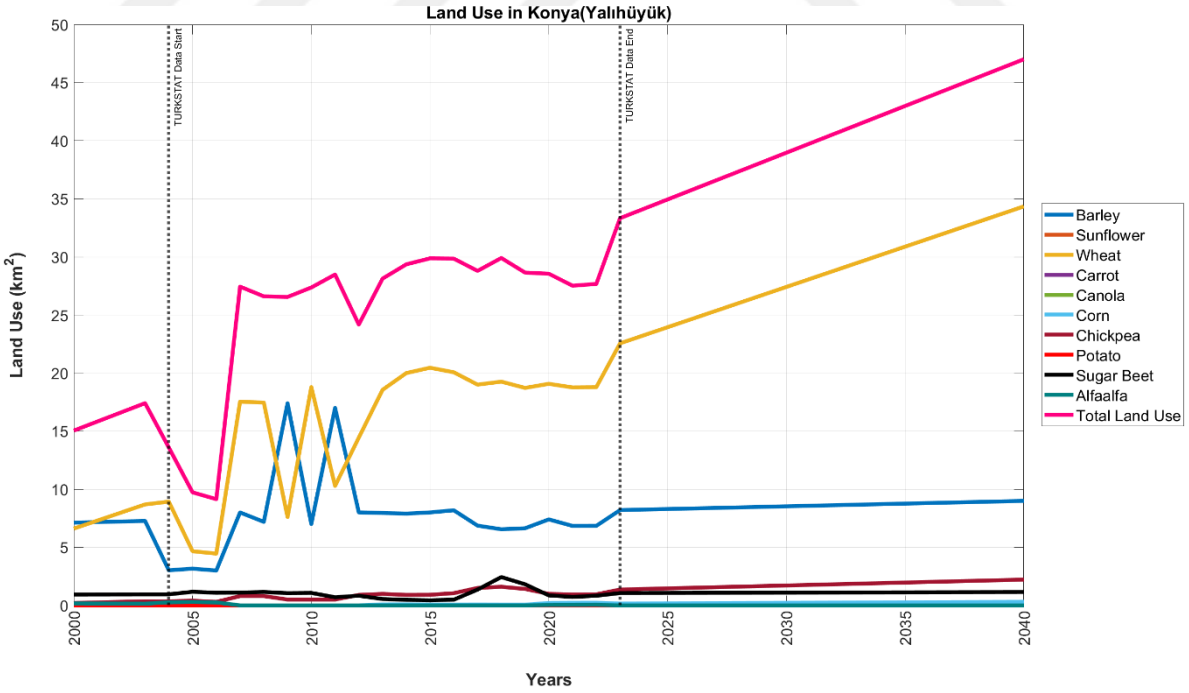

Figure B.32. Forecasted land use for the town of Yalıhüyük, Konya.

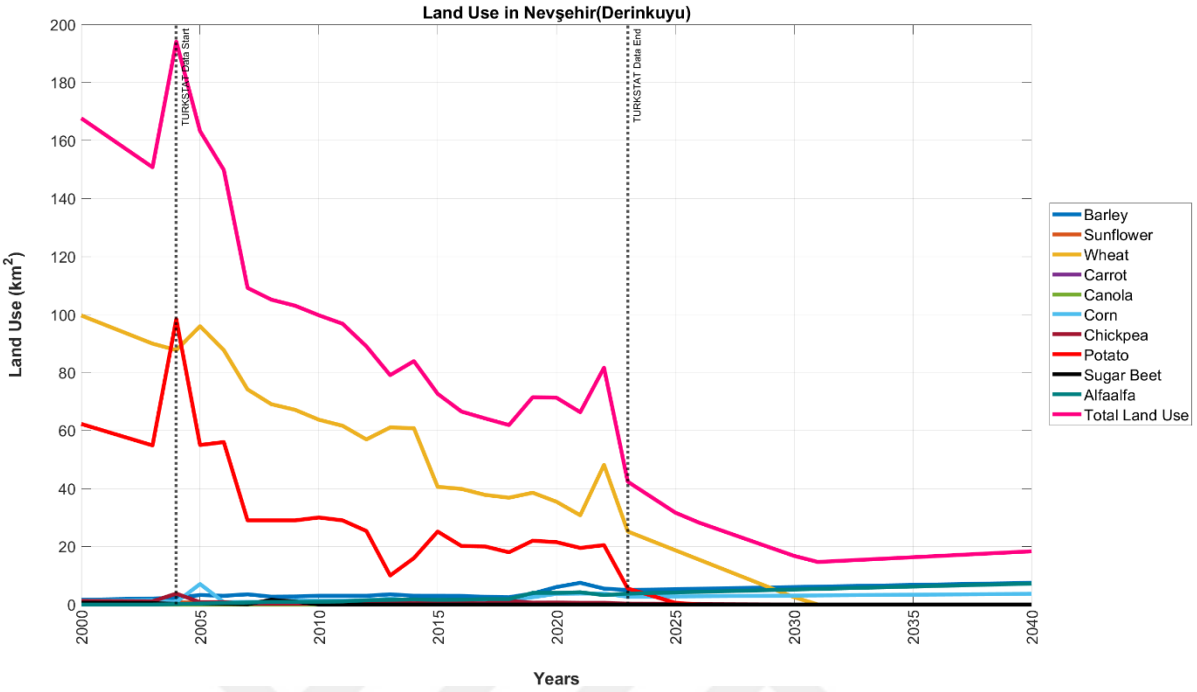

Figure B.33. Forecasted land use for the town of Derinkuyu, Nevşehir.

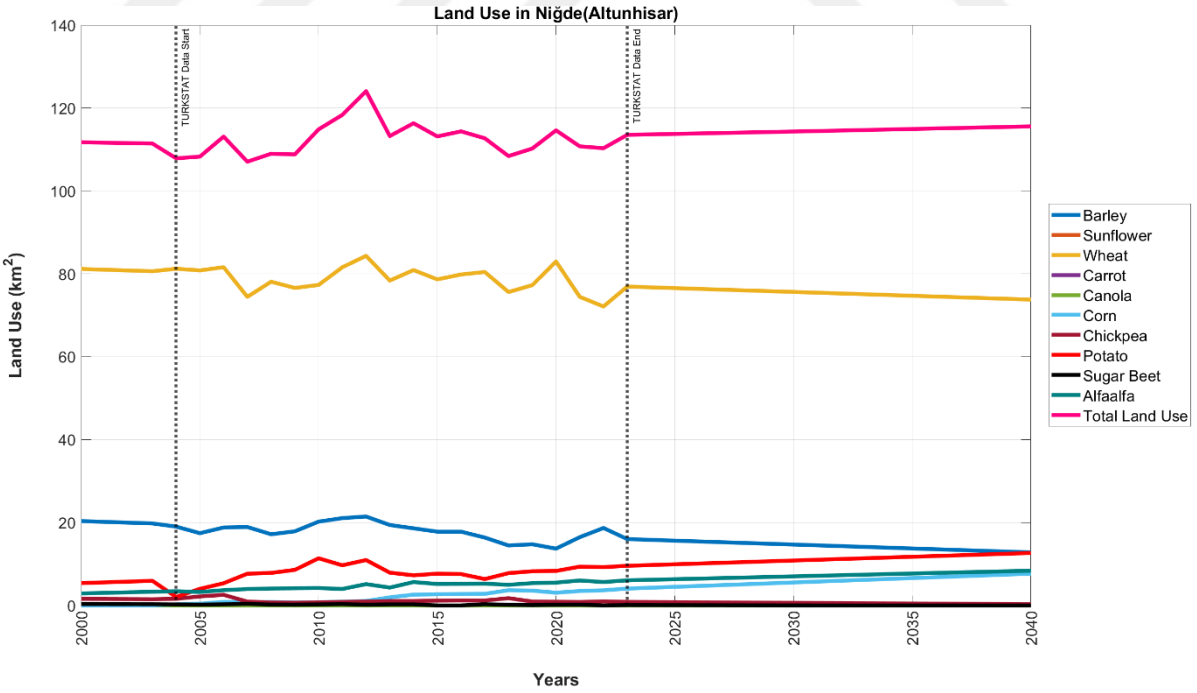

Figure B.34. Forecasted land use for the town of Altunhisar, Niğde.

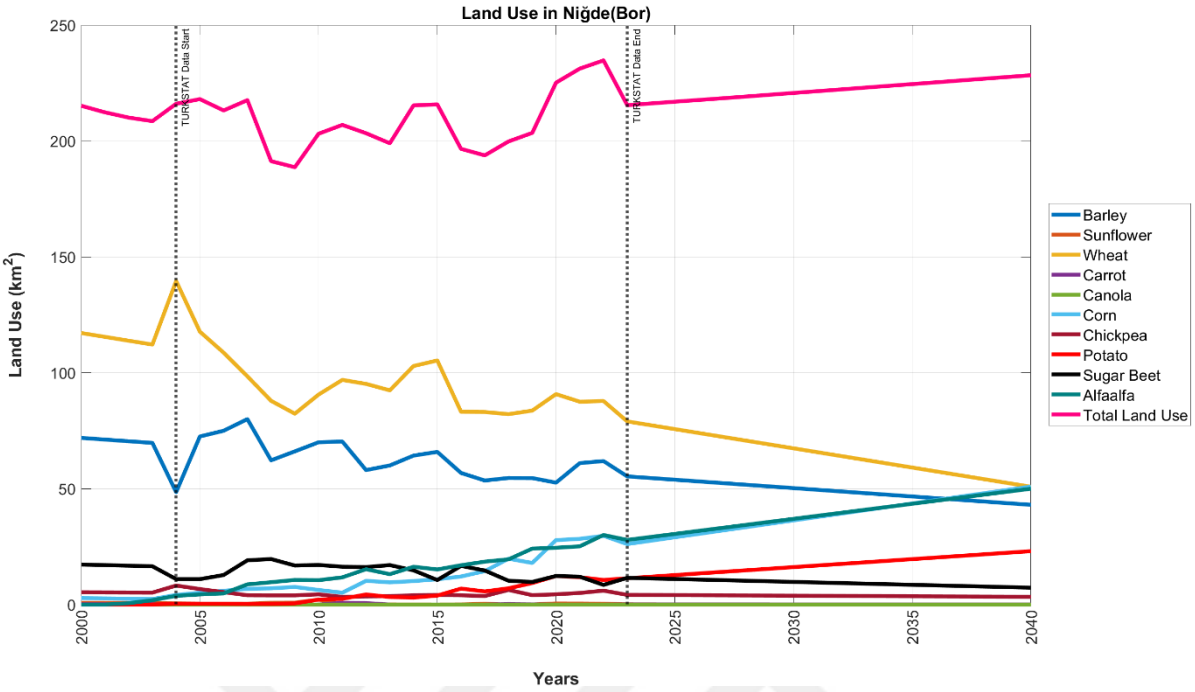

Figure B.35. Forecasted land use for the town of Bor, Niğde.

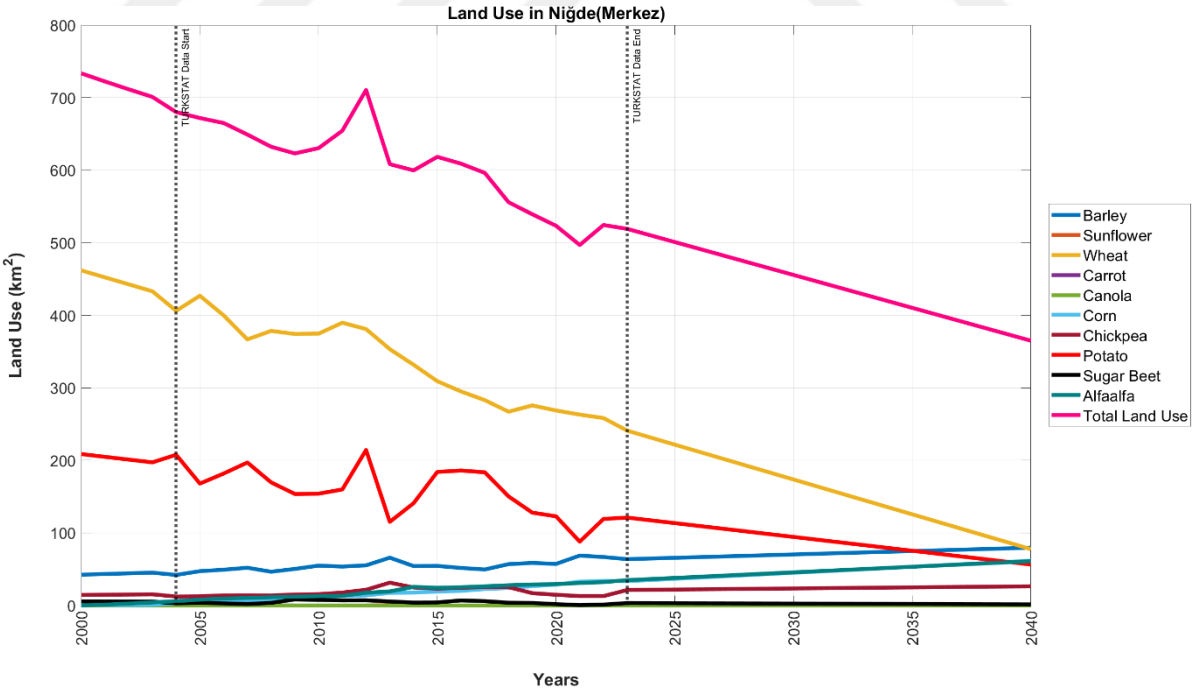

Figure B.36. Forecasted land use for the town of Merkez, Niğde.

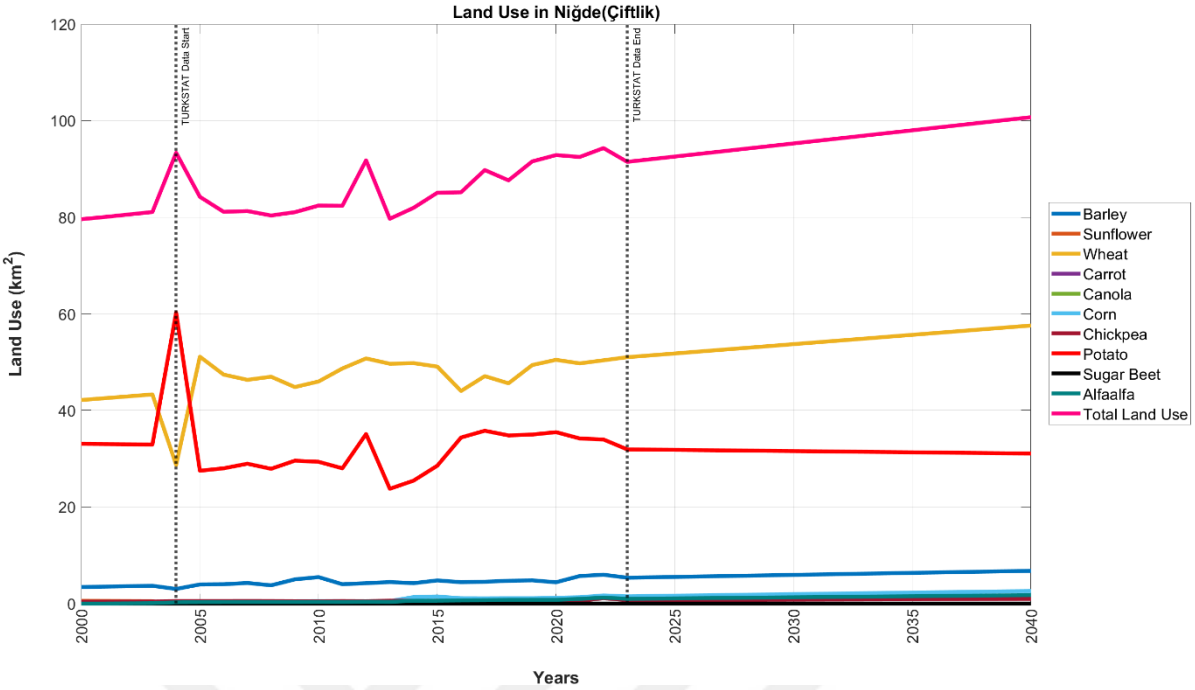

Figure B.37. Forecasted land use for the town of Çiftlik, Niğde.

APPENDIX C: PUMPING TEST RESULTS

Table C.1. Pumping test results from Yeşil Reports of State Hydraulic Works

Well ID	Well Name	Year	Water Yielding Layer	Spesific Capacity (lt/sec/m)	Aquifer Thickness (m)	Transmissibility Coefficient (m3/day/m)
182	Batum	1968	Limestone	2.9	125	1900
243	Göztepe	1958	-	6.3	193*	400
246	Beydili	1958	-	1.9	225*	600
251	Aşiran Yaylası	1961	-	3.4	193*	300
253	Şarlak Höy.	1968	Limestone	4.0	39	3300
292	Kulu (TMO)	-	Conglomerate	0.17	15	20
295	Kepir Y.	-	Conglomerate	1.1	32	100
297	Hacıbektaş	-	Conglomerate	0.37	21	120
329	Akköy	-	Miocene limestone	13.4	125	4200
345	Kiledere	-	Sand-Gravel-Tuff	23	230	6320
346	Ağçasar	-	Sand-Gravel	6	117	480
351	Bekarköy	-	Sand-Gravel-Tuff	1.5	190	160
1669	Merdivenli Kuyu	1967	Sand-Gravel	2.4	63	1580
2842	Edikli	-	Sand-Gravel-Tuff	1.3	144	150
5652	Tömek	1964	Limestone	10.8	152	1250
6488	Ölmezköy	-	Miocene limestone	26.4	30	7030
6489	Zıvarık	-	Miocene limestone	6.5	21	1866
6796	Toplanı Hayrat	1965	-	2.4	75.45*	150
7032	Höyük İstasyonu	-	Tuff	1.2	136	250
7033	Alayköy	-	Tuff-Basalt	18.5	164	3600
7803	Edikli	-	Sand-Gravel	0.4	42	20
7804	Misli Çayırı	-	Sand-Gravel	1	141	140
8076	Hatip	1966	Serpentine	5.52	28	650
8077	Hatip	1966	Serpentine	6.29	50	3150
8078	Karaman Kooperatifi	1967	-	8	311*	2974

8095	Hatip	1966	Limestone-Serpentine	1	55	1400
8096	Hatip	1966	Serpentine	2.4	42	1750
8159	Eğribayat	1968	Limestone-Serpentine	1	128	105
8184	Hatip	1966	Serpentine	8.81	57	870
8201	Hatip	1967	Serpentine	2.59	71	800
8219	Yeniköy	1967	Sand-Gravel	2.1	29	964
8220	Yeniköy	1967	Sand-Gravel	2.8	24	865
8221	Yeniköy	1967	Sand-Gravel	2.3	99	1360
8304	Yenibahçe	1967	Limestone	3.81	55	200
8305	Yenibahçe	1968	Limestone-Marl	60.4	67	800
8306	Yenibahçe	1967	Limestone	48.78	26	3160
8307	Yenibahçe	1967	Limestone-Marl	33.01	27	6270
8308	Yenibahçe	1968	Limestone-Marl	3.62	51	2000
8309	Yenibahçe	1967	Limestone-Marl	150	45	20500
8310	Yenibahçe	1967	Limestone	160	29	2100
8311	Yenibahçe	1967	Limestone	53.73	19	7900
8312	Yenibahçe	1967	Limestone	182	20	5300
8313	Yenibahçe	1967	Limestone-Marl	8.51	26	2280
8314	Yenibahçe	1967	Limestone	20.89	35	12600
8315	Yenibahçe	1967	Limestone-Marl	66	20	4500
9431	Alibeyhöyüğü	1968	Limestone-Marl	1.8	140	550
9432	Hatip	1967	Serpentine	3.47	44	3750
9433	Hatip	1967	Conglomerate-Serpentine	2.29	65	500
9543	Alibeyhöyüğü	1968	Limestone-Marl	4.32	162	4200
9544	Alibeyhöyüğü	1967	Limestone-Marl	3	109	1200
9545	Alibeyhöyüğü	1967	Limestone-Marl	5	132	1680
9546	Alibeyhöyüğü	1968	Limestone-Marl-Conglomerate	15.57	142	2400
9547	Alibeyhöyüğü	1967	Limestone-Marl	5.15	105	1460
9548	Alibeyhöyüğü	1967	Limestone-Marl	3.31	108	530
9553	Mandra	-	Sandstone-Conglomerate	0.39	75	32

9554	Hayret Y.	-	Conglomerate	1.62	21	650
9556	Tekiryaylası	-	Miocene limestone	2.15	34	500
9557	Tutup	-	Paleozoic limestone	Very High	13.5	8000
9841	Kayı Köyü	1967	Tuff-Sand-Gravel	8.9	114	3759
10024	Hasanoba	1968	Limestone-Marl	8	115	1500
10025	Hasanoba	1968	Limestone-Marl	81	129	1500
10026	Hasanoba	1968	Limestone-Marl	14.6	91	5400
10027	Hasanoba	1968	Limestone-Marl	23.1	108	4800
10028	Hasanoba	1968	Limestone-Marl	11.6	97	1200
10029	Hasanoba	1968	Limestone-Marl	11.9	97	3000
10030	Hasanoba	1968	Limestone-Marl	12.4	93	7000
10031	Hasanoba	1968	Limestone-Marl	12.25	83	4000
10464	Sarıcalar	1968	Limestone-Marl	1.06	63	500
10465	Sarıcalar	1968	Limestone-Marl	1.3	72	450
10466	Sarıcalar	1968	Limestone-Marl	2.56	48	450
10475	Sarıcalar	1968	Limestone-Marl	0.77	56	130
10476	Sarıcalar	1968	Limestone-Marl-Conglomerate	1.54	78	100
10477	Sarıcalar	1968	Limestone-Marl-Conglomerate	0.88	93	150
11143	Altınhisar	1968	Sand-Gravel	15.5	125	2500
11913	Altınhisar	1968	Sand-Gravel	9.2	142	6500
12154	Yeni Zengen	1969	Sand-Gravel	5.8	53	5277
12157	Yeni Zengen	1969	Tuff-Sand-Gravel-Limestone	4.2	80	3280

*The aquifer thickness is obtained from cross sections of hydrogeological maps which is shown in Figure C.2.

Table C.2. Pumping tests from SUİŞ report

Well ID	Well Name	Transmissibility Coefficient (m3/day/m)	Hydraulic Conductivity (m/day)
16001	Beyşehir-Kaşaklı	66	0.47
16002	Beyşehir-Kaşaklı	1976	8.2
16003	Beyşehir-Kaşaklı	1897	46
16004	Beyşehir-Kaşaklı	163	0.58

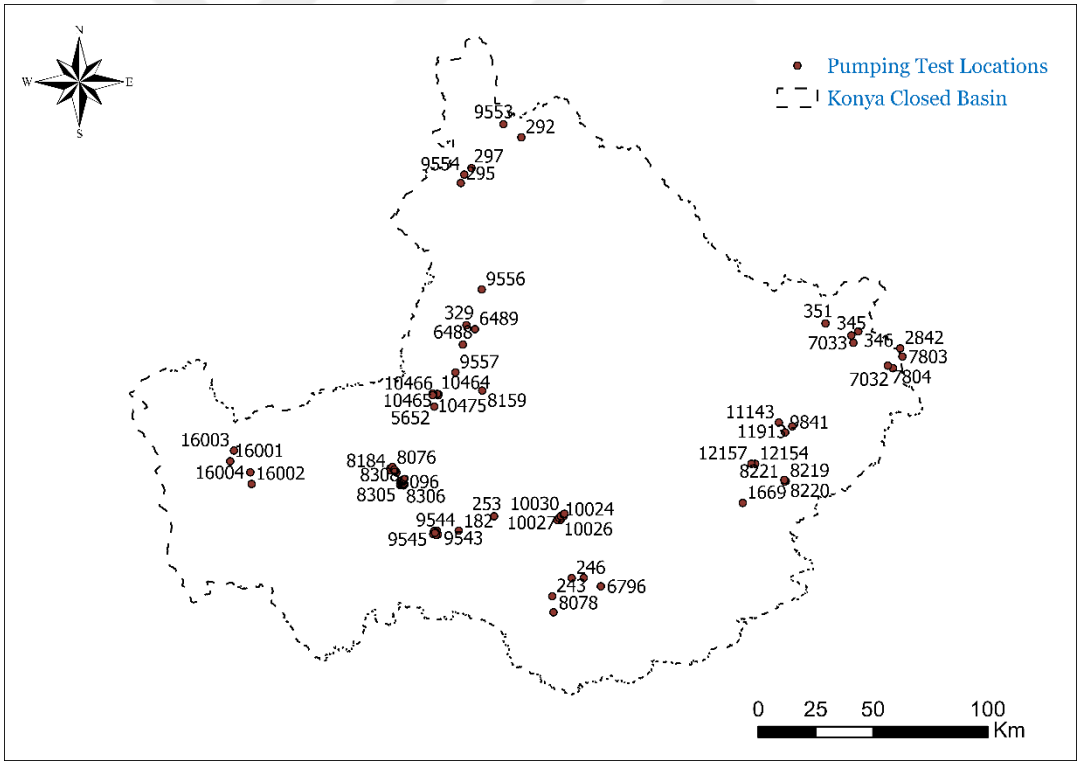

Figure C.1. Pumping test locations

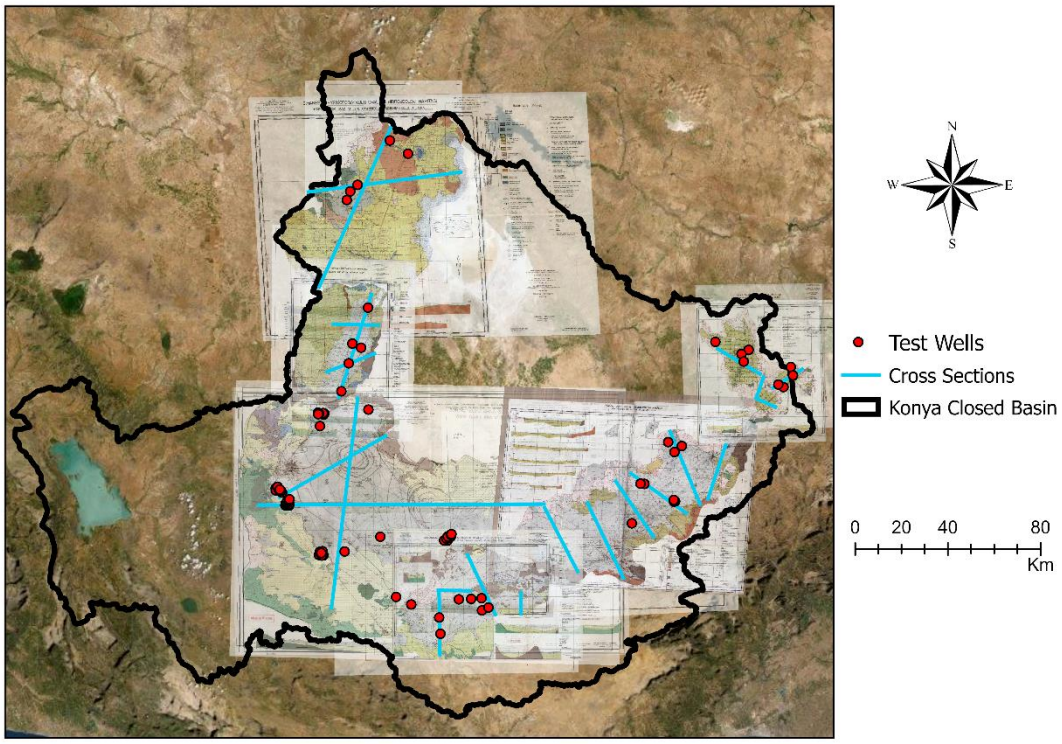

Figure C.2. Cross sections of hydrogeological maps of plains

APPENDIX D: PRECIPITATION AND TEMPERATURE UNDER REGIONAL CLIMATE MODELS FOR ALL STATIONS

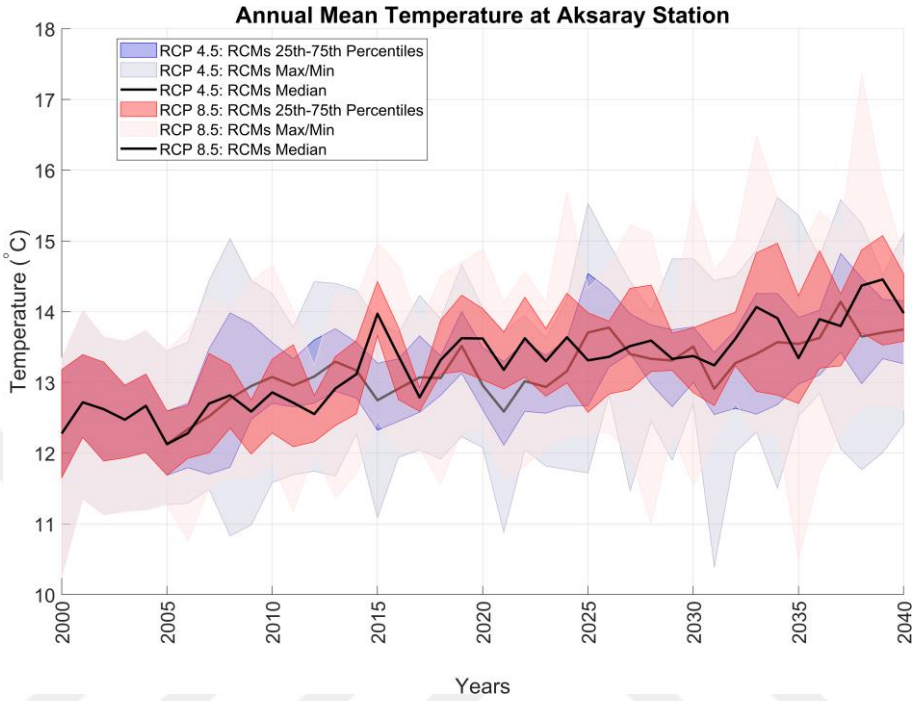

Figure D.1. Annual mean temperature according to 17 RCMs under RCP4.5 and RCP8.5 climatic pathways at Aksaray station.

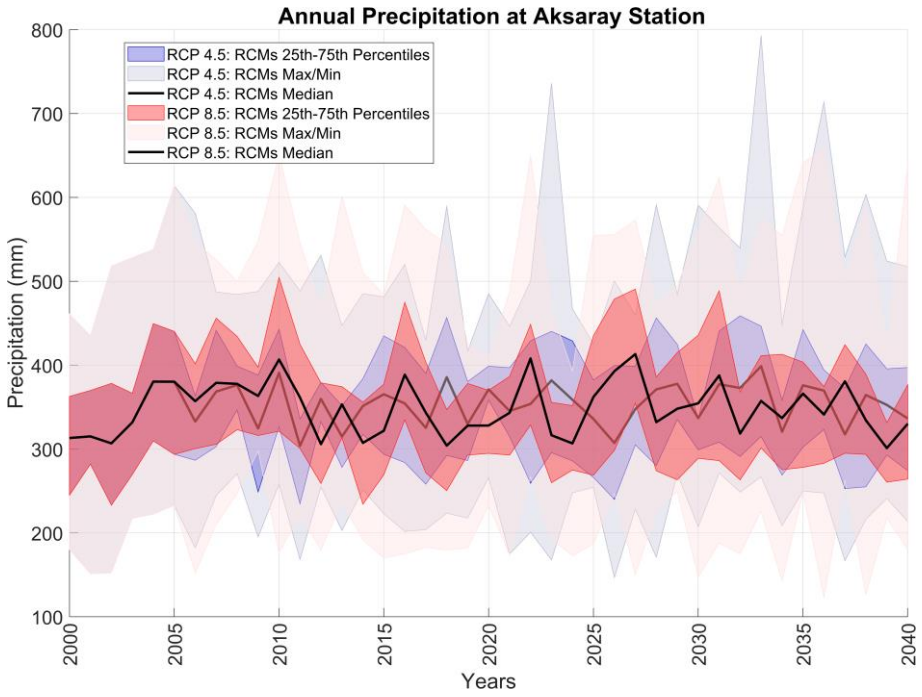

Figure D.2. Annual precipitation according to 17 RCMs under RCP4.5 and RCP8.5 climatic pathways at Aksaray station.

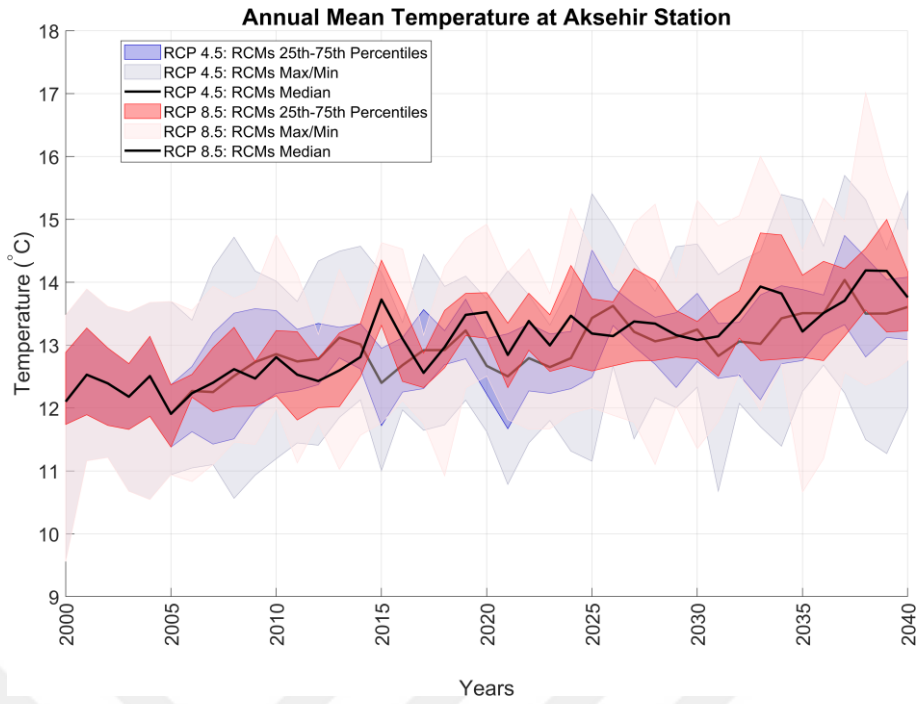

Figure D.3. Annual mean temperature according to 17 RCMs under RCP4.5 and RCP8.5 climatic pathways at Akşehir station.

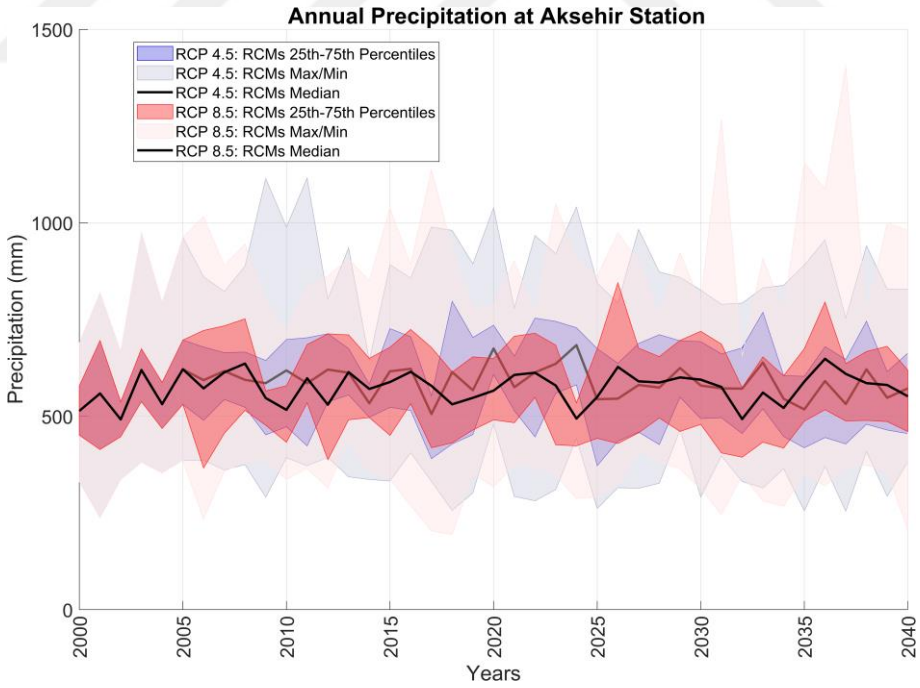

Figure D.4. Annual precipitation according to 17 RCMs under RCP4.5 and RCP8.5 climatic pathways at Akşehir station.

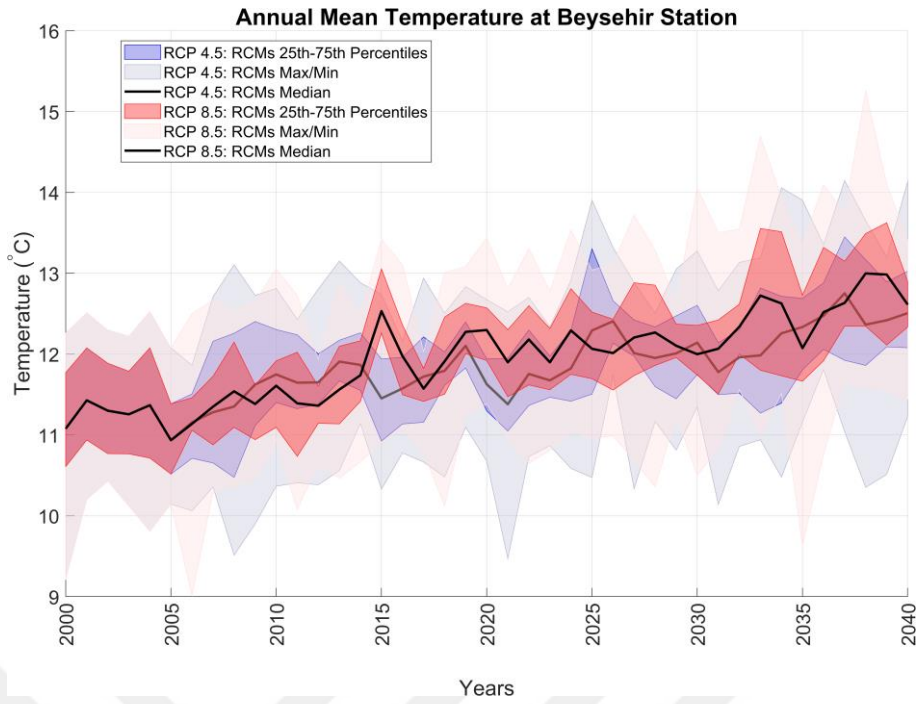

Figure D.5. Annual mean temperature according to 17 RCMs under RCP4.5 and RCP8.5 climatic pathways at Beyşehir station.

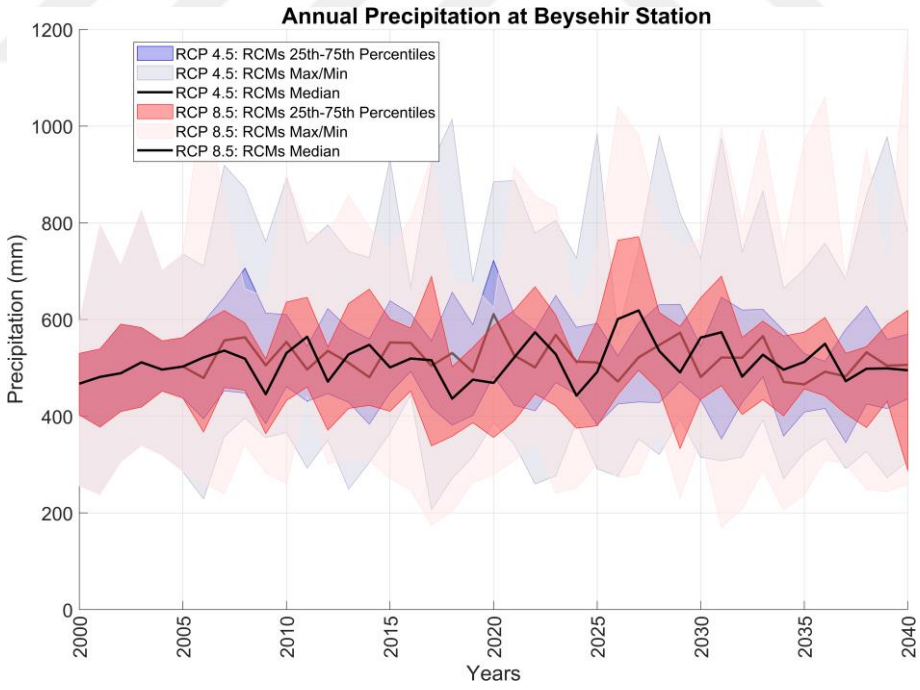

Figure D.6. Annual precipitation according to 17 RCMs under RCP4.5 and RCP8.5 climatic pathways at Beyşehir station.

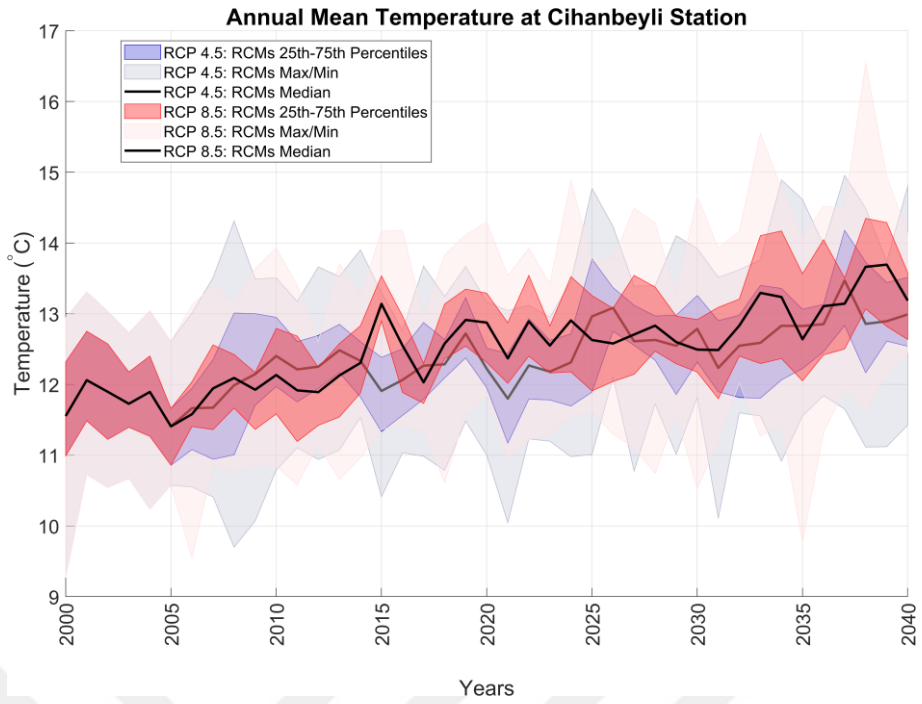

Figure D.7. Annual mean temperature according to 17 RCMs under RCP4.5 and RCP8.5 climatic pathways at Cihanbeyli station.

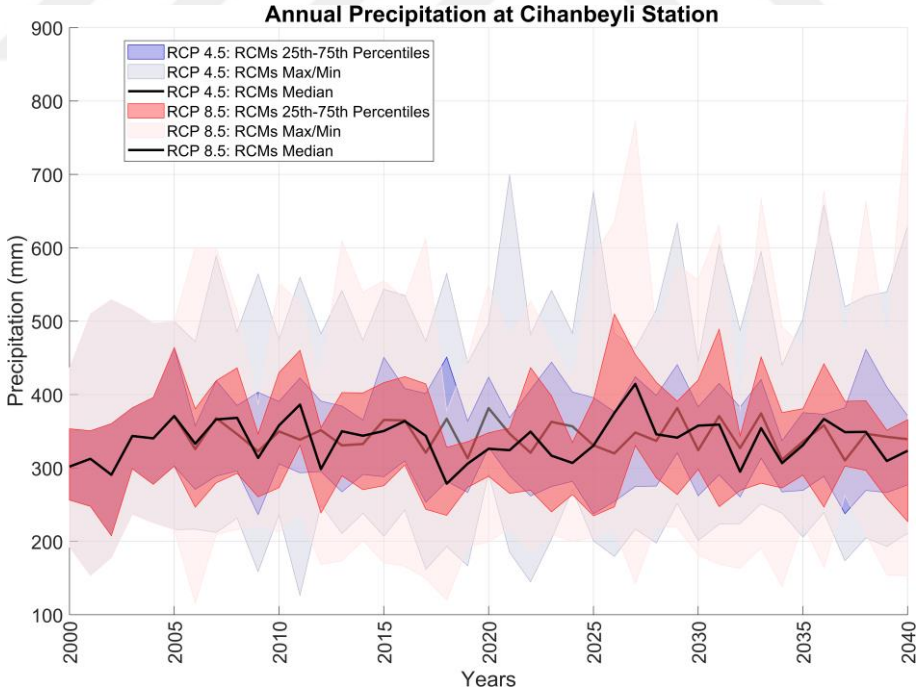

Figure D.8. Annual precipitation according to 17 RCMs under RCP4.5 and RCP8.5 climatic pathways at Cihanbeyli station.

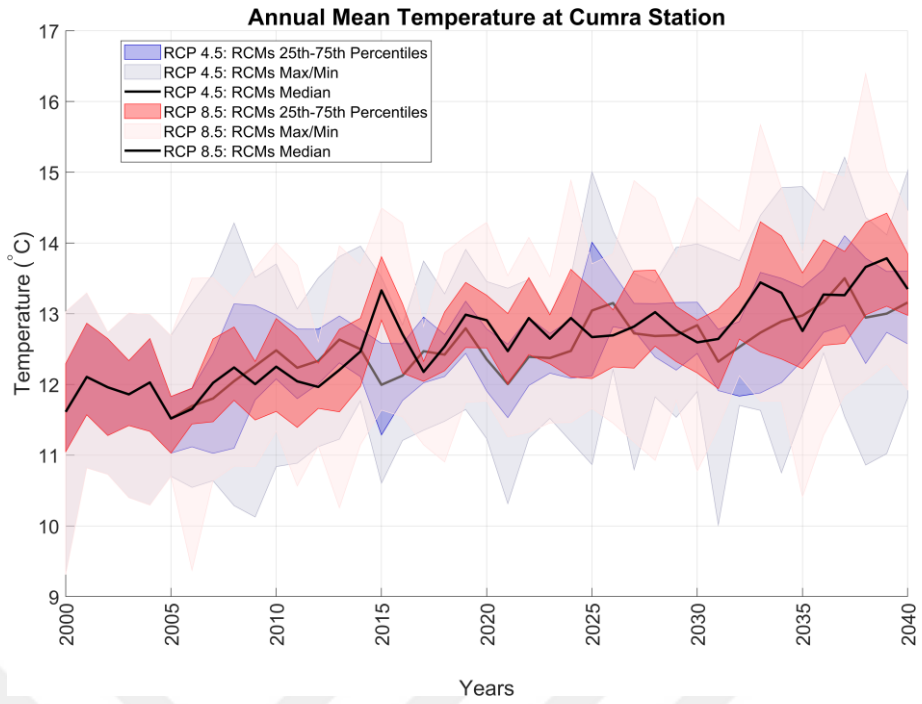

Figure D.9. Annual mean temperature according to 17 RCMs under RCP4.5 and RCP8.5 climatic pathways at Cumra station.

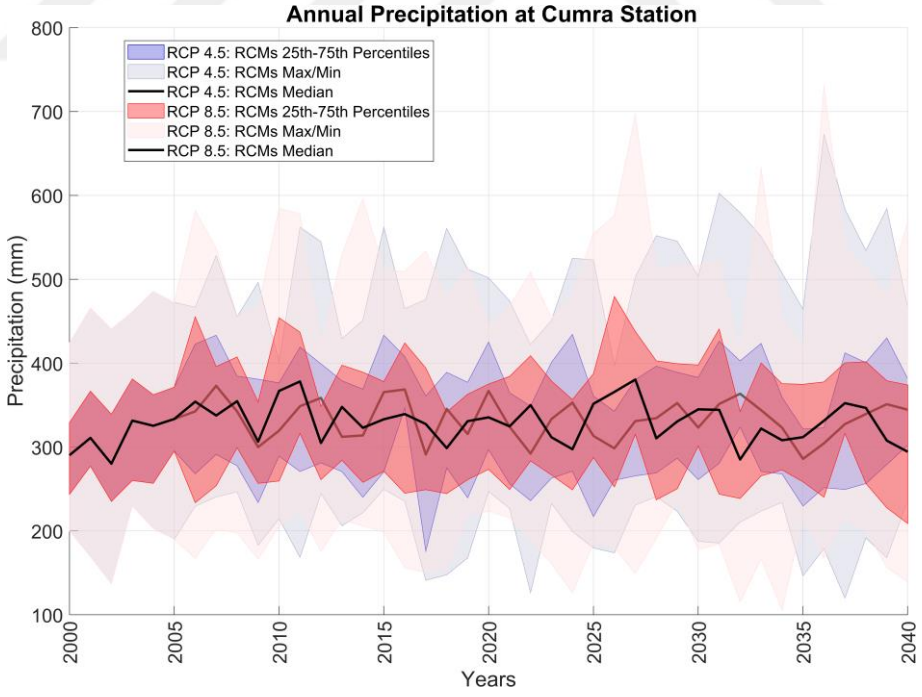

Figure D.10. Annual precipitation according to 17 RCMs under RCP4.5 and RCP8.5 climatic pathways at Çumra station.

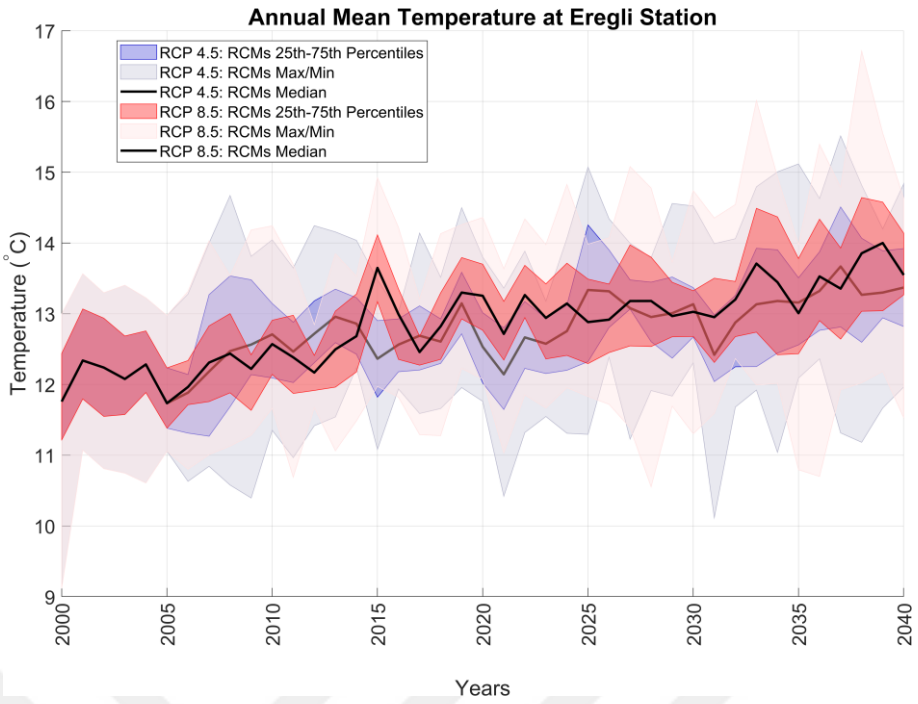

Figure D.11. Annual mean temperature according to 17 RCMs under RCP4.5 and RCP8.5 climatic pathways at Ereğli station.

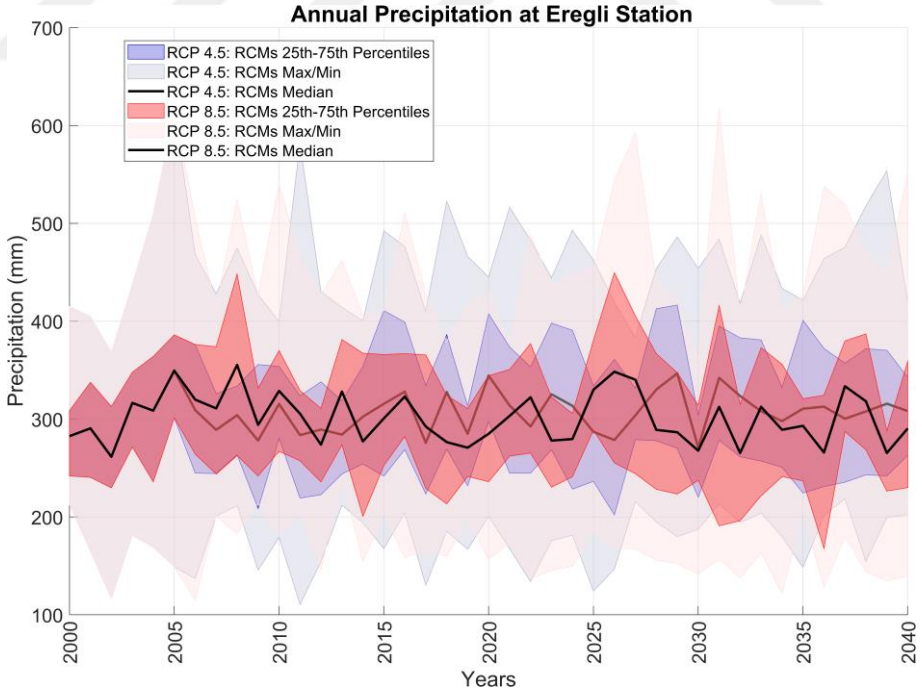

Figure D.12. Annual precipitation according to 17 RCMs under RCP4.5 and RCP8.5 climatic pathways at Ereğli station.

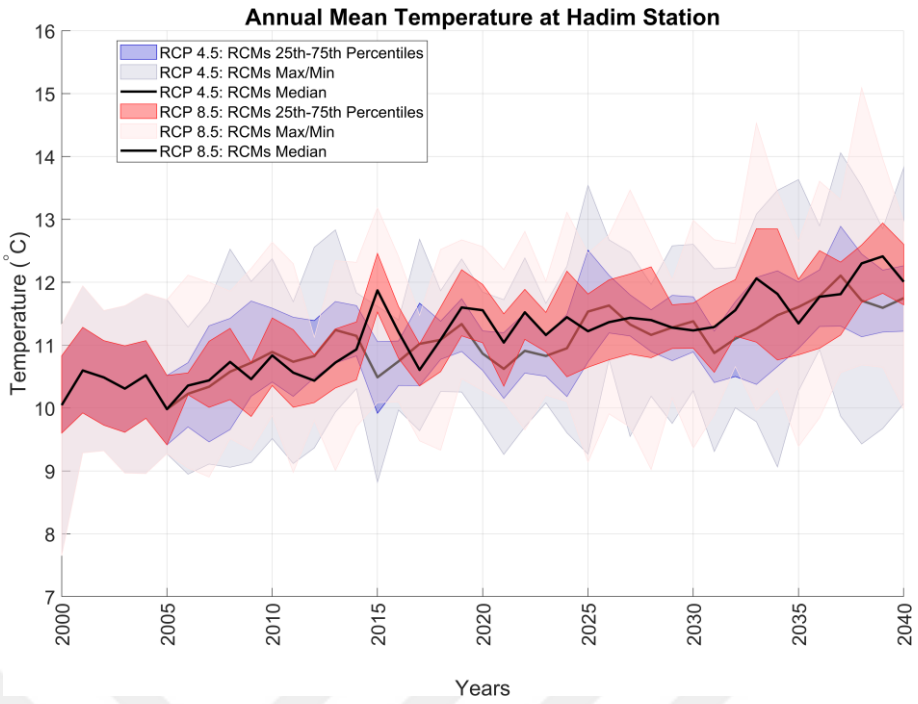

Figure D.13. Annual mean temperature according to 17 RCMs under RCP4.5 and RCP8.5 climatic pathways at Hadim station.

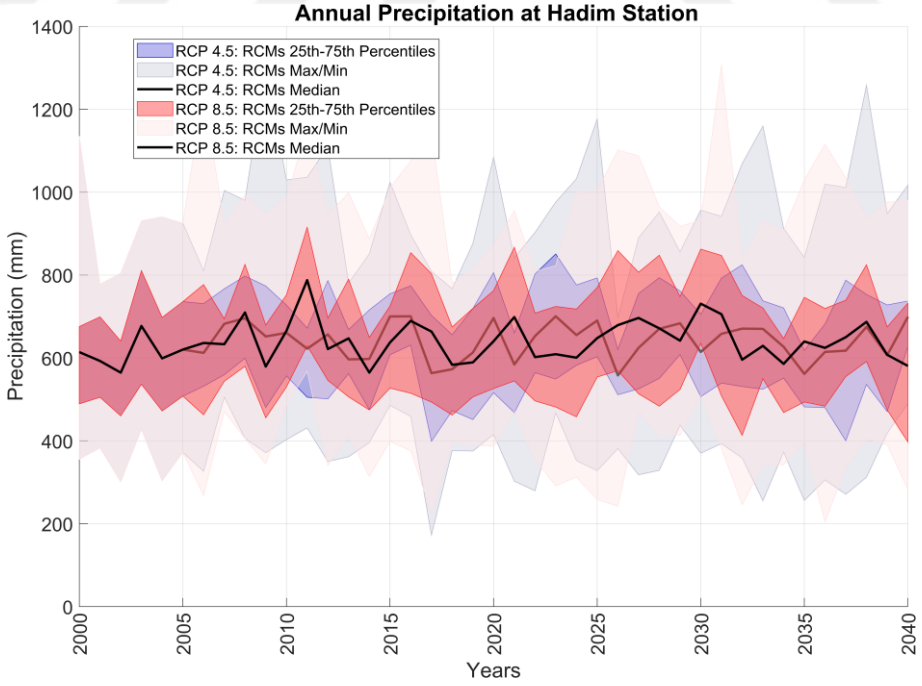

Figure D.14. Annual precipitation according to 17 RCMs under RCP4.5 and RCP8.5 climatic pathways at Hadim station.

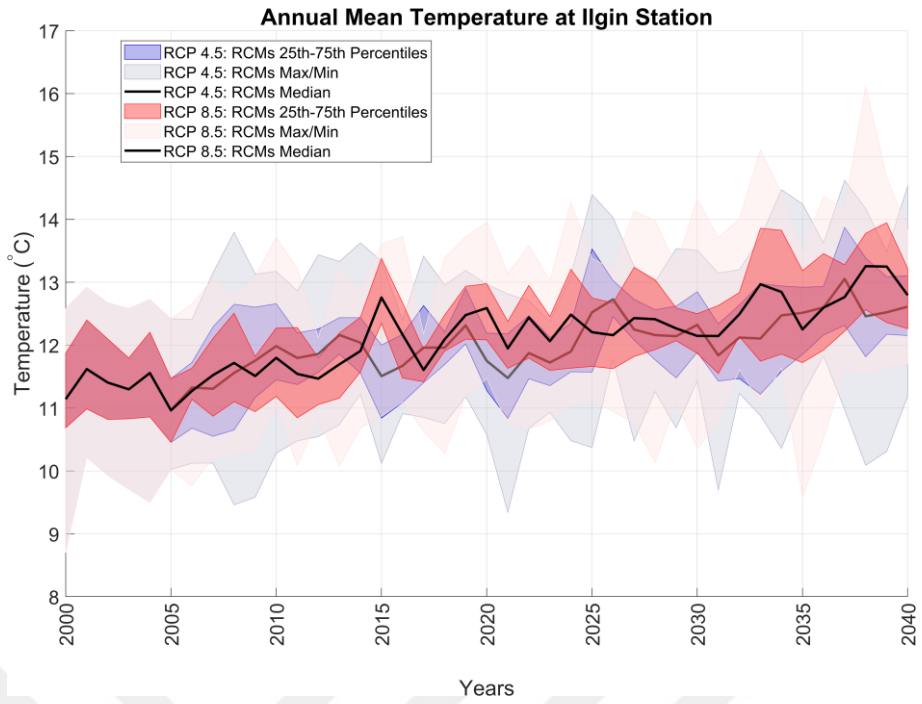

Figure D.15. Annual mean temperature according to 17 RCMs under RCP4.5 and RCP8.5 climatic pathways at Ilgın station.

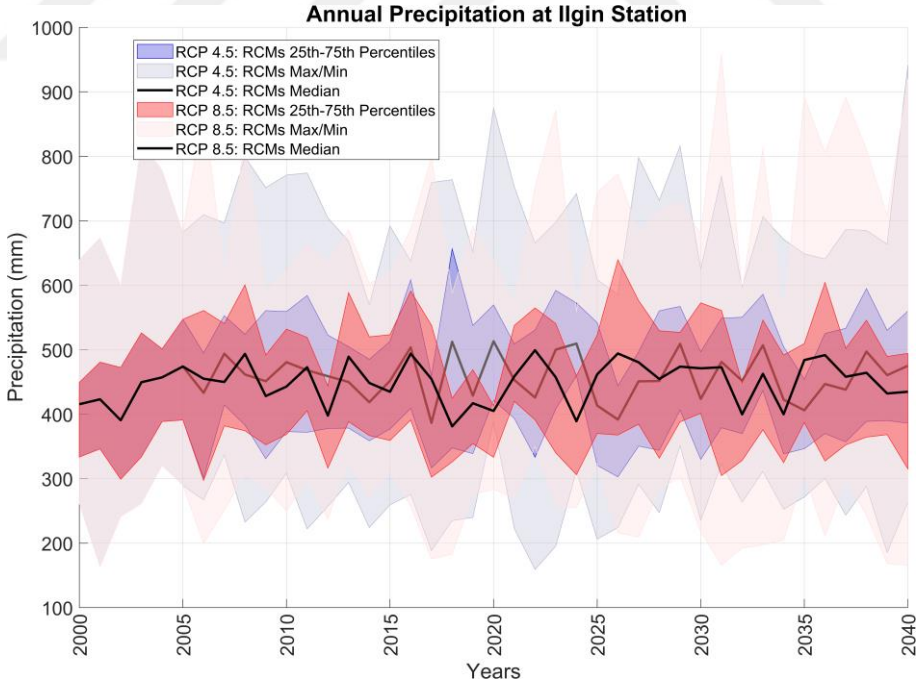

Figure D.16. Annual precipitation according to 17 RCMs under RCP4.5 and RCP8.5 climatic pathways at Ilgın station.

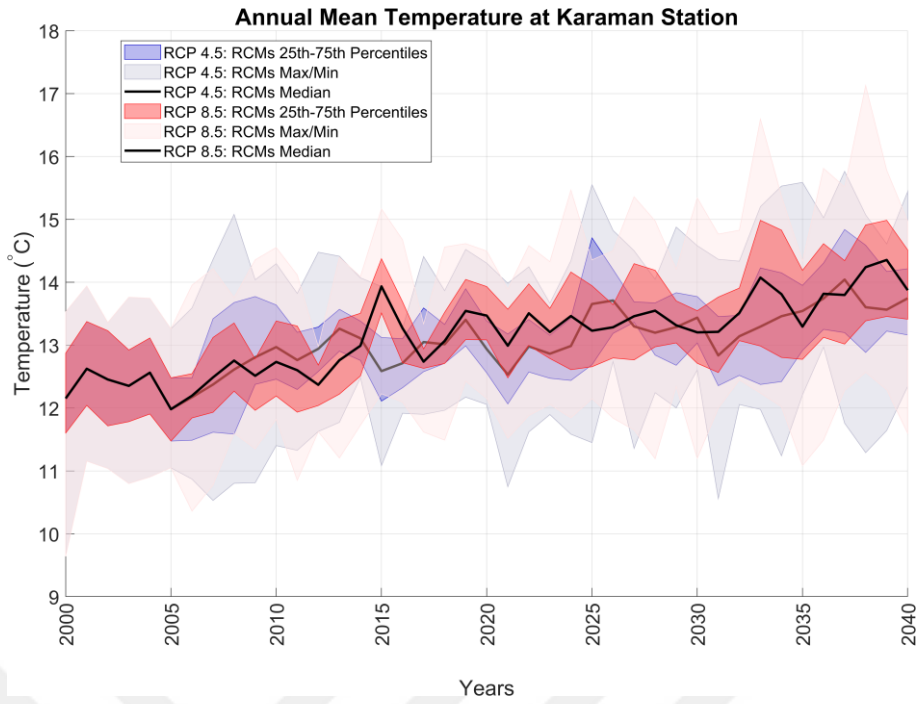

Figure D.17. Annual mean temperature according to 17 RCMs under RCP4.5 and RCP8.5 climatic pathways at Karaman station.

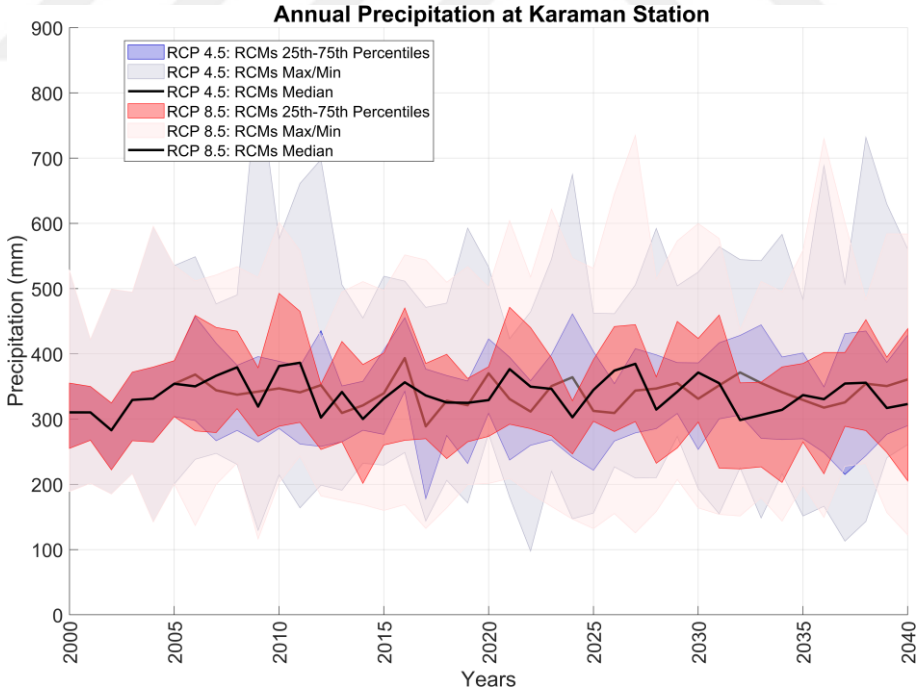

Figure D.18. Annual precipitation according to 17 RCMs under RCP4.5 and RCP8.5 climatic pathways at Karaman station.

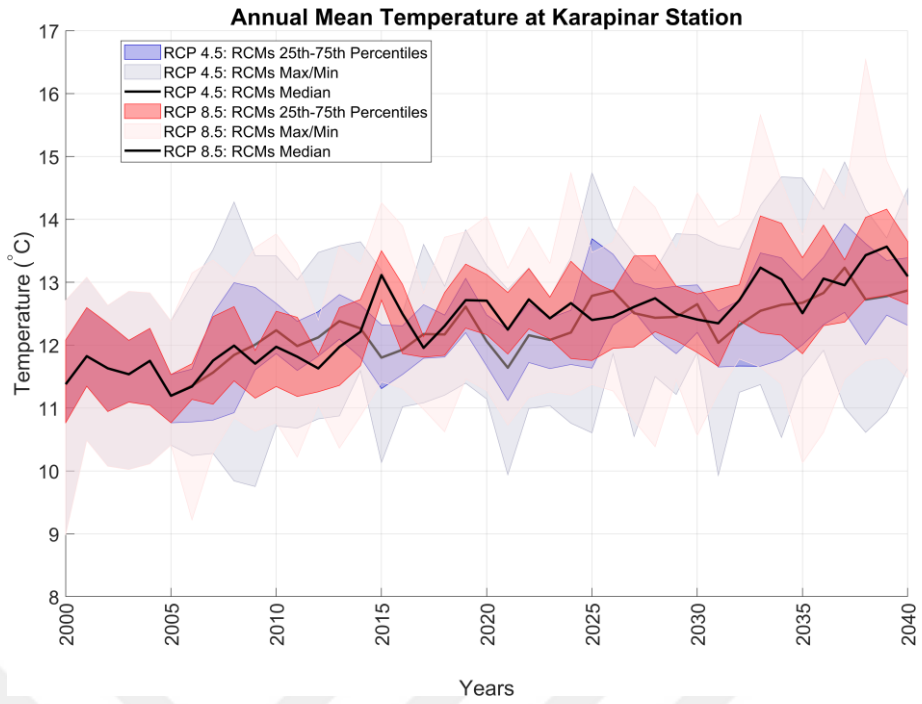

Figure D.19. Annual mean temperature according to 17 RCMs under RCP4.5 and RCP8.5 climatic pathways at Karapınar station.

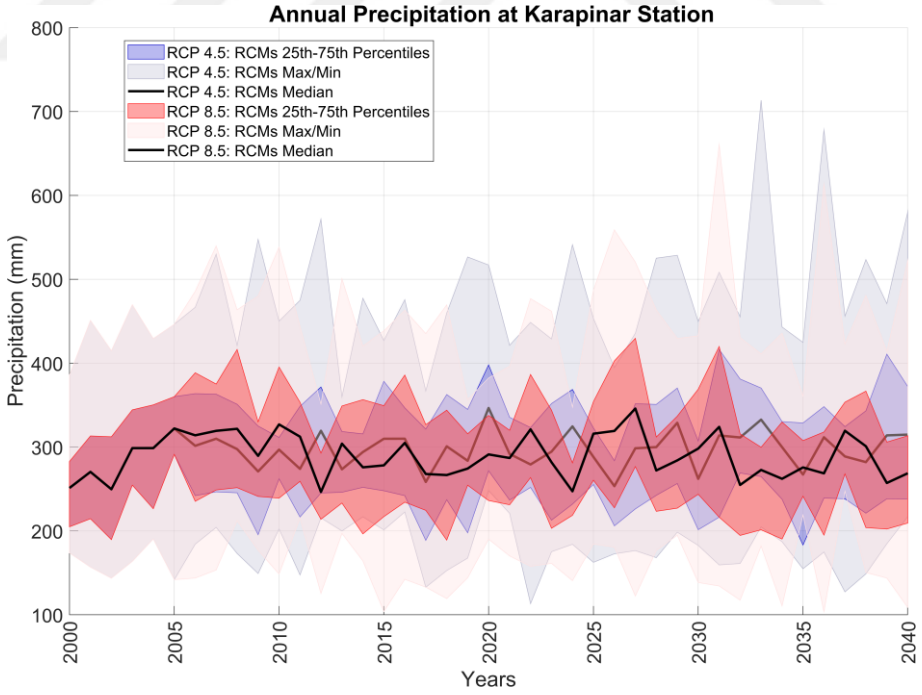

Figure D.20. Annual precipitation according to 17 RCMs under RCP4.5 and RCP8.5 climatic pathways at Karapınar station.

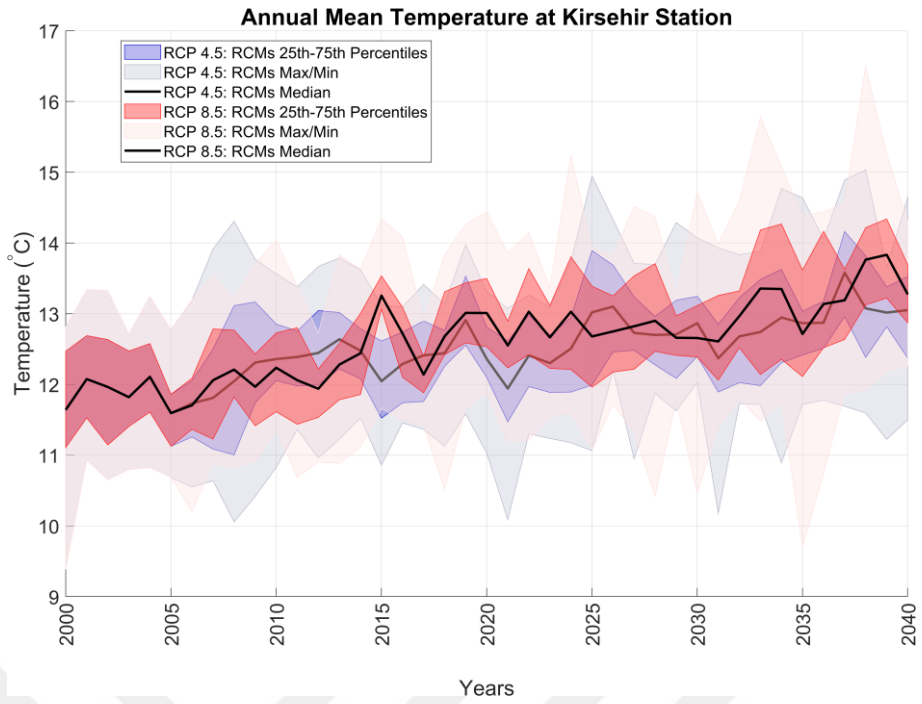

Figure D.21. Annual mean temperature according to 17 RCMs under RCP4.5 and RCP8.5 climatic pathways at Kırşehir station.

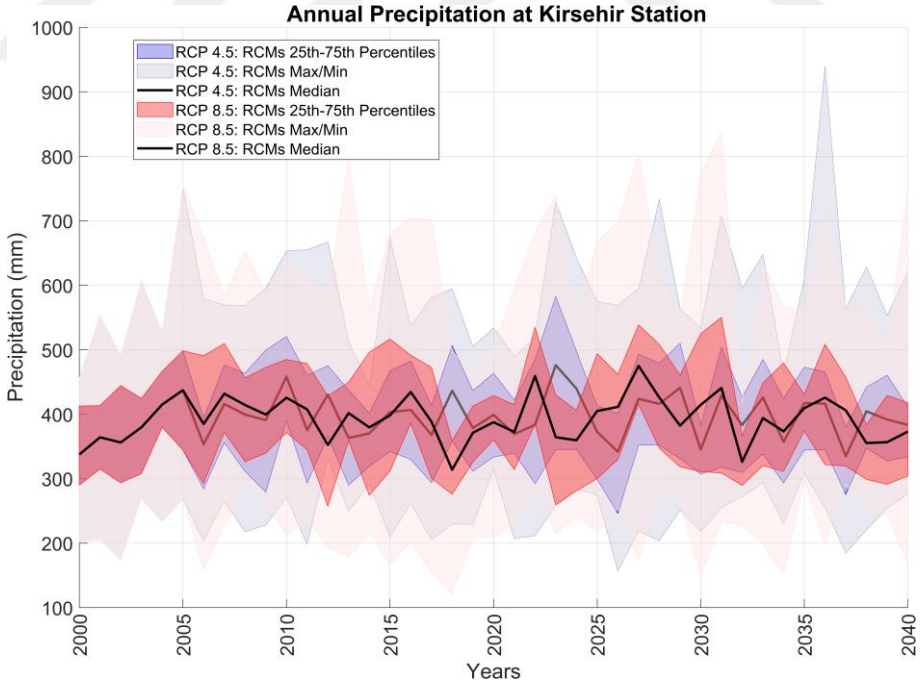

Figure D.22. Annual precipitation according to 17 RCMs under RCP4.5 and RCP8.5 climatic pathways at Kırşehir station.

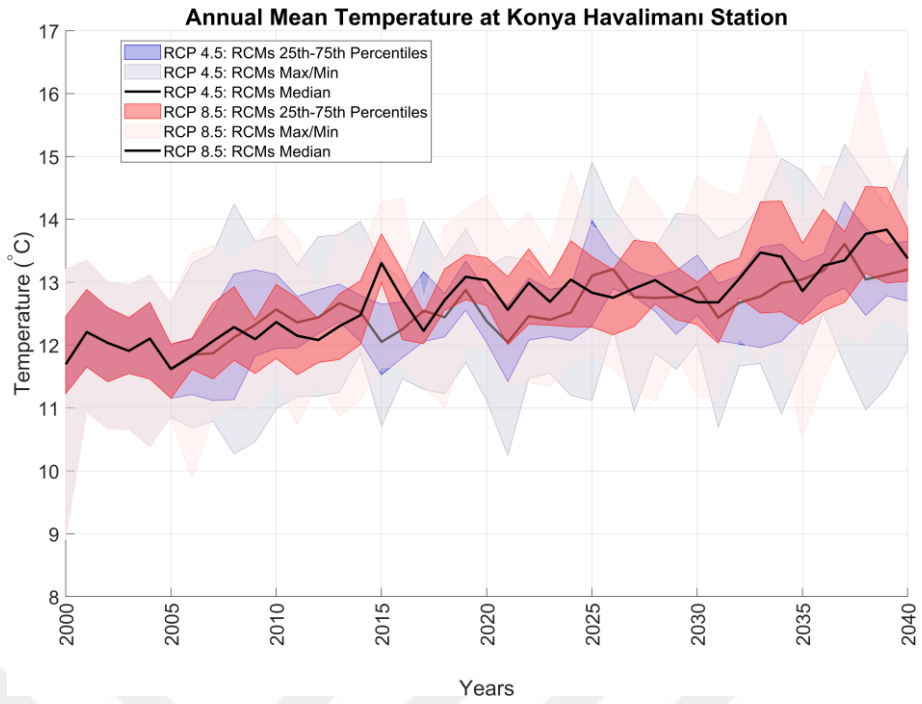

Figure D.23. Annual mean temperature according to 17 RCMs under RCP4.5 and RCP8.5 climatic pathways at Konya Airport station.

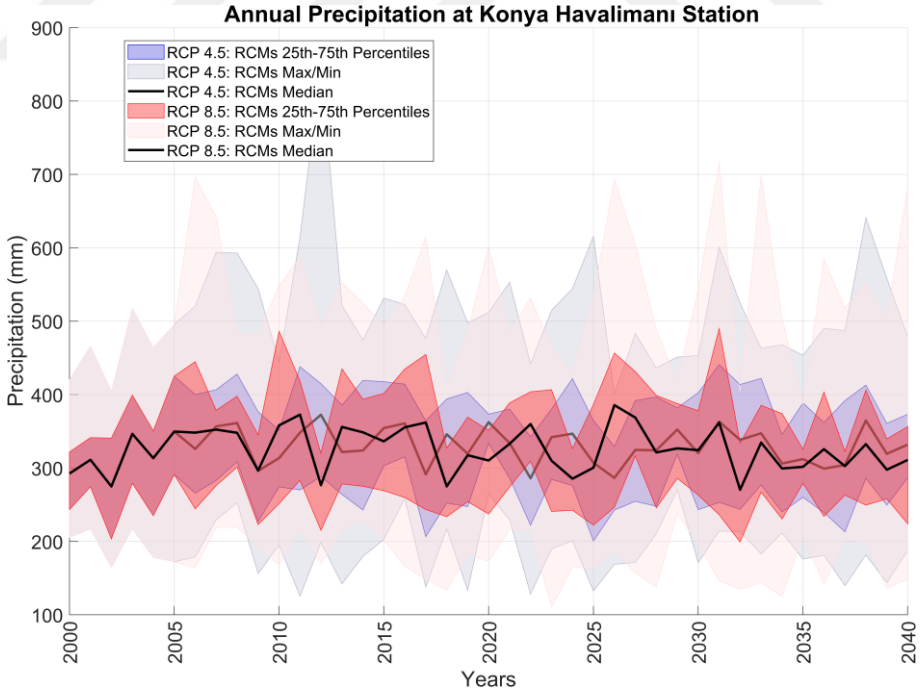

Figure D.24. Annual precipitation according to 17 RCMs under RCP4.5 and RCP8.5 climatic pathways at Konya Airport station.

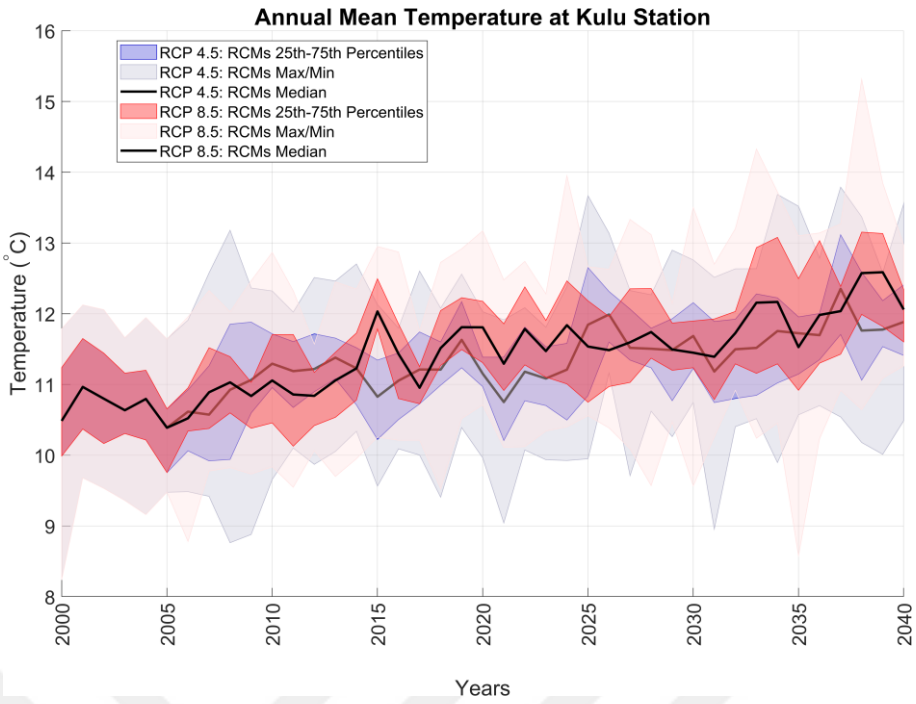

Figure D.25. Annual mean temperature according to 17 RCMs under RCP4.5 and RCP8.5 climatic pathways at Kulu station.

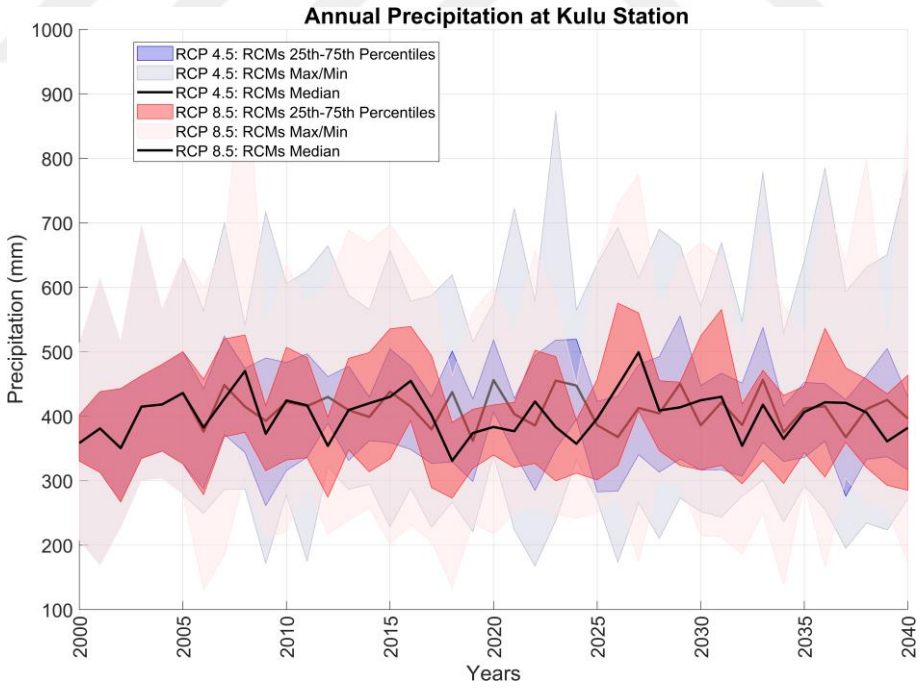

Figure D.26. Annual precipitation according to 17 RCMs under RCP4.5 and RCP8.5 climatic pathways at Kulu station.

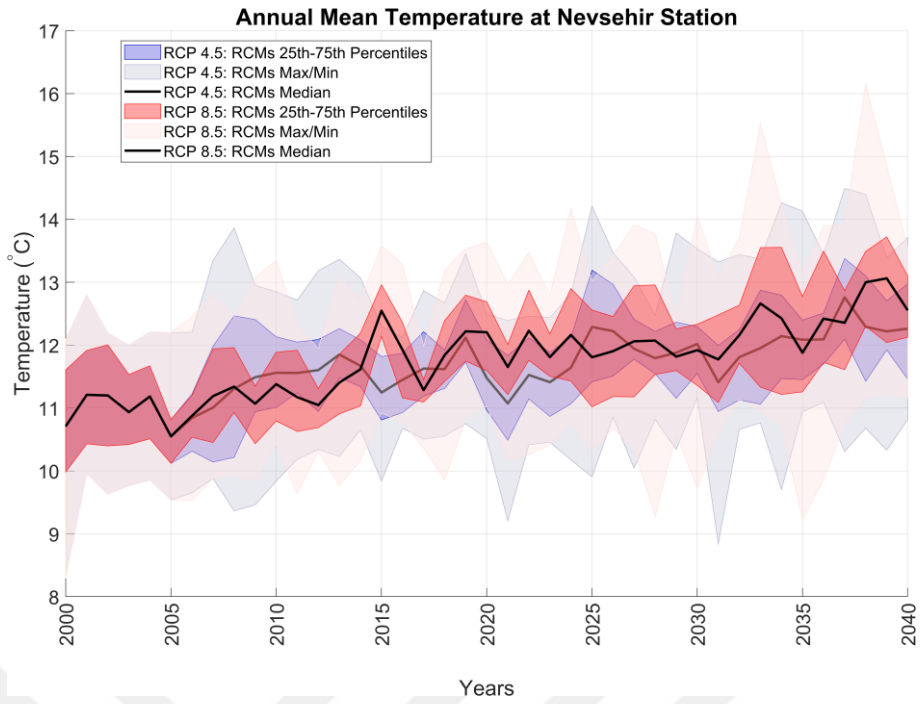

Figure D.27. Annual mean temperature according to 17 RCMs under RCP4.5 and RCP8.5 climatic pathways at Nevşehir station.

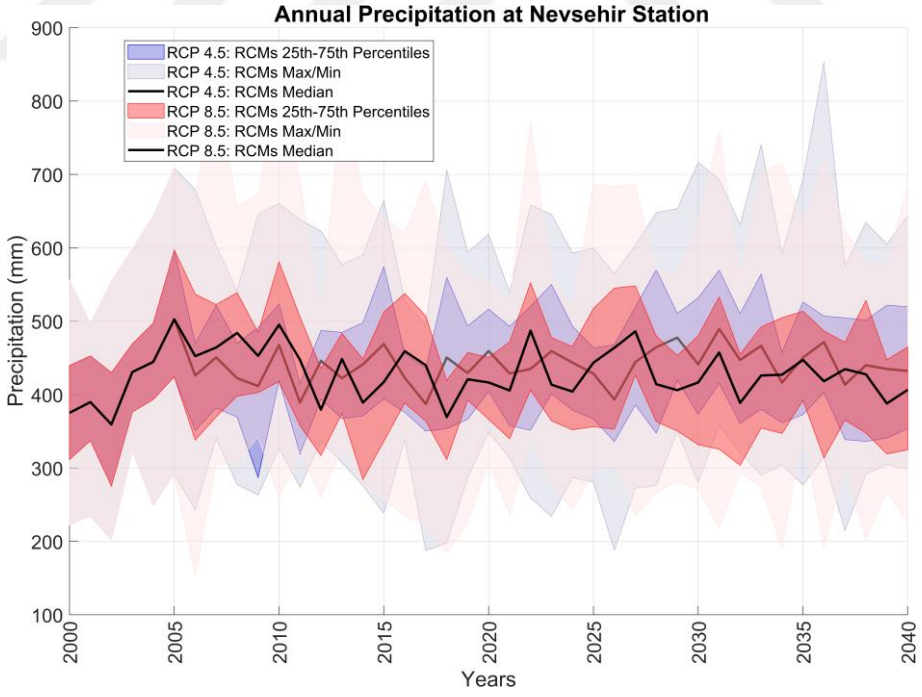

Figure D.28. Annual precipitation according to 17 RCMs under RCP4.5 and RCP8.5 climatic pathways at Nevşehir station.

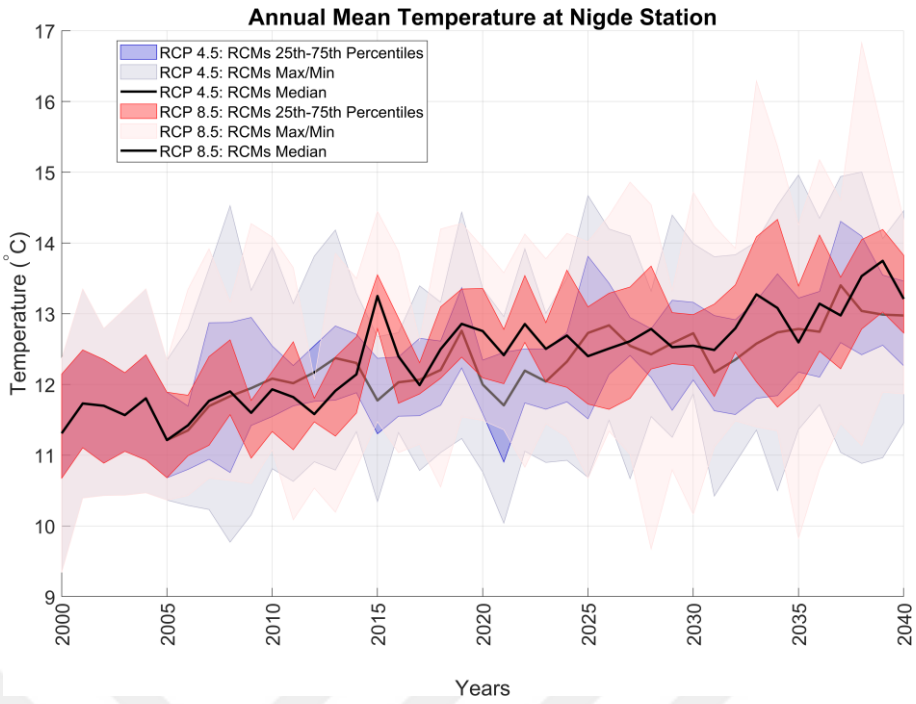

Figure D.29. Annual mean temperature according to 17 RCMs under RCP4.5 and RCP8.5 climatic pathways at Niğde station.

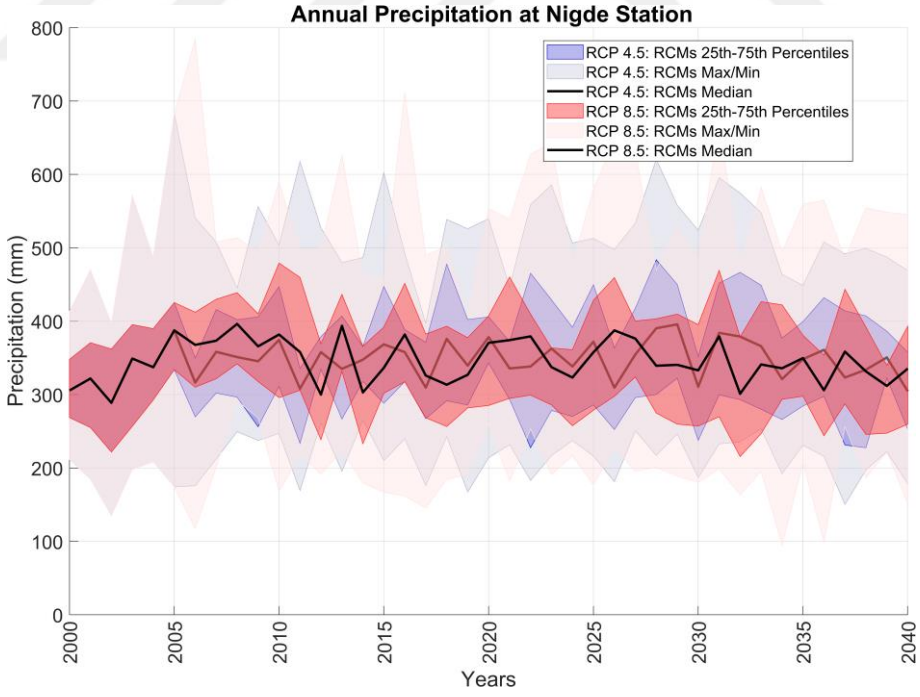

Figure D.30. Annual precipitation according to 17 RCMs under RCP4.5 and RCP8.5 climatic pathways at Niğde station.

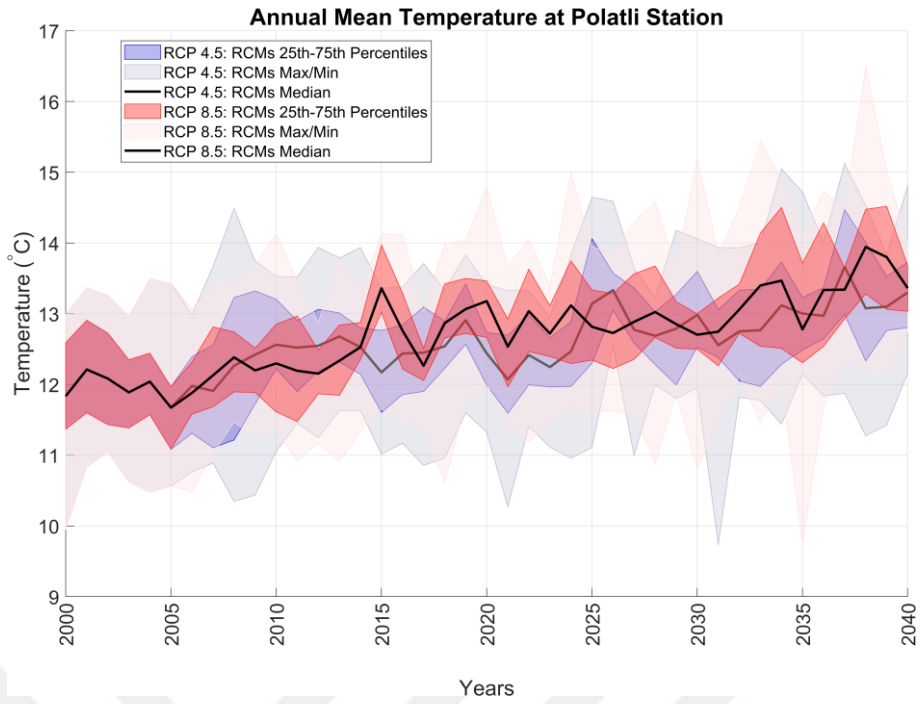

Figure D.31. Annual mean temperature according to 17 RCMs under RCP4.5 and RCP8.5 climatic pathways at Polatlı station.

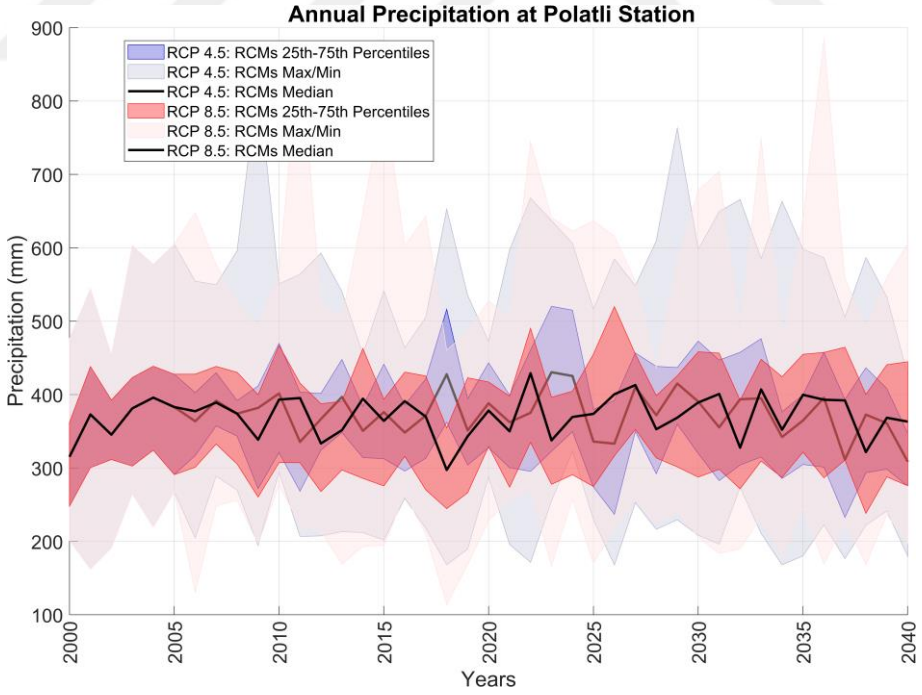

Figure D.32. Annual precipitation according to 17 RCMs under RCP4.5 and RCP8.5 climatic pathways at Polatlı station.

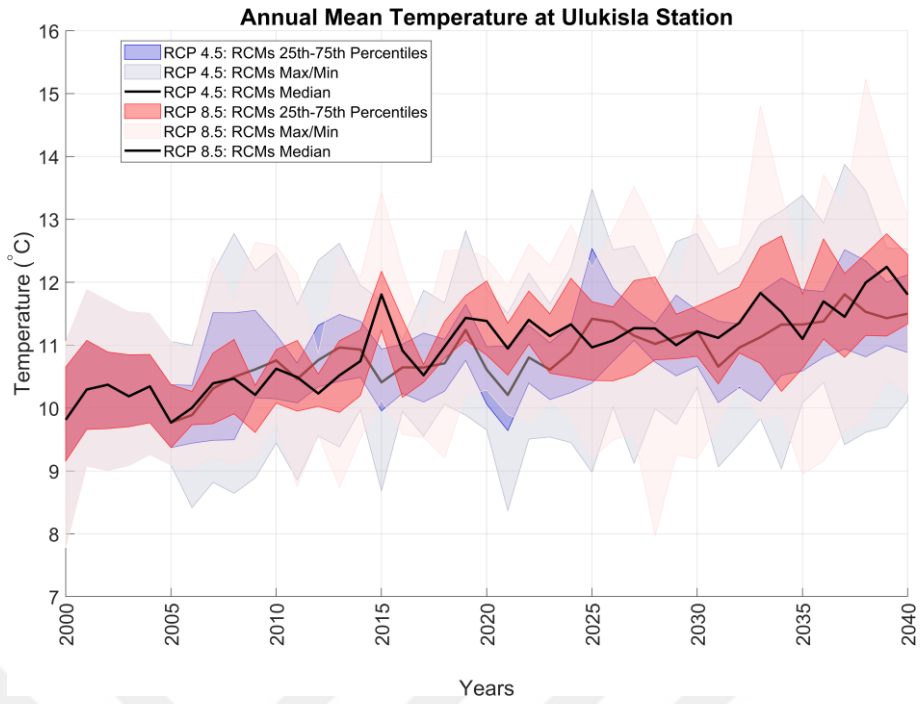

Figure D.33. Annual mean temperature according to 17 RCMs under RCP4.5 and RCP8.5 climatic pathways at Ulukışla station.

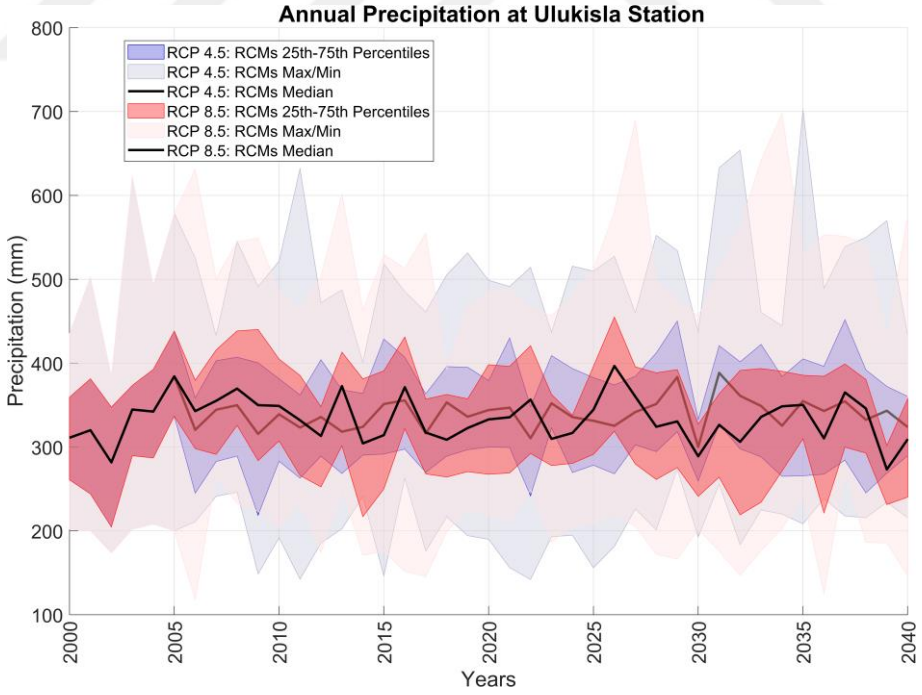

Figure D.34. Annual precipitation according to 17 RCMs under RCP4.5 and RCP8.5 climatic pathways at Ulukışla station.

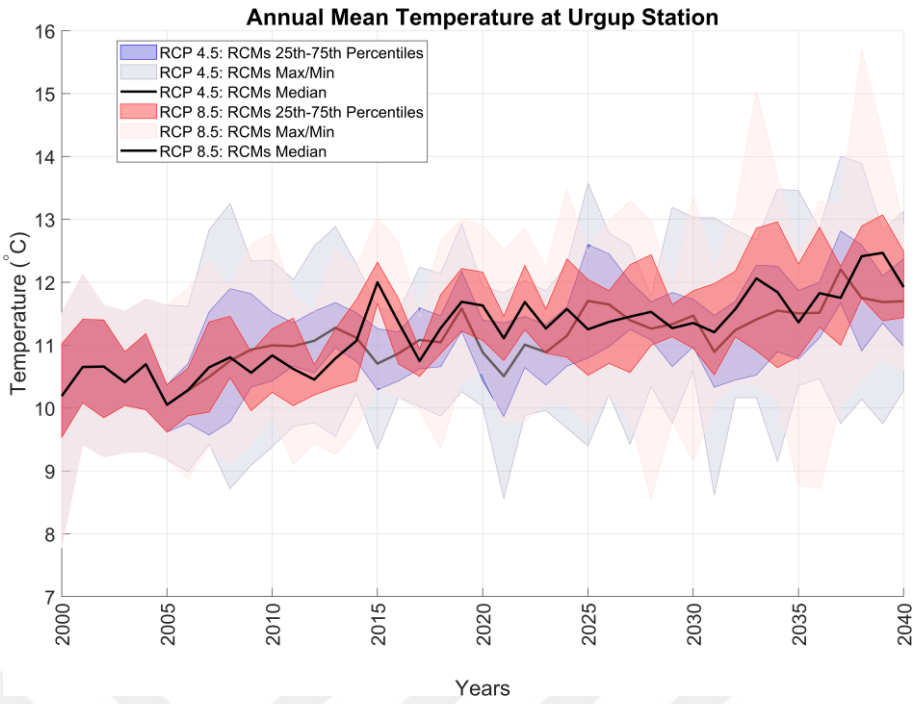

Figure D.35. Annual mean temperature according to 17 RCMs under RCP4.5 and RCP8.5 climatic pathways at Ürgüp station.

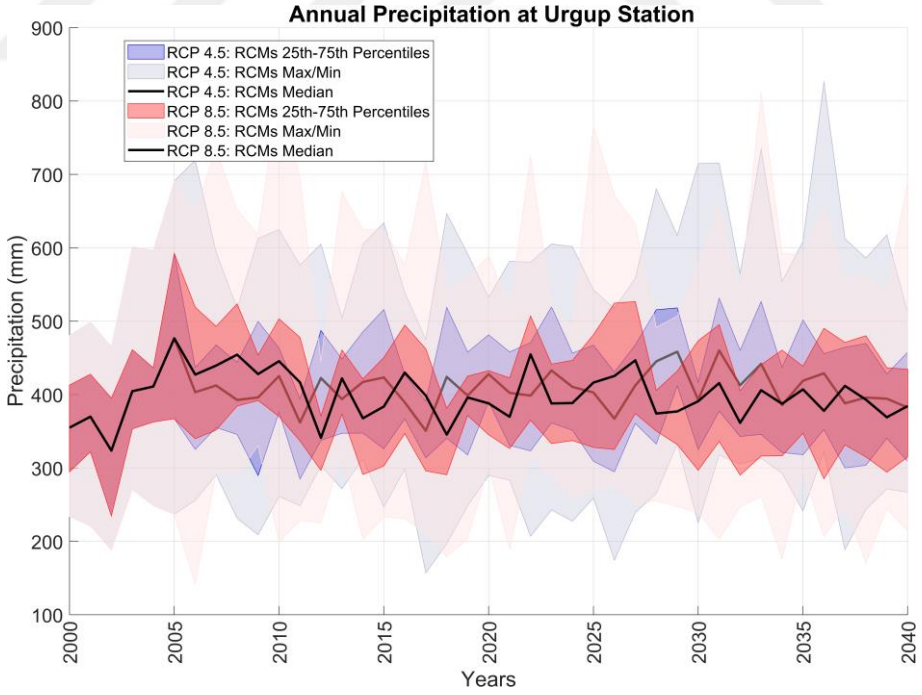

Figure D.36. Annual precipitation according to 17 RCMs under RCP4.5 and RCP8.5 climatic pathways at Ürgüp station.